

Sheet feedback control design in a printer paper path

Citation for published version (APA):

Bukkems, B. H. M. (2007). *Sheet feedback control design in a printer paper path*. [Phd Thesis 1 (Research TU/e / Graduation TU/e), Mechanical Engineering]. Technische Universiteit Eindhoven.
<https://doi.org/10.6100/IR625902>

DOI:

[10.6100/IR625902](https://doi.org/10.6100/IR625902)

Document status and date:

Published: 01/01/2007

Document Version:

Publisher's PDF, also known as Version of Record (includes final page, issue and volume numbers)

Please check the document version of this publication:

- A submitted manuscript is the version of the article upon submission and before peer-review. There can be important differences between the submitted version and the official published version of record. People interested in the research are advised to contact the author for the final version of the publication, or visit the DOI to the publisher's website.
- The final author version and the galley proof are versions of the publication after peer review.
- The final published version features the final layout of the paper including the volume, issue and page numbers.

[Link to publication](#)

General rights

Copyright and moral rights for the publications made accessible in the public portal are retained by the authors and/or other copyright owners and it is a condition of accessing publications that users recognise and abide by the legal requirements associated with these rights.

- Users may download and print one copy of any publication from the public portal for the purpose of private study or research.
- You may not further distribute the material or use it for any profit-making activity or commercial gain
- You may freely distribute the URL identifying the publication in the public portal.

If the publication is distributed under the terms of Article 25fa of the Dutch Copyright Act, indicated by the "Taverne" license above, please follow below link for the End User Agreement:

www.tue.nl/taverne

Take down policy

If you believe that this document breaches copyright please contact us at:

openaccess@tue.nl

providing details and we will investigate your claim.

Sheet Feedback Control Design in a Printer Paper Path

This PhD-study has been carried out as part of the Boderc project under the responsibility of the Embedded Systems Institute. This project is partially supported by the Netherlands Ministry of Economic Affairs under the Senter TS program.

A catalogue record is available from the Library Eindhoven University of Technology

Bukkems, Björn H.M.

Sheet Feedback Control Design in a Printer Paper Path / by Björn H.M. Bukkems. – Eindhoven : Technische Universiteit Eindhoven, 2007.

Proefschrift. – ISBN-13: 978-90-386-0974-4

NUR 978

Trefwoorden: document doorvoer systemen / terugkoppelingsgebaseerde regeling van de velloop / hiërarchisch regelen / stuksgewijs lineaire systemen / robuust regelen / lineaire matrix ongelijkheden / experimentele validatie

Subject headings: document handling systems / sheet feedback control / hierarchical control / piecewise linear systems / robust control / linear matrix inequalities / experimental validation

Copyright © 2007 by B.H.M. Bukkems.

All rights reserved. This publication may not be translated or copied, in whole or in part, or used in connection with any form of information storage and retrieval, electronic adaptation, electronic or mechanical recording, including photocopying or by any similar or dissimilar methodology now known or developed hereafter, without the written permission of the copyright holder.

This thesis was prepared with the \LaTeX 2_ε documentation system.

Cover Design: Oranje Vormgevers, Eindhoven, The Netherlands.

Reproduction: Universiteitsdrukkerij TU Eindhoven, Eindhoven, The Netherlands.

Sheet Feedback Control Design in a Printer Paper Path

PROEFSCHRIFT

ter verkrijging van de graad van doctor
aan de Technische Universiteit Eindhoven,
op gezag van de Rector Magnificus, prof.dr.ir. C.J. van Duijn,
voor een commissie aangewezen door het College voor Promoties
in het openbaar te verdedigen
op dinsdag 5 juni 2007 om 16.00 uur

door

Björn Hubertus Maria Bukkems

geboren te Geldrop

Dit proefschrift is goedgekeurd door de promotor:

prof.dr.ir. M. Steinbuch

Copromotor:

dr.ir. M.J.G. van de Molengraft

Contents

I	Introduction	I
1.1	The Boderc Research Project	I
1.2	Sheet Handling in a Printer Paper Path	4
1.3	Sheet Flow Modeling and Control	6
1.4	Contribution of the Thesis	9
1.5	Outline of the Thesis	II
2	The Sheet Feedback Control Architecture	13
2.1	Basic Paper Path Setup	13
2.2	Paper Path and Sheet Flow Modeling	14
2.3	Decomposition of the Sheet Handling Control Problem	17
3	State Feedback Control Design	23
3.1	The Tracking Control Problem	23
3.2	Nominal Sheet Feedback Control Design	26
3.2.1	Controller Synthesis	26
3.2.1.1	Linearizing Controller Synthesis	31
3.2.1.2	Partially linearizing Controller Synthesis	32
3.2.2	Control Design Results	33
3.2.2.1	Linearizing Feedback Control Design Results	34
3.2.2.2	Partially Linearizing Feedback Control Design Results	35
3.2.3	Simulation Results	36
3.2.3.1	Linearizing Feedback Controller Results	37
3.2.3.2	Partially Linearizing Feedback Controller Results	38
3.3	Analysis of the Perturbation of Paper Path Parameters	41
3.3.1	Influence of Parameter Perturbations	43
3.3.2	Simulation Results	46
3.4	Evaluation	51

4	Output Feedback Control Design	53
4.1	The Tracking Control Problem	53
4.2	Nominal Sheet Feedback Control Design	55
4.2.1	Controller Synthesis	55
4.2.2	Control Design Results	60
4.2.3	Simulation Results	64
4.3	Robust Sheet Feedback Control Design	66
4.3.1	Uncertainty Modeling	66
4.3.2	Controller Synthesis	68
4.3.3	Control Design Results	72
4.3.4	Simulation Results	76
4.4	Stability Analysis for Non-ideal Low Level Dynamics	77
4.5	Evaluation	78
5	The Experimental Paper Path Setup	81
5.1	The Sheet Transportation Unit	81
5.2	Sheet Position Measurement	83
5.2.1	Sensor Selection	83
5.2.2	Implementation	84
5.2.2.1	Calibration	85
5.2.2.2	Sheet Position Measurement	86
6	Experimental Results	89
6.1	Low Level Motor Dynamics	89
6.2	Experimental Validation Results - The State Feedback Control Approach	93
6.3	Experimental Validation Results - The Output Feedback Control Approach	100
6.3.1	Stability Analysis in Case of Non-ideal Low Level Dynamics	100
6.3.2	Robustness Experiments	101
7	Extensions of Sheet Feedback Control to Real Printer Paper Paths	107
7.1	Challenges in Industrial Paper Paths	107
7.2	Duplex Loop Modeling and Control	108
7.2.1	The Tracking Control Problem	108
7.2.2	Sheet Feedback Control Design	111
7.2.3	Simulation Results	112
7.3	Sheet Transport via Multiple Pinches	113
7.3.1	The Tracking Control Problem	113
7.3.2	High Level Sheet Flow Modeling and Control Design	116
7.3.3	Low Level Motor Control Design	117
7.3.3.1	Feedforward Control Structure	118
7.3.3.2	Feedforward Control Design Results	120

7.3.3	Feedback Control Design Results	121
7.3.4	Validation Results	123
7.4	Coupling Pinches into Sections	128
7.5	Evaluation	130
8	Conclusions and Recommendations	133
8.1	Conclusions	133
8.2	Recommendations	135
8.2.1	Recommendations for the Control Design Approaches	136
8.2.2	Recommendations for Integration and Implementation	137
A	Linearizing Change of Variables	139
	Bibliography	141
	Summary	149
	Samenvatting	151
	Dankwoord	155
	Curriculum Vitae	157

CHAPTER ONE

Introduction

1.1	The Boderc Research Project	I
1.2	Sheet Handling in a Printer Paper Path	4
1.3	Sheet Flow Modeling and Control	6
1.4	Contribution of the Thesis	9
1.5	Outline of the Thesis	II

1.1 The Boderc Research Project

A general trend in the design of high-tech systems as, for example, wafer steppers, electron microscopes, and document handling systems, is the increasing number of requirements imposed by its users. More functionality is asked for, while already existing functional properties must be preserved or, even more likely, improved. On the other hand, industrial constraints are becoming tighter. Product design cycles must be shortened and development costs must be decreased to keep a competitive position in the market. A consequence of this trend is an increasing complexity of the overall system design, which has to be realized in less time and in close co-operation by multiple monodisciplinary engineering disciplines, such as mechanical, electrical, software, and control engineering [36]. In each of these disciplines, the increasing system complexity results in an increase of the number of design decisions to be made. Erroneous decisions, especially the ones made in early design phases, can have a significant impact during product integration phases, as many other decisions will be based on them. Corrections in later project phases are difficult to make and can therefore lead to a longer development period than planned or can lead to a less optimal product [58].

Given the increasing design complexity in combination with industrial constraints that are becoming tighter, the need for a new system design approach arises. In conventional design approaches, both systems engineering [7] and the monodisciplinary engineering disciplines play an important role. On the one hand, systems engineering focuses on defining customer needs and required functionality early in the development cycle. Moreover, the focus is on the documentation of requirements, design synthesis, and system validation [43]. In many cases, qualitative, non-executable models are used, which give an insight in the functionality of the system. On the other hand, the monodisciplinary engineering disciplines focus on the functionality of parts of the system, using detailed, executable models to predict and quantify the subsystem behavior. The positioning of both systems engineering and the monodisciplinary engineering disciplines with respect to the number of details used in their models is schematically depicted in the pyramid shown in Fig. 1.1 [36]. The goal of the new system design approach is to develop a model-based design methodology that can cope with the increasing complexity by using low-detailed, executable models. By making use of this type of models, the methodology must support multi-disciplinary design space exploration and it must be able to predict the performance at the system level, i.e. in terms of the system functionalities [21, 36]. Hence, the design activities should be concentrated in the middle of the pyramid, as indicated in Fig. 1.1.

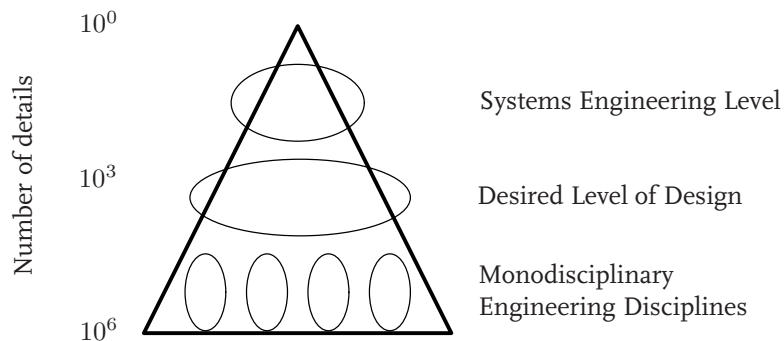


Figure 1.1 / Schematic indication of the level of detail of models used in system design.

To facilitate the realization of the desired new system design approach for high-tech systems, the Boderc research project has been initiated [21]. The intended model-based design methodology encompasses four different elements: *formalisms*, i.e. languages (syntax) used for modeling (parts of) the system behavior and to formalize the system requirements, *techniques*, used to retrieve information from models, *tools*, used to support the efficient application of formalisms and techniques, and *methods*, that give guidelines on how to use the formalisms, techniques, and tools [38]. Within the context of the Boderc project, the models, techniques, and methods are particularly developed for application

in the early design phases and must satisfy industrial application constraints. Moreover, they should enable fast design cycles to quickly yield insight in the influence of changing design choices on the system performance. To facilitate this, a systematic design is required, which, among others, can be realized by deriving low-detailed, yet adequate, models that are capable of making predictions at the system level.

To realize the Boderc research goal, the industry-as-laboratory approach [55] has been used, see [9] for an example. In this approach, the actual industrial setting is exploited as a test environment, which ensures the research question to be based on real industrial problems. In case of the Boderc project, the industrial setting consists of high volume document printing systems, as shown in Fig. 1.2. Since in these xerographic systems [33, 68] requirements at the system level, e.g. high throughput, reliability, and user-friendliness, are connected with subsystem requirements such as timing and synchronization requirements, they form a suitable test environment.



Figure 1.2 / The Boderc industrial setting: high volume document printing systems.

Given this type of systems as a case-study, the Boderc project addresses the overall system design problem at the system level and, after decomposition, at the subsystem level. This yields system-level methods and models on the one hand, and subsystem-level models on the other hand [36]. Each of the models makes use of its own tools, e.g. spreadsheet programs or Matlab/Simulink [78], whereas in the methods techniques like performance analysis or controller synthesis are used. Examples of system-level methods are the key driver method [37], in which the system requirements are obtained in a systematic way that provides a structured overview, the threads of reasoning method [65], which aims at providing a clear overview on how conflicts in the design relate to key drivers, and a budget-based design method [26], which proposes a systematic approach for the distribution of resources in the system design. Examples of system-level models, on the other hand, are the Happy Flow model [3], used for performing a quick design space exploration with respect to the print job scheduling and the mechanical layout of the paper path, and models describing the performance of software when executed on

real platforms [81]. Zooming in at the subsystem level, examples of topics addressed in the Boderc project are event-driven control [64, 66], the effect of time delay in networked control systems [16], and analysis techniques for real-time properties of software [24]. Within the context of the project, one of the central questions is in which way control engineering can contribute to the realization of the Boderc research goal. In response to this question, this thesis takes as a case-study the design of a sheet handling system in the paper path of document printing systems, since the paper path is a significant unit of the complete printing system in which motion control plays an important part. In the next section, sheet handling in a printer paper path will be discussed in more detail.

1.2 Sheet Handling in a Printer Paper Path

An example of a printer paper path is shown in Fig. 1.3. Sheets enter the paper path at the Paper Input Module (PIM) and are transported to the Image Transfer Station (ITS) where the image is printed onto the sheet at high pressure and high temperature. The required high sheet temperature is realized using two preheater units that are located before the ITS. After the print has been made, sheets can either re-enter the first part of the paper path via the so-called duplex loop and go to the ITS for the second time for back side printing or they can go to the finisher (FIN), where they are collected. The transportation of sheets is carried out via pinches. A pinch is a set of rollers consisting of two parts: the driven roller that is actuated by a motor and the non-driven roller that is used to apply sufficient normal force, i.e. the force needed to prevent the sheet from slipping in the pinch. As can be seen from Fig. 1.3, pinches can be driven either individually or grouped together in sections. To realize the desired, prespecified printing quality, the sheets must be transported correctly in three directions: the longitudinal direction, i.e. the direction of the sheet flow, the lateral direction, i.e. the direction perpendicular to the direction of the sheet flow, and the skewness direction, i.e. the orientation with respect to the desired longitudinal orientation. Corrections in the first direction can be applied via the motor-pinch combinations, whereas for the correction of the latter two directions a registration unit is often used, in which the sheets are stopped and aligned in lateral and skewness direction.

The main objective of the printer's sheet handling system is to accurately deliver sheets at the ITS. Each sheet must synchronize with its corresponding image with respect to both the ITS entry time and the constant printing velocity to achieve a high printing quality. This desired printing quality is often realized by using a high precision mechanical design. In such design, manufacturing tolerances of the various components are small and the paper path frame is designed to be stiff to prevent undesired flexibilities. With such high precision mechanics, a predictable sheet flow can be realized and error cor-

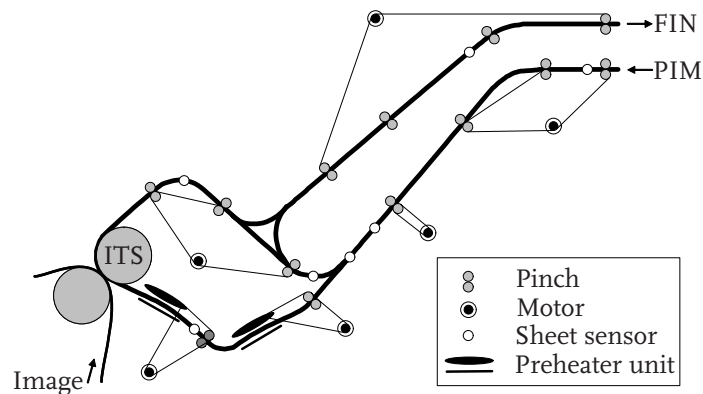


Figure 1.3 / Schematic representation of a printer paper path.

rection during the sheet transport can be done at a few fixed locations in the paper path only. At these locations optical I/O sheet sensors, indicated in Fig. 1.3, are mounted that can detect the presence of a sheet. Based on this sheet detection, the sheet reference motion profile can be slightly adjusted such that the sheet will meet its corresponding image in the ITS right on time. A drawback of this approach is the fact that the design of the discrete-event sheet controllers is not carried out systematically; for each new printer to be designed, it takes much effort to determine where and how feedback needs to be applied. Hence, fast design cycles in an early stage of the design are difficult to realize.

To improve the design trajectory of a sheet handling system, this thesis investigates how control engineering can contribute to the optimization of the design trajectory of such system. More specifically, having the Boderc research goal in mind, the question is if a model-based methodology for the design of such sheet handling system can be formulated from a control engineering point of view. In order to find an answer to this question, the goal of this thesis is to find a systematic approach for controlling the sheet flow, which is based on low-detailed, yet adequate models of the sheet flow and paper path dynamics. Such models should be both accurate enough to make useful predictions of the physical process and abstract enough to enable relevant reasoning with appropriate time-efficiency [4]. The approach to be designed should encompass three main characteristics. First of all, it should be applicable in early stages of the design process. Secondly, it should be generic such that it can be used in various printer design projects, and thirdly, it should allow for fast design cycles such that insight in the effect of certain design decisions can be quickly obtained. Hence, applying the approach for designing a sheet handling system in an industrial design process should result in both a decrease of the development time and an increase of the predictability of the design process.

1.3 Sheet Flow Modeling and Control

To realize the intended design of a sheet handling system, models of the sheet flow and paper path dynamics are needed. However, as we are dealing with a very specific application field, the amount of literature on paper path modeling is not too extensive. Yet, [32] and [31] present a compositional model of sheet transportation in a printer paper path. The model is meant for simulation and diagnosis, and is applicable to a variety of configurations. The models presented cannot be directly used for model-based sheet controller synthesis, but the key feature linking to the work presented in this thesis is the level of abstraction used in the modeling. More specifically, the model presented in [32] abstracts away from the physical forces and reasons only about velocities. Nonetheless, it succeeds in determining essential features of the motion of the sheet of paper like buckling and tearing.

Similar to paper path modeling, (model-based) control design for sheet handling systems of document printing systems has not received widespread attention in the control literature either [33]. One of the first contributions that is considered relevant for the work described in this thesis, is presented in [56]. A hybrid hierarchical control architecture for the transportation of sheets in a paper path is discussed. The transition from the open-loop operation of sheet handling mechanisms to the introduction of sheet feedback control is discussed. A hybrid hierarchical control system architecture is proposed, in which a central supervisory controller plans overall trajectories for each sheet of paper. These trajectories are communicated to the low-level systems, i.e. to the motor-pinch combinations that track the trajectories and provide an estimate of the motion of the sheet to the central controller. Based on this estimation, a new sheet trajectory can be planned when collisions become likely to occur.

Elaborating on the results presented in [56], the work presented in [12, 46] discusses in more detail the use of closed-loop longitudinal motion control of sheets in a printer paper path. Motivated by the increasing demands on sheet handling capabilities, i.e. sheets with a wider range of characteristics that have to be transported at higher speeds, a redesign of the paper path hardware and software is proposed. By introducing feedback of the sheet position information, variations in sheet properties, operating velocities and machine variations are shown to have a minimal impact on the machine performance. The design of the closed-loop sheet feedback control system is based on dynamic paper path models. In [12, 46], the paper path model is split up into two parts: the section dynamics and the sheet dynamics. The section dynamics map the motor currents to section velocities, so these dynamics consist essentially of integrators. The sheet dynamics, on the other hand, consist of switching integrators, as the section transporting the sheet changes as a function of the sheet position. A finite state machine is used to describe the discrete switching

of a sheet between different sections: when entering a new section, the sheet velocity is dictated by the velocity of that section. The mapping from sheet velocities to sheet positions is described by regular integrators. The combination of the finite state machine with the regular integrators results in a hybrid dynamic model, also known as a hybrid automaton [39]. On the basis of this model, a distributed, hybrid hierarchical control approach is adopted, which controls the spacings between the sheets [13, 14]. The controller structure used in this approach is depicted in Fig. 1.4, which is taken from [12, 46]. In this figure, the finite state machine representing the sheet dynamics can be recognized, together with low level controllers for the sections and high level controllers generating the reference velocities for the low level section control loops. At the supervisory level, the overall mode of operation is determined. To correct for deviations from the desired inter sheet spacing, proportional controllers are used in the high level control blocks. The outputs of these controllers are saturated according to the actuator constraints of the corresponding sections. Moreover, for a proper synchronization of the section velocities, needed to prevent buckling or tearing of the sheets, funnel-shaped velocity bounds¹ are used. These bounds limit the allowable velocity range of a section when the most downstream sheet in this section approaches the next one. If the velocity remains inside the funnel at all times, the sections will synchronize at or before the transfer of the sheet. As recognized in [12, 46], the control design is done intuitively and verified only by simulation. Stability of the closed-loop system is not proven and disturbances and uncertainties present in the printer paper path are not taken into account in the control design, which makes it hard to prove the controller works under all conditions. Examples of possible disturbances present in the paper path are the asymmetry of rollers driving the sheet through the paper path, variations in sheet properties, and slip between rollers and sheet, whereas tolerances on the radii of rollers or on transmission ratios between motors and rollers are examples of uncertainties in the paper path. In this thesis, the control design is fully model-based and uncertainties are taken into account in the control design, as will be discussed in Section 1.4. Hence, guarantees on stability and performance in the presence of uncertainties can be given.

The results discussed so far only apply to sheet control in the longitudinal direction. However, as mentioned in Section 1.2, most document printing systems also require precise lateral and skewness control of the sheets. Hence, accurate control of the sheets along two additional in-plane degrees of freedom is required. This problem is addressed in [61, 62, 63], where a steerable pinch mechanism is proposed for the actuation of sheets in lateral and skewness direction.

The hierarchy introduced in the paper path control design discussed in [12, 46, 56] has served as a basis for further research on paper path control. In [27], for example, coordi-

¹Upper and lower velocity bounds that both converge to the velocity of the next section.

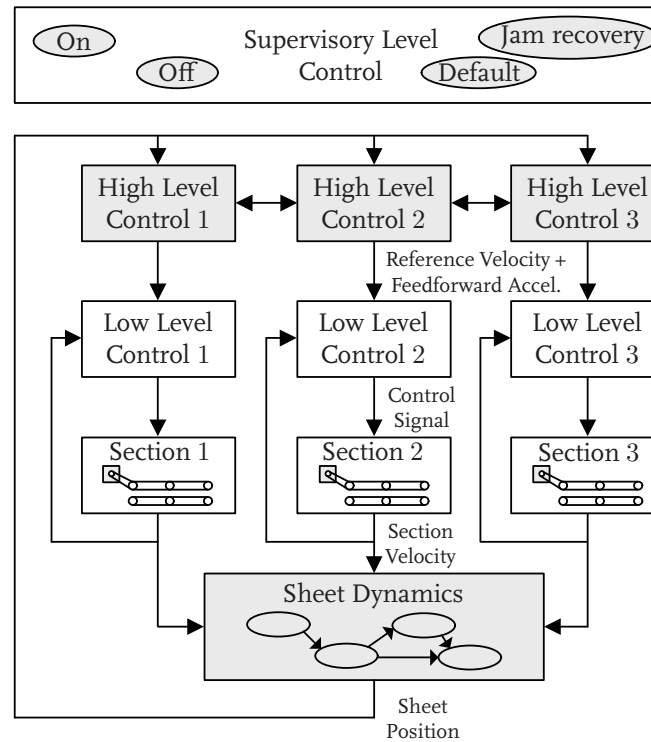


Figure 1.4 / Overview of the controller structure used in [12, 46].

nated control in highly modular printing systems is discussed, making use of the control hierarchy proposed by [12, 46, 56]. The coordination task, i.e. the proper transportation of a sheet by several sections at the same time, is assigned to a sheet controller instead of being solved by using funnel-shaped velocity bounds. This controller communicates with all section controllers currently interacting with the sheet, as well as those about to interact with it. The section controllers, in turn, are responsible for tracking the trajectories provided by the sheet controller. Also in [40], the hierarchical control setup is used in a case-study from the document printing domain to study the synchronization of controller states.

Besides the sheet transportation domain, the hybrid hierarchical control approach used in [12, 46] can also be applied in other domains. Its hierarchical structure reduces the design complexity, since different levels of abstraction are used. On the other hand, the overall performance of the system can benefit from the hybrid character of the controller. An example of another domain can be found in the area of manufacturing transport systems. In [79], for instance, a hybrid control scheme similar to the one used in [12, 13, 46] is proposed for this type of systems. Since they deal with the transport of packages via multiple transportation units, the link with sheet transport in a printer paper path can be easily made. This can be observed in [48], in which the inter sheet spacing control algorithm used in [12, 14, 46] is applied to a manufacturing transport system.

1.4 Contribution of the Thesis

In this thesis a systematic, model-based design methodology for applying sheet control in a printer paper path is proposed. Since the main focus will be on control design for stability and robustness, we will concentrate on feedback design only, while realizing that for achieving a good tracking performance in practical situations, adding a motion feedforward controller can be beneficial. To be able to judge the quality of the tracking behavior realized using the sheet feedback controllers, performance properties have been defined. Based on requirements and responses of real printers, the tracking performance realized using the sheet feedback controllers designed in this thesis is said to be good when the maximum transient responses and the steady state tracking error do not exceed $3 \cdot 10^{-3}$ m and $5 \cdot 10^{-4}$ m, respectively. The value of the maximum transient responses is well acceptable considering the fact that a typical value of the distance between the sheet and its upstream or downstream neighbor is $40 \cdot 10^{-3}$ m [15], whereas the value of the steady state tracking error is typically used for quantifying print quality.

To realize the desired model-based sheet feedback control design approach, this thesis starts with a case-study on control design for a basic printer paper path that describes the sheet flow in its most elementary form. By considering this basic version, the essence of the control problem, i.e. the switching nature of the system, caused by the consecutive changing of the driving pinch, becomes clear. For the modeling of the sheet flow, the thesis proposes to use a high level of abstraction [32]. Hence, a simple model of the sheet flow in longitudinal direction, that can take into account parametric uncertainties, is derived and formulated in the piecewise linear (PWL) modeling *formalism* [72]. As will be discussed in Chapter 2, the benefits of choosing this formalism are the fact that the system behavior can be very well captured in this formalism, together with the availability of *techniques* for both controller synthesis and analysis. For a simplification of the control design, the control problem is split up into low level motor control loops and a high level sheet control loop that can be designed independently. Hence, the hierarchy of the control architecture of [12, 46] is adopted. For a further simplification of the control design, the low level motor control loops are assumed to be ideal, reducing the overall sheet handling design problem to the design of sheet feedback controllers only.

Based on the sheet flow model, this thesis presents two approaches for sheet feedback control design. In the first approach, the system is formulated in terms of its error dynamics, given a predefined class of sheet reference profiles. By working in the tracking error domain, stabilization of the error dynamics is directly linked to tracking performance. In contrast with the formulation of linear models in the error domain, the formulation of the PWL sheet flow model in error space yields a discontinuous model of the error dynamics. More specifically, the resulting model consists of both flow conditions, describing

the dynamics in each regime, and jump conditions, describing the error dynamics at the switching boundaries. Given the model in error space, a stabilizing state feedback control law is proposed. Rendering the zero tracking error situation an equilibrium of the error dynamics imposes a restriction on the admissible controllers, i.e. controllers that result in either full or partial linearization of the system must be synthesized to realize the desired equilibrium. Given the control law, relations between the type of controller and the type of Lyapunov function needed for the stability analysis are derived. The actual calculation of the controller gains is carried out by solving a set of linear matrix inequalities (LMIs). For the case parameter uncertainties are present in the system, both the flow conditions and the jump conditions are derived. Based on the latter conditions, an analysis for predicting the effect of the uncertainties on the sheet tracking error is carried out. In the second control design approach, dynamic output feedback controllers are directly synthesized based on the switching sheet flow dynamics. The synthesis is also formulated in terms of a set of LMIs and combines linear H_∞ control design techniques for the individual regimes of the sheet flow dynamics with stability and performance requirements for the overall switched system. Initially, control design based on the nominal sheet flow model is considered, after which the approach is extended to take into account parametric model uncertainties within a prespecified bound, yielding controllers that result in both robust stability and robust performance of the switched closed-loop system.

This thesis also discusses the practical validation of both control design approaches. For this purpose, an experimental paper path setup, shown in Fig. 1.5, has been designed and built. To gain access of the sheet position information, the use of cheap optical mouse sensors is proposed as an alternative for the application of an asynchronous observer used for the estimation of the sheet position [47]. A benefit of directly measuring the sheet displacement is the accuracy of the sheet position information in case of unmodeled disturbances and uncertainties that are present in the paper path. Because of the simplifying assumptions on ideal motor dynamics, made in the sheet feedback control design approaches, a stability analysis procedure is presented to verify the stability of the overall closed-loop dynamics, i.e. including the low level controlled motor dynamics.

With the experimental validation of the sheet feedback control design approaches, the design cycle is complete. The PWL modeling *formalism* and the *techniques* for controller synthesis, together with the supportive *tools* for the calculation of the controller gains and the *method* of applying these in combination with simulations and experiments yields the desired methodology for applying sheet feedback control in a basic printer paper path.

The final contribution of the thesis is the extension of the control design towards real printer paper paths. Because of the possibility to carry out control design for robustness, and because most design freedom is obtained, the second approach is proposed for control design in a duplex loop and for cases in which sheets are driven by multiple sections.



Figure 1.5 / Photo of the experimental paper path setup.

For the latter case, we propose to adapt the low level motor control design to satisfy additional no-slip and no-buckling constraints. As a result, additional elements in the control loop, such as funnel-shaped velocity bounds [12, 46], are not necessary anymore. With these extensions, the basis of a reusable, systematic, and model-based design approach for sheet handling in printer paper paths is proposed in this thesis. The approach allows for fast design cycles and can be applied in early design stages to investigate the effect of certain design decisions. Hence, the proposed approach is expected to contribute to both a decrease of the development time and an increase of the predictability of the design process of the printer paper path design.

1.5 Outline of the Thesis

This thesis is organized in the following way. In Chapter 2 the basic paper path case-study, that serves as a basis for sheet feedback control design, will be presented. Given this case-study, various possibilities of modeling the paper path and sheet flow dynamics are presented, leading to a linear model of the controlled motor dynamics and a low-detailed, yet adequate PWL model of the sheet flow. Given the models for the paper path and sheet flow dynamics, the sheet handling control problem is decomposed into a high level sheet control loop and low level motor control loops and the hierarchical control layout is presented. Furthermore, an assumption on ideal low level motor control loops is made and the control goal for the remaining sheet flow dynamics is presented.

In Chapter 3, the first design approach for sheet feedback control is presented. First the sheet flow dynamics are represented in the error domain, yielding a nominal model of the sheet error dynamics that serves a basis for the control design. Based on this nominal

model, two types of controllers are proposed. The relation between the feedback controllers and the type of Lyapunov function for proving the stability of the closed-loop system is analyzed, together with the effect of parameter perturbations on the sheet tracking error. Simulations are carried out for the validation of the synthesis and analysis results.

The second approach for sheet feedback control design is presented in Chapter 4. Based on models of the sheet flow dynamics, control designs for both the nominal case and the case in which parametric uncertainties are present are discussed. Also for this control design approach, simulations are carried out. Furthermore, a procedure for the stability analysis of the overall system, i.e. including a model of the controlled motor dynamics, is derived.

Chapter 5 presents the experimental setup used for the practical validation of the control design approaches. The selection of an appropriate sensor for obtaining the sheet position information is discussed, yielding optical mouse sensors as the most suitable option. After describing the calibration procedure, the derivation of the sheet position information from multiple sensors is discussed.

In Chapter 6, the results of the validation experiments are presented. First the dynamics of the motor-pinch combinations are identified. Based on measured data, models are designed that need to be taken into account in the stability analysis of the overall system. Furthermore, suitable feedback controllers for the low level motor-pinch systems are designed. The sheet feedback controllers obtained from both control design approaches are implemented and the resulting responses are analyzed.

The extensions of sheet feedback control to industrial printer paper paths is discussed in Chapter 7. First the challenges in this type of paper paths are discussed, after which the second approach is chosen to be extended for application. Modeling and control of the sheet flow in a duplex loop are discussed, together with the case in which a sheet is driven by multiple pinches. In the latter case, an adaptation of the low level motor control design is proposed, needed to take into account additional constraints imposed by the new case.

Conclusions and recommendations regarding the work presented in this thesis are discussed in Chapter 8.

The Sheet Feedback Control Architecture

2.1	Basic Paper Path Setup	13
2.2	Paper Path and Sheet Flow Modeling	14
2.3	Decomposition of the Sheet Handling Control Problem	17

2.1 Basic Paper Path Setup

In this chapter the design of the architecture for model-based sheet feedback controller synthesis is discussed. To understand the essence of the control problem, a case-study is adopted that contains the most elementary elements present in a paper path. Given this case-study, the approach for modeling the sheet flow in the paper path is presented, resulting in a sheet flow model based on which the control design can be carried out. To facilitate this design, the sheet handling control problem is decomposed, resulting in a multi-level control hierarchy.

The case-study we adopt as a starting point for the design of the model-based sheet handling system is based on the most essential characteristic present in each printer paper path, i.e. sheets being driven by motor-pinch combinations in a sequential manner. This leads to a basic paper path case-study that reveals the essence of the control problem, i.e. the switching nature of the system caused by the consecutive changing of the driving pinch. By considering this basic version, a number of characteristics present in real printer paper paths, as the one shown in Fig. 1.3, are initially left out of consideration. The most important examples of these characteristics are the duplex loop for backside printing, the grouping of pinches into sections, and the transport of sheets by

multiple pinches. Extensions to the basic paper path that include these characteristics will be discussed in Chapter 7.

The basic paper path initially used for the design of the sheet handling system is depicted in Fig. 2.1. Since we consider the motion of sheets only when they are in the paper path, the paper input module and finisher are not taken into account. The considered paper path consists of three pinches (P_1 , P_2 , and P_3), each of which is driven by a separate motor (M_1 , M_2 , and M_3 , respectively). Hence, each sheet can be controlled independently from the others, since at all time instants each sheet has its own motor-pinch combination that determines its motion. The locations of the three pinches in the paper path are represented by x_{P_1} , x_{P_2} , and x_{P_3} , respectively. These locations are initially chosen such that the distance between two pinches is equal to a fixed sheet length L_s . Since the thickness of the sheet is neglected, the sheet can only be in one pinch at the time. Consequently, buckling or tearing of sheets due to a difference in the circumferential velocities of the pinches is not possible. A second consequence of this choice of pinch locations is that the dynamics of different motor-pinch combinations cannot be coupled via the sheet. The sheet position is defined as x_s and is assumed to be known at all time instants. In practice, this can for example be realized by measuring. As optical sensors, like the ones used in optical mouse devices, are cheap nowadays, sheet position measurement using these sensors is becoming a serious option in sheet feedback control design. An alternative would be to use an observer in combination with the optical sheet sensors as present in the paper path shown in Fig. 1.3 [47].

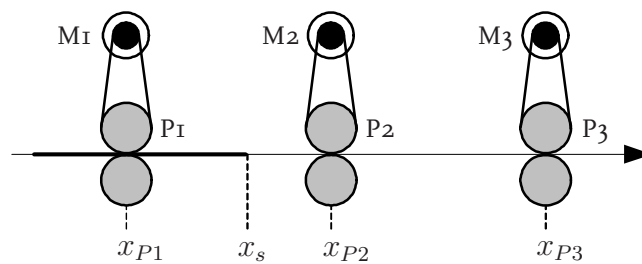


Figure 2.1 / Schematic representation of the basic printer paper path.

2.2 Paper Path and Sheet Flow Modeling

In deriving a model for the sheet flow in the basic printer paper path, we take the physical process as a starting point. Focussing on one single motor-pinch-sheet combination, it can be observed that there is a single source of actuation in this subsystem, i.e. the motor.

This motor is coupled to the driven roller of the pinch via a gear belt and therefore the motion of the driven roller is determined by the motor. The second coupling is present between the driven roller of the pinch and the sheet and therefore the sheet motion is determined by this driven roller. The non-driven roller of the pinch contributes in the transportation of the sheet by applying sufficient normal force to prevent the sheet from slipping in the pinch.

In the approach of modeling the various parts present in the paper path, we start with the description of the motor behavior, since the motor eventually determines the motion of the sheet. Moreover, we take into account the driven roller of the pinch, because of its direct connection to the motor. As can be seen in Fig. 2.2, the central question in the motor modeling process is whether or not to take into account the limited mechanical stiffness of the gear belt that connects motor and driven roller, i.e. if flexibilities in the connection between motor and pinch are present. A positive answer to this question yields a motor model that interacts with a model of the driven roller via a dynamic coupling. More specifically, in this case the motor motion and the motion of the driven roller influence each other via forces that are transmitted by the gear belt. The alternative is to neglect the flexibilities, yielding a kinematic coupling between the motor model and the model of the driven roller.

Given either coupling between the motor and the driven roller, the coupling between this roller and the sheet can be considered. As can be seen in Fig. 2.2, the central question regarding this coupling is whether or not to take into account slip between the roller and the sheet. If no slip is assumed to be present, a kinematic coupling between the sheet and the driven roller can be used to describe the sheet motion, given the motion of the driven roller. Otherwise, nonlinear stick-slip modeling is necessary to describe the sheet motion, resulting in a dynamic coupling between the sheet on the one hand and the driven roller on the other hand.

With the Boder research goal in mind, we are interested in using a high level of abstraction in the modeling procedure [32], resulting in low-detailed models for controller design, that can still give a good prediction of the system behavior. Realizing this high level of abstraction is supported by the physics of the system at hand. More specifically, in printers a high stiffness of the gear belt connecting the motor and driven roller is enforced to accurately drive this roller via the controlled motor for realizing the desired sheet motion. This high stiffness causes flexibilities to show up only at high frequencies. Therefore these flexibilities are not taken into account in the model, resulting in a kinematic coupling between the motor and the driven roller, as indicated by the gray block in Fig. 2.2. The answer to the question whether or not to take into account slip in the modeling approach can be derived from the basic paper path case-study. Since in this case-study the sheet is driven by a single motor-pinch combination at all time instants, no

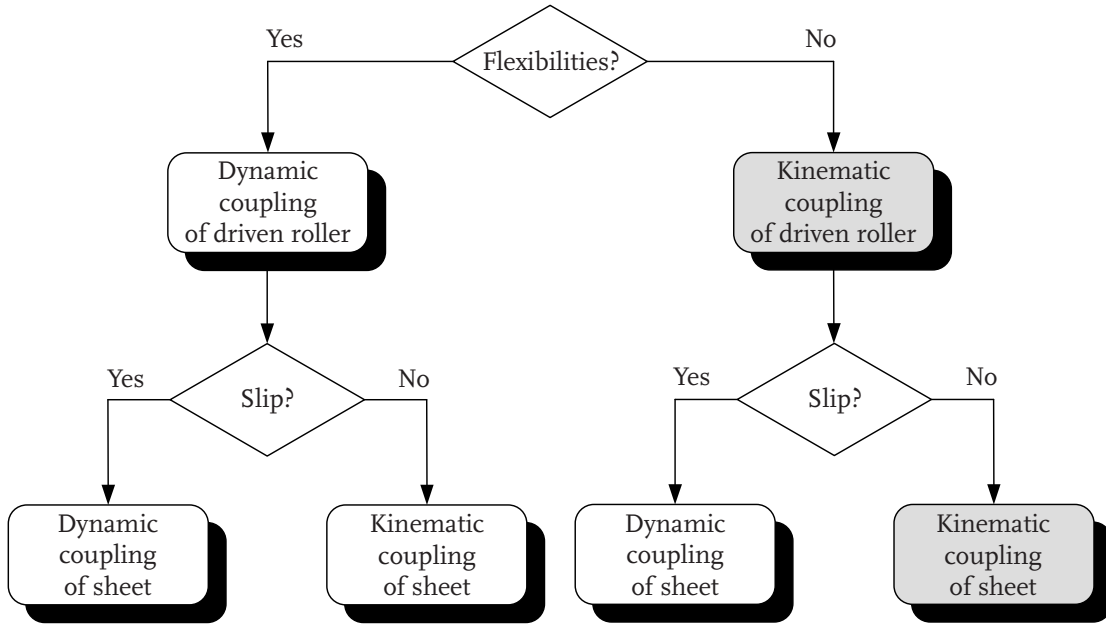


Figure 2.2 / Overview on paper path and sheet flow modeling possibilities.

other forces than the one resulting from the driven roller are acting on the sheet. Hence, assuming the non-driven roller supplies sufficient normal force, it is reasonable not to take into account slip in the model. This results in a kinematic coupling between the driven roller and the sheet, which is also indicated by the gray block in Fig. 2.2. The comparison of the experimental results and the simulation results, presented in Chapter 6, will approve the modeling choices made in this section.

Given the design choices taken in the modeling approach, the actual models can be derived. Since the flexibility of the gear belt is neglected, the motor dynamics are modeled as a single inertia, with the torque $T_{\phi,i}$ as input and the motor velocity ω_{Mi} as output of motor Mi :¹

$$\dot{\omega}_{Mi} = \frac{1}{J_{Mi}} T_{\phi,i}, \quad i \in \mathcal{I}. \quad (2.1)$$

In (2.1), $\mathcal{I} = \{1, 2, 3\}$ represents the index set of motor-pinch combinations, whereas J_{Mi} represents the inertia of motor Mi . Because of the assumptions made in the modeling process, the inertia of the rollers and the mass of the sheet can be taken into account in J_{Mi} as well.

In the derivation of this sheet flow model for the basic paper path case-study, we take into account the fact that at each time instant the sheet is only driven by one motor-pinch combination. Hence, only one of the motor velocities acts as an input for the sheet

¹By considering velocities as output of the motor model instead of positions, initial conditions concerning the motor positions do not have to be taken into account in the sheet flow model.

motion. As the sheet moves through the paper path, this input will change when the sheet arrives at the next pinch. This switching behavior can be easily captured in the PWL modeling formalism [72]. In the resulting sheet flow model, the mass of the sheet is not taken into account, as the effect of this mass is negligible with respect to the effect of the inertia of the motor-pinch combinations. Since flexibilities of the gear belts and slip between the sheet and the pinches are also not taken into account, the sheet velocity can be derived from the motor velocities via straightforward holonomic kinematic constraint relations that describe the relation between motor velocity and pinch velocity, and pinch velocity and sheet velocity, respectively. The sheet position is obtained by integrating the sheet velocity. The nominal high level sheet model, i.e. the sheet model without parameter uncertainties and disturbances, therefore consists of a switching integrator that can be represented as

$$\dot{x}_s = B_i \underline{u} \quad \text{for } x_s \in \mathcal{X}_i, i \in \mathcal{I}, \quad (2.2)$$

with the input matrices B_i defined as $B_1 = [n_1 r_{P1} \ 0 \ 0]$, $B_2 = [0 \ n_2 r_{P2} \ 0]$, and $B_3 = [0 \ 0 \ n_3 r_{P3}]$, respectively. In these definitions, n_i represents the transmission ratio between motor M_i and pinch P_i and r_{P_i} represents the radius of the driven roller of pinch i . Furthermore, \underline{u} is the column with inputs of the high level sheet dynamics: $\underline{u} = [\omega_{M1} \ \omega_{M2} \ \omega_{M3}]^T$. The partitioning of the state space into the three regions is represented by $\{\mathcal{X}_i\}_{i \in \mathcal{I}} \subseteq \mathbb{R}$. Here, $\mathcal{X}_1 = \{x_s | x_s \in [x_{P1}, x_{P2})\}$, $\mathcal{X}_2 = \{x_s | x_s \in [x_{P2}, x_{P3})\}$, and $\mathcal{X}_3 = \{x_s | x_s \in [x_{P3}, x_{P3} + L_s)\}$, since $x_{P2} - x_{P1} = L_s$ and $x_{P3} - x_{P2} = L_s$.

2.3 Decomposition of the Sheet Handling Control Problem

To create an inventory of the possibilities for designing the layout of the control architecture of the sheet handling system, we consider the possibilities of measuring the motor position, the position of the driven roller, and the sheet position, together with the detection of the sheet edges. These four types of measurements are schematically depicted in Fig. 2.3. When the paper path is not subject to disturbances and uncertainties, sheet control can be carried out using motor position information or position information of the driven roller, possibly in combination with the information obtained from the edge detection sensors. Based on the measured information, the sheet position can be derived via the straightforward holonomic kinematic constraint relations used in (2.2). However, when disturbances and uncertainties that affect the motion of the sheet are present in the paper path, the kinematic constraints do not provide an accurate sheet position estimation anymore. Hence, in this case accurate sheet control is difficult to realize. To achieve the desired sheet tracking behavior under the influence of disturbances and uncertainties, the measurement of the sheet position information is required. Therefore,

we consider the following three options of using position information for controlling the sheet flow:

1. sheet control based on the measurement of the sheet position information only,
2. sheet control based on the measurement of both the motor position and the sheet position,
3. and sheet control based on the measurement of both the position of the driven roller and the sheet position.

When option 1 is chosen for implementation, a control problem can be obtained in which the goal is to find a single controller for the combination of the motor, the driven roller, and the sheet. In contrast with this option, options 2 and 3 allow us to split up the sheet handling control problem into two levels, as done in [12, 46]. At the low level, model-based collocated (option 2) or non-collocated (option 3) motor control design is considered, whereas on the high level the focus is on model-based control of the sheet flow. This subdivision is possible since both the sheet position and the position of the motor or the driven roller are available and because of the no-slip condition between the pinch and the sheet. Breaking up the control problem into two parts seems natural for the system at hand and replaces the overall design question by two separate, less complex, control questions. Hence, options 2 and 3 are preferred over option 1. Since in a non-collocated control architecture high bandwidths are more difficult to realize than in collocated control architectures, collocated motor control is preferred. Moreover, considering the application of sheet feedback control in real printer paper paths, in which pinches are often coupled into sections that are driven by a single motor, option 2 is also preferred over option 3. This results from a technical point of view on the one hand, i.e. switching between position information would be needed in option 3 as the sheet is transported through the section, and from an economical point of view on the other hand, i.e. less encoders are needed in option 2, resulting in a less expensive printer. Hence, in this thesis option 2 is chosen as a basis for controlling the sheet flow.

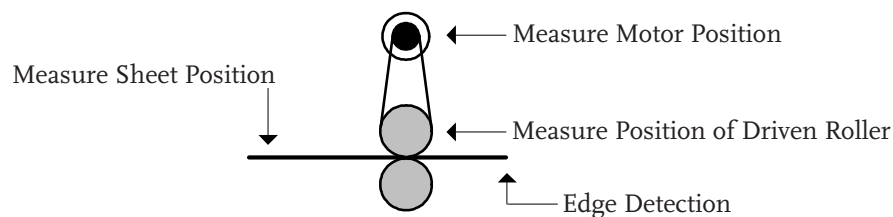


Figure 2.3 / Four possibilities for measuring: the motor position, the position of the driven roller, the sheet position, and the detection of the edge of the sheet.

The low level motor control loops are used to tackle disturbances and uncertainties at the motor level, e.g. cogging and friction in the bearings. In many cases, the controlled motor dynamics can be very well described by a linear model. Hence, each motor control loop in the paper path can be designed on the basis of well-known linear single-input single-output motion control techniques [25]. The closed-loop linear motor dynamics in the Laplace domain can be represented by

$$\Omega_{Mi}(s) = T_i(s)\Omega_{Mi,r}(s), i \in \mathcal{I}, \quad (2.3)$$

when assuming zero initial conditions. In (2.3), $T_i(s)$ represents the complementary sensitivity function of controlled motor Mi , which maps the input of the low level closed-loop system, i.e. the motor reference velocity $\omega_{Mi,r}$, with $\omega_{Mi,r}$ the inverse Laplace transform of $\Omega_{Mi,r}(s)$, $s \in \mathbb{C}$, to its output, i.e. the actual motor velocity ω_{Mi} , with Laplace transform $\Omega_{Mi}(s)$.

By introducing feedback of the sheet position information, robustness can be obtained for disturbances and uncertainties at the sheet level. One can think of, for example, varying sheet characteristics related to geometry or roughness, tolerances on pinch radii and transmission ratios, or slip between the sheet and pinches. By splitting up the control problem into two levels, an hierarchical control structure is obtained in which the inner loops (the low level motor control loops) are closed within the outer loop (the high level sheet control loop). In the design of both control loops, the goal is to make the inner loop much faster than the outer loop [69]. In this way, disturbances and uncertainties at the motor level are attenuated quickly such that they do not affect the sheet control loop [34, 50]. To realize this goal, the motor control loops are designed to have a higher bandwidth than the sheet control loop. In this design, rules of thumb regarding the ratio between the bandwidths of the different control loops are used, as this ratio is generally not strictly quantified [69, 75]. Furthermore, a good tracking behavior in the low level motor control loops is enforced. As a result, a stable overall system is obtained in which the inner loops will closely track the reference profiles generated by the outer loop [8]. This is schematically depicted in Fig. 2.4, which shows the control architecture of the basic printer paper path. In this figure we can recognize the three low level closed-loop systems, representing the three motor control loops. The goal of each LLT² is to have the actual motor velocity ω_M , i.e. the LLT's output, track the motor reference velocity $\omega_{M,r}$, i.e. the LLT's input, as close as possible. According to the nominal high level sheet model (2.2), the actual motor velocities determine the sheet motion and are therefore the inputs of the high level plant (HLP), i.e. the high level sheet dynamics. The output of these dynamics is the actual sheet position x_s , which is fed back and compared with the sheet reference position $x_{s,r}$, yielding the sheet tracking error e_s . Based on this tracking

²In this thesis, a low level closed-loop system is denoted by LLT, with T the symbol representing the closed-loop transfer function.

error, the High Level sheet Controllers (HLCs) calculate the motor reference velocities to be tracked by the LLTs. From Fig. 2.4 it can be seen that the sheet tracking error is chosen to be the input of all three high level sheet controllers at all times. Consequently, once the sheet has entered the first pinch, motors M2 and M3, and therefore pinches P2 and P3, will already have a nonzero velocity when the sheet enters these pinches. As a result, large transient responses when entering the pinches P2 and P3 will be avoided.

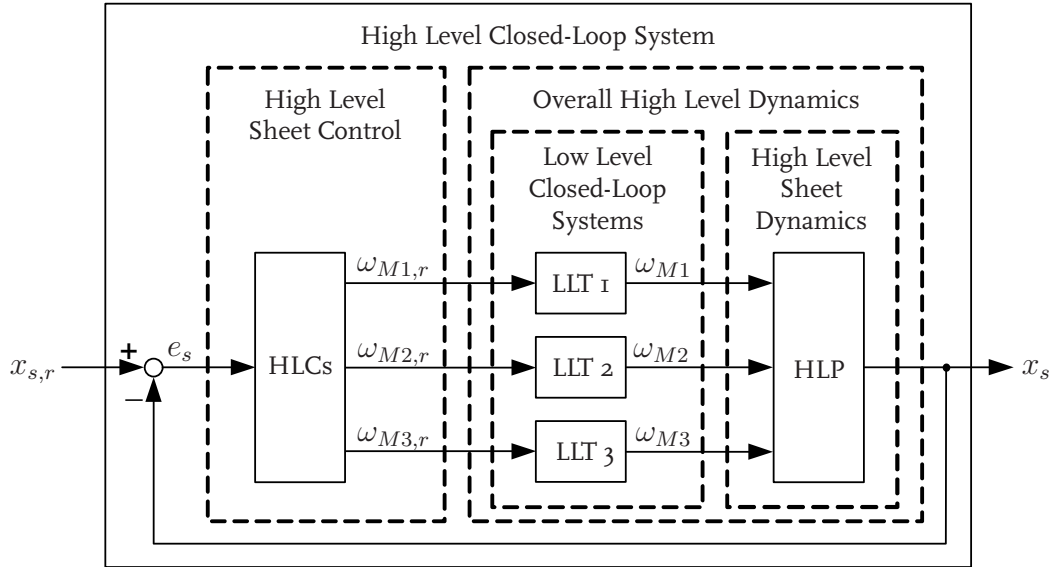


Figure 2.4 / Block diagram of the overall control scheme.

Based on the decomposition of the sheet feedback control design problem into a high level sheet control loop and low level motor control loops, an additional reduction of the complexity of the control problem can be realized by assuming perfect tracking behavior of the controlled motors, i.e. $T_i(s) = 1, \forall s \in \mathbb{C}, \forall i \in \mathcal{I}$ in (2.3). More specifically, in the sheet feedback control design approach we do not take into account any motor modeling and control design for the LLTs. This is shown in Fig. 2.5, which represents an updated block diagram of the control system at hand. The result of the assumption on ideal low level motor behavior is that the inputs of the high level sheet dynamics, stacked in the column \underline{u} , will be directly calculated by the high level sheet controllers. In practical situations, the assumption on perfect tracking behavior of the controlled motors cannot be realized. This is not a problem as long as the low level bandwidth is sufficiently higher than the bandwidth of the high level control loop and when the tracking error in the low level motor control loops is sufficiently small. Similar to the choices made in the modeling process, the assumption on perfect tracking behavior of the controlled motors will be approved by the experimental results, presented in Chapter 6.

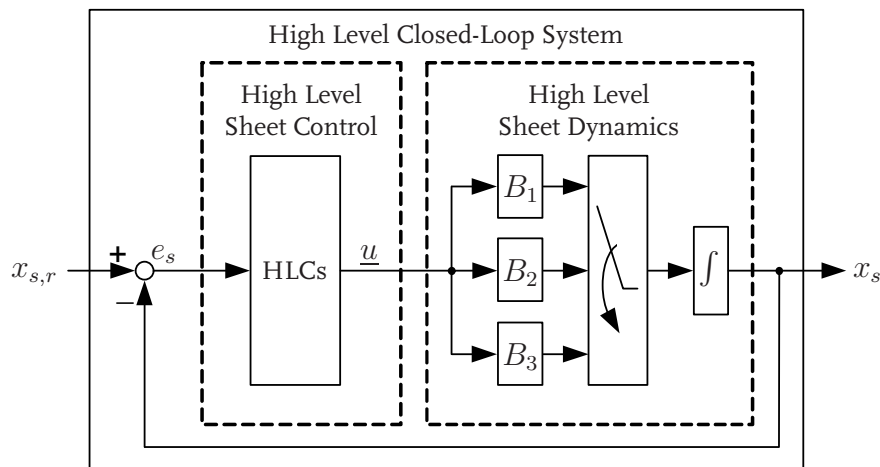


Figure 2.5 / Updated block diagram of the sheet feedback control scheme.

Given the sheet feedback control architecture of Fig. 2.5, the control goal we adopt for the basic paper path case-study is the systematic synthesis of robust sheet feedback controllers that yield a stable high level closed-loop system that is capable of accurately tracking the sheet reference profile, i.e. satisfying the performance properties presented in Section 1.4. As can be seen from Fig. 2.5, this controller synthesis is facilitated by the fact that the overall sheet handling control problem has been reduced to a control synthesis problem for a PWL system that, due to simplifying assumptions in the modeling approach, contains simple dynamics in each region. The choice of the sheet reference motion profile for each sheet in the paper path is based on the type of sheet control. Possible choices are Absolute Reference Tracking Control (ARTC) and Inter Sheet Spacing Control (ISSC). In the former option each sheet has to track a prespecified reference profile that is directly generated by the sheet flow scheduler [3], whereas in case of ISSC sheets have to track their downstream neighbor at a prespecified constant distance [12, 14, 46]. In this thesis, ARTC has been chosen given the current paper path layout of many printers. More specifically, since many paper paths are often equipped with a registration unit in which sheets are stopped for position corrections in the lateral and skewness directions, ARTC is more suitable for this type of paper paths than ISSC.

At this point one could pose the question why to use a PWL model as the basis for sheet feedback control design. More specifically, in the basic paper path at hand there will be no coupling between the various motor-pinch combinations due to the assumption on the distance between the pinches being equal to the sheet length. Hence, sheet feedback controllers can also be designed based on local models of the sheet flow in each separate motor-pinch combination. The reason for choosing the PWL sheet flow model as a basis for sheet feedback control design is the fact that the intrinsic switching character of the system under consideration is taken into account in the control design. Hence, the stability of the closed-loop dynamics can be guaranteed for arbitrary switching and

performance and robustness guarantees can be given for the overall system, i.e. the sheet motion in the complete paper path, which can in general not be done using individual designs only. Moreover, a generic framework is obtained, which can be used for extended problem formulations. Given this motivation, two approaches for controller synthesis based on the PWL model of the sheet flow will be presented in Chapters 3 and 4.

CHAPTER THREE

State Feedback Control Design

3.1	The Tracking Control Problem	23
3.2	Nominal Sheet Feedback Control Design	26
3.3	Analysis of the Perturbation of Paper Path Parameters	41
3.4	Evaluation	51

3.1 The Tracking Control Problem

This chapter presents the first approach for sheet feedback control design for the basic paper path case-study presented in Section 2.1. The goal is to synthesize sheet feedback controllers that make the sheets in the paper path track a reference trajectory that is known a priori, satisfying the performance properties presented in Section 1.4. To meet these specifications in practical situations, the use of a motion feedforward controller can be beneficial. However, the focus in this thesis will be on control design for robustness, and therefore we will concentrate on feedback design only. Initially, we will concentrate on control design based on the nominal high level sheet model (2.2). Based on this model, two synthesis approaches will be presented with which controllers can be designed that meet the desired performance properties. Given these controllers, the effect of perturbations of the system parameters will be analyzed. Therefore, the nominal sheet flow model will be extended such that it includes parametric uncertainties present in the paper path. Based on the resulting model, an analysis technique will be presented that enables the prediction of the increase in sheet position and velocity errors originating from the parameter perturbations.

Control design and analysis of PWL systems has been given much attention in literature lately, see for example [19] for an overview. In [44], piecewise quadratic Lyapunov functions were proposed for the analysis of PWL systems. In [57], the use of piecewise quadratic cost functions is extended from stability analysis to performance analysis and optimal control. In [35], analysis and controller synthesis of PWL systems is considered, based on constructing (piecewise) quadratic Lyapunov functions that prove stability and performance of the system. It is shown that proving stability and performance, as well as designing controllers, can be expressed as convex optimization problems involving LMIs. The work is extended in [59] to obtain an iterative method that can be used to design state and output feedback controllers with various constraints on the continuity and smoothness of the Lyapunov Function and control signals. In [23], an H_∞ controller synthesis method for PWL systems based on a piecewise smooth Lyapunov function is presented. A stabilizing controller is synthesized that results in disturbance attenuation up to a prescribed level. This work is extended in [11, 22] to be able to deal with uncertain PWL systems. A regulation control problem is considered for which a control design approach is presented for the stabilization with H_∞ performance of the closed-loop system. An alternative H_∞ control design approach for uncertain PWL systems, that can be used for solving tracking control problems, will be the subject of Chapter 4.

A common property of the work presented in [35, 44, 57, 59] is the focus on the stabilization of the system dynamics, i.e. regulation problems are considered, whereas tracking control problems are given less attention, as recognized in [60, 71]. In our case, however, the goal is to have the sheets in the paper path track a reference trajectory that is known a priori. Hence, we are dealing with a tracking problem and we will therefore formulate the system in terms of its error dynamics. By working in the tracking error domain, as is common for the linear case [25], stabilization of the error dynamics is directly linked to tracking performance. Note that if a fast decay of transient error responses is desired, one has to ensure that the equilibrium in error space is reached quickly. Hence, given a system formulation in terms of the error dynamics, the control goal becomes to find a feedback controller that results in regulation of the error dynamics, in such a way that all error states go to zero with a prescribed convergence rate. This automatically implies that the actual sheet position will become equal to the desired one and, hence, the desired tracking performance can be obtained [8, 10]. Hence, the basic idea of [35, 44, 57, 59], i.e. controller synthesis and stability analysis using a common or piecewise quadratic Lyapunov function, will be applied in this chapter. However, as we will see, formulation of the PWL sheet flow model in terms of its error dynamics will lead to a distinguishing feature, i.e. the introduction of jumps in the state variables.

For the derivation of the error dynamics of the nominal high level PWL sheet model (2.2), we use the error-space approach of [25] and extend it to the PWL case. As far as the sheet reference profile is concerned, needed in the derivation of the error dynam-

ics, in real printer paper paths piecewise linear velocity profiles are commonly used. In this case, however, we will consider a first order sheet reference profile for simplicity to focus on the essence of the resulting control problem. Hence, the second time derivative of the sheet reference position, i.e. the sheet reference acceleration, is taken zero in the derivation of the sheet error dynamics:

$$\ddot{x}_{s,r} = 0. \quad (3.1)$$

The sheet tracking error is defined as the difference between the sheet reference position and the actual sheet position:

$$e_s = x_{s,r} - x_s. \quad (3.2)$$

Substitution of the nominal high level sheet model (2.2) in the time derivative of (3.2) yields

$$\begin{aligned} \dot{e}_s &= \dot{x}_{s,r} - \dot{x}_s \\ &= \dot{x}_{s,r} - B_i \underline{u} \quad \text{for } x_{s,r} - e_s \in \mathcal{X}_i, i \in \mathcal{I}. \end{aligned} \quad (3.3)$$

Due to the switching character of the system, the right hand side of (3.3) can be discontinuous. Therefore the model of the sheet error dynamics will consist of two parts: the flow conditions that hold for the error dynamics of the various subsystems and the jump conditions that describe the relation of both e_s and \dot{e}_s just before and just after the switching moment.

For the derivation of the flow conditions, we differentiate (3.3) one more time, since then explicit dependencies on $x_{s,r}$ and its time derivatives vanish, yielding

$$\ddot{e}_s = -B_i \dot{\underline{u}} \quad \text{for } x_{s,r} - e_s \in \mathcal{X}_i, i \in \mathcal{I}. \quad (3.4)$$

Next, the time derivative of the control input \underline{u} is replaced by the control input in error-space [25], which is defined as

$$\underline{\mu} = \dot{\underline{u}}. \quad (3.5)$$

When we define the state vector of the error dynamics as

$$\underline{q} = [e_s \quad \dot{e}_s]^T, \quad (3.6)$$

we can write the flow conditions in error space in standard state-variable form:

$$\dot{\underline{q}} = F \underline{q} + G_i \underline{\mu} \quad \text{for } (x_{s,r} - [1 \quad 0] \underline{q}) \in \mathcal{X}_i, i \in \mathcal{I}. \quad (3.7)$$

In this notation, the system matrix is defined as $F = \begin{bmatrix} 0 & 1 \\ 0 & 0 \end{bmatrix}$, whereas the input matrix is defined as $G_i = [\underline{0} \quad -B_i^T]^T$.

Regarding the jump conditions, the physical interpretation of the system at hand shows that switching from regime k to regime $k + 1$ and vice versa is possible, with

$k \in \mathcal{K}$, $\mathcal{K} = \{1, 2\}$.¹ When we consider the transition from regime k to regime $k + 1$, the following relation holds for the sheet tracking error at the switching boundary:

$$e_s^+(t_s) = e_s^-(t_s), \quad (3.8)$$

with $e_s^+(t_s) := \lim_{t \downarrow t_s} e_s(t)$ and $e_s^-(t_s) := \lim_{t \uparrow t_s} e_s(t)$, and with t_s the switching time. From (3.8) it can be seen that e_s is continuous at the switching boundary, which is supported by the physics of the system, as the sheet cannot make instantaneous jumps. The jump conditions for \dot{e}_s are derived from (3.3). For $\dot{e}_s^+(t_s)$, the following relation holds:

$$\dot{e}_s^+(t_s) = \dot{x}_{s,r}(t_s) - B_{k+1}\underline{u}(t_s), k \in \mathcal{K}, \quad (3.9)$$

whereas for $\dot{e}_s^-(t_s)$ it holds that

$$\dot{e}_s^-(t_s) = \dot{x}_{s,r}(t_s) - B_k\underline{u}(t_s), k \in \mathcal{K}. \quad (3.10)$$

Subtraction of (3.10) from (3.9) yields the desired jump condition for \dot{e}_s :

$$\dot{e}_s^+(t_s) = \dot{e}_s^-(t_s) + (B_k - B_{k+1})\underline{u}(t_s), k \in \mathcal{K}. \quad (3.11)$$

Given (3.8) and (3.11), the jump conditions can be represented as

$$\underline{q}^+(t_s) = \begin{bmatrix} 1 & 0 \\ 0 & 1 \end{bmatrix} \underline{q}^-(t_s) + \begin{bmatrix} \underline{0}^T \\ B_k - B_{k+1} \end{bmatrix} \underline{u}(t_s), k \in \mathcal{K}, \quad (3.12)$$

with $\underline{q}^-(t_s) := [e_s^-(t_s) \quad \dot{e}_s^-(t_s)]^T$ and $\underline{q}^+(t_s) := [e_s^+(t_s) \quad \dot{e}_s^+(t_s)]^T$.² Hence, the complete model of the open-loop sheet dynamics in error space is given by the flow conditions (3.7) and the jump conditions (3.12).

3.2 Nominal Sheet Feedback Control Design

3.2.1 Controller Synthesis

For controlling the piecewise linear flow dynamics in error space (3.7) in combination with the jump conditions (3.12), we propose a control law that is based on state feedback of the error dynamics:

$$\underline{\mu} = -K\underline{q}, \quad (3.13)$$

¹For clarity, note that in this chapter the index k is used to indicate the regimes between which a transition is made, whereas the index i is used to indicate the regimes in all other cases.

²Note that these particular jump conditions result from the assumptions made in the modeling process. If, for example, the mass would have been taken into account, slightly different jump conditions would have been obtained, as otherwise infinitely large forces would be needed to realize the jump in \dot{e}_s , which is not realistic.

with K the matrix with state feedback gains to be calculated. From (3.13), it can be seen that the controller calculates the three control inputs of the high level sheet dynamics, i.e. the three motor reference velocities, independent of the location of the sheet in the paper path, i.e. no regional information is used in the definition of the control law. Hence, the controller itself is not switching and the structure of the input matrices of the sheet flow dynamics makes sure that the correct control input influences the sheet motion. Substitution of (3.13) into (3.7) yields the closed-loop flow dynamics in error space:

$$\dot{\underline{q}} = (F - G_i K) \underline{q} \quad \text{for } (x_{s,r} - [1 \ 0] \underline{q}) \in \mathcal{X}_i, i \in \mathcal{I}. \quad (3.14)$$

For the derivation of the closed-loop jump conditions, first \underline{u} is derived by substitution of (3.13) into (3.5) and integration of the resulting equation. Hence, for each i -th element of \underline{u} , u_i , the following relation holds:

$$u_i(t) = -K(i, 1) \int_{t_0}^t e_s(\tau) d\tau - K(i, 2) e_s(t), i \in \mathcal{I}, \quad (3.15)$$

with t_0 the initial time, $u_i(t_0) = 0$, and $K(i, j)$ the j -th element of the i -th row of K , $j \in \{1, 2\}$. As can be seen from (3.15), the control law for each region consists of a proportional-integral (PI) controller.

The second step in deriving the closed-loop jump conditions is substitution of (3.15) into (3.11), yielding the closed-loop jump condition for \dot{e}_s when considering the transition from regime k to regime $k + 1$:

$$\begin{aligned} \dot{e}_s^+(t_s) &= \dot{e}_s^-(t_s) - B_k(k) \left(K(k, 1) \int_{t_0}^{t_s} e_s(\tau) d\tau + K(k, 2) e_s(t_s) \right) + \\ &+ B_{k+1}(k+1) \left(K(k+1, 1) \int_{t_0}^{t_s} e_s(\tau) d\tau + K(k+1, 2) e_s(t_s) \right), k \in \mathcal{K}. \end{aligned} \quad (3.16)$$

In (3.16), $B_k(k)$ represents the k -th element of B_k , i.e. its only nonzero element. Given (3.8) and (3.16), the closed-loop jump conditions can be represented as

$$\begin{aligned} \underline{q}^+(t_s) &= \begin{bmatrix} 1 & 0 \\ B_{k+1}(k+1)K(k+1, 2) - B_k(k)K(k, 2) & 1 \end{bmatrix} \underline{q}^-(t_s) + \\ &+ \begin{bmatrix} 0 \\ B_{k+1}(k+1)K(k+1, 1) - B_k(k)K(k, 1) \end{bmatrix} \int_{t_0}^{t_s} e_s(\tau) d\tau \\ &= R_{k,k+1} \underline{q}^-(t_s) + \begin{bmatrix} 0 \\ B_{k+1}(k+1)K(k+1, 1) - B_k(k)K(k, 1) \end{bmatrix} \int_{t_0}^{t_s} e_s(\tau) d\tau, \end{aligned} \quad \begin{matrix} k \in \mathcal{K}. \\ (3.17) \end{matrix}$$

From (3.17), it can be seen that if it is desired not to have jumps in \dot{e}_s at the switching boundaries, the controller gains should be chosen such that both $B_{k+1}(k+1)K(k+1, 2) = B_k(k)K(k, 2)$ and $B_{k+1}(k+1)K(k+1, 1) = B_k(k)K(k, 1)$. When the resulting

controller is applied to the nominal high level sheet model (2.2), it can be seen that a linear closed-loop system is obtained, from which we can conclude that the controller linearizes the sheet dynamics. Furthermore, from (3.14) it can be seen that in this case $\underline{q} = \underline{0}$ is an equilibrium point of the closed-loop system. As $\underline{q} = \underline{0}$ implies $e_s = 0$ and $\dot{e}_s = 0$, this is the equilibrium point we are interested in. However, to ensure that $\underline{q} = \underline{0}$ is an equilibrium point, it is not necessary to enforce both $B_{k+1}(k+1)K(k+1, 2) = B_k(k)K(k, 2)$ and $B_{k+1}(k+1)K(k+1, 1) = B_k(k)K(k, 1)$. More specifically, the only necessary condition for $\underline{q} = \underline{0}$ to be an equilibrium point is that the second term of (3.17) is equal to $\underline{0}$, as can be seen from (3.14) and (3.17). Clearly, a sufficient condition for this to realize is $B_{k+1}(k+1)K(k+1, 1) = B_k(k)K(k, 1)$ via the choice of $K(k, 1)$ and $K(k+1, 1)$. If the integral term in (3.17) is nonzero, which is to be expected in practical cases, the above mentioned condition is also a necessary one. In other words, the feedback controllers (3.15) have to be at least partially linearizing to enforce the origin to be a globally asymptotically stable equilibrium in the sense of Lyapunov. In summary, two types of controllers are considered:

- *Fully linearizing controllers.* To obtain this type of controllers, the gains should be chosen such that both $B_{k+1}(k+1)K(k+1, 2) = B_k(k)K(k, 2)$ and $B_{k+1}(k+1)K(k+1, 1) = B_k(k)K(k, 1)$. Given this type of controllers, $\underline{q} = \underline{0}$ is an equilibrium point of the closed-loop system and jumps in the error states will not occur.
- *Partially linearizing controllers.* To obtain this type of controllers, the gains should be chosen such that $B_{k+1}(k+1)K(k+1, 1) = B_k(k)K(k, 1)$. Given this type of controllers, $\underline{q} = \underline{0}$ is an equilibrium point of the closed-loop system and jumps in \dot{e}_s will not be eliminated.

Regarding the partially linearizing controllers, more freedom in the choice of the controller parameters is obtained. As a result, the behavior of the system could be improved or additional characteristics could be introduced. One could think of, for example, improvement of the performance index containing the control input, as in LQR control problems [25, 69], or the possibility to design for different control bandwidths in the various subsystems.

Given a partially linearizing feedback controller, the expression for the closed-loop jump conditions becomes:

$$\underline{q}^+ = R_{k,k+1}\underline{q}^-, k \in \mathcal{K}. \quad (3.18)$$

In analogy with the derivation of (3.18), the closed-loop jump conditions can also be derived when the transition from regime $k+1$ to regime k is considered, i.e. when the system switches back to the previous regime. This could occur, for example, in a registration unit of a real printer paper path, or after a change in direction of motion of the

sheet when leaving the duplex loop. In this case, the expression for the closed-loop jump conditions becomes:

$$\begin{aligned} \underline{q}^+ &= \begin{bmatrix} 1 & 0 \\ B_k(k)K(k, 2) - B_{k+1}(k+1)K(k+1, 2) & 1 \end{bmatrix} \underline{q}^- \\ &= R_{k+1,k} \underline{q}^-, k \in \mathcal{K}. \end{aligned} \quad (3.19)$$

From (3.17) and (3.19) it can be observed that switching forward and backward has the same influence on the magnitude of a jump, whereas the sign of the jump differs. Hence, $R_{k,k+1}$ and $R_{k+1,k}$ are related via

$$R_{k,k+1} = R_{k+1,k}^{-1}, k \in \mathcal{K}. \quad (3.20)$$

Focussing again on the transition from region k to region $k+1$, the stability analysis of the closed-loop error dynamics (3.14), (3.18) encompasses two parts: the stability analysis of the flow dynamics in each regime and the stability analysis at the switching boundary connecting two regimes. By making use of the work presented in [6, 19], it can be analyzed whether the closed-loop flow dynamics in error space in (3.14) are Globally Exponentially Stable (GES). By considering exponential stability, the rate of convergence of the tracking error to zero can be adjusted such that the performance properties presented in Section 1.4 are satisfied. For the stability analysis, a piecewise quadratic Lyapunov function candidate is proposed:

$$V_i(\underline{q}) = \underline{q}^T P_i \underline{q}, i \in \mathcal{I}, \quad (3.21)$$

with

$$P_i = P_i^T \succ 0, i \in \mathcal{I}. \quad (3.22)$$

To prove that the flow dynamics are GES, the following set of matrix inequalities in P_i and K must hold:

$$\begin{aligned} 0 &\succ \dot{V}_i(\underline{q}) + \alpha V_i(\underline{q}) = \\ &= (F - G_i K)^T P_i + P_i (F - G_i K) + \alpha P_i, i \in \mathcal{I}, \end{aligned} \quad (3.23)$$

with $\alpha > 0$ representing the decay rate of the Lyapunov function. This parameter is chosen a priori in relation to the transient behavior of the error dynamics, and therefore in relation to the desired tracking performance. A large value of α results in a fast convergence of the error to zero. However, it is possible that beyond some value of α , no feasible solution of (3.23) can be obtained anymore. From (3.23), it becomes clear that both the stability analysis of the flow dynamics and the calculation of the controller gains K can be carried out by solving a single set of matrix inequalities. In other words, the free parameters to be solved, i.e. the Lyapunov matrices P_i and the matrix with controller gains K , depend on each other.

This dependency is also present in the stability analysis at the switching boundary connecting two regimes. To characterize the dependency, we consider both the transition from regime k to regime $k + 1$ and vice versa. In both transitions, no extra energy is allowed to enter the system, i.e. the Lyapunov function active in a new regime must be smaller than or equal to the Lyapunov function active in the previous regime. Keeping this in mind, we start with the transition from regime k to regime $k + 1$, and we require:

$$(\underline{q}^+)^T P_{k+1} \underline{q}^+ \leq (\underline{q}^-)^T P_k \underline{q}^-, k \in \mathcal{K}. \quad (3.24)$$

To show the relation between P_i and the controller parameters, two inequalities describing the relation between P_k , P_{k+1} , $R_{k,k+1}$, and $R_{k+1,k}$ can be derived from (3.24) by making use of the closed-loop jump conditions (3.18). First of all, (3.18) is substituted into (3.24) to obtain a relation between P_k , P_{k+1} , and $R_{k,k+1}$:

$$(\underline{q}^-)^T R_{k,k+1}^T P_{k+1} R_{k,k+1} \underline{q}^- \leq (\underline{q}^-)^T P_k \underline{q}^-, k \in \mathcal{K}. \quad (3.25)$$

In the derivation of the second inequality, first an expression for \underline{q}^- is derived from (3.18) and (3.20):

$$\begin{aligned} \underline{q}^- &= R_{k,k+1}^{-1} \underline{q}^+ \\ &= R_{k+1,k} \underline{q}^+, k \in \mathcal{K}. \end{aligned} \quad (3.26)$$

Substitution of (3.26) into (3.24) yields the desired second inequality, which describes the relation between P_{k+1} , P_k , and $R_{k+1,k}$:

$$(\underline{q}^+)^T P_{k+1} \underline{q}^+ \leq (\underline{q}^+)^T R_{k+1,k}^T P_k R_{k+1,k} \underline{q}^+, k \in \mathcal{K}. \quad (3.27)$$

In finding a relation between P_i and the controller parameters, the second transition we consider is the one from regime $k + 1$ to regime k . In analogy with the derivation of (3.25) and (3.27), two additional relations between P_k , P_{k+1} , $R_{k,k+1}$, and $R_{k+1,k}$ can be obtained:

$$(\underline{q}^-)^T R_{k+1,k}^T P_k R_{k+1,k} \underline{q}^- \leq (\underline{q}^-)^T P_{k+1} \underline{q}^-, k \in \mathcal{K}, \quad (3.28)$$

$$(\underline{q}^+)^T P_k \underline{q}^+ \leq (\underline{q}^+)^T R_{k,k+1}^T P_{k+1} R_{k,k+1} \underline{q}^+, k \in \mathcal{K}. \quad (3.29)$$

From the combination of (3.25) and (3.29), which hold for all \underline{q}^- and \underline{q}^+ , we know that

$$P_k = R_{k,k+1}^T P_{k+1} R_{k,k+1}, k \in \mathcal{K}, \quad (3.30)$$

whereas the combination of (3.27) and (3.28), which also hold for all \underline{q}^- and \underline{q}^+ , results in

$$P_{k+1} = R_{k+1,k}^T P_k R_{k+1,k}, k \in \mathcal{K}. \quad (3.31)$$

Note that (3.30) can be rewritten into (3.31) and vice versa via (3.20).

With the derivation of (3.30) and (3.31) we have obtained the desired relations between P_i and the controller parameters. From these relations, a number of interesting observations can be made. First of all, if the controller structure is chosen such that a linear

closed-loop system is obtained, there will be no jumps in e_s and \dot{e}_s , independent of their values at the switching boundary. Then, from (3.18) and (3.19), we know that for that case $R_{k,k+1} = R_{k+1,k} = I$ has to hold. With this relation it can be observed that $P_k = P_{k+1}$ in (3.30) and (3.31), and hence, a common quadratic Lyapunov function can be used to prove the stability of the closed-loop system under arbitrary switching. This reasoning can also be carried out in the opposite direction. Suppose a common quadratic Lyapunov function is used to prove the stability of the closed-loop system under arbitrary switching. According to (3.30), the following holds for P in that case:

$$\begin{aligned} P &= R_{k,k+1}^T P R_{k,k+1} \\ \underbrace{\begin{bmatrix} p_1 & p_2 \\ p_2 & p_4 \end{bmatrix}}_{>0} &= \begin{bmatrix} 1 & \gamma_{k,k+1} \\ 0 & 1 \end{bmatrix} \begin{bmatrix} p_1 & p_2 \\ p_2 & p_4 \end{bmatrix} \begin{bmatrix} 1 & 0 \\ \gamma_{k,k+1} & 1 \end{bmatrix} \\ &= \begin{bmatrix} p_1 + 2\gamma_{k,k+1}p_2 + \gamma_{k,k+1}^2 p_4 & p_2 + \gamma_{k,k+1}p_4 \\ p_2 + \gamma_{k,k+1}p_4 & p_4 \end{bmatrix}, k \in \mathcal{K}, \end{aligned} \quad (3.32)$$

with $\gamma_{k,k+1} = B_{k+1}(k+1)K(k+1, 2) - B_k(k)K(k, 2)$. Since the symmetric matrix P has to be positive definite, we know from Sylvester's theorem [70] that the following necessary and sufficient conditions have to hold:

$$p_1 + 2\gamma_{k,k+1}p_2 + \gamma_{k,k+1}^2 p_4 > 0, k \in \mathcal{K}, \quad (3.33)$$

$$\det(P) > 0, k \in \mathcal{K}. \quad (3.34)$$

If we now suppose that $\gamma_{k,k+1} \neq 0$, then both p_2 and p_4 have to be equal to zero to fulfill (3.32). However, in that case (3.34) cannot hold anymore. Therefore, $\gamma_{k,k+1}$ has to be equal to 0, which implies that $B_{k+1}(k+1)K(k+1, 2) = B_k(k)K(k, 2)$ and, hence, $R_{k,k+1} = I$. Hence, suppose there exists a partially linearizing controller K for controlling the sheet dynamics in error space under consideration, and there exists a piecewise quadratic Lyapunov function. Then the controller results in a linear closed-loop system if and only if the Lyapunov function is a common one.³

Having derived these observations, the remainder of this section will focus on the synthesis of both linearizing and partially linearizing controllers. Furthermore, the control design and simulation results obtained using the two controllers will be presented.

3.2.1.1 Linearizing Controller Synthesis

When it is desired to use a sheet feedback controller that completely linearizes the system, the jump conditions can be left out of consideration since $\underline{q}^+ = \underline{q}^-$ in (3.18)-(3.19).

³Note that in case of piecewise smooth Lyapunov functions, the equivalent of (3.30) can also be derived, yielding $V_k(\underline{q}) = V_{k+1}(R_{k,k+1}\underline{q})$. Also in this case it holds that if $R_{k,k+1} = I$, a common Lyapunov function will be obtained.

Hence, in that case we only have to consider the flow dynamics in the controller synthesis. From Section 3.2.1 we know that when all transitions from regime k to regime $k + 1$ and vice versa are allowed, a linearizing feedback controller will be obtained if a common quadratic Lyapunov function is adopted for the stability analysis, i.e. $P_i = P$ in (3.22)-(3.23). However, since these matrix inequalities are nonlinear in the unknown matrices P_i and K , a linearizing change of variable variables is applied [6]. More specifically, we pre- and post-multiply (3.22) and (3.23) with P^{-1} and substitute $X = P^{-1}$ and $Y = KP^{-1}$ to obtain the following set of LMIs in the free variables X and Y :

$$0 \prec X = X^T, \quad (3.35)$$

$$0 \succ FX + XF^T - G_i Y - Y^T G_i^T + \alpha X, i \in \mathcal{I}. \quad (3.36)$$

The calculation of the free variables amounts to solving a feasibility problem for which efficient software is available [28]. After solving the LMIs (3.35)-(3.36), the controller gains can be calculated using

$$K = YX^{-1}. \quad (3.37)$$

3.2.1.2 Partially linearizing Controller Synthesis

To exploit the possibilities of using a feedback controller that does not completely linearize the system, with the consequence that more freedom in the choice of the controller parameters is obtained, this section presents an approach for calculating these parameters. For simplicity, we use a rather ad-hoc approach. Further research should be carried out to investigate if the calculation of the controller parameters and the Lyapunov functions can be reformulated in terms of LMIs [6] or Bilinear Matrix Inequalities (BMIs) [41].

For the calculation of the parameters of a feedback controller that does not completely linearize the system, we have to consider both the flow conditions and the jump conditions in the synthesis. Focussing first on subsystem 1, the controller parameters for this subsystem can be calculated by solving (3.22)-(3.23). In analogy with Section 3.2.1.1, (3.35) and (3.36) can be derived with $X = X_1$ and $Y = Y_1$. Via (3.37), the controller parameters for the first subsystem, i.e. $K(1, \bullet)$, can be calculated. For the calculation of the controller parameters for the second subsystem, i.e. $K(2, \bullet)$, the following approach can be used:

- I. To ensure that $\underline{q} = \underline{0}$ is an equilibrium of our system, the equality $B_2(2)K(2, 1) = B_1(1)K(1, 1)$ has to be enforced, as recognized in Section 3.2.1. Hence, $K(2, 1)$ can be calculated according to

$$K(2, 1) = s_2 K(1, 1), \quad (3.38)$$

with $s_2 := \frac{B_1(1)}{B_2(2)}$ the scaling factor for the second subsystem.

2. Given $K(2, 1)$, $K(2, 2)$ remains the only unknown controller parameter for the second subsystem, as the Lyapunov matrix P_2 can be expressed as a function of this parameter via (3.31). Given this matrix, both (3.22) and (3.23) are evaluated for $i = 2$, given a range of values of $K(2, 2)$. This range can, for example, be chosen in the neighborhood of the value for $K(2, 2)$ that linearizes the system built up from the first and second subsystem, i.e. $K(2, 2) = s_2 K(1, 2)$.
3. From the values of $K(2, 2)$ for which (3.22) and (3.23) are satisfied, one can be chosen that does not linearize the system, i.e. for which $K(2, 2) = s_2 K(1, 2)$ does not hold. The actual choice of $K(2, 2)$ depends on the requirements, e.g. the minimization of a performance index containing the control input or the enforcement of different control bandwidths in the various subsystems. With the choice of $K(2, 2)$, the partially linearizing controller for the second subsystem has been found.

The calculation of the controller parameters for the third subsystem can be carried out in analogy with steps 1-3 described above.

3.2.2 Control Design Results

Given the approaches for synthesizing both fully and partially linearizing feedback controllers, the controller parameters can be calculated. In both approaches, α can be used to influence the gains of the controller. Choosing a large value for α will result in a fast convergence of the tracking error towards zero, resulting in large controller gains. Such high gains could lead to high demands on actuators in the low level control loop or to a large amplification of measurement noise in practical situations. Moreover, implementing the resulting controller in practical cases might lead to instability of the system when the bandwidth⁴ in one of the regimes of the high level closed-loop system is close to or larger than the bandwidth of the corresponding low level control loop. Therefore, to obtain a bandwidth that is significantly lower than the typical bandwidth of the low level motor control loop, which is in the range of 50 Hz, and to satisfy the rule of thumb regarding the ratio between the bandwidths of the different control loops in hierarchical control systems, mentioned in Section 2.3, the value of α will be determined via an iterative process that is schematically depicted in Fig. 3.1. An initial value of α is chosen and the controller synthesis described in Section 3.2.1.1 or 3.2.1.2 is carried out. If the obtained high level bandwidth in each regime, obtained by inspection of the Bode plots of the loop gains, is either too low or too high, the value of α will be decreased or increased, respectively. After carrying out the synthesis again and calculating new controller gains, the high level

⁴In this thesis, the bandwidth of a system is defined as the crossover frequency.

bandwidth in each regime can again be obtained. If necessary, more iterations can be carried out until the desired bandwidth is obtained, before implementing the resulting controller.

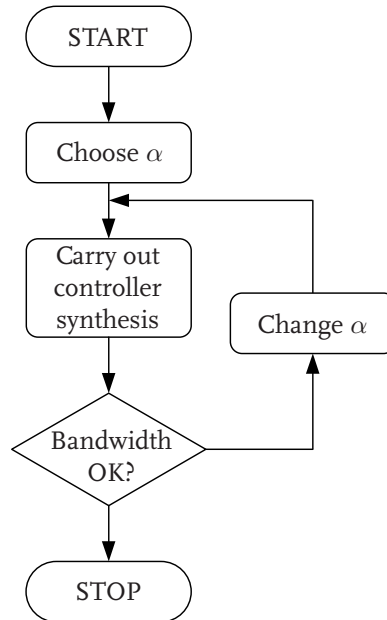


Figure 3.1 / Schematic representation of the iterative process for choosing α .

3.2.2.1 Linearizing Feedback Control Design Results

In the design of a linearizing feedback controller, the paper path parameters collected in Table 3.1 have been used. As can be seen, the radii of the driven rollers of the pinches are all chosen to be equal to each other. The transmission ratios, on the other hand, have been chosen different with respect to each other to resemble real paper path configurations. Given the parameters of the basic paper path, the state feedback controller gains can be calculated and the stability of the closed-loop error dynamics, in case of a linearizing feedback controller described by the closed-loop flow dynamics in error space (3.14), can be verified by solving the set of LMIs given by (3.35)-(3.36). A positive definite, symmetric matrix P has been found, which proves that the closed-loop error dynamics are GES. Using the iterative process shown in Fig. 3.1, the final value of α was chosen to be $\alpha = 30$. Given this value, the controller gains K to be used in the control law are the following:

$$K = \begin{bmatrix} -2.3 \cdot 10^5 & -9.9 \cdot 10^3 \\ -2.4 \cdot 10^5 & -1.0 \cdot 10^4 \\ -2.2 \cdot 10^5 & -9.6 \cdot 10^3 \end{bmatrix}. \quad (3.39)$$

Substitution of $K(2, 1)$ and $K(1, 1)$ into (3.38) shows that $s_2 = \frac{B_1(1)}{B_2(2)} = \frac{K(2,1)}{K(1,1)}$. Since also $\frac{K(2,2)}{K(1,2)} = s_2$ and $s_3 = \frac{B_1(1)}{B_3(3)} = \frac{K(3,1)}{K(1,1)} = \frac{K(3,2)}{K(1,2)}$, with s_3 the scaling factor for the third subsystem, we can conclude that the feedback controller completely linearizes the system, as expected.

Parameter	Nominal Value
n_1	18/37
n_2	14/30
n_3	15/30
r_{P1}	$14 \cdot 10^{-3}$ m
r_{P2}	$14 \cdot 10^{-3}$ m
r_{P3}	$14 \cdot 10^{-3}$ m

Table 3.1 / Paper path parameters for the nominal control design.

3.2.2.2 Partially Linearizing Feedback Control Design Results

The control design of a partially linearizing feedback controller has also been carried out using the paper path parameters listed in Table 3.1. Given these parameters, the controller gains have been calculated using the approach presented in Section 3.2.1.2.

Focussing first on subsystem 1, the controller parameters for this subsystem have been calculated using (3.37), after solving (3.35) and (3.36) with $X = X_1$ and $Y = Y_1$. In the calculation of these controller gains, the iterative process shown in Fig. 3.1 has been used to check whether the desired bandwidth has been realized for the first subsystem. Choosing $\alpha = 40$ resulted in $K(1, 1) = -2.3 \cdot 10^5$ and $K(1, 2) = -8.6 \cdot 10^3$. For the calculation of $K(2, 2)$ and $K(2, 3)$, the range of values for these gains has been chosen such that $K(2, 2) = s_2 K(1, 2) \pm 5 \cdot 10^2$ and $K(3, 2) = s_3 K(1, 2) \pm 5 \cdot 10^2$, respectively. In each of these ranges, several values of $K(2, 2)$ and $K(3, 2)$ satisfy (3.22) and (3.23) for $i = 2$ and $i = 3$, respectively. For illustration purposes, $K(2, 2)$ and $K(3, 2)$ were chosen such that the largest difference with $s_2 K(1, 2)$ and $s_3 K(1, 2)$ was obtained, in order to obtain the largest discontinuity in \dot{e}_s . This resulted in the following controller gains K to be used in the control law:

$$K = \begin{bmatrix} -2.3 \cdot 10^5 & -8.6 \cdot 10^3 \\ -2.3 \cdot 10^5 & -9.5 \cdot 10^3 \\ -2.2 \cdot 10^5 & -8.9 \cdot 10^3 \end{bmatrix}. \quad (3.40)$$

Substitution of $K(2, 2)$ and $K(1, 2)$ into (3.38) shows that $\frac{K(2,2)}{K(1,2)} \neq s_2$. Similarly, it can be seen that $\frac{K(3,2)}{K(1,2)} \neq s_3$, which shows that the resulting controller does indeed not completely linearize the system.

3.2.3 Simulation Results

To demonstrate the effectiveness of the control design approach, simulations have been conducted for the basic paper path case-study. An A4-format sheet, the length of which is $L_s = 0.21$ m, enters the paper path at $t = 0.25$ s. The sheet has to be transported at a velocity of 0.3 m/s and leaves the paper path when its trailing edge has left pinch P3. Given this desired sheet reference velocity, a throughput of 72 pages per minute can be realized when an inter sheet spacing of $40 \cdot 10^{-3}$ m is adopted. This inter sheet spacing is a typical value used in the design of sheet schedules [15], but could even be reduced, since the sheet flow becomes more predictable compared with traditional designs. According to the assumption made in Section 2.1, the distance between the pinches is chosen to be equal to the sheet length: $x_{P1} = 0$ m, $x_{P2} = L_s$ m, and $x_{P3} = 2L_s$ m. Furthermore, the pinch radii and transmission ratios used in the simulations are equal to the ones adopted in the control design. The paper path parameters used in this section have been collected in Table 3.2, which is an extended version of Table 3.1, as a reference for future sections. For completeness, the actual transmission ratios of the second and third motor-pinch combination and the uncertainty bounds on these ratios have also been included in Table 3.2. These parameters will be used in Section 3.3 for the analysis of the influence of perturbation of the paper path parameters on the sheet tracking error and the sheet velocity error. The other paper path parameters will not be perturbed in the basic paper path case-study, as indicated by "—" for their uncertainty bound.

Parameter	Nominal Value	Actual Value	Uncertainty Bounds
n_1	18/37	18/37	$\frac{26}{555}$
n_2	14/30	16/30	$\frac{1}{15}$
n_3	15/30	18/37	$\frac{1}{30}$
r_{P1}	$14 \cdot 10^{-3}$ m		—
r_{P2}	$14 \cdot 10^{-3}$ m		—
r_{P3}	$14 \cdot 10^{-3}$ m		—
$\dot{x}_{s,r}$	0.3 m/s		—
L_s	0.21 m		—
x_{P1}	0 m		—
x_{P2}	L_s m		—
x_{P3}	$2L_s$ m		—

Table 3.2 / Nominal and actual paper path parameters, together with the uncertainty bounds on the transmission ratios.

3.2.3.1 Linearizing Feedback Controller Results

For the validation of the linearizing controller design, simulations of the nominal high level sheet model (2.2) in combination with the sheet feedback controllers (3.15) have been carried out, using the controller gains given in (3.39). In these simulations, the sheet tracking error depicted by the thick line in Fig. 3.2(a) has been obtained. It can be seen that the sheet controller anticipates quickly to the increasing error right after $t = 0.25$ s, which is due to the difference in actual and desired sheet velocity at the moment the sheet enters the paper path. Furthermore, it can be noticed that after the transient response the error remains zero, also at the switching boundaries. This corresponds to the fact that there are no jumps in e_s and \dot{e}_s , as can be seen from (3.18), since $R_{k,k+1} = I$ for a linearizing controller. This also implies that the Lyapunov function is continuous on the switching boundaries. This can be observed from Fig. 3.2(b), which shows the value of the Lyapunov function along the sheet error trajectory.

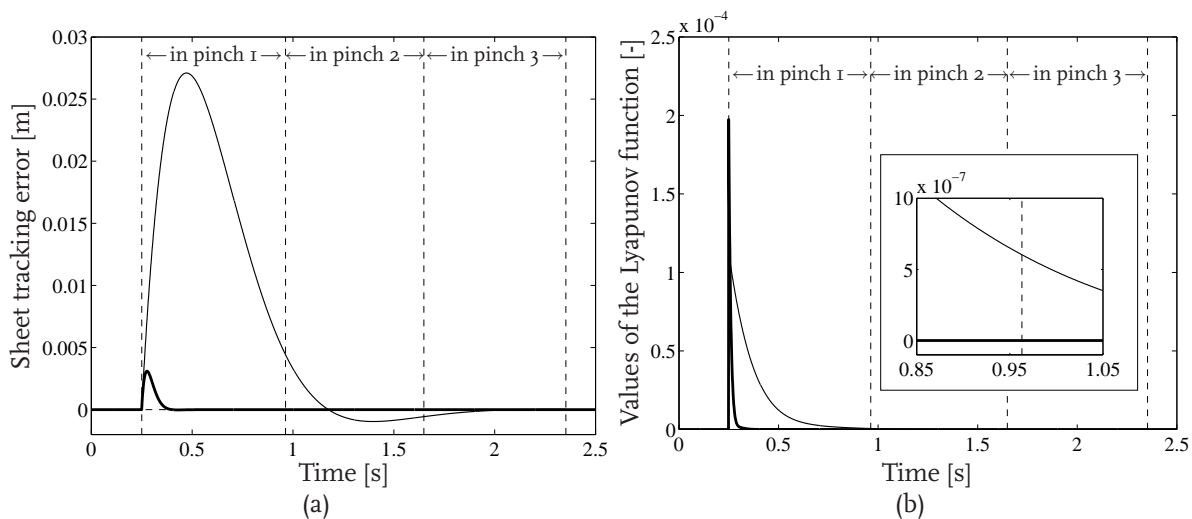


Figure 3.2 / Sheet tracking error obtained in simulation using a fully linearizing feedback controller for $\alpha = 30$ (thick) and $\alpha = 5$ (thin) (a), and the values of the corresponding Lyapunov function along the sheet error trajectories (b).

To demonstrate the effect of changes in α , Fig. 3.2(a) also shows the tracking error obtained using controller gains resulting from setting $\alpha = 5$. A decrease of the value of this parameter results in a slower transient response and in a nonzero tracking error when transferring the sheet from pinch P1 to pinch P2 and from pinch P2 to pinch P3. As can be seen, also during these switches between the regions the error is not amplified. This again implies that the Lyapunov function is continuous on the switching boundaries,

which can be observed from Fig. 3.2(b). The slow transient response results from the decrease of the controller gains, which in turn is caused by the decrease of α . These lower controller gains result in a decrease in bandwidth of the controlled system. This can be seen from Fig. 3.3, which shows the Bode plots of the loopgains of the first subsystem for $\alpha = 5$ and $\alpha = 30$. Although not shown here, similar Bode plots have been obtained for the second and third subsystem. As can be seen from Fig. 3.3, the bandwidths of the two controlled systems are approximately 1 Hz and 11 Hz, respectively. These bandwidths are both significantly lower than the typical bandwidths of the low level motor control loops, which is in correspondence with the rule of thumb for hierarchical control systems, mentioned in Section 2.3. From Fig. 3.3 we can also observe the stability of the first subsystem, as this is guaranteed by the design. Since at the crossover frequencies the phase lags are approximately 120° and 110° , respectively, the subsystem is stable in both cases and the phase margins are approximately 60° and 70° , respectively.

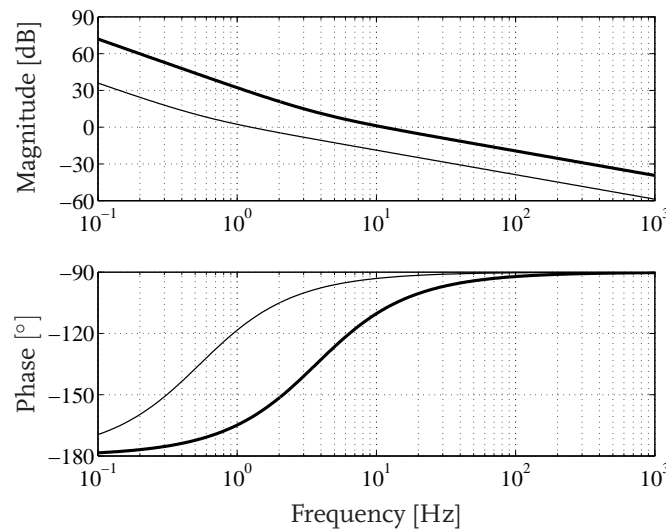


Figure 3.3 / Bode plot of the loop gain of the first subsystem for $\alpha = 30$ (thick) and $\alpha = 5$ (thin).

3.2.3.2 Partially Linearizing Feedback Controller Results

To validate the design results for the partially linearizing feedback controller, simulations of the nominal high level sheet model (2.2) in combination with the sheet feedback controllers (3.15) have been carried out, using the controller gains given in (3.40). In these simulations, the (nominal) paper path parameters shown in Table 3.2 have been used. The sheet tracking error obtained in these simulations is depicted by the thick line in Fig. 3.4. It can be seen that also this sheet controller anticipates quickly to the increasing error right after $t = 0.25$ s, which is due to the difference in actual and desired sheet ve-

locity at the moment the sheet enters the paper path. Furthermore, it can be noticed that also in this case the error remains zero after the transient response, also at the switching boundaries. This corresponds to the fact that there are no jumps in \dot{e}_s , as can be expected from (3.18). Since $\underline{q}^- \approx \underline{0}$, also $\underline{q}^+ \approx \underline{0}$, despite the fact that $R_{k,k+1} \neq I$. Since there are no jumps in \dot{e}_s , also the value of the Lyapunov function will not increase at the switching boundary.

To investigate the behavior of the system when $e_s(t_s) \neq 0$, sheet feedback controllers have been designed according to the approach presented in Section 3.2.1.2, only this time with $\alpha = 5$. The results of the simulations carried out using the new controller are also shown in Fig. 3.4. As can be seen from this figure, larger transient errors have been obtained, resulting from the decreased controller parameters, which in turn result from the decrease in α . Furthermore, it can be observed that the sheet tracking error is nonzero during the transfer from pinch P1 to pinch P2. Fig. 3.4 also shows that the sheet tracking error is continuous, as expected. However, the sheet velocity error is discontinuous, since the slopes of $e_s^-(t_s)$ and $e_s^+(t_s)$ differ from each other.

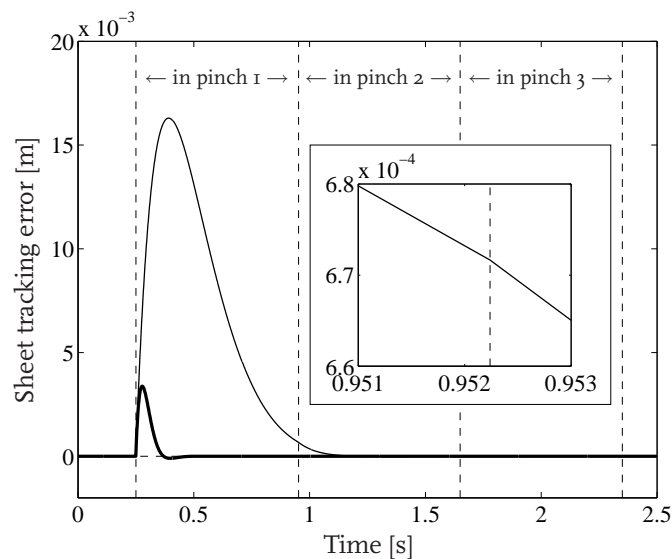


Figure 3.4 / Sheet tracking error obtained in simulation using a partially linearizing feedback controller for $\alpha = 40$ (thick) and $\alpha = 5$ (thin).

The discontinuity in \dot{e}_s can also be observed from Fig. 3.5, which shows the sheet velocity error obtained in simulation. When the sheet enters the first pinch at $t = 0.25$ s, $\dot{e}_s = 0.3$ m/s since the first pinch is not in motion at that time. At the transition from pinch P1 to pinch P2, the sheet velocity error jumps from $\dot{e}_s^-(t_s) = -6.55 \cdot 10^{-3}$ m/s to $\dot{e}_s^+(t_s) = -8.74 \cdot 10^{-3}$ m/s. This latter value of \dot{e}_s can also be calculated from the closed-loop jump conditions (3.18):

$$\begin{aligned}
\dot{e}_s^+(t_s) &= (B_2(2)K(2,2) - B_1(1)K(1,2))e_s^-(t_s) + \dot{e}_s^-(t_s) \\
&= (B_2(2)K(2,2) - B_1(1)K(1,2))6.72 \cdot 10^{-4} - 6.55 \cdot 10^{-3} \\
&= -8.74 \cdot 10^{-3} \text{ m/s.}
\end{aligned} \tag{3.4I}$$

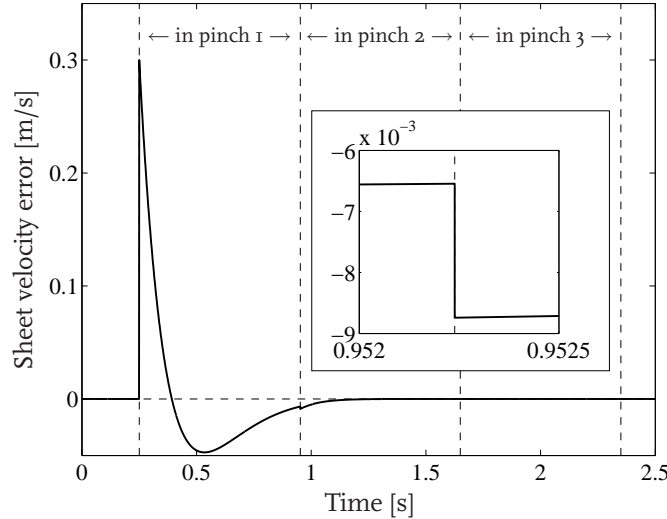


Figure 3.5 / Time derivative of the sheet tracking error obtained in simulation using a partially linearizing feedback controller for $\alpha = 5$.

The discontinuity in \dot{e}_s also affects the values of the three Lyapunov functions used in the controller synthesis, as can be observed from Fig. 3.6. From a global perspective, it seems that the three Lyapunov functions are all decreasing. However, zooming in on the switching boundary between pinch P1 and pinch P2, it can be observed that the values of all Lyapunov functions increase as a result of the jump in \dot{e}_s . However, at this switching boundary, also the switch from Lyapunov function V_1 , i.e. the one indicated by the thick black line in Fig. 3.6, to Lyapunov function V_2 , i.e. the one indicated by the gray line, is made. Regarding this switch, it can be observed that the overall Lyapunov function is continuous, i.e. $V_1^-(t_s) = V_2^+(t_s)$. Although not shown in the figure, the same phenomenon can be observed when switching from pinch P2 and pinch P3. Hence, the simulations confirm the use of piecewise quadratic Lyapunov functions for the proof of the stability of the closed-loop system and the synthesis of partially linearizing feedback controllers.

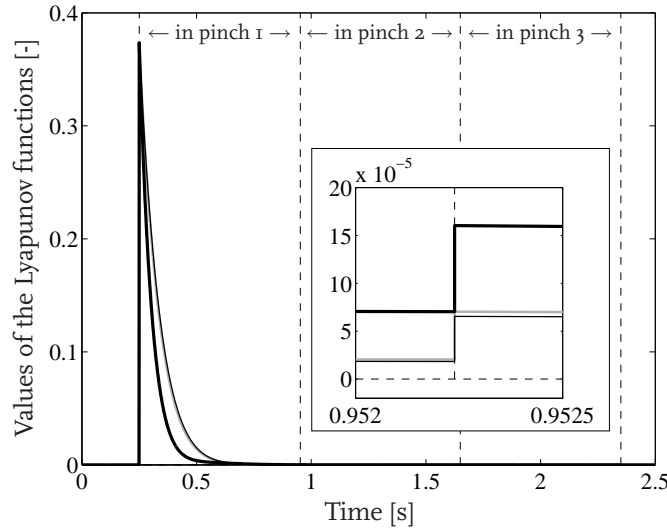


Figure 3.6 / Values of the Lyapunov functions along the sheet error trajectories obtained from simulation using a partially linearizing feedback controller for $\alpha = 5$: $V_1(\underline{q}(t))$ (black, thick), $V_2(\underline{q}(t))$ (gray), $V_3(\underline{q}(t))$ (black, thin).

3.3 Analysis of the Perturbation of Paper Path Parameters

Up to now, control design and analysis have been carried out for the nominal basic printer paper path, i.e. disturbances and uncertainties have not been taken into account yet. As such, the possibilities of incorporating parametric uncertainties in the control design and analysis are investigated in this section. Therefore, first the flow conditions and jump conditions in error space are derived. The first step in this derivation is the extension of the nominal high level sheet model (2.2) such that it incorporates parametric uncertainties:

$$\dot{x}_s = (B_i + \Delta B_i) \underline{u} \quad \text{for } x_s \in \mathcal{X}_i, i \in \mathcal{I}, \quad (3.42)$$

with ΔB_i the constant uncertainty term of the i -th subsystem.⁵ In this model, this term can represent, for example, an uncertainty in the transmission ratio between motor M_i and pinch P_i or an uncertainty in the radius of the driven roller of pinch i .

Given the high level sheet model subject to parametric uncertainties (3.42), the flow conditions in error space in standard state-variable form can be derived in analogy with Section 3.1, yielding

$$\dot{\underline{q}} = F \underline{q} + (G_i + \Delta G_i) \underline{\mu} \quad \text{for } x_{s,r} = \begin{bmatrix} 1 & 0 \end{bmatrix} \underline{q} \in \mathcal{X}_i, i \in \mathcal{I}. \quad (3.43)$$

In this notation, the state vector \underline{q} , the input vector $\underline{\mu}$, the system matrix F , and the

⁵Note that ΔB_i has the same structure as B_i , i.e. $\Delta B_1 = \begin{bmatrix} \Delta(n_1 r_{P1}) & 0 & 0 \end{bmatrix}$, $\Delta B_2 = \begin{bmatrix} 0 & \Delta(n_2 r_{P2}) & 0 \end{bmatrix}$, and $\Delta B_3 = \begin{bmatrix} 0 & 0 & \Delta(n_3 r_{P3}) \end{bmatrix}$.

nominal input matrices G_i are defined as in Section 3.1. The uncertainty terms of the input matrices are defined as $\Delta G_i = [\underline{0} \quad -(\Delta B_i)^T]^T$.

Similar to the flow conditions, also the jump conditions of the error dynamics can be derived in analogy with Section 3.1, yielding

$$\underline{q}^+(t_s) = \begin{bmatrix} 1 & 0 \\ 0 & 1 \end{bmatrix} \underline{q}^-(t_s) + \begin{bmatrix} \underline{0}^T \\ B_k + \Delta B_k - B_{k+1} - \Delta B_{k+1} \end{bmatrix} \underline{u}(t_s), k \in \mathcal{K}. \quad (3.44)$$

Hence, the complete model of the uncertain open-loop sheet dynamics in error space is given by the flow conditions (3.43) and the jump conditions (3.44).

As in Section 3.2.1, the goal is to control the error dynamics using a state feedback control law (3.13). Using, this control law, the closed-loop flow dynamics in error space can be derived:

$$\dot{\underline{q}} = (F - (G_i + \Delta G_i) K) \underline{q} \quad \text{for} \quad (x_{s,r} - [1 \quad 0] \underline{q}) \in \mathcal{X}_i, i \in \mathcal{I}. \quad (3.45)$$

When we consider the transition from regime k to regime $k + 1$, the closed-loop jump conditions can be derived from the open-loop jump conditions (3.44) in combination with the control law u_i (3.15), yielding

$$\begin{aligned} \underline{q}^+(t_s) = & \begin{bmatrix} 1 & 0 \\ (B_{k+1}(k+1) + \Delta B_{k+1}(k+1)) K(k+1, 2) - & 1 \\ & - (B_k(k) + \Delta B_k(k)) K(k, 2) \end{bmatrix} \underline{q}^-(t_s) + \\ & + \begin{bmatrix} 0 \\ (B_{k+1}(k+1) + \Delta B_{k+1}(k+1)) K(k+1, 1) - & \int_{t_0}^{t_s} e_s(\tau) d\tau \\ & - (B_k(k) + \Delta B_k(k)) K(k, 1) \end{bmatrix}, k \in \mathcal{K}. \end{aligned} \quad (3.46)$$

For $\underline{q} = \underline{0}$ to be the desired equilibrium point of the closed-loop error dynamics, the second term of (3.46) should be equal to $\underline{0}$. In analogy with Section 3.2.1, we know that enforcing $(B_{k+1}(k+1) + \Delta B_{k+1}(k+1)) K(k+1, 1)$ to be equal to $(B_k(k) + \Delta B_k(k)) K(k, 1)$ would result in $\underline{q} = \underline{0}$ to be the desired equilibrium point. However, since the actual values of the uncertainty matrices ΔB_k are assumed to be unknown, the feedback controllers (3.15) cannot fully or partially linearize the system for all uncertainties. *Therefore, $\underline{q} = \underline{0}$ is not an equilibrium point of the system and we cannot synthesize a stabilizing controller for the uncertain error dynamics using the approach presented in Section 3.2.1.* Hence, instead of carrying out robust control design, the focus in the remainder of this section is on analysis. More specifically, given bounds on the uncertainties present in the paper path, the goal is to derive expressions for predicting the influence of these uncertainties on the magnitude of the jumps in \dot{e}_s . Moreover, based on the resulting expressions, the effect of these jumps on the evolution of the sheet tracking error will be investigated, with the goal to be able to analytically predict this evolution and

the maximum error value, and, hence, to be able to evaluate the system's performance analytically.

3.3.1 Influence of Parameter Perturbations

In this section, first the influence of the parametric uncertainties on the jumps in \dot{e}_s is analyzed. Hence, the goal is to derive an expression for $\dot{e}_s^+(t_s)$ as a function of these uncertainties, the input matrices of the high level sheet flow model, and the controller parameters. To realize this goal, we start from the relation for $\dot{e}_s^+(t_s)$ in (3.46):⁶

$$\begin{aligned} \dot{e}_s^+(t_s) = & ((B_{k+1} + \Delta B_{k+1}) K(k+1, 2) - (B_k + \Delta B_k) K(k, 2)) e_s^-(t_s) + \dot{e}_s^-(t_s) + \\ & + \underbrace{((B_{k+1} + \Delta B_{k+1}) K(k+1, 1) - (B_k + \Delta B_k) K(k, 1)) \int_{t_0}^{t_s} e_s(\tau) d\tau}_{c_k}, \\ & k \in \mathcal{K}. \end{aligned} \quad (3.47)$$

To express $\dot{e}_s^+(t_s)$ as a function of the uncertainties, the input matrices, and the controller parameters, the next step is to rewrite the unknown integral term in c_k in (3.47). In doing this, we calculate $\dot{x}_s^-(t_s)$ in the k -th subsystem of the high level sheet flow model (3.42), with the control law substituted, given the initial condition $\underline{u}(t_0) = \underline{0}$:

$$\dot{x}_s^-(t_s) = - (B_k + \Delta B_k) K(k, 1) \int_{t_0}^{t_s} e_s(\tau) d\tau - (B_k + \Delta B_k) K(k, 2) e_s^-(t_s), k \in \mathcal{K}. \quad (3.48)$$

Rewriting (3.48) yields the desired expression for the integral term:

$$\int_{t_0}^{t_s} e_s(\tau) d\tau = \frac{-\dot{x}_s^-(t_s) - (B_k + \Delta B_k) K(k, 2) e_s^-(t_s)}{(B_k + \Delta B_k) K(k, 1)}, k \in \mathcal{K}. \quad (3.49)$$

With this expression, c_k in (3.47) can be written as follows

$$c_k = \left(\frac{-(B_{k+1} + \Delta B_{k+1}) K(k+1, 1)}{(B_k + \Delta B_k) K(k, 1)} + 1 \right) (\dot{x}_s^-(t_s) + (B_k + \Delta B_k) K(k, 2) e_s^-(t_s)), \quad k \in \mathcal{K}. \quad (3.50)$$

If we now adopt the linearizing or partially linearizing controllers designed in Section 3.2.1, we know that

$$K(k, 1) = \frac{B_{k+1}}{B_k} K(k+1, 1), k \in \mathcal{K}. \quad (3.51)$$

⁶To simplify the notation, in the remainder of this section $B_k(k)$, $B_{k+1}(k+1)$, $\Delta B_k(k)$, and $\Delta B_{k+1}(k+1)$ have been replaced by B_k , B_{k+1} , ΔB_k , and ΔB_{k+1} , respectively.

Substitution of this relation into (3.50) yields the following expression for c_k :

$$\begin{aligned} c_k &= \left(\frac{-(B_{k+1} + \Delta B_{k+1})K(k+1,1)}{(B_k + \Delta B_k) \frac{B_{k+1}}{B_k} K(k+1,1)} + 1 \right) (\dot{x}_s^-(t_s) + (B_k + \Delta B_k) K(k,2) e_s^-(t_s)), \\ &= \left(\frac{-B_k \Delta B_{k+1} + B_{k+1} \Delta B_k}{B_{k+1}(B_k + \Delta B_k)} \right) (\dot{x}_s^-(t_s) + (B_k + \Delta B_k) K(k,2) e_s^-(t_s)), k \in \mathcal{K}. \end{aligned} \quad (3.52)$$

With this expression for c_k , the desired relation between $\dot{e}_s^+(t_s)$ and the uncertainties, the input matrices of the high level sheet flow model, and the controller parameters now becomes:

$$\begin{aligned} \dot{e}_s^+(t_s) &= ((B_{k+1} + \Delta B_{k+1}) K(k+1,2) - (B_k + \Delta B_k) K(k,2)) e_s^-(t_s) + \dot{e}_s^-(t_s) + \\ &\quad \left(\frac{-B_k \Delta B_{k+1} + B_{k+1} \Delta B_k}{B_{k+1}(B_k + \Delta B_k)} \right) (\dot{x}_s^-(t_s) + (B_k + \Delta B_k) K(k,2) e_s^-(t_s)), k \in \mathcal{K}. \end{aligned} \quad (3.53)$$

From (3.47) it can be observed that for the prediction of the jump in \dot{e}_s , the sheet tracking error and its time derivative right before switching are required, together with the actual sheet velocity at this time instant. Since these are in general not known beforehand, the desired prediction cannot be made. However, from the simulation results presented in Section 3.2.3 it could be observed that with the sheet controllers calculated using the large values of α , i.e. $\alpha = 30$ and $\alpha = 40$, and with a sheet reference velocity of 0.3 m/s, a zero tracking error and a zero velocity error could be realized at t_s with both the fully and the partially linearizing feedback controller. If we assume that in case parameter uncertainties are present in the paper path, $e_s^-(t_s) = 0$ and $\dot{e}_s^-(t_s) = 0$ can also be realized, a significant simplification of (3.53) can be obtained. Since under these assumptions $\dot{x}_s^-(t_s) = \dot{x}_{s,r}$, $\dot{e}_s^+(t_s)$ can be expressed as a function of the uncertainties and the input matrices of the high level sheet flow model:

$$\dot{e}_s^+(t_s) = \left(\frac{-B_k \Delta B_{k+1} + B_{k+1} \Delta B_k}{B_{k+1}(B_k + \Delta B_k)} \right) \dot{x}_{s,r}, k \in \mathcal{K}. \quad (3.54)$$

As can be seen from (3.54), the jump in \dot{e}_s is in this case only a function of the nominal system parameters, the uncertainty terms, and the sheet reference velocity. More specifically, *in the case of fully or partially linearizing feedback controllers, the controller gains do not influence the jump in \dot{e}_s , since this jump is fully determined by the system parameters.* Since the nominal system parameters and the sheet reference velocity are assumed to be known, (3.54) can be evaluated for various values of the uncertainty terms within the upper and lower bounds on these terms. This way, insight is obtained in the influence of various combinations of the uncertainty terms on the value of the jump in \dot{e}_s . One of these combinations can already easily be obtained from (3.54): if there are no uncertainties present, there will be no jumps in \dot{e}_s on the transitions between two regimes, which coincides with the closed-loop jump conditions (3.46).

Once the jump in \dot{e}_s can be predicted, this prediction can be used to evaluate the effect on the sheet tracking error. For analysis purposes, we consider the transition from regime

k to regime $k + 1$, assuming the sheet is not forced back into the previous pinch, i.e. no immediate switching back to the previous regime occurs. Since the states of the error dynamics are both assumed to be equal to zero just before the transition occurs, $\underline{q}^+(t_s) = [e_s^+(t_s) \ \dot{e}_s^+(t_s)]^T$ can be considered as an initial condition of the flow dynamics active in regime $k + 1$, with $e_s^+(t_s) = 0$ since $e_s^+(t_s) = e_s^-(t_s)$ and with $\dot{e}_s^+(t_s)$ calculated from in (3.54). By solving the set of differential equations in (3.45), the evolution of the sheet tracking error can be predicted as a function of time. Via this approach, also the evolution of the sheet tracking error in the first regime can be predicted. Given the second order dynamics active in each regime of the closed-loop system (3.45), it is plausible to assume that each subsystem has two complex eigenvalues $\lambda_{i,2} = \sigma_i \pm j\omega_i$, as a result of which the general solution of the set of differential equations for each subsystem is given by:

$$e_i(t) = C_{i,1}e^{\sigma_i t} \cos(\omega_i t) + C_{i,2}e^{\sigma_i t} \sin(\omega_i t), i \in \mathcal{I}, \quad (3.55)$$

with the constants $C_{i,1}$ and $C_{i,2}$ calculated from the initial conditions, leading to $C_{i,1} = 0$, $C_{i,2} = \frac{\dot{e}_s^+(t_s)}{\omega_i}$, and therefore

$$e_i(t) = \frac{\dot{e}_s^+(t_s)}{\omega_i} e^{\sigma_i t} \sin(\omega_i t), i \in \mathcal{I}. \quad (3.56)$$

Hence, using (3.56) the evolution of the sheet tracking error can be predicted. To calculate the maximum or minimum value of e_i , its time derivative, given by

$$\dot{e}_i(t) = \frac{\dot{e}_s^+(t_s)}{\omega_i} \sigma_i e^{\sigma_i t} \sin(\omega_i t) + \frac{\dot{e}_s^+(t_s)}{\omega_i} e^{\sigma_i t} \omega_i \cos(\omega_i t), i \in \mathcal{I}, \quad (3.57)$$

is set equal to zero. Solving the resulting equality for t yields the time t^* at which the sheet tracking error has its maximum or minimum value:

$$t^* = \frac{-\arctan\left(\frac{\omega_i}{\sigma_i}\right)}{\omega_i}, i \in \mathcal{I}. \quad (3.58)$$

Substitution of (3.58) into (3.56) yields the expression for calculating the maximum or minimum value of the tracking error in subsystem i :

$$e_i(t^*) = \frac{\dot{e}_s^+(t_s)}{\sqrt{\sigma_i^2 + \omega_i^2}} e^{-\frac{\sigma_i}{\omega_i} \arctan\left(\frac{\omega_i}{\sigma_i}\right)}, i \in \mathcal{I}. \quad (3.59)$$

With the derivation of (3.56) and (3.59), the evolution of the sheet tracking error and its maximum value can be predicted in case a zero tracking error and a zero velocity error are realized just before a transition to a subsequent regime occurs. In the next subsection, simulation results will be presented to judge the quality of these predictions.

3.3.2 Simulation Results

To analyze the behavior of the system subject to perturbations of the paper path parameters and to validate if the jumps in \dot{e}_s and the resulting maximum deviations of the sheet tracking error can be predicted correctly, simulations have been carried out using two types of controllers: the ones that result in a nonzero tracking error and velocity error right before switching and the ones that yield $e_s^-(t_s) = \dot{e}_s^-(t_s) \approx 0$. Initially, we start with the analysis of the results obtained using the latter type of sheet controllers. Hence, we make the assumption that the transient behavior in each regime, initiated by the perturbation of the paper path parameters, has decayed before the transition to the next regime occurs. Before presenting the simulation results, first (3.54) is evaluated for various uncertainties present in adjacent subsystems. The bounds on these uncertainties are quantified by introducing an additional transmission ratio of 16/30. Since this ratio is larger than the nominal ratios listed in Table 3.2, the maximum possible variations of the ratios, which will take the role of uncertainty bounds upon the nominal ratios, can be calculated. Given these uncertainty bounds, also listed in Table 3.2, (3.54) can be evaluated for various uncertainties within these bounds. The results of this evaluation are shown in Fig. 3.7. From Fig. 3.7(a), which shows the jump in \dot{e}_s as a function of ΔB_1 and ΔB_2 , it can be seen that for fixed values of ΔB_1 , the jump in \dot{e}_s varies linearly with changing values of ΔB_2 , as can be expected from (3.54). When considering fixed values of ΔB_2 , it can be observed that the jump in \dot{e}_s increases nonlinearly with increasing values of ΔB_1 . Given the ranges of uncertainty terms ΔB_1 and ΔB_2 , no large jumps in \dot{e}_s are predicted. Hence, the increase in tracking error after the transition from regime 1 to regime 2 due to the perturbations of the transmission ratios will be limited, as can be seen from (3.59). From Fig. 3.7(b), which shows the jump in \dot{e}_s as a function of ΔB_2 and ΔB_3 , similar conclusions can be drawn: for fixed values of ΔB_2 , the jump in \dot{e}_s varies linearly with changing values of ΔB_3 , whereas fixing the values of ΔB_3 results in jumps in \dot{e}_s that increase nonlinearly with an increasing ΔB_2 . Also in this case, relatively small jumps in \dot{e}_s , and therefore small increases in e_s after the transition will be obtained.

In the simulations that have been carried out, the actual paper path parameters listed in Table 3.2 have been used. Hence, the actual gains of the second and third subsystem vary 14% and -3% with respect to their nominal values, respectively. As an example, the fully linearizing controller designed in Section 3.2.2.1, i.e. with the decay rate of the Lyapunov function chosen to be $\alpha = 30$, has been used. Although not discussed here, similar results have been obtained using partially linearizing controllers. The tracking error obtained in simulation is depicted in Fig. 3.8. It can be seen that the tracking error increases in the negative direction right after the sheet enters the second pinch, which corresponds with the increased value of the second transmission ratio with respect to the one the feedback controller was designed for. On the other hand, a positive tracking error

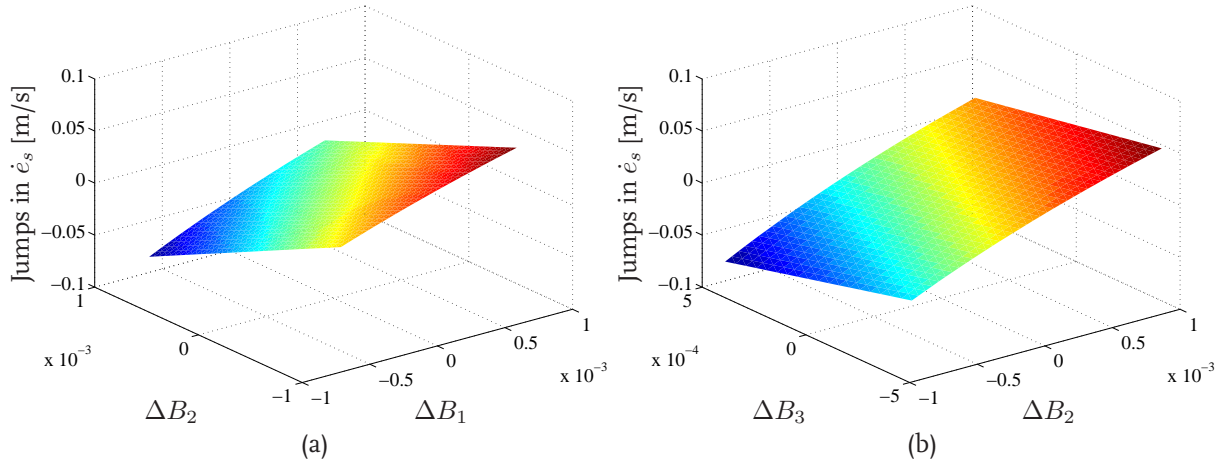


Figure 3.7 / Jumps in \dot{e}_s as a function of ΔB_1 and ΔB_2 (a), and ΔB_2 and ΔB_3 (b).

occurs right after entering pinch P₃, corresponding to the decrease of the third transmission ratio. Furthermore, it can be seen that the increases in tracking error are controlled to zero quickly. From Fig. 3.8, it can be concluded that the performance properties defined in Section 1.4 have been satisfied for this case.

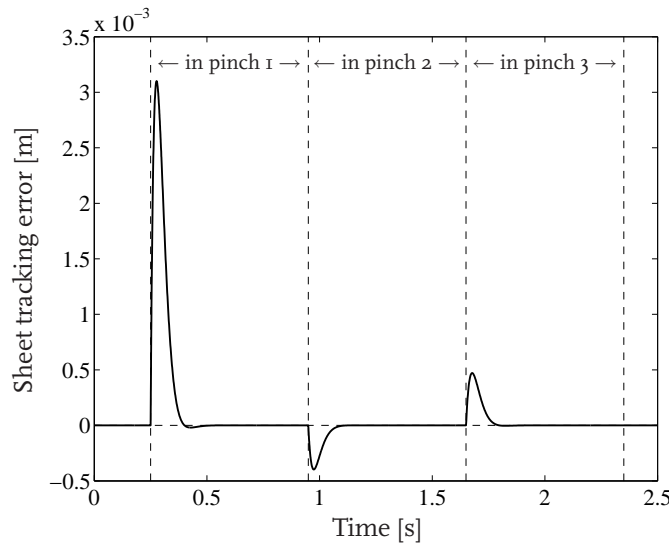


Figure 3.8 / Sheet tracking error obtained in simulation using a fully linearizing feedback controller for $\alpha = 30$, with perturbation of the paper path parameters.

Given the paper path parameters used in the simulation, the values of $\dot{e}_s^+(t_s)$ can be predicted using (3.54). Evaluation of this relation shows that $\dot{e}_s^+(t_s)$ at the transitions to the second and third regime are equal to $-4.29 \cdot 10^{-2}$ m/s and $4.46 \cdot 10^{-2}$ m/s, respectively.

To validate if these predicted values are correct, the sheet velocity error has been depicted in Fig. 3.9. From this figure, three jumps in \dot{e}_s can be observed, corresponding to the sheet entering the three pinches. The first jumps is equal to 0.3 m/s, which coincides with difference between the reference and initial actual velocity. Regarding the second and third jump, it can be observed that the predicted values of $\dot{e}_s^+(t_s)$ at the transitions to the second and third regime match the ones obtained in simulation.

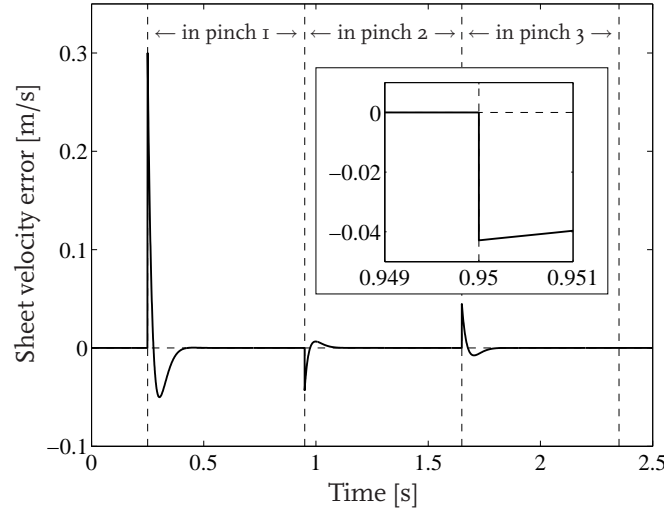


Figure 3.9 / Time derivative of the sheet tracking error obtained in simulation using a fully linearizing feedback controller for $\alpha = 30$, with perturbation of the paper path parameters.

Based on the values of $\dot{e}_s^+(t_s)$, the evolution of the sheet tracking error can be predicted using (3.55), whereas the maximum tracking errors can be calculated using (3.59). As an example, we consider the sheet tracking error in the second regime. From (3.59), a maximum sheet tracking error of $-4.0 \cdot 10^{-4}$ m is expected after the sheet enters the second pinch. Comparing this value with the tracking error shown in Fig. 3.8, it can be seen that the prediction is correct. Hence, (3.59) can be very well used to predict the deviations from the desired zero error level in case perturbations of the paper path parameters are known. Otherwise, if these perturbations are not known, the worst-case maximum values of e_s can be predicted given the maximum values of $\dot{e}_s^+(t_s)$ depicted in Figs. 3.7(a) and 3.7(b).

The second simulation is carried out using fully linearizing sheet controllers that result in a nonzero tracking error and velocity error at the switching boundaries, i.e. controllers designed using the procedure discussed in Section 3.2.1.1 with $\alpha = 5$.⁷ The parameters used are the actual ones listed in Table 3.2, resulting in the sheet tracking error shown

⁷Note that also in this case similar results have been obtained using partially linearizing controllers.

in Fig. 3.10. From this figure, it can be seen that the combination of the controllers and the perturbed parameters results in nonzero tracking errors larger than $5 \cdot 10^{-3}$ m before each transition. Therefore, and since the maximum transient responses are larger than $3 \cdot 10^{-3}$ m, in this case the performance properties defined in Section 1.4 have not been satisfied.

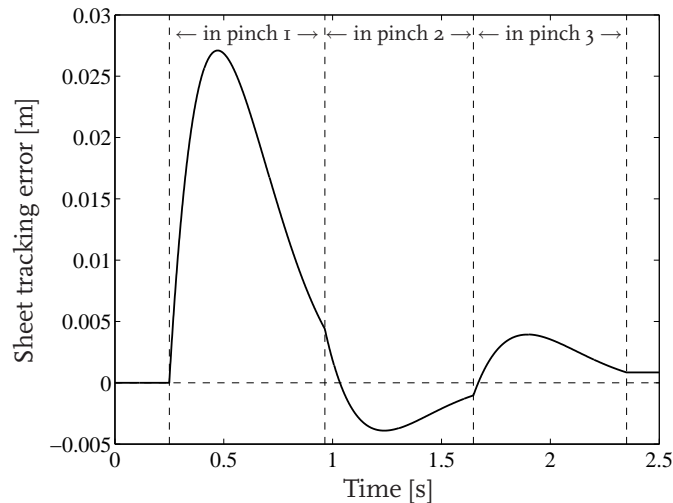


Figure 3.10 / Sheet tracking error obtained in simulation using a fully linearizing feedback controller for $\alpha = 5$, with perturbation of the paper path parameters.

Given the paper path parameters used in the simulation, together with the values of $e_s^-(t_s)$, $\dot{e}_s^-(t_s)$, and $\dot{x}_s^-(t_s)$, $\dot{e}_s^+(t_s)$ can be predicted using (3.53). Evaluation of this relation shows that $\dot{e}_s^+(t_s)$ is equal to $-8.05 \cdot 10^{-2}$ m/s and $4.97 \cdot 10^{-2}$ m/s at the transitions to the second and third regime, respectively. To validate if these predicted values are correct, the sheet velocity error has been depicted in Fig. 3.11. From this figure, three jumps in \dot{e}_s can be observed, corresponding to the sheet entering the three pinches. The first jumps is equal to 0.3 m/s, which again coincides with difference between the reference and initial actual velocity. Regarding the second and third jump, it can be observed that the predicted values of $\dot{e}_s^+(t_s)$ at the transitions to the second and third regime match the ones obtained in simulation.

At this point we reconsider the first simulation results described in this section, i.e. we again take a critical look at the sheet tracking error obtained in the first simulation, which is depicted in Fig. 3.8. From this figure, it can be observed that the deviation from the desired zero error level after entering the third pinch has approximately the same size as the deviation after entering the second pinch, while the perturbation of the transmission ratio is smaller. This can be explained by the sheet feedback control architectures shown in Figs. 2.4 and 2.5. When the sheet enters pinch P2, its velocity will increase

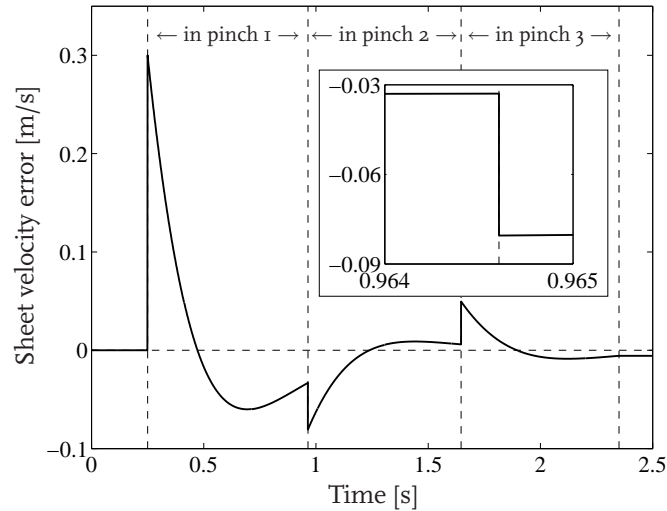


Figure 3.11 / Time derivative of the sheet tracking error obtained in simulation using a fully linearizing feedback controller for $\alpha = 5$, with perturbation of the paper path parameters.

due to the larger value of the actual transmission ratio with respect to the nominal one. Consequently, all three motor reference velocities will be decreased to compensate for the increasing sheet velocity in pinch P2, since the sheet tracking error is input of all three high level sheet controllers. After the sheet tracking error has settled at the desired zero level, all three motor reference velocities will have lower values compared with their original nominal ones. When the sheet enters the third pinch, the velocity of motor M3 is too low with respect to the nominal one, causing the sheet velocity to be too low as well, which results in an increase in the tracking error. This increase is amplified by the perturbation of the third transmission ratio, which in this case has a value smaller than the nominal one. The phenomenon described above occurs in a region of which the upstream neighbor has perturbed parameters, even when the parameters of the region itself are not perturbed. This can be seen in Fig. 3.12(a), which shows the sheet tracking error obtained in simulation when only the second transmission ratio has been perturbed according to the values shown in Table 3.2. As explained above, in this case the tracking error will also deviate from zero when entering the third pinch, even though the nominal and actual transmission ratios in this subsystem are equal. Fig. 3.12(b) shows the corresponding motor (reference) velocities. It can be seen that ω_{M3} responds to the increasing error of the sheet when entering pinch P2. After the sheet has entered pinch P3, the value of ω_{M3} becomes equal to its value during the time the sheet was in the first pinch.

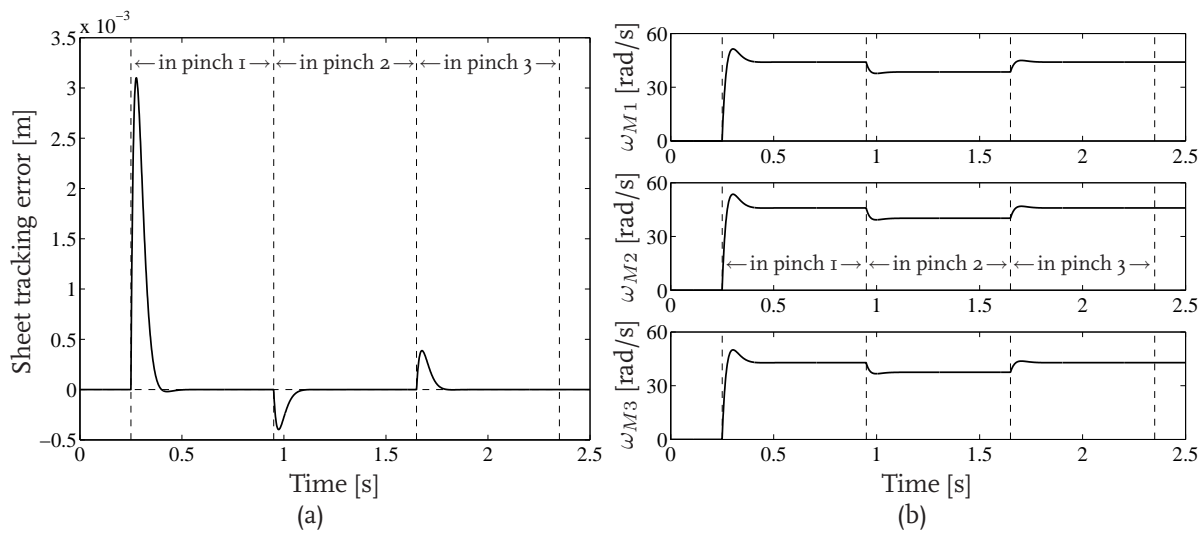


Figure 3.12 / Perturbation of n_2 : Sheet tracking error obtained in simulation using a fully linearizing feedback controller (a), and the motor (reference) velocities (b).

3.4 Evaluation

In this chapter, a design approach for sheet feedback control has been discussed, in which controllers based on a nominal PWL sheet flow model have been synthesized. This nominal model has been written in terms of its error dynamics. In contrast with the linear case that only contains flow dynamics, the PWL version of the error dynamics also contains jump conditions that describe the system behavior at the switching boundaries. Based on this model, both fully and partially linearizing feedback controllers have been designed. It has been analyzed that for the synthesis of fully linearizing controllers, a common quadratic Lyapunov function had to be adopted for proving the stability of the closed-loop system. On the other hand, the synthesis of partially linearizing controllers required the use of a piecewise quadratic Lyapunov function that is continuous on the switching boundaries. This continuity is related to the fact that stability had to be guaranteed for switching from regime k to regime $k + 1$, and vice versa. In the design of the latter type of controllers, more freedom in the choice of the parameters has been obtained. However, the exploitation of the increase in freedom is left open for future research.

In the third section of this chapter, the possibilities of extending the control design approaches to include parametric uncertainties have been investigated. It has been concluded that the approaches presented in Section 3.2 are not suitable for this purpose, since in case of uncertainties it is not possible to define an equilibrium point of the error dynamics. Hence, control design for robustness is not possible. Therefore, an a posteriori analysis technique has been derived that enables the investigation of the influence

of parametric uncertainties on the tracking performance of the system. In this analysis, two cases have been distinguished. In the first case, the sheet tracking error and its time derivative are assumed to be zero right before the sheet enters the new pinch, i.e. the linear subsystems are assumed to be fast enough to reach the steady state mode before switching. In the second case, nonzero tracking errors at the switching boundaries are considered. In the first case, it has been assumed for analysis purposes that after entering a new pinch, the sheet is not immediately forced back into the previous pinch, i.e. no immediate switching back to the previous regime is allowed to occur. The simulations showed that the performance properties are still satisfied. However, as the uncertainties were not incorporated in the control design, no a priori guarantees on the system behavior can be given from a control point of view. More specifically, the performance guarantees should be obtained from the mechanical design of the system, as the jumps in \dot{e}_s are not influenced by the controller gains, but only by the paper path parameters.

In the control design approaches presented in this chapter, the structure of the sheet feedback controllers solely depends on the order of the sheet reference profile that is taken into account in the derivation of the error dynamics. This implies that high order profiles lead to equally high order controllers. So far, only first order reference profiles have been considered, while in real printer paper paths piecewise linear velocity profiles are commonly used. Hence, a next step in sheet feedback control design using the approach presented in this chapter is the extension to take into account more realistic sheet reference profiles. Another observation regarding the control design presented in this chapter is that no additional dynamics have been added to the controller. One could think of, for example, a high frequency roll-off to prevent the low level motor control loops to be excited by high frequency components in the motor reference velocities that cannot be tracked. A third observation is that the controller design is frequency independent, i.e. possible a priori knowledge on important frequency ranges, e.g. ranges in which disturbances are likely to be present, is not taken into account in the design. Hence, an item for future research could be to incorporate additional dynamics in the design of the sheet feedback controllers, while still using the design approach presented in this chapter.

Given the evaluation of the control design presented in this chapter, in the next chapter an alternative control design procedure will be presented for both the nominal and the uncertain high level sheet flow model. The main reasons for considering this alternative are the possibility to carry out control design for robustness, the independency of the control design and the controller structure with respect to the order of the sheet reference profiles, and the possibility to incorporate bandwidth requirements and possible a priori knowledge on important frequency ranges. More specifically, in the alternative approach, disturbance attenuation properties can be incorporated into the design via frequency dependent weighting filters. Using this approach, controllers can be shaped according to the designer's demands.

Output Feedback Control Design

4.1	The Tracking Control Problem	53
4.2	Nominal Sheet Feedback Control Design	55
4.3	Robust Sheet Feedback Control Design	66
4.4	Stability Analysis for Non-ideal Low Level Dynamics	77
4.5	Evaluation	78

4.1 The Tracking Control Problem

In this chapter, the second approach for sheet feedback control design for the basic paper path case-study is presented. The goal of the control design procedure is the same as the one in Chapter 3, i.e. the synthesis of sheet feedback controllers that make the sheets in the paper path track a reference trajectory, satisfying the performance properties presented in Section 1.4. In contradiction to Chapter 3, in which the influence of parametric uncertainties on the tracking performance of the system was considered via an a posteriori analysis technique, in this chapter the focus will eventually be on control design for robustness. Hence, also in this chapter we will concentrate on feedback design only, leaving feedforward control design out of consideration.

As already shortly mentioned in Section 3.1, the focus in this chapter is on control design that guarantees performance in the H_∞ sense. Known results from literature regarding this topic can be found in [23, 57], in which state feedback control design for PWL systems is proposed. Given the control law, it is shown that upper bounds on the induced L_2 -norm of the operator from the control input [57] or the disturbance input [23]

to the controlled output can be given. Based on the work presented in [23], extensions for controlling uncertain PWL systems via state feedback are presented in [11, 22]. In this chapter we will take an alternative approach. First of all, we will present a controller synthesis technique that is based on output feedback. Secondly, we will make use of frequency domain weighting filters to shape the closed-loop dynamics in each regime of the PWL sheet flow model. Hence, the novelty of the controller synthesis that will be carried out in this chapter is that linear H_∞ output-based control design techniques [69] for the dynamics of each subsystem are combined with stability and performance requirements for the switched system. For carrying out the controller synthesis, LMI-based approaches for linear systems known in literature, e.g. [29, 30, 67], are extended to the PWL case. More specifically, the stability and performance requirements for both the subsystems, incorporated via frequency dependent weighting filters, and the switched system, using L_2 -gains, are combined into a joint optimization problem, enforcing both (robust) stability and (robust) performance of the subsystems and the closed-loop switched system.

As in Chapter 3, we will focus initially on sheet feedback control design based on the nominal sheet flow model (2.2), after which control design will be considered that guarantees robust stability and robust performance of the closed-loop system. In this case, however, the output feedback controllers will be based on the dynamics described by the PWL sheet flow model itself, instead of the sheet dynamics in error space. Hence, in this approach the sheet reference profile is not taken into account and does therefore not enforce the structure of the designed controllers, i.e. the resulting controllers are not necessarily PI feedback controllers. By making use of the frequency domain weighting filters for the dynamics in each region of the PWL sheet model, bandwidth requirements on the sheet control loop can be incorporated in the control design. Moreover, the influence of disturbances can be penalized in frequency ranges in which they are present, and desired properties of the controllers, e.g. integral action and high frequency roll-off, can be enforced. Hence, in this way both performance and stability of the closed-loop system in each region can be guaranteed.

Preliminary results of applying nominal H_∞ control design to the paper path case-study are presented in [18]. In [18], the dynamics of the low level motor control loops were taken into account in the design of the sheet feedback controllers. Consequently, the stability of the overall system could be guaranteed via the controller synthesis. However, the approach presented in [18] resulted in sheet feedback controllers of 24-th order. Since in an embedded environment often no dedicated processors are available exclusively for real-time motion control tasks, it is desirable to keep the controller order low to reduce the computational burden imposed by the sheet feedback control loops. Therefore, in this chapter controllers are initially designed based on the nominal PWL sheet flow dynamics in which the controlled motor dynamics are not taken into account, leading to lower order sheet feedback controllers.

After carrying out the nominal control design, extensions to guarantee robust stability and robust performance are presented. Furthermore, as the rule of thumb describing the relation between the high level and low level bandwidth is generally not strictly quantified, a founded stability analysis of the overall system, i.e. the system including the non-ideal low level dynamics, could be desired. As the structure of the model and controller used in this chapter easily allow for a stability analysis, the technique for carrying out this analysis will be presented. Note however, that we do not consider this stability analysis to be a necessary step in the design of sheet feedback control.

4.2 Nominal Sheet Feedback Control Design

4.2.1 Controller Synthesis

In the design of nominal sheet feedback controllers, uncertainties in the system parameters and external disturbances acting on the system are assumed not to be present. Hence, H_∞ feedback controllers will be designed based on the nominal high level PWL sheet model (2.2). Regarding these controllers, there are several desirable properties to be satisfied. From Chapter 3, we know that these controllers should contain an integral action to be able to track linear sheet position profiles with zero error. Secondly, we would like the amplitude of the controllers to roll-off at high frequencies to prevent the low level motor control loops to be excited by high frequency components in the motor reference velocities that cannot be tracked, as in reality the low level motor control loops are not ideal, i.e. not satisfying $T_i(s) = 1, \forall s \in \mathbb{C}, \forall i \in \mathcal{I}$ in (2.3). A third requirement regarding the control design is that it should be possible to take into account bandwidth constraints. All three requirements can be satisfied by designing an augmented plant that, besides the sheet model, contains weighting filters for shaping the closed-loop transfer functions [69]. The augmented plant P_i for region i of the high level sheet model is schematically depicted in the standard plant configuration in Fig. 4.1. The exogenous input w of the augmented plant is chosen to be the sheet reference position. The outputs to be minimized are the weighted sheet tracking error z_e and the weighted high level sheet control output z_u . The measured output v is the sheet tracking error and the output of the high level sheet controller, i.e. the column with motor reference velocities, is represented by \underline{u} . As can be seen from Fig. 4.1, the filter W_e is used to shape the (output) sensitivity function

$$S_i = (I + G_i K_i)^{-1}, i \in \mathcal{I}, \quad (4.1)$$

where G_i represents the high level sheet dynamics in region i , and where K_i represents the high level sheet controller for region i . With this filter the desired bandwidth of the

sheet control loop and the integral action in the controller can be enforced. The single-input single-output (SISO) filter W_e can be represented as follows:

$$\begin{aligned}\dot{\underline{x}}_{W_e} &= A_{W_e}\underline{x}_{W_e} + B_{W_e}v \\ z_e &= C_{W_e}\underline{x}_{W_e} + D_{W_e}v\end{aligned}\quad (4.2)$$

with \underline{x}_{W_e} the state vector of the filter and with A_{W_e} , B_{W_e} , C_{W_e} , and D_{W_e} representing the state matrix, the input matrix, the output matrix, and the throughput matrix of the weighting filter, respectively.

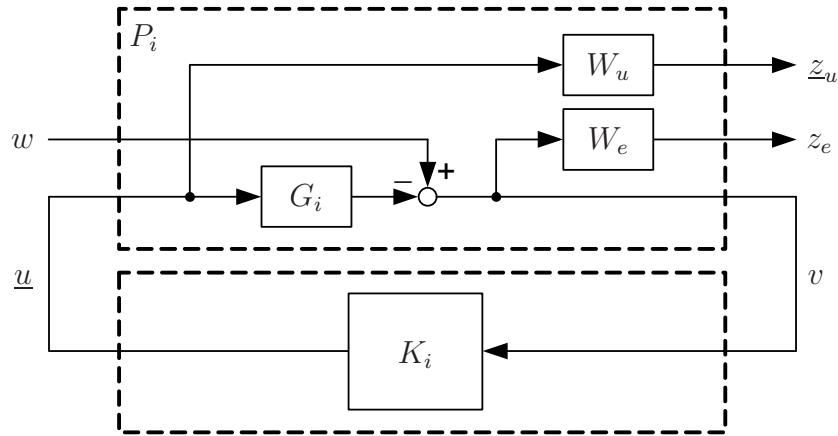


Figure 4.1 / Standard plant configuration for region i .

When (4.1) is reconsidered, it can be observed from the index i of K_i that, in contradiction to Chapter 3, in this chapter different feedback controllers will be used in the various regimes of the high level sheet dynamics. More specifically, sheet feedback controllers are adopted in this chapter that switch synchronously with the sheet dynamics at the switching boundaries. Within each region, the sheet feedback controller that is active will calculate the three control inputs, i.e. the three motor reference velocities, of the high level sheet dynamics. Similar to Chapter 3, the structure of the input matrices of the sheet flow dynamics makes sure that, given the three control inputs calculated, the correct one influences the sheet motion.

Besides W_e , a second filter W_u is used to shape control sensitivity transfer function of region i , defined by

$$R_i = (I + K_i G_i)^{-1} K_i, i \in \mathcal{I}. \quad (4.3)$$

This filter is used to enforce the desired high frequency roll-off in the high level sheet controllers for each regime. This multiple-input multiple-output (MIMO) filter can be represented as

$$\begin{aligned}\dot{\underline{x}}_{W_u} &= A_{W_u}\underline{x}_{W_u} + B_{W_u}\underline{u} \\ \underline{z}_u &= C_{W_u}\underline{x}_{W_u} + D_{W_u}\underline{u}\end{aligned}\quad (4.4)$$

with \underline{x}_{W_u} the state vector of the filter and with A_{W_u} , B_{W_u} , C_{W_u} , and D_{W_u} representing the state matrix, the input matrix, the output matrix, and the throughput matrix of the weighting filter, respectively.

From Fig. 4.1, the interconnection matrices of the augmented plant P_i can be derived. After stacking the inputs and outputs of P_i in columns, we get for P_i

$$\begin{aligned} \begin{bmatrix} z_e \\ \underline{z}_u \\ v \end{bmatrix} &= P_i \begin{bmatrix} w \\ \underline{u} \end{bmatrix} \\ &= \begin{bmatrix} W_e & -W_e G_i \\ 0 & W_u \\ I & -G_i \end{bmatrix} \begin{bmatrix} w \\ \underline{u} \end{bmatrix} \\ &= \begin{bmatrix} P_{11,i} & P_{12,i} \\ P_{21,i} & P_{22,i} \end{bmatrix} \begin{bmatrix} w \\ \underline{u} \end{bmatrix}, i \in \mathcal{I}. \end{aligned} \quad (4.5)$$

Based on the interconnection matrices, the closed-loop transfer functions from w to $\underline{z} = [z_e \ \underline{z}_u^T]^T$ are given by the lower linear fractional transformation (LFT) [69]

$$\underline{z} = N_i w, i \in \mathcal{I}, \quad (4.6)$$

where

$$\begin{aligned} N_i = F_l(P_i, K_i) &\triangleq P_{11,i} + P_{12,i} K_i (I - P_{22,i} K_i)^{-1} P_{21,i} \\ &= \begin{bmatrix} W_e S_i \\ W_u R_i \end{bmatrix}, i \in \mathcal{I}. \end{aligned} \quad (4.7)$$

Besides the requirements on the shape of the closed-loop transfer functions of the individual subsystems, enforced via the weighting filters W_e and W_u in N_i , requirements have also been formulated for the overall switched system. First of all, the stability of the closed-loop switched system has to be guaranteed and, secondly, the switched system has to satisfy performance guarantees in the H_∞ sense, interpreted as an induced L_2 -gain. Before specifying these requirements in further detail, first the closed-loop dynamics of the switched linear system are derived. Hereto, the state space realization of the augmented plant dynamics is derived from the interconnection of the nominal PWL high level sheet dynamics (2.2) and the weighting filters W_e (4.2) and W_u (4.4):

$$\begin{aligned} \dot{\underline{x}} &= A_i \underline{x} + B_{w,i} w + B_{u,i} \underline{u} \\ \underline{z} &= C_{z,i} \underline{x} + D_{zw,i} w + D_{zu,i} \underline{u}, i \in \mathcal{I}. \\ v &= C_{v,i} \underline{x} + D_{vw,i} w \end{aligned} \quad (4.8)$$

In (4.8), $\underline{x} = [x_s \ \underline{x}_{W_e}^T \ \underline{x}_{W_u}^T]^T$ represents the state vector of the augmented plant dynamics, containing the state of the sheet flow model and the states of the filters of the augmented plant. As mentioned in Section 4.1, we propose the use of dynamic output feedback controllers of the form:

$$\begin{aligned}\dot{\underline{\xi}} &= A_{K,i}\underline{\xi} + B_{K,i}v, \\ \underline{u} &= C_{K,i}\underline{\xi} + D_{K,i}v,\end{aligned} \quad i \in \mathcal{I}, \quad (4.9)$$

with $\underline{\xi}$ representing the controller state vector, which is shared by the controllers active in the three regimes, and which therefore remains continuous at the switching boundary, and with $A_{K,i}$, $B_{K,i}$, $C_{K,i}$, and $D_{K,i}$ representing the state matrix, the input matrix, the output matrix, and the throughput matrix of the feedback controller, respectively. Substitution of (4.9) into (4.8) yields the closed-loop dynamics of the switched system:

$$\begin{aligned}\dot{\underline{x}}_{CL} &= \mathcal{A}_i \underline{x}_{CL} + \mathcal{B}_i w, \\ \underline{z} &= \mathcal{C}_i \underline{x}_{CL} + \mathcal{D}_i w,\end{aligned} \quad i \in \mathcal{I}, \quad (4.10)$$

with

$$\left[\begin{array}{c|c} \mathcal{A}_i & \mathcal{B}_i \\ \hline \mathcal{C}_i & \mathcal{D}_i \end{array} \right] = \left[\begin{array}{cc|c} A_i + B_{u,i}D_{K,i}C_{v,i} & B_{u,i}C_{K,i} & B_{w,i} + B_{u,i}D_{K,i}D_{vw,i} \\ B_{K,i}C_{v,i} & A_{K,i} & B_{K,i}D_{vw,i} \\ \hline C_{z,i} + D_{zu,i}D_{K,i}C_{v,i} & D_{zu,i}C_{K,i} & D_{zw,i} + D_{zu,i}D_{K,i}D_{vw,i} \end{array} \right], \quad i \in \mathcal{I}, \quad (4.11)$$

and with $\underline{x}_{CL} = [\underline{x}^T \quad \underline{\xi}^T]^T$ the state vector of the closed-loop dynamics.

Regarding the stability requirement for the closed-loop switched system, it is known that the existence of a *common* quadratic Lyapunov function is a sufficient condition for proving stability of the closed-loop dynamics (4.10) under arbitrary switching:

$$V(x_{CL}) = \underline{x}_{CL}^T \mathcal{P} \underline{x}_{CL}, \quad (4.12)$$

with $\mathcal{P} = \mathcal{P}^T \succ 0$, such that

$$0 \succ \mathcal{A}_i^T \mathcal{P} + \mathcal{P} \mathcal{A}_i, \quad i \in \mathcal{I}. \quad (4.13)$$

The performance requirements for the switched system, on the other hand, are specified by requiring that for zero initial conditions, i.e. $\underline{x}_{CL}(0) = \underline{0}$, the following inequality has to hold:

$$\|\underline{z}\|_2 \leq \gamma \|w\|_2, \quad (4.14)$$

with $\|\underline{z}\|_2^2 := \int_{t_0}^t \underline{z}(\tau)^T \underline{z}(\tau) d\tau$ and $\|w\|_2^2 := \int_{t_0}^t w(\tau)^T w(\tau) d\tau$. This means that the induced L_2 -norm of the operator from w to \underline{z} should be smaller than γ under zero initial conditions for all nonzero $w \in L_2$. This can be obtained via a dissipativity approach [6], by requiring that

$$V(\underline{x}_{CL}(t)) - V(\underline{x}_{CL}(t_0)) \leq \int_{t_0}^t (-\underline{z}(\tau)^T \underline{z}(\tau) + \gamma^2 w(\tau)^T w(\tau)) d\tau, \quad (4.15)$$

with $\gamma \geq 0$, holds under zero initial conditions. Since $V(x_{CL}(t)) \geq 0$ and $V(x_{CL}(t_0)) = 0$, we know that

$$\int_{t_0}^t (-\underline{z}(\tau)^T \underline{z}(\tau) + \gamma^2 w(\tau)^T w(\tau)) d\tau \geq 0, \quad (4.16)$$

which in turn implies (4.14), as required. Since it is possible for the system to stay in only one of the three regimes, (4.14) also has to hold for the individual linear subsystems. In that case, the induced L_2 -norm of the operator from w to \underline{z} represents the H_∞ -norm of N_i [69]:

$$\begin{aligned} \|N_i\|_\infty &= \max_{w \neq 0} \frac{\|\underline{z}\|_2}{\|w\|_2} \\ &\leq \gamma, i \in \mathcal{I}, \end{aligned} \quad (4.17)$$

with

$$\|N_i\|_\infty = \max_{\omega} \bar{\sigma}(N_i(j\omega)), i \in \mathcal{I}. \quad (4.18)$$

Since N_i is defined by (4.7), solving the control design problem for the switched linear system at hand can be interpreted by solving the mixed-sensitivity H_∞ control problem [5, 17, 69] in linear control design cases.

Given the techniques presented in [29, 30, 67], the stability and performance requirements can be formulated in terms of a set of matrix inequalities that, if feasible, guarantee stability of the closed-loop switched system (4.10), together with an upper bound γ on the induced L_2 -norm of the operator from w to \underline{z} :

$$0 \prec \mathcal{P} = \mathcal{P}^T, \quad (4.19)$$

$$0 \succ \begin{bmatrix} \mathcal{A}_i^T \mathcal{P} + \mathcal{P} \mathcal{A}_i & \mathcal{P} \mathcal{B}_i & \mathcal{C}_i^T \\ \mathcal{B}_i^T \mathcal{P} & -\gamma I & \mathcal{D}_i^T \\ \mathcal{C}_i & \mathcal{D}_i & -\gamma I \end{bmatrix}, i \in \mathcal{I}. \quad (4.20)$$

The inequalities (4.19)-(4.20) are matrix inequalities in the free variables \mathcal{P} , γ , $A_{K,i}$, $B_{K,i}$, $C_{K,i}$, and $D_{K,i}$, $i \in \mathcal{I}$. By applying the linearizing change of variables discussed in Appendix A [67], the matrix inequalities (4.19)-(4.20) can be rewritten into the following LMIs with the free variables X , Y , γ , \hat{A}_i , \hat{B}_i , \hat{C}_i , and \hat{D}_i , $i \in \mathcal{I}$:

$$0 \prec \begin{bmatrix} X & I \\ I & Y \end{bmatrix}, \quad (4.21)$$

$$0 \succ \begin{bmatrix} A_i X + X A_i^T + B_{u,i} \hat{C}_i + (B_{u,i} \hat{C}_i)^T & \hat{A}_i^T + (A_i + B_{u,i} \hat{D}_i C_{v,i}) & * & * \\ \hat{A}_i + (A_i + B_{u,i} \hat{D}_i C_{v,i})^T & A_i^T Y + Y A_i + \hat{B}_i C_{v,i} + (\hat{B}_i C_{v,i})^T & * & * \\ (B_{w,i} + B_{u,i} \hat{D}_i D_{vw,i})^T & (Y B_{w,i} + \hat{B}_i D_{vw,i})^T & -\gamma I & * \\ C_{z,i} X + D_{zu,i} \hat{C}_i & C_{z,i} + D_{zu,i} \hat{D}_i C_{v,i} & D_{zw,i} + D_{zu,i} \hat{D}_i D_{vw,i} & -\gamma I \end{bmatrix}, \quad (4.22)$$

where $*$ replaces blocks that can be derived by symmetry. Since γ enters linearly in (4.22), it can be directly minimized by LMI optimization to find the smallest achievable induced L_2 -norm of the operator from w to \underline{z} of the closed-loop system (4.10). If a feasible solution has been found, first nonsingular matrices M and N have to be calculated. From the derivation of the linearizing change of variables in Appendix A, the following relation can be derived:

$$MN^T = I - XY. \quad (4.23)$$

From the singular value decomposition of $I - XY$, M and N can be calculated. Given these nonsingular matrices, the controller matrices can be calculated as follows:

$$\begin{aligned}
 D_{K,i} &= \widehat{D}_i \\
 C_{K,i} &= \left(\widehat{C}_i - D_{K,i} C_{v,i} X \right) M^{-T} \\
 B_{K,i} &= N^{-1} \left(\widehat{B}_i - Y B_{u,i} D_{K,i} \right) \\
 A_{K,i} &= N^{-1} \left(\widehat{A}_i - N B_{K,i} C_{v,i} X - Y B_{u,i} C_{K,i} M^T - Y (A_i + B_{u,i} D_{K,i} C_{v,i}) X \right) M^{-T} \\
 & \quad i \in \mathcal{I}.
 \end{aligned} \tag{4.24}$$

4.2.2 Control Design Results

In the H_∞ control design, the nominal paper path parameters in Table 3.2 have been used. Given these parameters, the design of the weighting filters can be carried out. In each region the same weighting filter for shaping the sensitivity function, W_e , and the same filter for shaping the control sensitivity function, W_u , is chosen, such that in each region the corresponding transfer functions are designed to have the same shape. Both filters are designed to be both stable and biproper. The filter W_e is used to enforce a desired bandwidth and an integral action in the high level sheet controllers. Since in each region the plant to be controlled consists of an integrator, a second order filter is needed to enforce the integral action:

$$W_e(s) = \frac{1}{S_0} \frac{\frac{1}{4\pi^2 f_{BW} f_I} s^2 + \left(\frac{0.7}{2\pi f_{BW}} + \frac{0.7}{2\pi f_I} \right) s + 1}{\frac{S_\infty}{4\pi^2 S_0 f_{BW} f_I} s^2 + \frac{2 \cdot 0.7 \sqrt{S_\infty}}{2\pi \sqrt{S_0} f_{BW} f_I} s + 1}. \tag{4.25}$$

Here, f_{BW} is used to tune the bandwidth and f_I represents the desired cut-off frequency of the integral action. Furthermore, S_0 represents the upper bound on the amplitude of the sensitivity function for $s \rightarrow 0$, whereas S_∞ represents the upper bound on the amplitude for $s \rightarrow \infty$. In the paper path case-study, f_{BW} has been chosen to be 12 Hz, i.e. slightly larger than the desired bandwidth of 10 Hz, since the sensitivity function will not be exactly equal to the inverse of its weighting filter. The cut-off frequency of the integral action has been chosen to be $f_I = 1/5 \cdot f_{BW} = 2.4$ Hz to prevent much phase lag at the desired bandwidth. The low frequency and high frequency bounds on the sensitivity function have been chosen to be -150 dB and 6 dB, respectively, yielding $S_0 = 10^{-\frac{150}{20}}$ and $S_\infty = 10^{\frac{6}{20}}$. The low frequency bound has been chosen such that an integral action is obtained in a large low frequency range, whereas the high frequency bound has been chosen to limit the maximum magnitude of the sensitivity function to 6 dB. The resulting

weighting filter W_e is depicted in Fig. 4.2(a). As can be seen, in the low-frequency range W_e has a zero slope to prevent inserting a pole in $\omega = 0$ in the augmented plant, that cannot be stabilized by the controller. For mid-range frequencies W_e has a slope of -2 , corresponding to the desired -1 slope of the controller, i.e. the integral action, and the -1 slope of the high level sheet dynamics. For high frequencies, W_e again has a zero slope.

In Fig. 4.1, W_u is selected to represent a matrix with a SISO weighting filter w_u on each diagonal element and with zeros on all other elements. By weighting each control input with the weighting filter given by

$$w_u(s) = \frac{\frac{1}{2\pi f_{ro}}s + 1}{\frac{R_\infty}{2\pi f_{ro}}s + R_0}, \quad (4.26)$$

a high frequency roll-off can be enforced in the controller. In (4.26), f_{ro} represents the desired roll-off frequency, whereas R_0 and R_∞ represent the upper bound on the amplitude of the control sensitivity when $s \rightarrow 0$ and $s \rightarrow \infty$, respectively. In (4.26), f_{ro} has been chosen to be $f_{ro} = 50$ Hz, i.e. equal to the expected bandwidth of the motor control loops. The low frequency and high frequency bounds on the control sensitivity function have been chosen to be 100 dB and 40 dB, respectively, yielding $R_0 = 10^{\frac{100}{20}}$ and $R_\infty = 10^{\frac{40}{20}}$. These bounds have been chosen such that the sheet feedback controllers will have a roll-off characteristic in a large frequency range. The choices on the filter parameters result in the weighting filter shown in Fig. 4.2(b). Since $S_i \approx 1$ for frequencies well above the bandwidth, the control sensitivity R_i can be approximated by the controller in this region. Hence, for high frequencies we are weighing the controller and therefore the desired roll-off can be shaped.

Given the high level sheet dynamics (2.2), together with the weighting filters (4.25) and (4.26), a feasible solution of the LMIs (4.21)-(4.22) can be found. The resulting value of γ obtained after optimization is $\gamma \approx 0.58$. Also the H_∞ -norms of N_i are $\|N_i\|_\infty \approx 0.58$. From Fig. 4.3, which shows the maximum singular values of the first closed-loop subsystem as a function of the frequency, it can be seen that the resulting value of γ is approached by these maximum singular values, but not exceeded.¹ To obtain an indication about the loss of subsystem performance due to the controller design based on the PWL sheet flow model, carried out for giving stability and performance guarantees of the switched system, H_∞ feedback controllers have also been calculated based on the dynamics of the individual subsystems. The resulting values of γ are all approximately equal to 0.56, which is only a little smaller than the γ -value obtained from the combined control design. Hence, the loss of performance in the proposed approach is limited.

¹The discussion on the control design results obtained in this subsection will mainly focus on the results obtained for the first subsystem. Similar results have been obtained for the second and third subsystem and will therefore not be discussed.

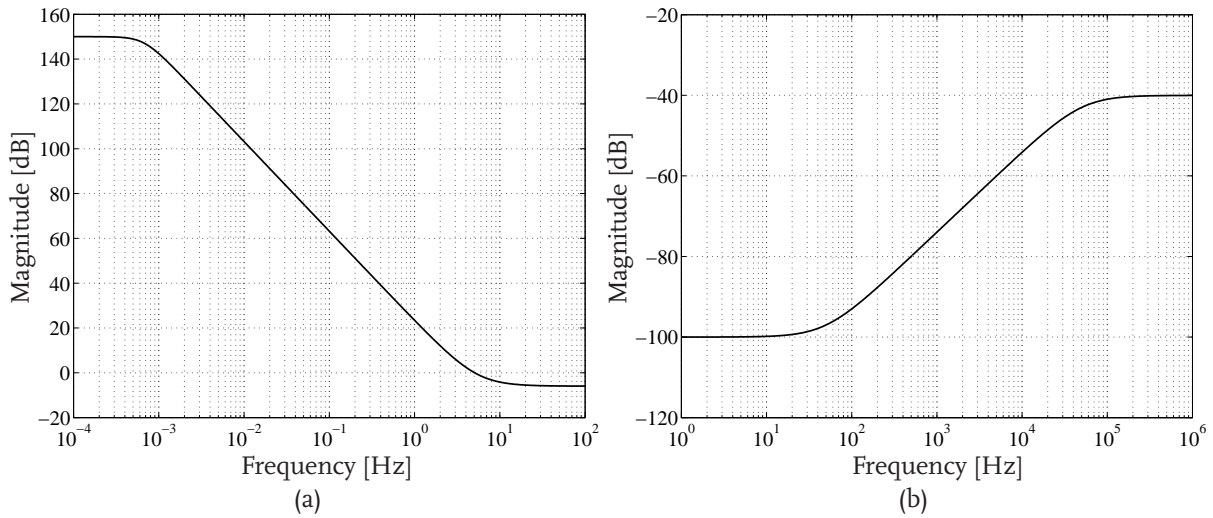


Figure 4.2 / Bode plots of the weighting filters W_e (a), and w_u (b).

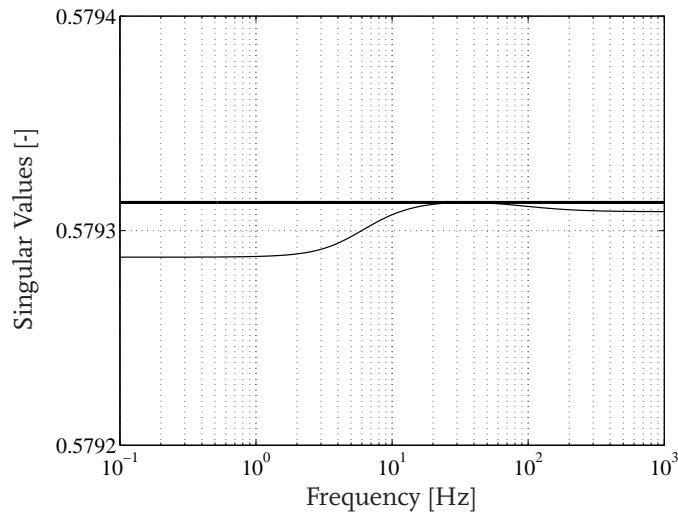


Figure 4.3 / Maximum singular values of N_1 as a function of frequency (thin) together with the value of γ (thick).

The Bode plot of the controller for the first subsystem of the sheet dynamics can be seen in Fig.4.4(a). From the figure it becomes clear that both the desired integral action and the high frequency roll-off have been realized. Using the controller and the sheet dynamics active in the first region of the PWL sheet model, the loop gain for this region can be calculated, resulting in the Bode plot shown in Fig.4.4(b). From this figure, it can be seen that the bandwidth of the first controlled subsystem is approximately 10 Hz, i.e. significantly lower than typical bandwidths of the low level motor control loops, as desired according to Section 2.3. From Fig. 4.4(b) we can also observe the stability of

the first subsystem, as this is guaranteed by the design. Since at the crossover frequency the phase lag is approximately 110° , the subsystem is stable and the phase margin is approximately 70° .

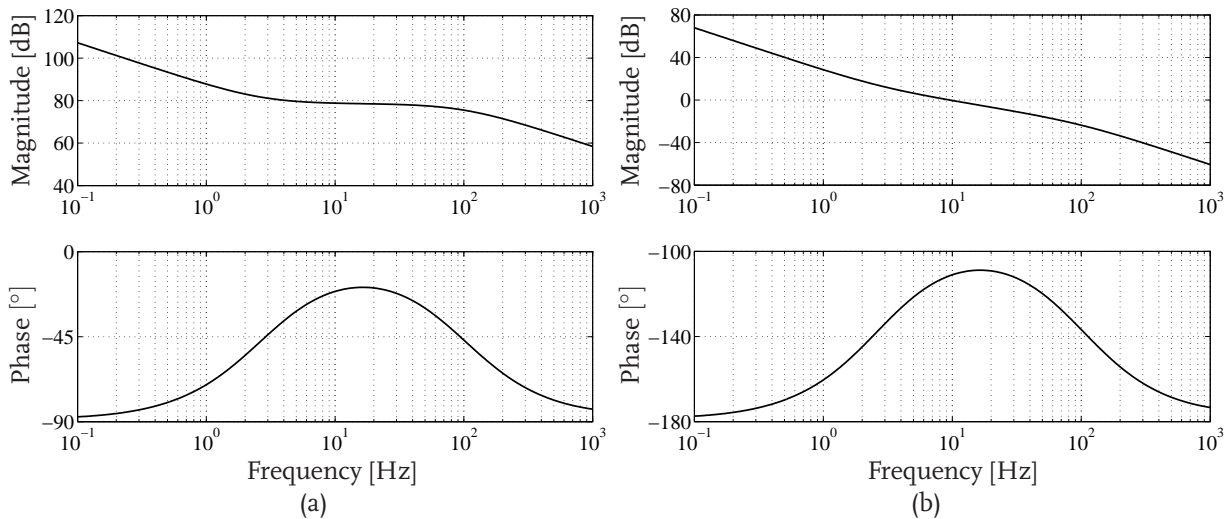


Figure 4.4 / Bode plots of the sheet feedback controller (a), and the loop gain (b) of the first subsystem.

In Fig. 4.5(a) the Bode plot of the designed sensitivity function of the first subsystem is shown, together with the inverse of the weighting filter W_e . As already expected from the fact that $\gamma < 1$, it can be seen that $|S_1(j\omega)| < |W_e^{-1}(j\omega)|, \forall \omega$, which leads to the conclusion that the obtained sensitivity function meets the design criteria. The same conclusion can be drawn for the control sensitivity function that has been designed. As can be seen from Fig. 4.5(b), which shows the inverse of the weighting filter w_u together with the control sensitivity function of the first subsystem, also in this case the inverse of the weighting filter upperbounds the corresponding closed-loop transfer function: $|R_1(j\omega)| < |w_u^{-1}(j\omega)|, \forall \omega$.

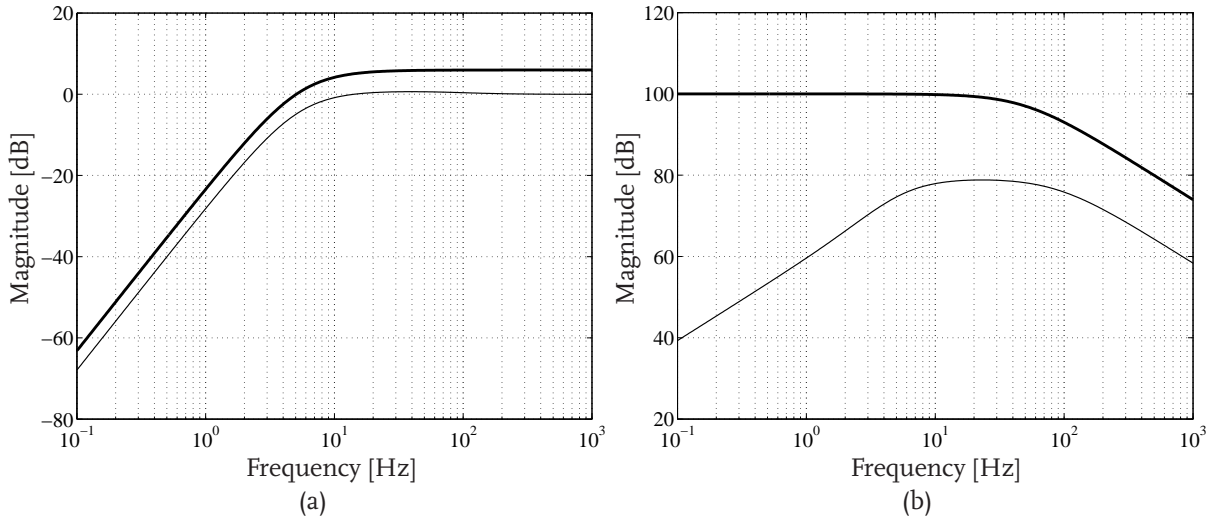


Figure 4.5 / Bode plots of the inverse of W_e (thick) and S_1 (thin) (a), and the inverse of w_u (thick) and R_1 (thin) (b).

4.2.3 Simulation Results

As in Sections 3.2.3 and 3.3.2, simulations of the nominal high level sheet flow model in combination with the designed sheet feedback controllers have been conducted for the basic paper path case-study to demonstrate the effectiveness of the control design approach. In these simulations, the nominal paper path and sheet parameters in Table 3.2 have been used. The difference with the simulations carried out in the previous chapter is that in this case we are dealing with a switching controller. This implies that state information of the plant dynamics, i.e. the sheet position, is needed in the implementation of the switching controller. More specifically, the sheet position is needed to properly switch between controllers based on the active regime of these dynamics.

Given the calculated sheet feedback controllers, the sheet tracking error depicted in Fig. 4.6 is obtained. It can be seen that a similar response to the ones shown in Figs. 3.2(a) and 3.4 has been obtained, i.e. the sheet controller anticipates quickly to the initial error, due to the difference in actual and desired sheet velocity at $t = 0.25$ s. Zooming in on the obtained tracking error shows two phenomena. First of all, it can be seen that the steady state tracking error in the regimes is not equal to zero. This is caused by the fact that the controller does not contain a pure integrator, which results from the fact that W_e has a zero slope in the low-frequency range. Furthermore, from Fig. 4.6 an increase of the sheet tracking error of approximately $5 \cdot 10^{-7}$ m when entering the next pinch can be observed. This indicates that a jump in \dot{e}_s has occurred resulting from the fact that the circumferential pinch velocities are not completely synchronized when transferring

a sheet from one pinch to the other. This phenomenon may occur since this synchronization was not taken into account in the control design. At this point, a connection to Chapter 3 can be made, since also in that chapter it was shown that jumps in \dot{e}_s can occur. The difference between this chapter and the previous one is that in Chapter 3 the system was formulated in terms of its error dynamics. Hence, in that case \dot{e}_s was part of the system's state vector and therefore explicitly taken into account in the Lyapunov function. Consequently, the sheet feedback controller was forced to have a certain structure to enforce the origin to be a globally asymptotically stable equilibrium in the sense of Lyapunov. In this chapter, \dot{x}_s , i.e. the variable related to \dot{e}_s , is not part of the state vector of the closed-loop dynamics. Hence, no structure of the sheet feedback controller has to be enforced in this case and the whole design procedure implicitly accounts for possible discontinuities in \dot{x}_s and \dot{e}_s .

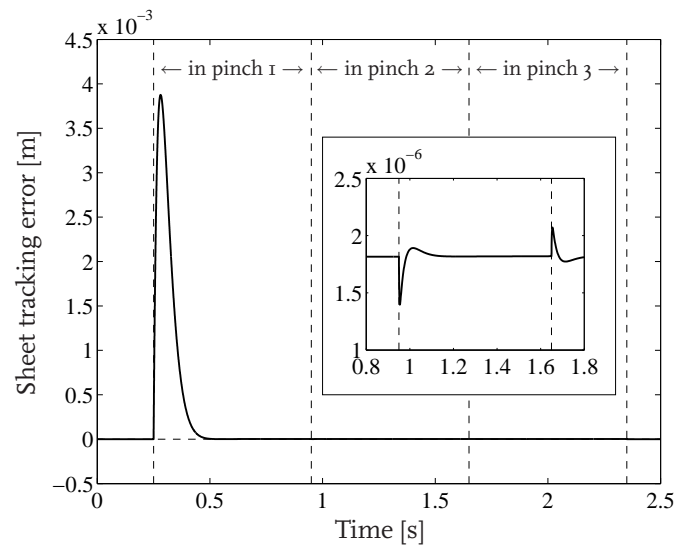


Figure 4.6 / Sheet tracking error obtained in simulation.

Despite the fact that perturbations of the paper path parameters were not taken into account in the control design, an indication about the robustness of the closed-loop system obtained using the nominal sheet feedback controllers can be obtained via simulations. For this purpose, the actual gains of the second and third subsystem vary 14% and 3% with respect to their nominal values, respectively. Hence, the actual values presented in Table 3.2 have been used in the simulation. The tracking error obtained using these perturbed gains is depicted in Fig. 4.7. It can be seen that the closed-loop system is again stable. The tracking error deviates from zero right after the switching boundaries, caused by the perturbation of the transmission ratios. The maximum deviation from the desired zero error level is approximately $5.8 \cdot 10^{-4}$ m. This is slightly larger than the maximum deviation obtained in Section 3.3.2, which is caused by the fact that the bandwidth of the controlled system in that section was slightly larger than the one obtained in Section 4.2.2.

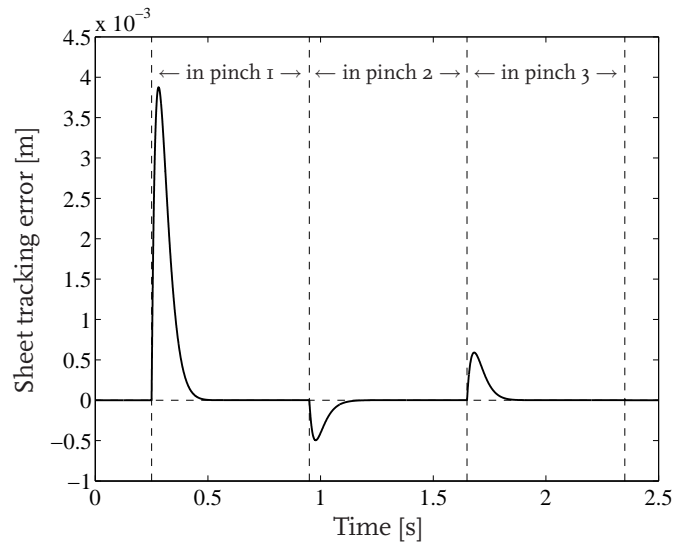


Figure 4.7 / Sheet tracking error obtained in simulation, with perturbation of the nominal transmission ratios.

From Fig. 4.7 we can conclude that the performance properties defined in Section 1.4 are satisfied for this case, despite the fact that the parameter uncertainties have not been taken into account in the control design procedure. Hence, a priori guarantees on robust stability and robust performance cannot be given. To be able to give such guarantees, in the next section we will extend the control design approach such that parameter uncertainties are incorporated in the synthesis.

4.3 Robust Sheet Feedback Control Design

4.3.1 Uncertainty Modeling

The robust control design discussed in this section will be carried out based on the PWL high level sheet model with uncertain paper path parameters (3.42), presented in Section 3.3. The control goal in this section is to make the system robustly stable for the parameter uncertainties. Furthermore, robust performance has to be realized. This implies that performance conditions will have to be satisfied for all possible plants, i.e. including the worst-case uncertainty [69]. To realize this goal, we will use the H_∞ control paradigm presented in Section 4.2.1 and we will extend it to include the uncertainties in the parameters into the design framework.

The first topic to be addressed in the robust control design approach is to determine the uncertainty set, i.e. to find a mathematical representation of the model uncer-

tainty [69, 77]. From the PWL high level sheet model with uncertain paper path parameters (3.42), it can be observed that the structure of the model is assumed to be known, but some of the parameters are uncertain. Therefore, we are dealing with parametric, real-valued uncertainties. These uncertainties are quantified by assuming that the parameter combinations $\psi_i = n_i r_{\psi_i}$ in the input matrices B_i are bounded and their values are assumed to be in a known region $[\underline{\psi}_i, \bar{\psi}_i]$. In other words, parameter sets of the form

$$\psi_i = \tilde{\psi}_i (1 + r_{\psi_i} \delta_i), i \in \mathcal{I}, \quad (4.27)$$

can be formulated. In (4.27), $\tilde{\psi}_i \triangleq \frac{\bar{\psi}_i + \underline{\psi}_i}{2}$ represents the mean parameter value, $r_{\psi_i} = \frac{\bar{\psi}_i - \underline{\psi}_i}{\bar{\psi}_i + \underline{\psi}_i}$ represents the relative uncertainty, and δ_i is any real scalar satisfying $|\delta_i| \leq 1$. Since the perturbation δ_i is real-valued, the parametric uncertainty can be represented in the H_∞ framework [69]. This can be illustrated by rewriting the model of the sheet dynamics in each region in transfer function format:

$$G_{\delta,i}(s) = \Psi_i G_{0,i}(s), i \in \mathcal{I}, \quad (4.28)$$

with $G_{\delta,i}$ representing the set of possible plants, $G_{0,i}(s) = \frac{1}{s}$, and $\Psi_1 = [\psi_1 \ 0 \ 0]$, $\Psi_2 = [0 \ \psi_2 \ 0]$, and $\Psi_3 = [0 \ 0 \ \psi_3]$. Given this representation, the parametric, real-valued uncertainty can be rewritten as a multiplicative input uncertainty:

$$G_{\delta,i}(s) = \underbrace{\tilde{\Psi}_i G_{0,i}(s)}_{G_i(s)} (I + W_{\delta,i} \Delta), i \in \mathcal{I}, \quad (4.29)$$

with $\tilde{\Psi}_i$ defined as $\tilde{\Psi}_1 = [\tilde{\psi}_1 \ 0 \ 0]$, $\tilde{\Psi}_2 = [0 \ \tilde{\psi}_2 \ 0]$, and $\tilde{\Psi}_3 = [0 \ 0 \ \tilde{\psi}_3]$. Furthermore, $G_i(s)$ represents the nominal plant, $W_{\delta,i}$ is the uncertainty matrix for region i containing the relative uncertainty r_{ψ_i} on the i -th diagonal element and zeros on the other elements, and Δ is a diagonal matrix containing the real-valued scalars δ_i , with $|\delta_i| \leq 1$. Hence, for Δ it holds that $\|\Delta\|_\infty \leq 1$. This multiplicative input uncertainty can be represented by the block diagram in Fig. 4.8.

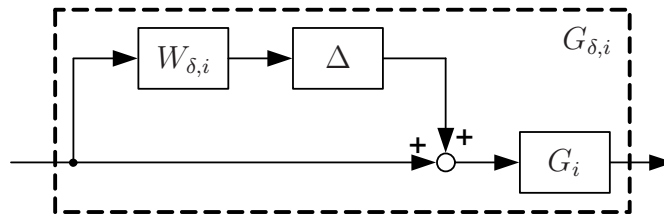


Figure 4.8 / Block scheme representing the multiplicative input uncertainty of subsystem i .

4.3.2 Controller Synthesis

Given the description of the uncertainty present in the system, in this section the goal is to synthesize sheet feedback controllers such that the performance properties presented in Section 1.4 are satisfied for all possible plants. As in Section 4.2.1, also in this case the sheet feedback controllers should have an integral action to closely track the sheet reference profiles, and a high frequency roll-off to prevent the low level motor control loops to be excited by high frequency components in the motor reference velocities. Moreover, it should be possible to tune the sheet controllers such that a desired bandwidth can be realized. To realize this goal, we combine the standard plant configuration for region i , shown in Fig. 4.1 with the multiplicative input uncertainty of the dynamics in this region. This results in the standard plant configuration shown in Fig. 4.9. In this configuration, the exogenous inputs \underline{w}_1 and w_2 represent the input resulting from the uncertainty and the sheet reference position, respectively, whereas z_1 represents the output resulting from the uncertainty. As in Section 4.2.1, the outputs to be minimized, i.e. z_u and z_e , represent the weighted high level sheet control output and the weighted sheet tracking error, whereas the measured output v represents the sheet tracking error and the output of the high level sheet controller is represented by \underline{u} .

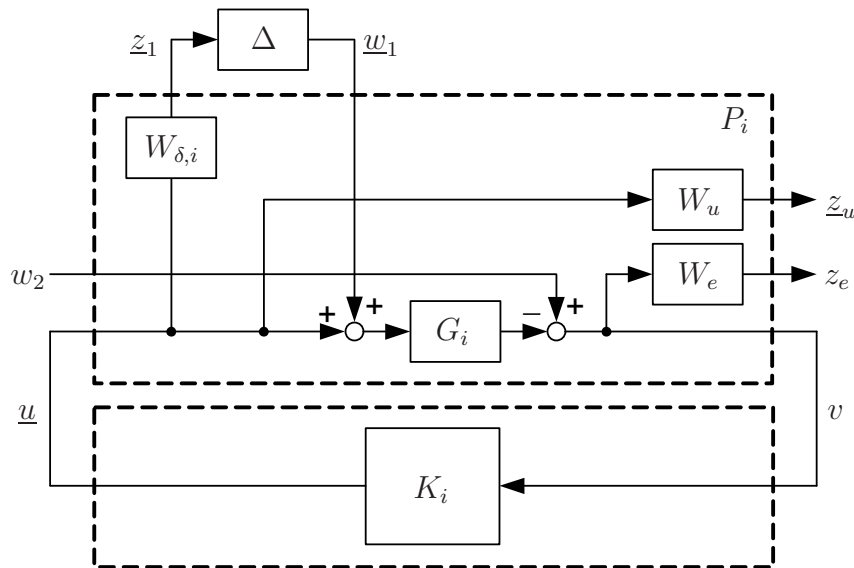


Figure 4.9 / Standard plant configuration for region i .

Given the augmented plant P_i shown in Fig. 4.9, its interconnection matrices can be derived:

$$\begin{aligned}
\begin{bmatrix} \underline{z}_1 \\ z_e \\ \underline{z}_u \\ v \end{bmatrix} &= P_i \begin{bmatrix} \underline{w}_1 \\ w_2 \\ \underline{u} \end{bmatrix} \\
&= \left[\begin{array}{cc|c} 0 & 0 & W_{\delta,i} \\ -W_e G_i & W_e & -W_e G_i \\ 0 & 0 & W_u \\ \hline -G_i & I & -G_i \end{array} \right] \begin{bmatrix} \underline{w}_1 \\ w_2 \\ \underline{u} \end{bmatrix}, i \in \mathcal{I}.
\end{aligned} \tag{4.30}$$

Based on the interconnection matrices, the closed-loop transfer functions from $\underline{w} = [\underline{w}_1^T \ w_2]^T$ to $\underline{z} = [\underline{z}_1^T \ z_e \ \underline{z}_u^T]^T$ are again given by the lower LFT

$$\underline{z} = N_i \underline{w}, i \in \mathcal{I}, \tag{4.31}$$

with

$$N_i = \left[\begin{array}{c|c} -W_{\delta,i} T_i & W_{\delta,i} R_i \\ \hline -W_e S_{p,i} & W_e S_i \\ -W_u T_i & W_u R_i \end{array} \right], i \in \mathcal{I}. \tag{4.32}$$

In (4.32)

$$T_i = (I + K_i G_i)^{-1} K_i G_i, i \in \mathcal{I}, \tag{4.33}$$

represents the (input) complementary sensitivity function of subsystem i , whereas

$$S_{p,i} = (I + G_i K_i)^{-1} G_i, i \in \mathcal{I}, \tag{4.34}$$

represents the (output) process sensitivity function. By inspection of (4.32) it can be seen that W_e will affect both the sensitivity function and the process sensitivity function. Since this filter is designed to weigh the sensitivity function to create an integral action in the controller at low frequencies, applying this weight to the process sensitivity function will result in a penalty at low frequencies that is too demanding, resulting in a double integral action in the controller. To avoid this, a different standard plant configuration will be used, which is shown in Fig. 4.10. In this configuration, the exogenous input \underline{w}_2 is chosen as a disturbance acting on the high level sheet control output \underline{u} , instead of the sheet reference position. This choice does not change our control problem, as we use this control design approach to shape certain closed-loop transfer functions. Since the outputs to be minimized, i.e. \underline{z}_u and z_y represent in this case the weighted high level sheet control output and the weighted high level plant output, respectively, weighing of the complementary sensitivity function and the process sensitivity function is possible. The weighting filter W_u penalizes the control input \underline{u} and can therefore be used to enforce a high frequency roll-off in the controller. Furthermore, in combination with the filter W_y , it can be used to realize the desired bandwidth of the controlled system. Furthermore, the filter W_y is used for penalizing the plant output y and can therefore be used to enforce the integral action in the controller. Both filters can be represented in analogy with (4.4) and (4.2), respectively.

the feedback controllers (4.9), the closed-loop dynamics of the uncertain switched system can be represented by (4.10)-(4.11). As in Section 4.2.1, a common quadratic Lyapunov function is proposed for proving the stability of the closed-loop system subject to parametric uncertainties. Regarding the performance specifications, it is required that the induced L_2 -norm of the operator from the performance input \underline{w}_2 to the performance output $[z_y \ z_u^T]^T$ is smaller than γ under zero initial conditions and for all plants in the uncertainty set $G_{\delta,i}$. This can be achieved by requiring that the matrix inequalities (4.19)-(4.20) hold for a $\gamma \leq 1$. Indeed, this would imply that for a common quadratic Lyapunov function $V(\underline{x}_{CL}) = \underline{x}_{CL}^T \mathcal{P} \underline{x}_{CL}$ the following inequality holds under zero initial conditions:

$$\begin{aligned} V(\underline{x}_{CL}(t)) - V(\underline{x}_{CL}(t_0)) &\leq \int_{t_0}^t (-\underline{z}(\tau)^T \underline{z}(\tau) + \gamma^2 \underline{w}(\tau)^T \underline{w}(\tau)) \, d\tau \\ &= \int_{t_0}^t (-\underline{z}_1(\tau)^T \underline{z}_1(\tau) - z_y(\tau)^T z_y(\tau) - \underline{z}_u(\tau)^T \underline{z}_u(\tau)) \, d\tau \\ &\quad + \gamma^2 \int_{t_0}^t (\underline{w}_1(\tau)^T \underline{w}_1(\tau) + \underline{w}_2(\tau)^T \underline{w}_2(\tau)) \, d\tau, \end{aligned} \quad (4.38)$$

with $\gamma \geq 0$. Since $\|\Delta\|_\infty \leq 1$, the following holds:

$$\|\underline{w}_1\|_2^2 \leq \|\underline{z}_1\|_2^2. \quad (4.39)$$

Consequently,

$$\int_{t_0}^t -\underline{z}_1(\tau)^T \underline{z}_1(\tau) \, d\tau + \gamma^2 \int_{t_0}^t \underline{w}_1(\tau)^T \underline{w}_1(\tau) \, d\tau \leq 0, \quad (4.40)$$

with $\gamma^2 \leq 1$. From the combination of (4.38) and (4.40), it can be concluded that, since $V(\underline{x}_{CL}(t)) \geq 0$ and $V(\underline{x}_{CL}(t_0)) = 0$, the induced L_2 -norm of the operator from the performance input \underline{w}_2 to the performance output $[z_y \ z_u^T]^T$ is smaller than γ under zero initial conditions and for all plants in the uncertainty set $G_{\delta,i}$:

$$\| [z_y \ z_u^T]^T \|_2 \leq \gamma \|\underline{w}_2\|_2, \quad (4.41)$$

with $0 \leq \gamma \leq 1$.

Given this result, the robust controller synthesis procedure can be applied in analogy with the one described in Section 4.2.1, i.e. the set of matrix inequalities (4.19)-(4.20) can be rewritten into the LMIs (4.21)-(4.22) after applying the linearizing change of variables discussed in Appendix A. The goal is again to minimize γ by LMI optimization to find the smallest achievable induced L_2 -norm of the operator from \underline{w} to \underline{z} of the closed-loop system, while requiring $0 \leq \gamma \leq 1$. At this point it should be noted that, similar as in robust H_∞ control design for non-switched systems, conservatism in the analysis of the robust performance property will occur. For the latter class of systems μ -analysis [20, 49, 69, 83] or μ -synthesis [69, 74, 84] can be carried out in order to avoid such conservatism. For switched systems, however, this analysis cannot be directly applied. Since the control design results presented in the next subsection turn out to be satisfactory, this type of analysis and synthesis is not further explored in this specific case. Consequently, when interpreting the obtained results, one should realize that these results can be conservative and that improvements in the design might be possible.

4.3.3 Control Design Results

The robust H_∞ control design has been carried out based on the paper path parameters presented in Table 3.2. The introduction of the additional transmission ratio of 16/30, used to verify the robustness of the system, results in uncertainty matrices $W_{\delta,i}$ containing the relative uncertainties $r_{\psi,1} = 0.05$, $r_{\psi,2} = 0.07$, and $r_{\psi,1} = 0.03$, respectively. The filters W_y and W_u , are used to realize the desired shape of the high level sheet controllers. As in Section 4.2.2, the filters W_y and W_u are again chosen the same for each region to enforce the same performance for each subsystem.

As can be seen from (4.37), W_y is used to shape the process sensitivity function and can therefore be used to enforce an integral action in the controller. Since in each region the plant to be controlled consists of an integrator, whereas the desired sensitivity function has a +2 slope for low frequencies, the desired process sensitivity has a +1 slope in that frequency range. Therefore, W_y is chosen to be a first order filter:

$$W_y(s) = \frac{\frac{1}{2\pi f_I} s + 1}{\frac{S_{p,\infty}}{2\pi f_I} s + S_{p,0}}. \quad (4.42)$$

Here, f_I represents the desired cut-off frequency of the integral action, whereas $S_{p,0}$ and $S_{p,\infty}$ represent the upper bound on the amplitude of the process sensitivity function for $s \rightarrow 0$ and $s \rightarrow \infty$, respectively. To facilitate the design of this filter, the plant dynamics have been scaled such that its gain is equal to 0 [dB] at the desired bandwidth, i.e. at 10 Hz. Since also the magnitude of the sensitivity function is approximately equal to 0 [dB] around the bandwidth, the magnitude of the process sensitivity will be in the proximity of 0 [dB] at this frequency as well. As a result, the magnitude of the weighting filter W_y can now be easily chosen. The parameter f_I has been chosen to be 4 Hz, i.e. well below the desired bandwidth of 10 Hz to avoid much phase lag at this frequency. The low frequency and high frequency bounds on the process sensitivity function have been chosen to be 12 dB and -60 dB, respectively, yielding $S_{p,0} = 10^{\frac{-60}{20}}$ and $S_{p,\infty} = 10^{\frac{12}{20}}$. This way, the inverse of W_y properly overbounds the process sensitivity function and the integral action in the controller is present in a large low frequency range. Using these parameters, the filter shown in Fig. 4.11(a) has been obtained.

The weighting filter w_u is used for shaping the complementary sensitivity function T_i , as can be seen from (4.37). Since $T_i \approx K_i G_i$ for frequencies well above the bandwidth, w_u can be used to enforce a high frequency roll-off in the controller by shaping T_i . To realize this, a second order filter is needed, coinciding with the -2 slope of $K_i G_i$ at high frequencies:

$$w_u(s) = \frac{1}{T_\infty} \frac{\frac{1}{4\pi^2 f_{BW} f_{ro}} s^2 + \left(\frac{0.7}{2\pi f_{BW}} + \frac{0.7}{2\pi f_{ro}} \right) s + 1}{\frac{T_0}{4\pi^2 T_\infty f_{BW} f_{ro}} s^2 + \frac{2 \cdot 0.7 \sqrt{T_0}}{2\pi \sqrt{T_\infty} f_{BW} f_{ro}} s + 1}. \quad (4.43)$$

In (4.43), f_{BW} is used to tune the bandwidth and f_{ro} represents the desired roll-off frequency. Furthermore, T_0 represents the upper bound on the amplitude of the complementary sensitivity function for $s \rightarrow 0$, whereas T_∞ represents the upper bound on the amplitude for $s \rightarrow \infty$. The parameter f_{BW} has been tuned to realize the desired bandwidth, yielding $f_{BW} = 7$ Hz and f_{ro} has been chosen to be $f_{ro} = 50$ Hz, i.e. equal to the expected bandwidth of the motor control loops. The bounds on the amplitude of the complementary sensitivity function have been chosen to be 12 dB and -120 dB, respectively, yielding $T_0 = 10^{-\frac{120}{20}}$, and $T_\infty = 10^{\frac{12}{20}}$. This way, the inverse of w_u properly overbounds the complementary sensitivity function and the roll-off in the controller is present in a large frequency range. The resulting weighting filter w_u is depicted in Fig. 4.11(b).

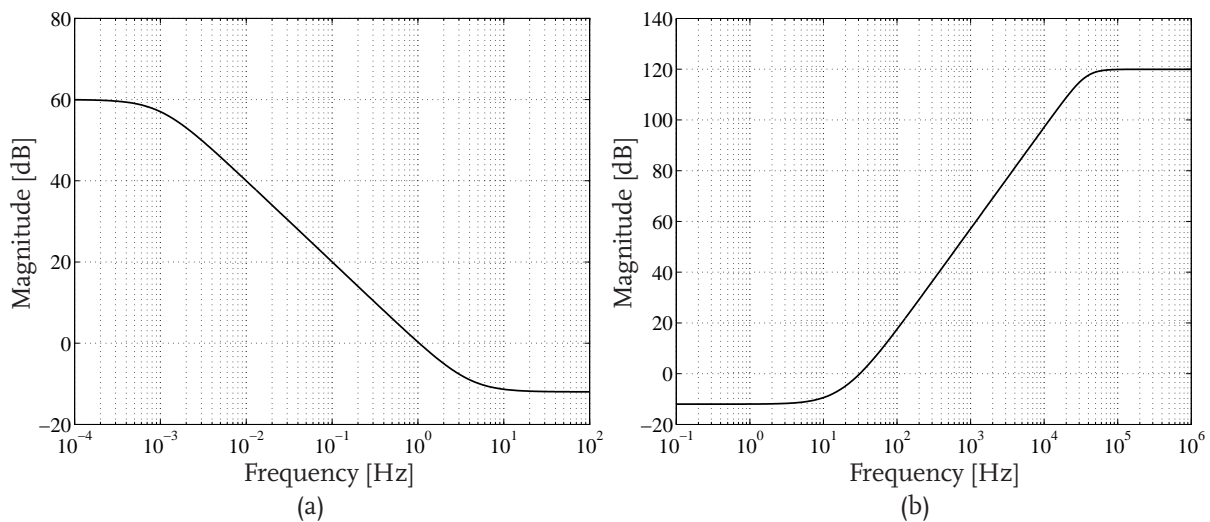


Figure 4.11 / Bode plots of the weighting filters W_y (a), and w_u (b).

Based on the high level sheet dynamics, together with the designed weighting filters, a feasible solution of the LMIs (4.21)-(4.22) can be found, resulting in $\gamma \approx 0.89$. Note that in the robust control design approach performance was traded in for robustness, as the obtained value of γ is larger than the one obtained in the nominal control design. The H_∞ -norms of N_i are $\|N_i\|_\infty \approx 0.88$. In Fig. 4.12 the maximum singular values of the first closed-loop subsystem are shown as a function of the frequency. It can be seen that the resulting value of γ is not exceeded by these singular values.² Since the H_∞ -norm of the Δ block shown in Fig. 4.10 is smaller than 1, and since also $\gamma < 1$, robust stability and robust performance of the closed-loop system have been obtained. Hence, it can be concluded that the small-gain theorem [17, 49, 69] for linear systems also holds for switched linear systems.

²The discussion on the control design results obtained in this subsection will again mainly focus on the results obtained for the first subsystem. Similar results have been obtained for the second and third subsystem and will therefore not be discussed.

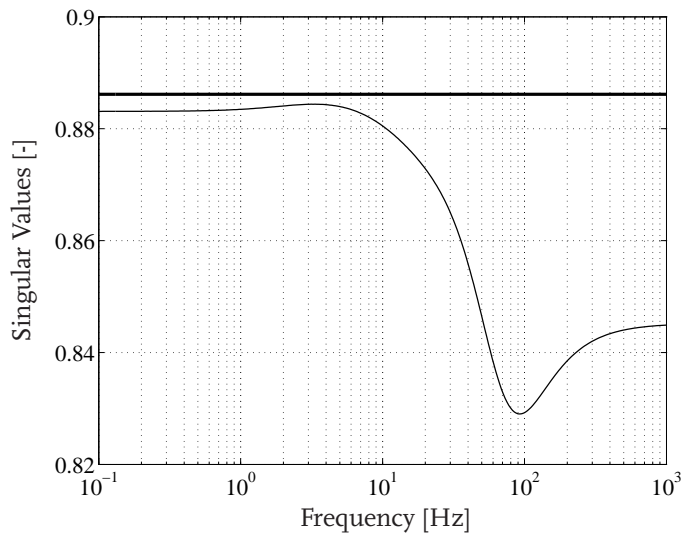


Figure 4.12 / Maximum singular values of N_1 as a function of frequency (thin) together with the value of γ (thick).

Also for the robust control design case, controllers have been designed based on the dynamics in the individual subsystems to obtain an indication about the loss of subsystem performance due to the fact the controller design is based on the PWL sheet flow model. The resulting values of γ are all approximately equal to 0.59, which is smaller than the γ -value obtained from the combined control design. Hence, in case of robust control design based on the switched dynamics, some subsystem performance is lost in comparison with the individual control design.

In Fig. 4.13(a), the Bode plot of the controller for the first subsystem of the sheet dynamics is shown. From the figure it becomes clear that both the desired integral action and the high frequency roll-off have been realized. Comparing Fig. 4.13(a) with Fig. 4.4(a), a large difference in gain can be noticed. This is due to the scaling of the plant in the design of the weighting filters. Before implementation in simulation or experiments, the controllers should be scaled with the same factor as used in scaling the plant dynamics. Given the sheet feedback controller and the sheet dynamics in the first region of the PWL model, the loop gain for this region can be calculated, resulting in the Bode plot shown in Fig. 4.13(b). From this figure, it can be seen that the bandwidth of the first controlled subsystem is approximately 10 Hz, i.e. significantly lower than typical bandwidths of the low level motor control loops, as desired according to Section 2.3. From Fig. 4.13(b) we can also observe the stability of the first subsystem, as this is guaranteed by the design. Since at the crossover frequency the phase lag is approximately 110° , the subsystem is stable and the phase margin is approximately 70° .

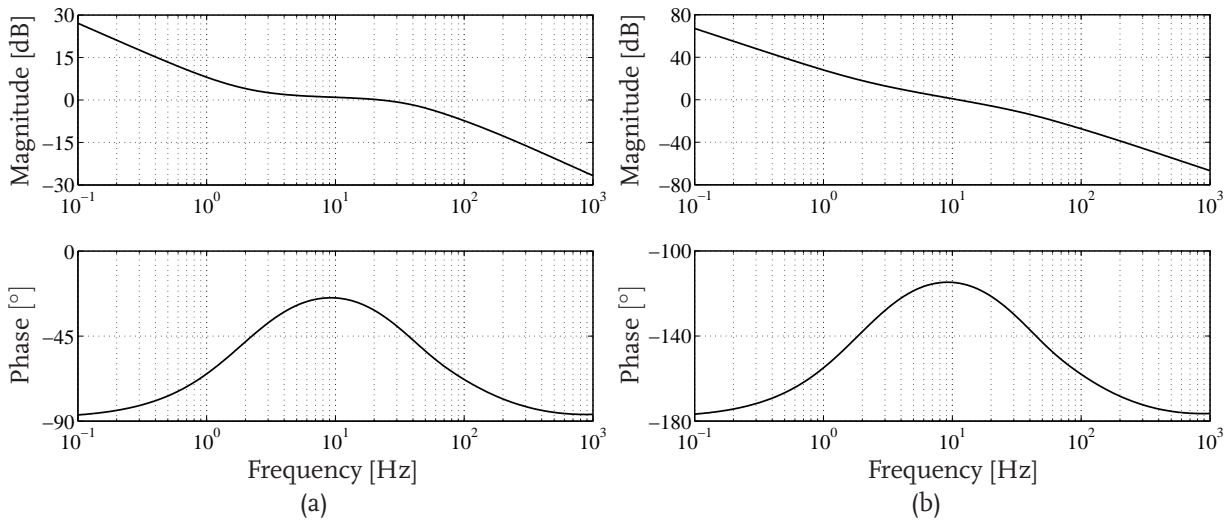


Figure 4.13 / Bode plots of the (scaled) sheet feedback controller (a), and the loop gain (b) of the first subsystem.

The Bode plot of the designed process sensitivity function of the first subsystem is shown in Fig. 4.14(a), together with the inverse of the weighting filter W_y . Since $|S_{p,1}| < |W_y^{-1}|, \forall \omega$, which was already expected from the fact that $\gamma < 1$, it can be concluded that the obtained process sensitivity function meets the design criteria. Since also $|T_1| < |w_u^{-1}|, \forall \omega$, as can be seen in Fig. 4.14(b), the same conclusion can be drawn for the complementary sensitivity function.

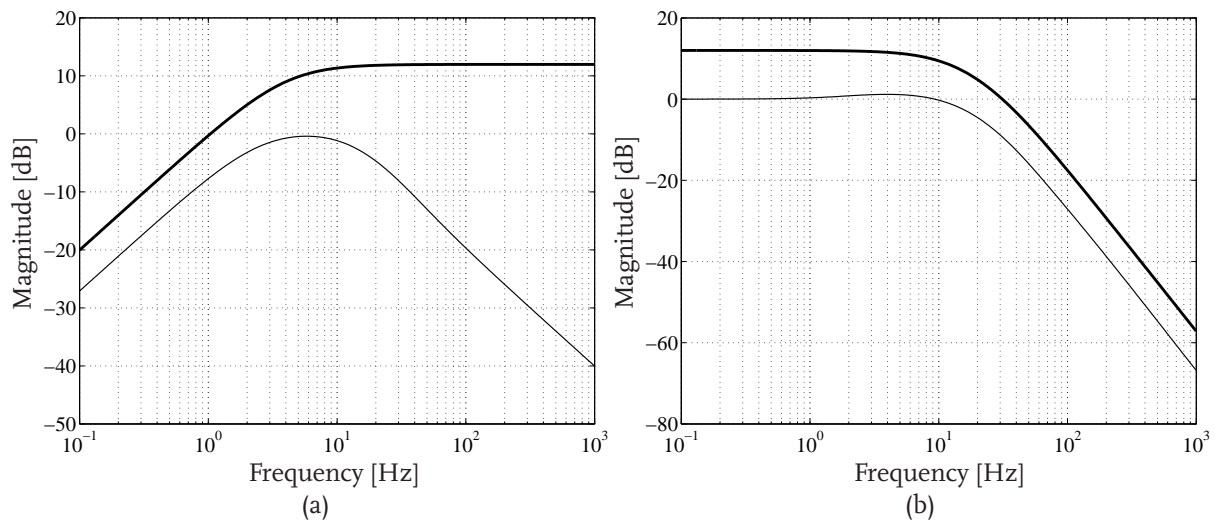


Figure 4.14 / Bode plots of the inverse of W_y (thick) and $S_{p,1}$ (thin) (a), and the inverse of W_u (thick) and T_1 (thin) (b).

4.3.4 Simulation Results

For the validation of the robust H_∞ control design approach, simulations of the uncertain high level sheet model in combination with the sheet feedback controllers designed in Section 4.3.3 have been conducted. In these simulations, the actual paper path and sheet parameters from Table 3.2 have been chosen. Hence, the transmission ratios of the second and third subsystem deviate from the nominal values used in the control design by 14% and -3% , respectively. As in the previous section, also in this case the sheet position has been used to properly switch between controllers based on the active regime of these dynamics. The sheet tracking error obtained in simulation, shown by the black line in Fig. 4.15, is similar to the one shown in Fig. 3.8. The maximum deviation from the desired zero error level after the switching moments is approximately $3.8 \cdot 10^{-4}$ m, which is much smaller than the maximum transient response defined by the performance properties in Section 1.4. The sheet tracking error depicted in Fig. 4.15 shows the predicted stable behavior of the closed-loop system and it shows that for the parametric uncertainties under consideration the performance properties presented in Section 1.4 are satisfied.

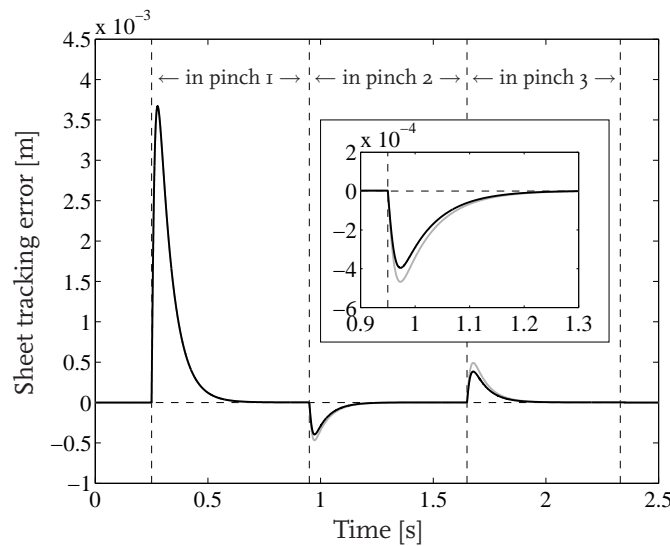


Figure 4.15 / Sheet tracking error obtained in simulation using robust (black) and nominal (gray) sheet feedback controllers.

To compare the obtained simulation results with results obtained from nominal H_∞ control design, controllers have been synthesized based on the modified standard plant configuration shown in Fig. 4.10, in which the uncertainty channel has been omitted, i.e. in which no uncertainties have been taken into account. Since the weighting filters in the design have been chosen identical to the ones used in the robust control design, a fair comparison can be made. The simulation results obtained using the new set of nominal

sheet feedback controllers are also depicted in Fig. 4.15. It can be seen that these results show a somewhat larger tracking error after the sheet has entered a subsequent pinch. Since the bandwidths of the closed-loop systems in the nominal and robust case are the same, it can be concluded that using the robust controllers a slightly better performance can be realized.

4.4 Stability Analysis for Non-ideal Low Level Dynamics

In the sheet control design procedure presented in Section 4.3, stability was proven under the assumption of perfect low level motor behavior. However, the calculated controllers will also be applied in practical cases in which the controlled motors will not behave ideally. Therefore, in the control design we made sure that the high level bandwidth in each regime was significantly smaller than the corresponding low level bandwidth. Since the required ratio between the high level and low level bandwidth is generally not strictly quantified to guarantee closed-loop stability, i.e. rules of thumb or assumptions are used [69, 75], it could be desired to carry out a founded stability analysis. As mentioned in Section 4.1, however, this stability analysis is not considered to be a necessary step in the sheet feedback control design methodology, but will be given since the model and controller structure used in this chapter easily allow for the analysis.

For the construction of the analysis technique, the closed-loop dynamics are derived, only this time models of the motor and driven roller are included. According to Fig. 2.2, taking into account the flexibility between the motor and driven roller leads to a dynamic coupling of this driven roller to the model of the motor. Hence, a combined model of the motor-pinch dynamics is obtained that describes the relation between the motor reference velocity and the angular velocity of the driven roller. On the other hand, if the flexibilities in the drive line are not taken into account, the driven roller can be coupled to the motor via a straightforward holonomic constraint relation. In the derivation of the overall closed-loop dynamics, slip between the sheet and driven roller is assumed not to be present. Hence, the model of the high level sheet dynamics always consists of at least one holonomic kinematic constraint relation in combination with an integrator, independent of the choice of the coupling between the motor and driven roller. As a result, one single model of the closed-loop error dynamics can be derived, independent of the low level modeling choices.

The low level closed-loop systems can be represented as follows:

$$\begin{aligned} \dot{\underline{x}}_{LLT,i} &= A_{LLT,i}\underline{x}_{LLT,i} + B_{LLT,i}u_{LLT,i}, \\ y_{LLT,i} &= C_{LLT,i}\underline{x}_{LLT,i} + D_{LLT,i}u_{LLT,i}, \end{aligned} \quad i \in \mathcal{I}, \quad (4.44)$$

with $u_{LLT,i}$ the reference velocity for motor M_i , calculated by the sheet feedback controller of the i -th subsystem, and $y_{LLT,i}$ the i -th input of the high level sheet dynamics. More specifically, $y_{LLT,i}$ represents the actual velocity of motor M_i in case the flexibility between motor and driven roller is neglected, or it represents the velocity of pinch i , in case the flexibility is taken into account. Furthermore, $A_{LLT,i}$, $B_{LLT,i}$, $C_{LLT,i}$, and $D_{LLT,i}$ represent the state matrices, the input matrices, the output matrices, and the throughput matrices of the low level closed-loop systems.

The series connection of (4.44) and the model describing the high level sheet dynamics,

$$\dot{x}_s = B_{HLP,i} \begin{bmatrix} y_{LLT,1} \\ y_{LLT,2} \\ y_{LLT,3} \end{bmatrix} \quad \text{for } x_s \in \mathcal{X}_i, i \in \mathcal{I}, \quad (4.45)$$

yields the overall plant to be controlled by the high level sheet feedback controllers. In (4.45), $B_{HLP,i}$ is equal to B_i in (2.2) and (3.42) in case the flexibility between the motor and the driven roller is not taken into account in the modeling procedure. Otherwise, $B_{HLP,i}$ will only contain the radii of the driven rollers.

Given the model of the low level closed-loop systems (4.44), the model describing the high level sheet dynamics (4.45), and the robust H_∞ feedback controllers represented by (4.9), the model of the overall closed-loop system can be derived. Given this model, the LMIs in (4.19) and (4.13), with \mathcal{A}_i representing the state matrices of the model of the overall switched linear closed-loop system, can be used to check the stability of the switched linear closed-loop dynamics. The results of the stability analysis in case of non-ideal low level dynamics will be presented in Section 6.3.1, after the motor dynamics have been identified and modeled, as described in Section 6.1.

A next step in the stability analysis would be to consider robust stability of the system with non-ideal low level dynamics, i.e. to include the uncertainty terms of the high level sheet dynamics in the stability analysis. However, this extension will not be considered here and remains open for future research.

4.5 Evaluation

In this chapter, (robust) H_∞ controllers have been designed for the basic paper path case-study. The main beneficial differences with respect to the approach presented in Chapter 3 are the following. First of all, robustness against parameter perturbations within a prespecified region is guaranteed in the controller synthesis, that, similar to Chapter 3, is carried out without taking into account the controlled motor dynamics. Hence, no

a posteriori stability and performance analysis is needed. Secondly, the control design and the controller structure are independent of the sheet reference profile. Hence, additional dynamics, as for example high frequency roll-off, can be easily incorporated in the controller. The third benefit is that using the weighting filters in the control design, bandwidth requirements and disturbance attenuation properties can be incorporated in the controller design. Fourthly, in the approach presented in this chapter, no structure of the sheet feedback controllers has to be enforced to cope with possible jumps in \dot{x}_s and \dot{e}_s , as the design process implicitly accounts for these discontinuities. Besides these benefits, some concerns are present with respect to the approach presented in the previous chapter, especially considering the use of the methodology in an industrial environment [73].

One of the concerns is that choosing the right parameter values for the weighting filters is not straightforward. More specifically, in many cases iterations are required to achieve, for example, a desired value of $\gamma < 1$, stable controllers, and the desired bandwidth, although the bandwidth resulting from the initial filter choice is likely to be in the neighborhood of the desired one. Secondly, sensitivity for numerical ill-conditioning is relatively high. To reduce this sensitivity, scaling of the nominal model and weights and transformation to balanced realizations can be applied [74]. Furthermore, care has to be taken not to choose the dynamic ranges of the weighting filters too large, since this can result in numerical ill-conditioning of the resulting controller. A third concern is that using the H_∞ control design approach, no pure integral action and roll-off can be realized. This is due to the fact that the weighting filters are chosen to be biproper and stable to prevent inserting a pole in $\omega = 0$ in the augmented plant, that cannot be stabilized by the controller. Hence, care has to be taken not to place the poles in (4.25) and (4.42) at a frequency that is too high, since this could result in steady state sheet tracking errors that are too large.

Regarding the implementation of the controllers designed in this chapter, two disadvantages with respect to the controllers presented in the previous chapter exist. First of all, the controllers to be implemented are of 8-th order, which results in an increase in computational effort on a CPU compared with the effort needed in case of the first order controllers designed in Section 3.2.2.³ However, since the dynamics of the controllers we are interested in only consist of an integral action and a roll-off, reduction of the controller order might be possible, yielding second order controllers. The second disadvantage is the fact that state information of the plant dynamics is needed in the implementation of the controller, since switching synchronously with the plant dynamics is required. Hence, the switching controllers do not result in robustness for possible deviations of the pinch locations.

³When presenting the experimental results in Chapter 6, the computational effort needed for both controllers will be analyzed.

Given the control design results presented in the Sections 3.2.2 and 4.3.3, an experimental validation of the two approaches can be conducted. To facilitate these experiments, an experimental paper path setup has been built, that will be discussed in the next chapter.

The Experimental Paper Path Setup

5.1	The Sheet Transportation Unit	81
5.2	Sheet Position Measurement	83

5.1 The Sheet Transportation Unit

For the practical validation of the proposed control design approaches, an experimental paper path setup has been designed and built. Before designing the setup, a number of requirements was formulated [82]. One important requirement in the design encompassed the maximum achievable sheet velocity and acceleration, which were determined to be 1 m/s and 10 m/s² [15]. These requirements on the sheet motion profile in turn impose requirements on the actuators driving the pinches. Another condition that had to be taken into account in the design was the adaptability of the setup, such that controller designs for a wide range of case-studies could be experimentally validated. This condition was imposed considering the future extension of the basic paper path case-study to real printer paper path case-studies. For example, it had to be possible to change the location of pinches, such that the sheet can be driven by more than one pinch. Furthermore, grouping pinches into sections driven by a single motor had to be possible. In this case, an industrial paper path as the one shown in Fig. 1.3 could be mimicked.

Based on the requirements, the experimental paper path setup depicted in Fig. 5.1 has been realized. As can be seen in the figure, the setup consists of a PIM and a paper path with five pinches. Whereas in real printer paper paths aluminium plates are used to guide the sheets through the paper path, in the experimental setup thin steel wires

are used to prevent the sheets from dropping out of the path and to be able to visually observe the sheets when they are transported. In the experiments that will be described in Chapter 6, only the second, third, and fourth pinch have been used. For the sake of notation, in the remainder of this thesis we will refer to these pinches as pinch P_1 , pinch P_2 and pinch P_3 , respectively. Each pinch is connected to a motor via a gear belt. The transmission ratios between the motors and pinches match the ones used to study the influence of parameter perturbations and the robustness properties of the controlled system in Sections 3.3.2 and 4.3.4, respectively, and are therefore equal to the actual values presented in Table 3.2. Also the pinch radii match the ones used in the simulations, since $r_{P_i} = 14 \cdot 10^{-3}$ m. The normal force applied to the sheet by each non-driven roller can be adjusted by variation of the distance of this roller with respect to the driven roller.

The actuators in the paper path are chosen to be 10 W DC motors, driven by power amplifiers with built-in current controllers. The angular positions of the motor shafts are measured using optical incremental encoders with a resolution of 2000 increments per revolution, yielding a collocated low level motor control setup. Both the amplifiers and the encoders are connected to a PC-based control system. This system consists of a Pentium 4 host computer running RTAI/Fusion Linux [54] and Matlab/Simulink [78] and three TUEdACS USB I/O devices [80]. Each TUEdACS device is equipped with two 16 bits ADC channels, two 16 bits DAC channels, two quadrature encoder input counters, and eight digital I/O channels. Since typical motor control bandwidths are in the range of 50 Hz, a sampling frequency is chosen that is twenty times higher, i.e. $f_s = 1000$ Hz.

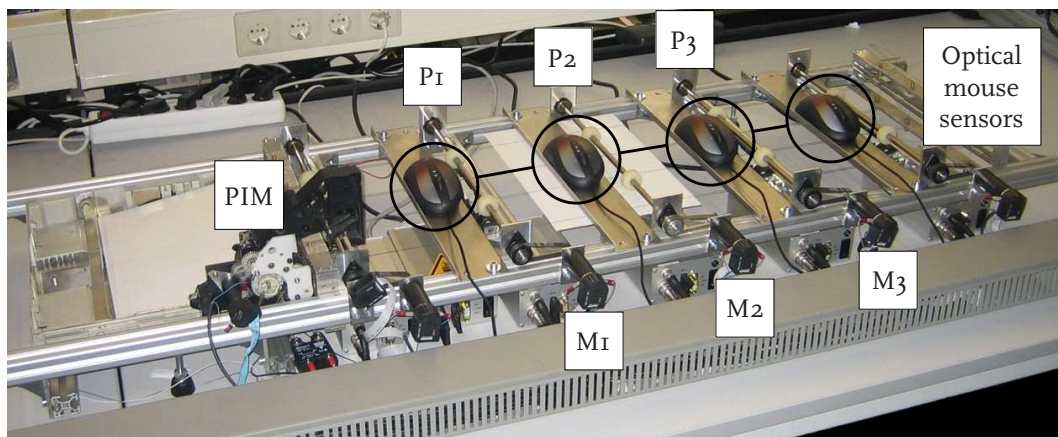


Figure 5.1 / Photo of the experimental paper path setup.

5.2 Sheet Position Measurement

5.2.1 Sensor Selection

To be able to implement the sheet feedback controllers in practice and to verify the robustness of the closed-loop system, the sheet position must be known at all time instants. Since our practical setup allows for a simple direct measurement of the state and output of the sheet flow model, i.e. the sheet position, no observer will be needed. As defined in Section 1.4, the maximum steady state sheet tracking error is $5 \cdot 10^{-4}$ m. From this we propose a resolution of $1 \cdot 10^{-4}$ m for the, preferably absolute and contactless, sheet position sensor. Two examples of commercially available absolute contactless position sensors are measuring light beams and photo-electric slot sensors [2]. Both systems use multiple small light beams that are interrupted when a sheet passes. However, as their resolution is $2.5 \cdot 10^{-3}$ m and $3 \cdot 10^{-4}$ m, respectively, they do not have the required resolution.

As an alternative for absolute position measurement systems, relative displacement sensors could be used. An example of a relative displacement sensor is the sensor used in optical mouse devices. These sensors are relatively cheap, and by placing them at a distance which is a little smaller than the sheet length, only a limited number of sensors is needed. Furthermore, today's mouse sensors have a very good resolution. An example of such sensor is the Agilent ADNS-6010 optical laser mouse sensor, supplied by Avago Technologies [1], which can be found in the Logitech G5 Laser mouse [51]. This sensor is suitable for high speed motion detection, with a maximal velocity and acceleration up to 1.14 m/s and 196 m/s^2 , respectively. The maximum sensor resolution is 2000 counts per inch (dpi), which corresponds to $12.7 \cdot 10^{-6}$ m per count. Since these specifications meet the requirements, the mouse sensors are chosen to act as a sheet position measurement system. However, care has to be taken when mounting the sensors onto the paper path, since the specifications given in the sensor's data sheet depend on several environmental properties, of which the distance between the sensor lens and the sheet surface is most crucial. The recommended range for this distance is $2.1 \cdot 10^{-3} - 2.7 \cdot 10^{-3}$ m.

The working principle of the optical mouse sensor is schematically depicted in Fig.5.2, which is taken from [1]. Light from a Vertical Cavity Surface Emitting Laser (VCSEL), represented by the thick gray line, is transported through a lens to illuminate the surface the mouse is working on. The reflected light is projected onto the mouse sensor, again via the lens. The sensor contains an Image Acquisition System (IAS), a Digital Signal Processor (DSP), and a serial port. The IAS acquires images, which are processed by the DSP. By comparing two sequentially taken images of the surface, the direction and the distance of the motion are determined, after which the relative displacement values in

the direction of the two principal axes are calculated. An external microcontroller reads the displacement information from the serial port and translates it into USB signals that are sent to the host PC [1].

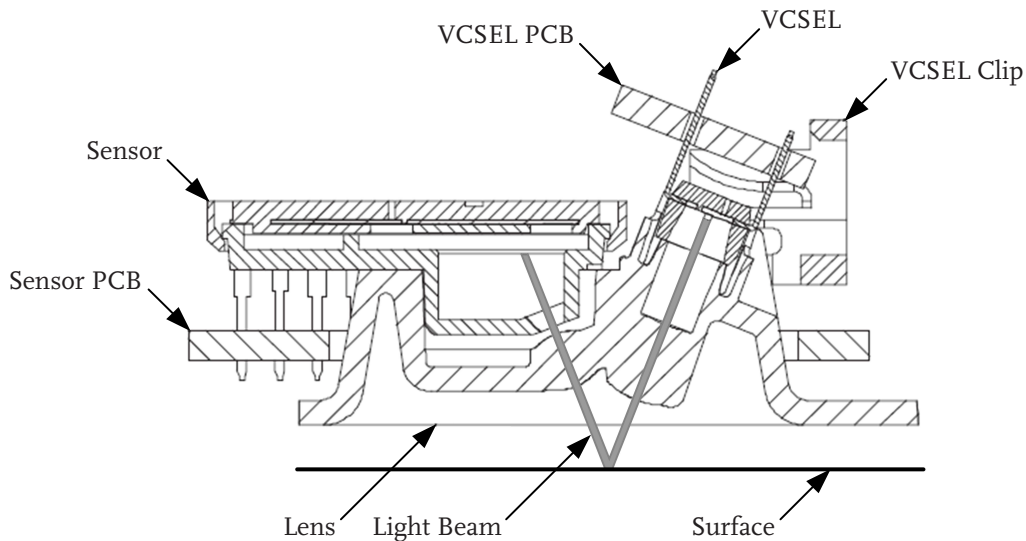


Figure 5.2 / Cross section of an optical laser mouse [1].

5.2.2 Implementation

To use the optical mouse sensor for sheet position measurement, first of all the displacement information sent by the microcontroller must be made available. Hereto, the mouse driver on the host PC is used. This driver collects the displacement information at a sampling frequency of $f_{s,m} = 500$ Hz and returns the number of counts in the direction of the two principal axes. To make the data available in Matlab/Simulink, a c-coded Simulink function has been written. In this function, the time stamps of the mouse events, i.e. the times at which the new displacement information was obtained, the mouse identification numbers, and the displacement information itself are collected from the mouse driver every 2 ms. The counts in both principal directions are added to the previous counter values and the overall displacement of the moving sheet (in counts) can be calculated. Before reconstructing the sheet position information from the sheet displacement measured by each sensor, first the sensors have to be calibrated, as will be discussed next.

5.2.2.1 Calibration

In the paper path setup, four mouse sensors are placed just above the thin steel wires guiding the sheet through the path. The distance between the sheet and the sensors will slightly vary from sensor to sensor. Since the resolution depends on this distance, a calibration procedure will be carried out. This procedure encompasses feeding n sheets of equal length to the paper path and transporting them at a constant velocity through the path. During this transportation, each sensor measures the displacement in counts for each individual sheet. After the calibration experiment, for each sensor the resolution of each individual sheet is calculated, yielding n resolutions. By averaging these resolutions, the final sensor resolution to be used in the experiments can be calculated. The results of the calibration experiment for 25 A4 sheets are given in Table 5.1 for two different sheet velocities. From this table, it can be seen that the difference in resolution for these two velocities, which is in the range of 10^{-7} m/count, can be neglected.

Mouse	Resolution [m/count]	
	$\dot{x}_s = 0.15$ m/s	$\dot{x}_s = 0.30$ m/s
1	$9.05 \cdot 10^{-6}$	$9.18 \cdot 10^{-6}$
2	$1.09 \cdot 10^{-5}$	$1.12 \cdot 10^{-5}$
3	$9.74 \cdot 10^{-6}$	$9.65 \cdot 10^{-6}$
4	$1.05 \cdot 10^{-5}$	$1.06 \cdot 10^{-5}$

Table 5.1 / Resolution of the mouse sensors.

Given the resolutions shown in Table 5.1, together with the number of increments of each sheet measured by the sensors during calibration, for each sensor the length of the sheets can be reconstructed by multiplication of the resolution with the measured number of increments. An example of the results of this reconstruction is depicted in Fig. 5.3, which shows the estimated length of the sheets by the first mouse sensor when the sheet velocity was $\dot{x}_s = 0.30$ m/s. It can be seen that with respect to the nominal sheet length of 0.21 m deviations occur up to $9 \cdot 10^{-4}$ m, which corresponds to an inaccuracy of approximately 0.4%. Since the variations in sheet length are one order lower, the deviations are attributed to the sensors or to the measurement procedure. The result of the measurement inaccuracy is that an exact continuous absolute position measurement of the sheets in the paper path cannot be carried out using these sensors. Therefore, more research on determining the absolute sheet position will have to be carried out before implementing the sheet feedback control design approaches of this thesis in an industrial environment. Nevertheless, for a practical proof of concept of our design approaches, the mouse sensors will suffice.

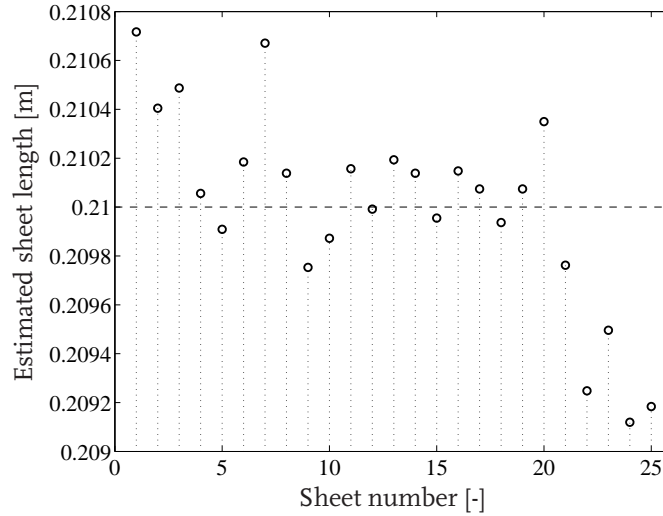


Figure 5.3 / Sheet lengths estimated by the first mouse sensor in the calibration procedure ($\dot{x}_s = 0.30$ m/s).

5.2.2.2 Sheet Position Measurement

Given the calibration procedure, the displacement of a sheet underneath each individual mouse can be measured. However, for closed-loop sheet feedback control, the measurements of the different sensors have to be synchronized online to obtain a single signal representing the sheet position. This synchronization is again realized via a c-coded Simulink function, based on the schematic representation of the sheet position measurement strategy depicted in Fig. 5.4. Initially, all displacements measured by the mouse sensors are set to zero, i.e. $x_{MS,k} = 0$, $k \in \{1, 2, 3, 4\}$. Furthermore, also the distances between the sensors are set to zero, i.e. $d_{l,l+1} = 0$, $l \in \{1, 2, 3\}$. When the leading edge of the sheet has passed the first mouse sensor, i.e. $x_{MS,1} > 0$, but has not yet passed the second mouse sensor, i.e. $x_{MS,2} = 0$, the sheet position is determined by the first sensor, i.e. $x_s = x_{MS,1}$. This corresponds to situation ① in Fig. 5.4. From situation ②, it can be seen that when the sheet has passed the second mouse sensor for no more than $5 \cdot 10^{-3}$ m, the sheet position is still determined by the first mouse sensor, despite the fact that the second mouse sensor is already measuring. This overlap is introduced for a safe detection of the sheet by the second sensor. When the leading edge of the sheet has passed the second sensor for over $5 \cdot 10^{-3}$ m, the distance between the first and second mouse sensor is determined once by subtracting the measurement of the second mouse sensor from the measurement of the first mouse sensor, i.e. $d_{1,2} = x_{MS,1} - x_{MS,2}$. From this point on, the sheet position is defined as the distance between the first and second mouse sensor plus the measurement of the second sensor, i.e. $x_s = d_{1,2} + x_{MS,2}$. This corresponds to situation ③ in Fig. 5.4. The determination of the sheet position at the third and fourth mouse sensor is carried out analogously.

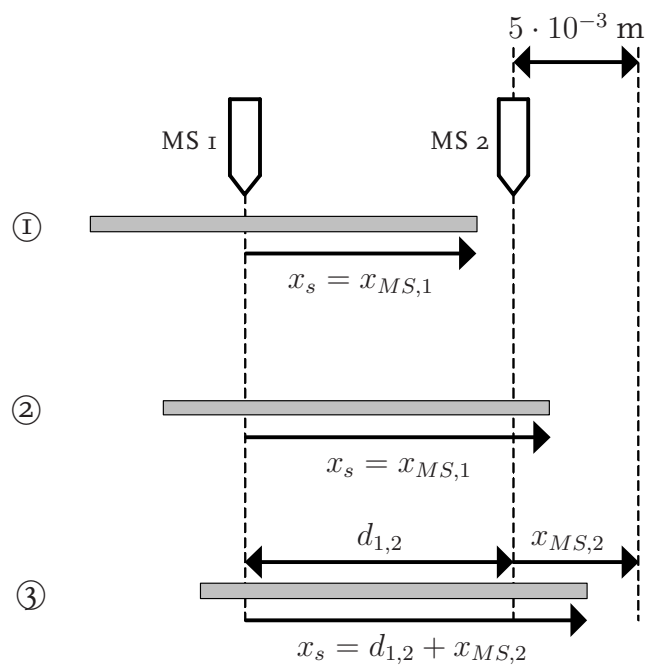


Figure 5.4 / Schematic representation of the sheet position measurement using two optical mouse sensors.

In the next chapter, the practical validation experiments of the control design approaches discussed in Chapters 3 and 4 will be presented, together with the identification, modeling, and control design of the low level motor dynamics.

CHAPTER SIX

Experimental Results

6.1	Low Level Motor Dynamics	89
6.2	Experimental Validation Results - The State Feedback Control Approach	93
6.3	Experimental Validation Results - The Output Feedback Control Approach	100

6.1 Low Level Motor Dynamics

In this chapter the practical validation experiments of the control design approaches presented in Chapters 3 and 4 will be described, together with the comparison with the corresponding simulation results. However, first identification and control design of the low level motor dynamics will be discussed, after which the models of the closed-loop motor dynamics, needed for carrying out the stability analysis of the complete system, will be derived.

In the design procedures of the sheet feedback controllers, perfect tracking behavior of the controlled motors was assumed, i.e. the motor control loops were assumed to have an infinite bandwidth. Furthermore, we assumed an infinitely stiff coupling between the motors and the pinches. In the experimental setup, however, these assumptions do not hold. The digital implementation of the controllers will cause a delay in the control loop, that will limit the attainable bandwidth. Another limitation results from the rubber belt that connects the motor with driven roller of the pinch. Since this belt has a finite stiffness, flexibilities will be present in the system that can limit the attainable bandwidth as well.

To identify the low level motor dynamics, frequency response function (FRF) measurements have been carried out under closed-loop conditions, using a sampling frequency of $f_s = 1$ kHz. Broadband noise is added to the controller output and besides this noise signal, both the total motor input signal as well as the motor tracking error are measured. From these measurements, the transfer function from the noise signal to the total motor input signal, i.e. the sensitivity function of the low level control loop, and the transfer function from the noise signal to the motor tracking error, i.e. the process sensitivity function of the low level control loop, are determined. By dividing both transfer functions, the remaining motor dynamics can be extracted. The results of this identification procedure are reliable in the frequency range above the bandwidth of the controlled system, which was 20 Hz in this case, since in this range the coherence of the measurement is good. This can be observed from Fig. 6.1, which shows the coherence of the sensitivity function, together with the FRF of the first motor-pinch combination. Although not shown, similar results have been obtained for the motors M2 and M3. The flexibility due to limited stiffness of the transmission belt results in an antiresonance and resonance peak in the frequency range between 200 – 500 Hz. The small antiresonance/resonance pair at 120 Hz, indicated by the circles in Fig. 6.1, results from the decoupling of the non-driven roller of the pinch. The phase lag due to the time delay in the control system can be observed from the two different phase plots depicted in Fig. 6.1.

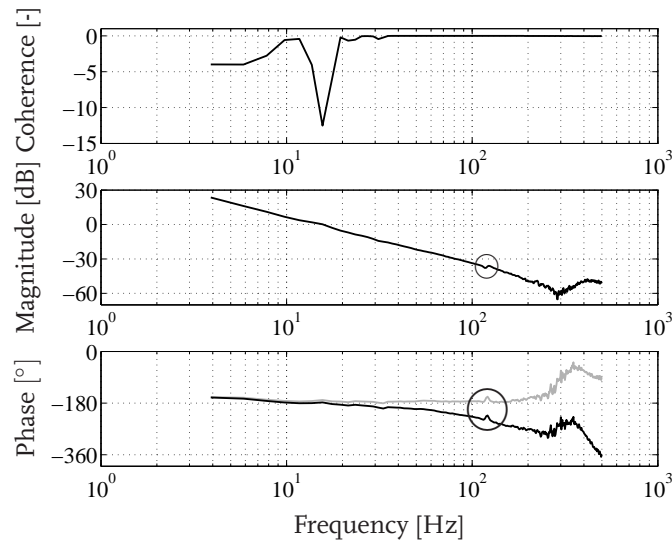


Figure 6.1 / Experimentally obtained FRF of motor M1 including delay (black) and with delay removed (gray).

To investigate the influence of the limited stiffness of a driving belt, two FRFs of the first motor-pinch combination in the paper path setup have been measured, since both this motor and the driven roller of this pinch are equipped with an optical incremental encoder. The first FRF measurement is equal to the one described above, whereas during

the second measurement the angular position of the driven roller is used for feedback instead of the angular motor position. The reconstruction of the FRF of the low level dynamics has been done in analogy with the first experiment. When the resulting FRF is divided by the FRF obtained from the first measurement, the FRF of the dynamics of the transmission between the motor and the driven roller is obtained. From this FRF, shown in Fig. 6.2, it can be seen that the assumption on the stiffness of the connection between motor and pinch only holds for frequencies up to approximately 60 Hz. In this frequency range, the measured transmission ratio coincides with the used transmission ratio of 18/37, which is equal to -6.3 [dB]. For higher frequencies the flexibility in the system becomes dominant.

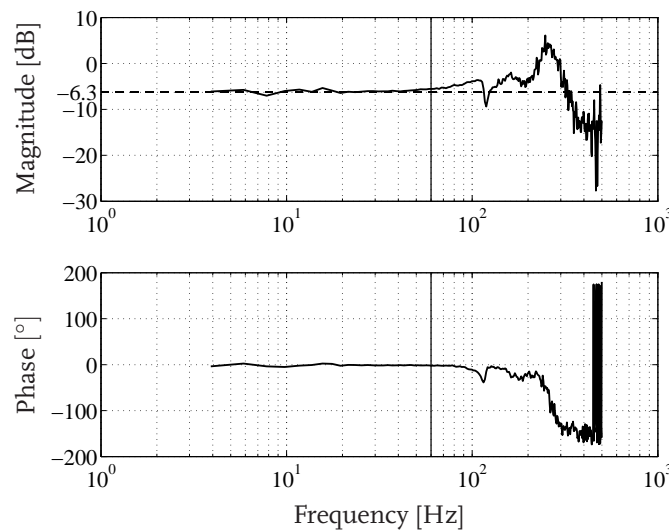


Figure 6.2 / Experimentally obtained FRF of the transmission between the first motor and driven roller in the setup (solid), and the nominal transmission ratio indicated in the magnitude plot (dashed).

Given the motor dynamics shown in Fig. 6.1, a collocated feedback controller, i.e. based on motor encoder feedback, has been designed using loopshaping techniques [25]. This controller consists of a lead filter in combination with an integral action. The zero and pole of the lead filter are located at $1/4 \cdot 50$ Hz and $4 \cdot 50$ Hz, respectively, whereas the cut-off frequency of the integral action is equal to $1/5 \cdot 50$ Hz. Given this controller, which is depicted in Fig. 6.3(a), a bandwidth of 53 Hz has been realized, as shown in Fig. 6.3(b). This is approximately five times higher than the bandwidth of the loop gain of the first high level subsystem, obtained using the controllers designed in Sections 3.2.2 and 4.3.3. Hence, the desired difference in bandwidth between the inner loop and the outer loop, discussed in Section 2.3, has been realized. The bandwidths of the second and third low level system are approximately 47 Hz and 50 Hz, respectively.

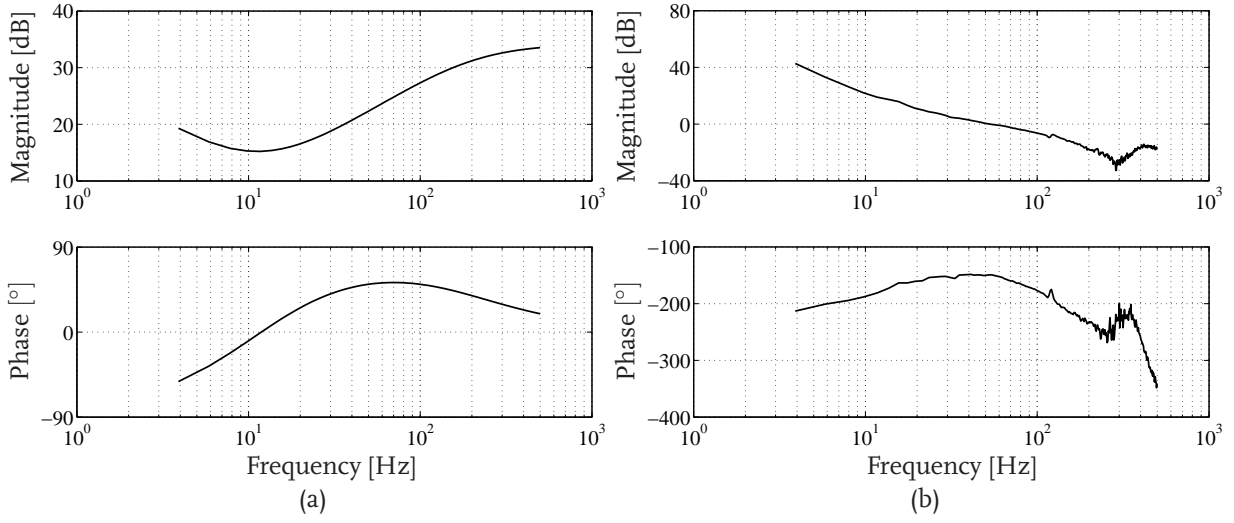


Figure 6.3 / Bode plot of the feedback controller (a), and the FRF of the loop gain (b) of the first controlled motor.

In the design of the low level feedback controllers, the delay present in the control system is the bandwidth limiting factor. Therefore, in modeling the low level motor dynamics, needed for the stability analysis of the overall closed-loop system, this delay is taken into account. On the other hand, the decoupling of the non-driven roller and flexibility due to the limited stiffness of the transmission belt are neglected, since these properties manifest themselves only considerably above the bandwidth. The low level motor dynamics are therefore modeled as double integrators

$$\frac{\Phi_{M_i}(s)}{U_i(s)} = \frac{K_{A_i}K_{M_i}}{J_i s^2} e^{-\tau s}, i \in \mathcal{I}, \quad (6.1)$$

where K_{A_i} represent the amplification factors of the current amplifiers in A/V, K_{M_i} are the motor constants in Nm/A, J_i are the inertias of the low level systems in kgm², and τ represents the delay present in the control system. Furthermore, $\Phi_{M_i}(s)$ and $U_i(s)$ are the Laplace transforms of the motor position ϕ_{M_i} and the motor control input u_i , respectively. The values of the parameters K_{A_i} and J_i , obtained via identification, and of the parameter K_{M_i} , obtained from the motor specifications, are given in Table 6.1. From the FRFs we know that the delay time τ is equal to $1.5 \cdot 10^{-3}$ s in every low level control loop. This delay can be approximated by a second order Padé approximation [69]:

$$e^{-\tau s} \approx \frac{(1 - \frac{\tau}{4}s)^2}{(1 + \frac{\tau}{4}s)^2}. \quad (6.2)$$

The resulting model of the first motor can be seen in Fig. 6.4(a), together with the identified motor dynamics. From this figure it can be seen that there is a close match

i	K_{Ai} [A/V]	K_{Mi} [Nm/A]	J_i [kgm ²]
$i = 1$	0.54	$4.38 \cdot 10^{-3}$	$2.9 \cdot 10^{-6}$
$i = 2$	0.51	$4.38 \cdot 10^{-3}$	$3.3 \cdot 10^{-6}$
$i = 3$	0.53	$4.38 \cdot 10^{-3}$	$2.9 \cdot 10^{-6}$

Table 6.1 / Parameter values of the low level motor dynamics.

between the model and the measured data in the frequency range up to 100 Hz. At higher frequencies, the differences between the model and the measured dynamics result from the fact that the model does not take into account the flexibilities. Given the model of the plant dynamics, together with the designed feedback controller, the model of the closed-loop motor dynamics can be derived. This model is shown in Fig. 6.4(b) for the first motor system, together with the FRF of the closed-loop system, derived from the identification of the motor dynamics and the designed feedback controller. It can be seen that also in this case a good match between model and measured data exists in the low frequency range, i.e. up to approximately 40 Hz. Furthermore, it can be seen that the assumption on perfect tracking behavior of the controlled motors, i.e. $T_i(s) = 1, \forall s \in \mathbb{C}, \forall i \in \mathcal{I}$ in (2.3) only holds up to 10 Hz. Hence, by designing the inner loops using the lead filter in combination with the integral action such that a 50 Hz bandwidth is realized, the motor control loops are capable of closely tracking reference profiles with a frequency content up to 10 Hz, generated by the sheet feedback controllers. At this point, it has to be noted that according to (2.3), the input and output of the motor control loops are the motor reference velocity and the actual motor velocity, respectively, whereas the motors are controlled by position feedback. However, this does not influence the closed-loop transfer function, as the transfer function from the motor reference velocity to the actual motor velocity is equal to the transfer function from the motor reference position to the actual motor position.

6.2 Experimental Validation Results - The State Feedback Control Approach

In this section, the experimental validation results of the two control design approaches presented in Section 3.2, i.e. the approaches leading to both linearizing and partially linearizing controllers, will be presented. In both experiments, the transmission ratios of the second and third motor-pinch combination have been changed with respect to ones used in the control design, in order to analyze the behavior of the system subject to perturbations of the paper path parameters. More specifically, the actual parameter values

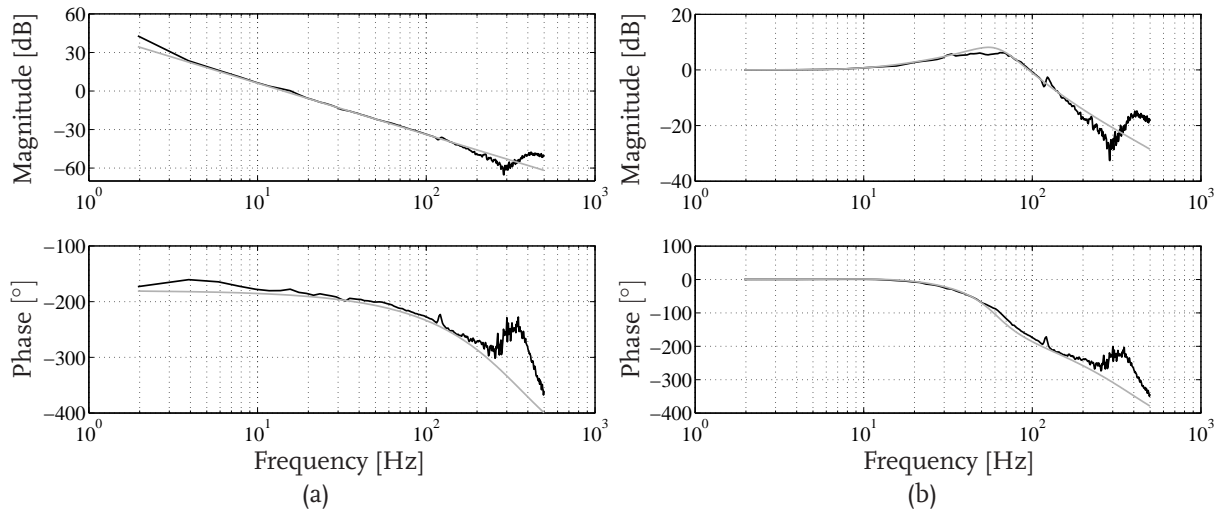


Figure 6.4 / FRFs (black) of the dynamics (a) and the complementary sensitivity function (b) of motor M1, together with the Bode plots of their corresponding models (gray).

listed in Table 3.2 have been used in the experiments. These parameter values match the ones used in the simulations described in Section 3.3.2, and therefore the resemblance between the simulations and the experiments can be investigated.

The experimentally obtained sheet tracking error using the fully linearizing sheet feedback controller is depicted in Fig. 6.5(a), whereas the tracking error obtained using the partially linearizing controller is shown in Fig. 6.5(b). It can be seen that the responses in both figures resemble each other strongly. The main difference between the two tracking errors is the maximum deviation from the desired zero error level after entering a new pinch, caused by a small difference in high level bandwidth: approximately 11 Hz and 10 Hz for the fully linearizing and partially linearizing controller, respectively. As in the simulation, the large transient behavior just after the moment the sheet enters the paper path is caused by the difference between the sheet reference velocity and the initial actual sheet velocity. Moreover, the increase in tracking error when the sheet enters the regimes two and three is caused by the deviation of the implemented transmission ratios with respect to their nominal values. Also these increases are controlled towards zero quickly. When the sheet is in pinch P1, a clear harmonic component with a frequency in the range of 7 – 8 Hz can be observed in the sheet tracking error. This component is caused by the rotation asymmetry of the first driven roller, a phenomenon that demonstrates itself less in the other two driven rollers.

For a frequency domain analysis of the sheet tracking errors, Figs. 6.6(a) and 6.6(b) show the cumulative power spectrum (CPS) of the measured sheet tracking error, to-

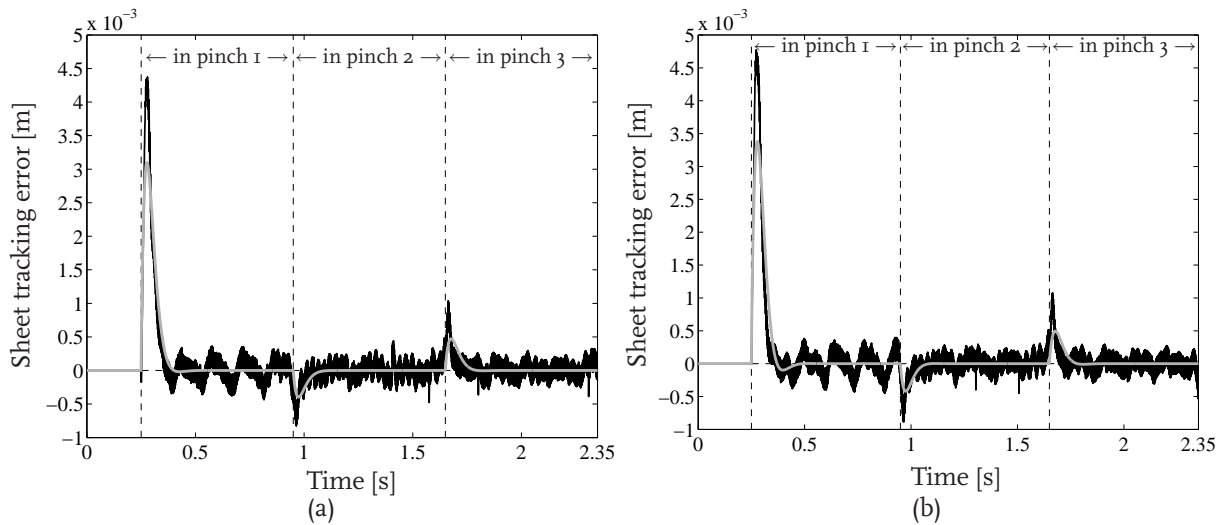


Figure 6.5 / Sheet tracking error obtained in experiments (black) and simulation (gray) using the linearizing (a) and the partially linearizing (b) sheet feedback controllers.

gether with the CPS of the error obtained in simulation obtained using the fully and partially linearizing sheet feedback controllers, respectively. The comparison of both figures shows that the power of the tracking errors, i.e. the value of the CPS at 500 Hz, obtained using the partially linearizing controllers is slightly larger than the power of the errors obtained using the fully linearizing controllers. This corresponds to the larger maximum deviation from the desired zero error level after entering a new pinch. From Figs.6.6(a) and 6.6(b), also the contribution of the rotation asymmetry to the measured tracking error can be observed, as it manifests itself as an increase of the frequency content in the range around 7 – 8 Hz.

In Figs. 6.5 and 6.6, the resemblance between the experimentally obtained tracking error and the error obtained in simulation can be observed in both feedback control cases. In Fig. 6.5, the good match between both tracking errors can be observed visually, whereas in Fig. 6.6 it can be seen that the power of both signals is in the same order of magnitude. Because of the close resemblance between both tracking errors, it can be concluded that the low-detailed simulation models have very good predicting capabilities. The small differences between the experimental and simulation results can be caused by, for example, unmodeled motor and pinch inertias, possible slip between the pinch and the sheet, and a slightly late arrival of the sheet at the first pinch, i.e. the sheet reference position has started to increase when the sheet is not in the pinch yet. The good resemblance between simulations and experiments justifies the assumption on ideal low level motor dynamics in the controller synthesis approach.

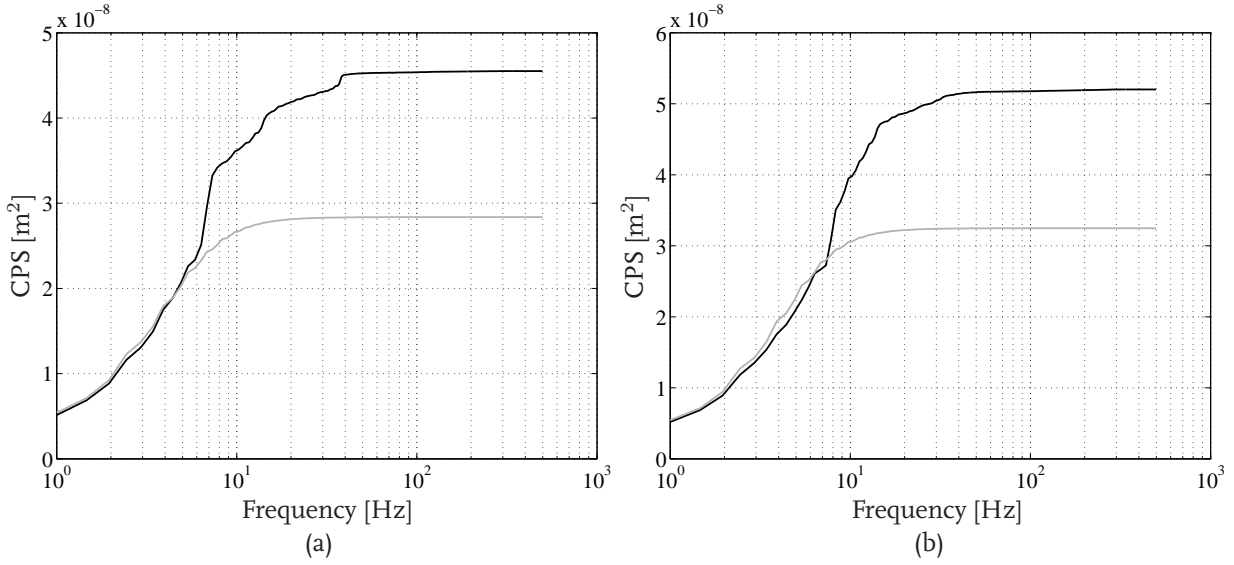


Figure 6.6 / Cumulative power spectra of the sheet tracking errors obtained in experiments (black) and simulation (gray) using the linearizing (a) and the partially linearizing (b) sheet feedback controllers.

To analyze the influence of the motor tracking errors on the sheet tracking error, the tracking errors of motor M_I, obtained in the two experiments, have been depicted in Fig. 6.7 as an example. As expected from the resemblance of the sheet tracking errors obtained using the fully and partially linearizing sheet feedback controllers, also the motor errors show comparable responses. As an example, we consider the tracking error of motor M_I depicted in Fig. 6.7(a). Observation of the transient motor response shows that a maximum error of $7.5 \cdot 10^{-2}$ rad has been obtained. Multiplying this maximum motor tracking error with the transmission ratio and pinch radius of the first subsystem yields a contribution to the sheet tracking error of $5.1 \cdot 10^{-4}$ m. In this calculation, no slip and an infinite stiff connection between motor and pinch are assumed. Comparing this calculated contribution with the maximum error obtained in simulation, which is $3.1 \cdot 10^{-3}$ m and fully caused by the difference between reference and initial actual velocity, it can be observed that the latter one is significantly higher. Hence, the contribution of the accelerating motor and pinch inertias to the sheet tracking error is limited. Looking at the steady state errors of motor M_I in the first regime, a maximum error of approximately $3.5 \cdot 10^{-2}$ rad can be observed. Multiplying this error with the transmission ratio and pinch radius of the first subsystem yields a sheet tracking error of $2.4 \cdot 10^{-4}$ m, which coincides with the corresponding measured sheet error. From Fig. 6.7(a) we can also observe a zero tracking error before the sheet enters pinch P_I, which can be expected since the motors are standing still before the sheet enters this pinch. Furthermore, it can be seen that the magnitudes of the steady state errors in the three regimes are all of equal

order, which indicates that the presence of a sheet does not influence these steady state motor tracking errors. From Fig. 6.7(a), peaks in the motor tracking error at the switching boundaries can be observed. This sudden decrease of increase of the motor tracking error is caused by the change in motor reference velocity, which in turn results from the perturbation of the paper path parameters. As an example we consider the motor tracking error at $t = 0.95$ s. At that time instant, the sheet enters pinch P2 which is rotating too fast for realizing a zero tracking error, since the transmission ratio is larger than the one the controller was designed for. The sheet controller reacts to the increasing sheet error by decreasing the motor reference velocity. This fast decrease in motor reference velocity, which can be observed in Fig. 6.8(a), causes the motor tracking error to decrease as well. The peak at $t = 1.65$ s, i.e. the moment the sheet enters the third pinch, can be explained analogously. From Fig. 6.7(b), it can be seen that there is no peak in the motor tracking error at $t = 1.65$ s. In this case, the sudden increase in tracking error due to the increase in motor reference velocity is counteracted by the increase in actual motor velocity, which is caused by the rotation asymmetry. More specifically, at $t = 1.65$ s the second motor-pinch combination starts accelerating after passing the point of maximum resistance in the rotation.

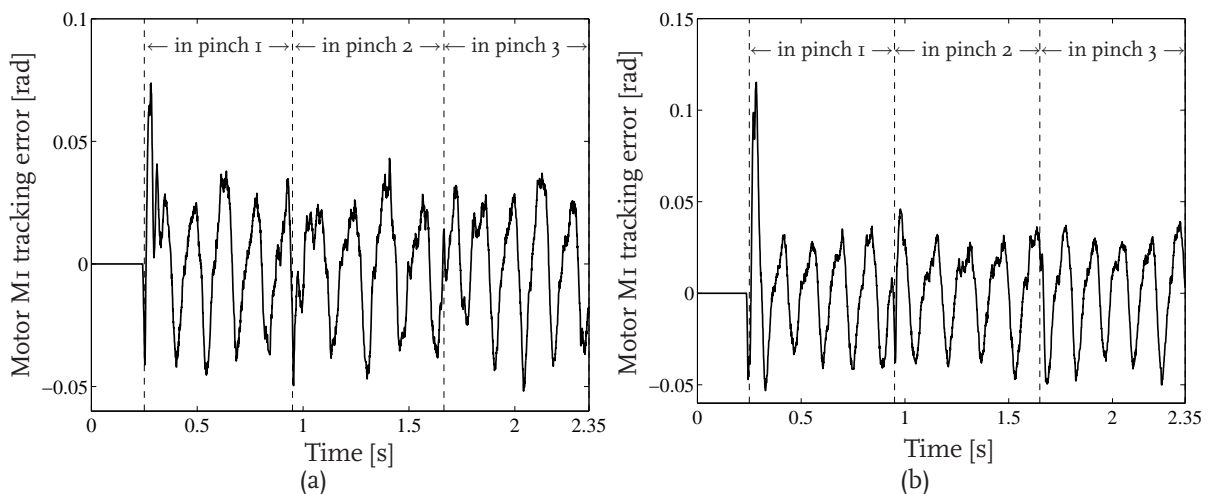


Figure 6.7 / Experimentally obtained tracking error of motor M_I using the linearizing (a) and the partially linearizing (b) sheet feedback controllers.

In Fig. 6.8, the high level control inputs of motor M_I , i.e. the motor reference velocities in the two experiments, are shown. As expected from the previous analysis of the two sheet and motor tracking errors, also the motor reference velocities show a strong resemblance. When the sheet is in pinch P1, again the rotation asymmetry of the first driven roller can be observed. The average steady state motor velocity in this regime is approxi-

mately 44 rad/s. Multiplying this velocity with the transmission ratio and pinch radius of the first subsystem yields a sheet velocity of 0.3 m/s, which equals the desired velocity. As mentioned, the velocity of motor M_I changes when the sheet enters the second and third pinch. This change corresponds to the increasing sheet tracking error when entering the next pinch. Hence, the sheet feedback controller adapts the reference velocity of motor M_I to account for the increasing tracking error, as if the sheet is still in pinch P_I .

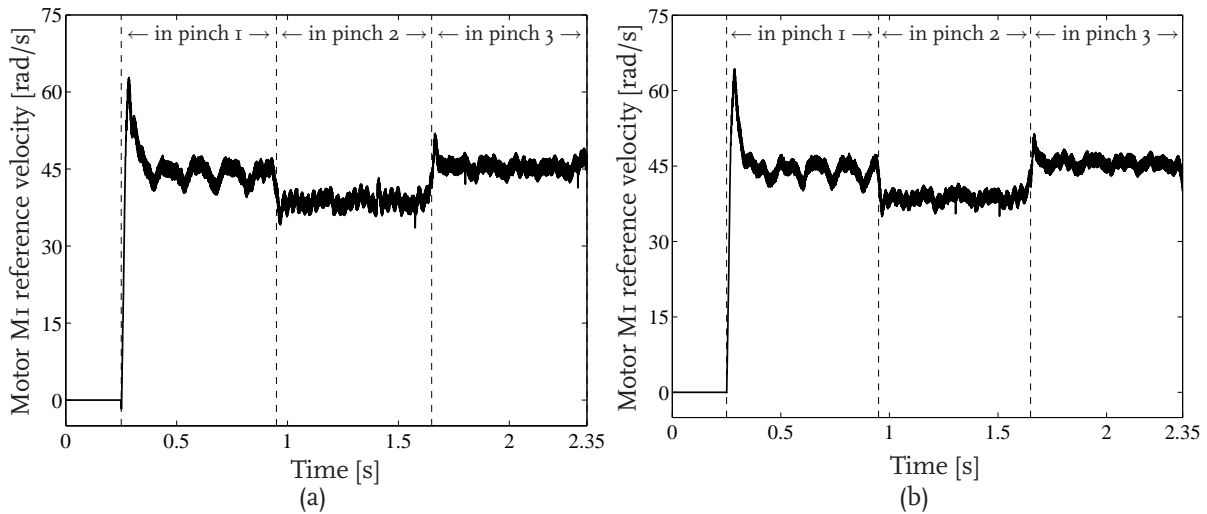


Figure 6.8 / Experimentally obtained reference velocity for motor M_I using the linearizing (a) and the partially linearizing (b) sheet feedback controllers.

For the frequency analysis of the high level control inputs, the CPSs of these inputs have been calculated. As an example, Fig. 6.9 shows the CPS of the reference velocities of motor M_I , obtained in both experiments. These spectra show that the majority of the frequency content is located in the low frequency range. This is desirable because the motors can only accurately track reference profiles within a limited low frequency range, as observed in Fig. 6.4(b). The harmonic component present in the motor reference velocities in the first regime, see Fig. 6.8, can also be observed in Fig. 6.9, as it manifests itself as an increase in the spectrum in the range around 7 – 8 Hz.

To study the effect of changes in the bandwidth of the low level control loops on the performance of the closed-loop system, several experiments have been carried out in which the low level bandwidth has been reduced. As an example, the experimentally obtained sheet tracking errors using a 25 Hz low level bandwidth, obtained using both the fully and partially linearizing sheet feedback controllers, are shown in Fig. 6.10. From this figure, a larger transient response and larger steady state errors can be observed, compared with the results presented in Fig. 6.5. Furthermore, it can be seen that the harmonic compo-

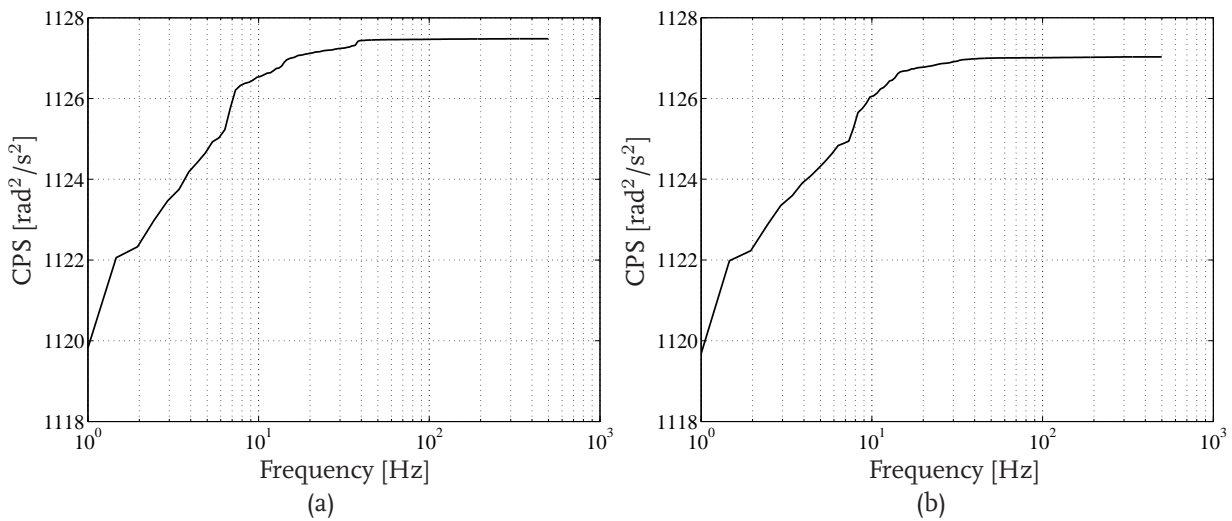


Figure 6.9 / Cumulative power spectra of the motor M1 reference velocities obtained in experiments using the linearizing (a) and the partially linearizing (b) sheet feedback controllers.

ment in the sheet tracking error in the first regime is still present, whereas the influence of the parameter perturbations is less evident than in Fig. 6.5. Since the maximum steady state tracking errors shown in Fig. 6.10 are larger than $5 \cdot 10^{-4}$ m, the performance properties defined in Section 1.4 are not satisfied in this case.

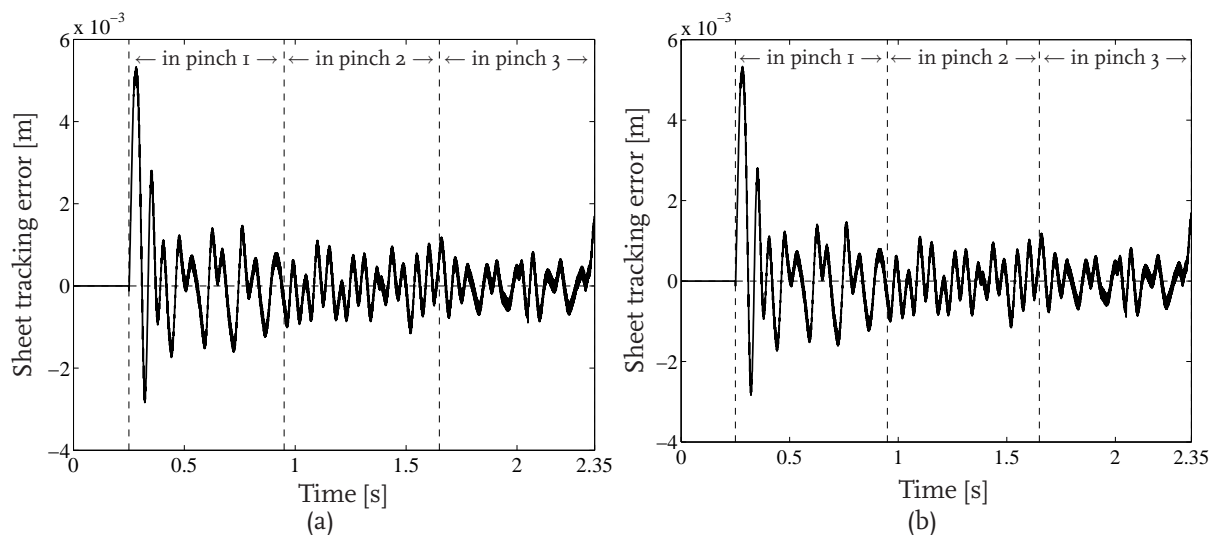


Figure 6.10 / Experimentally obtained sheet tracking errors using the linearizing (a) and the partially linearizing (b) sheet feedback controllers, given a low level bandwidth of 25 Hz.

6.3 Experimental Validation Results - The Output Feedback Control Approach

6.3.1 Stability Analysis in Case of Non-ideal Low Level Dynamics

Before implementing the designed controllers in practice, first the stability analysis discussed in Section 4.4 is performed, using the models of the closed-loop motor dynamics, derived in Section 6.1. Before analyzing the stability of the overall switched system, first the stability of the subsystems will be studied. Despite the fact that in some cases the switched system might be stable, although unstable subsystems exist, it is desired to also have stable subsystems in order to satisfy the performance properties defined in Section 1.4. For the subsystem stability analysis, the loop gain of the nominal first high level subsystem, shown in Fig. 4.13(b), is multiplied with the model of the closed-loop dynamics of the first motor-pinch combination, shown in Fig. 6.4(b), resulting in the overall loop gain of the first subsystem, which is shown by the black line in Fig. 6.11.¹ From this figure it can be seen that the phase lag at the crossover frequency, located at approximately 12.5 Hz, is approximately 115° , yielding a phase margin of 65° . Hence, the first subsystem is stable. Although not shown here, similar results have been obtained for the motors M2 and M3. Fig. 6.11 also shows the overall loop gain of the first subsystem, calculated using the fully linearizing sheet feedback controller designed in Section 3.2.2.1. Comparing this loop gain with the one calculated using the robust sheet feedback controller designed in Section 4.3.3, it can be seen that the magnitude of the latter one is approximately 20 dB lower at 500 Hz and that the phase lag is approximately 90° larger. This can be explained from the presence of a first order low-pass filter in the robust sheet feedback controller of Section 4.3.3.

Given the models of the controlled motor dynamics, derived in Section 6.1, the stability of the overall switched linear closed-loop system has been analyzed according to the method presented in Section 4.4. In this analysis, both nominal and perturbed high level sheet models have been used. Since a feasible solution of the set of LMIs consisting of (4.19) and (4.13) can be obtained in these cases, the overall switched linear closed-loop system is proven to be stable. The stability analysis discussed in this subsection has also been carried out using a model of the motor-pinch dynamics that takes into account the limited stiffness of the transmission belt. Also using this model, a feasible solution of the set of LMIs consisting of (4.19) and (4.13) can be found. Hence, also this overall switched linear closed-loop system is proven to be stable.

¹The stability analysis discussed in this subsection has also been carried out using the perturbed high level sheet model. Although not shown, similar results have been obtained.

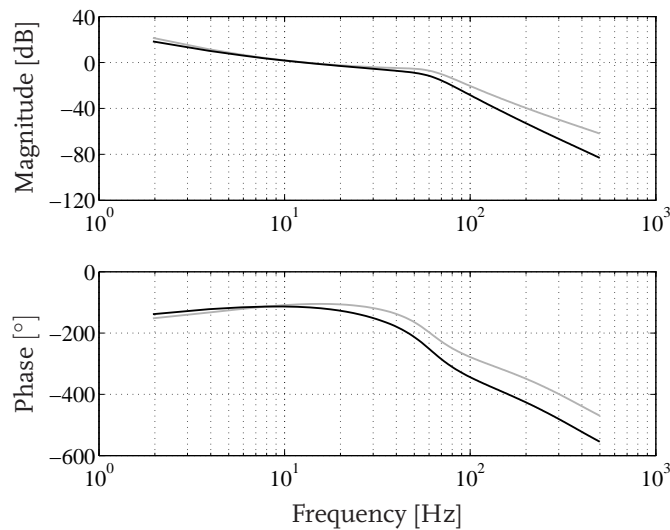


Figure 6.11 / Overall loop gains of the first subsystem, calculated using the robust sheet feedback controller designed in Section 4.3.3 (black) and the fully linearizing sheet feedback controller designed in Section 3.2.2.1 (gray).

6.3.2 Robustness Experiments

To study the robustness characteristics of the closed-loop system obtained using the feedback controllers designed in Section 4.3.3, experiments have been conducted. In these experiments, the same conditions have been created as in the simulations discussed in Section 4.3.4. Hence, the same switching controller and sheet reference motion task have been used, no feedforward control input has been added to the system, and the physical parameters match the ones used in the simulation, i.e. the actual values listed in Table 3.2 have been used. Consequently, the resemblance between simulation and experiment can be investigated.

The experimentally obtained sheet tracking error is depicted in Fig. 6.12(a). It shows the stable behavior of the closed-loop system and it shows that for the parametric uncertainties under consideration the performance properties presented in Section 1.4 are still satisfied. The transient responses, resulting from entering a new regime, are controlled towards zero quickly. Furthermore, the harmonic component in the sheet tracking error, caused by the rotation asymmetry of the first driven roller, can again be observed when the sheet is in the first pinch. For a frequency domain analysis of the sheet tracking error, Fig. 6.12(b) shows the CPS of the measured sheet tracking error, together with the CPS of the error obtained in simulation. Also from this figure, the contribution of the rotation asymmetry to the measured tracking error can be observed by the increase of the frequency content in the range around 7 – 8 Hz. From Fig. 6.12 it can be concluded that the resemblance between the experimentally obtained sheet tracking error and the error obtained in simulation, observed both visually in Fig. 6.12(a) and via the power spectrum of

both errors in Fig. 6.12(b), is good. Hence, it can again be concluded that the low-detailed simulation models have very good predicting capabilities.

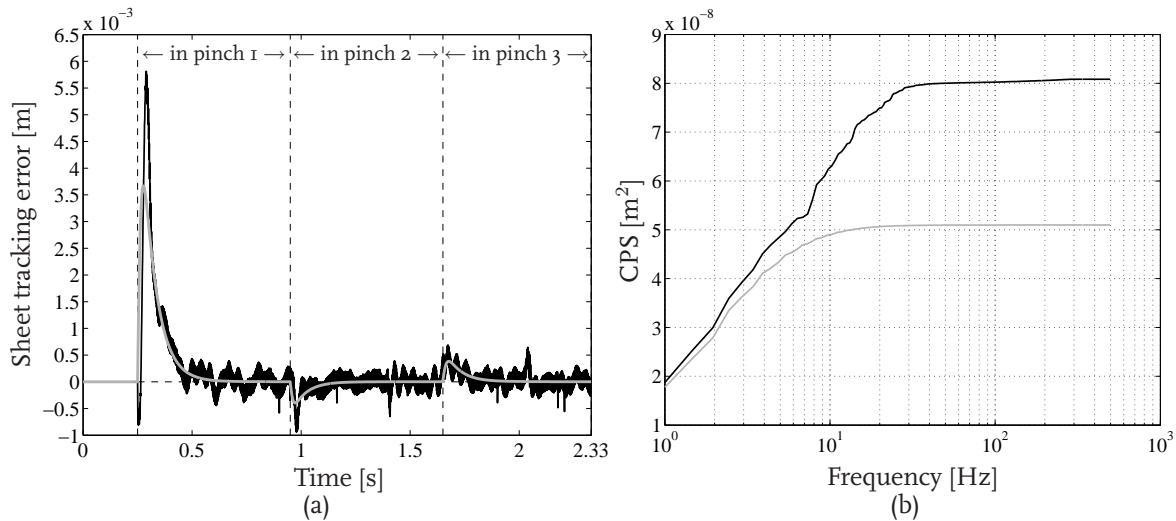


Figure 6.12 / Sheet tracking error obtained in experiments (black) and simulation (gray) (a), together with the corresponding cumulative power spectra (b).

In Fig. 6.13 the tracking error of motor M_I measured during the experiment is depicted. Similar to the motor tracking errors depicted in Fig. 6.7, a zero tracking error before the sheet enters pinch P_I can be observed, which can be expected since the motors are standing still before the sheet enters this pinch. Also in this case, the presence of a sheet does not seem to influence the steady state motor tracking error, as the magnitudes of these steady state errors in the three regimes are all of equal order. On the transition from the first to the second pinch, a peak in the motor tracking error can be observed. As explained in Section 6.2, this peak is caused by the change in motor reference velocity at the switching boundary. At the transition from the second to the third pinch, no peak in the motor tracking error can be observed. The sudden increase in tracking error due to the increase in motor reference velocity is also in this case counteracted by the increase in actual motor velocity due to the rotation asymmetry. Multiplication of the maximum amplitude level of the steady state motor errors obtained when the sheet is in pinch P_I, which is approximately $3.5 \cdot 10^{-2}$ rad, with the transmission ratio and pinch radius of the first subsystem yields also in this case a sheet tracking error of $2.4 \cdot 10^{-4}$ m, which again coincides with the results depicted in Fig. 6.12(a). Regarding the transient response resulting from a sheet entering the paper path, also in this case it can be concluded that the contribution of the accelerating motor and pinch inertias to the sheet tracking error is limited. More specifically, multiplication of the maximum motor tracking error in regime 1 with the transmission ratio and pinch radius yields a contribution to the sheet

tracking error of $8.9 \cdot 10^{-4}$ m, which is considerably smaller than the sheet error obtained in simulation.

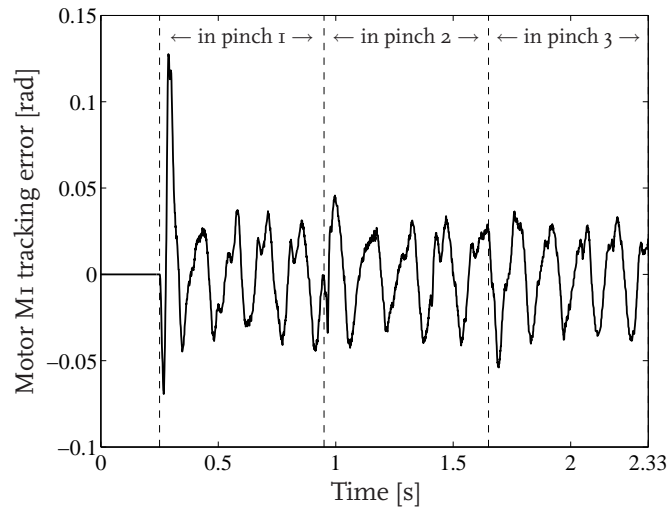


Figure 6.13 / Experimentally obtained tracking error of motor M1.

The high level control input of motor M1 is shown in Fig. 6.14(a). As in Fig. 6.8, the rotation asymmetry of the first driven roller can be observed, as well as the changes in velocity when the sheet enters the second and third pinch. For the frequency analysis of the high level control inputs, the CPS of these inputs have again been calculated. As an example, Fig. 6.14(b) shows the CPS of the reference velocity of motor M1. Also in this case the majority of the frequency content is located in the low frequency range, as desired. The harmonic component present in the motor reference velocity in the first regime, see Fig. 6.14(a), can also be observed in Fig. 6.14(b), as it manifests itself as an increase in the spectrum in the range around 8 Hz. Comparing Fig. 6.14(b) with Fig. 6.9, it can be seen that the power of the motor reference velocities is of equal order.

The major difference between Fig. 6.8 and Fig. 6.14(a) is that the high level control input shown in the latter one contains less high frequency components. This results from the fact that the high level sheet controllers designed in Section 4.3.3 contain a low-pass filter rejecting frequency components larger than 50 Hz. The decrease in frequency content can also be observed in Fig. 6.15. In this figure, the Power Spectral Densities (PSDs) of the high level control input of motor M1, calculated by the fully linearizing controller in Section 6.2 and the robust sheet feedback controller in this section, are shown. It can be seen that the frequency content of both control inputs is approximately the same for frequencies up to approximately 50 Hz, whereas the high frequency content of the control input obtained in this section is significantly smaller.

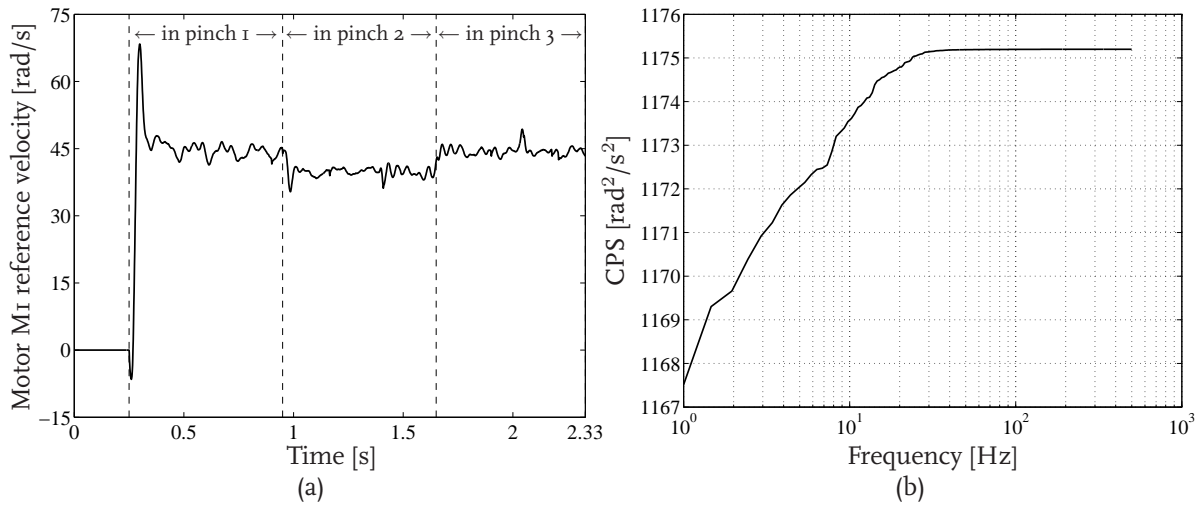


Figure 6.14 / Reference velocity for motor M1 (a), and its cumulative power spectrum (b).

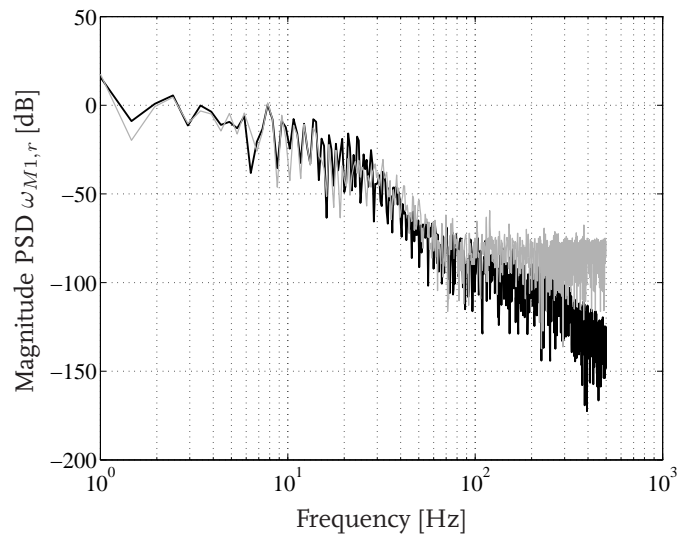


Figure 6.15 / Power Spectral Densities of the reference velocity of motor M1, resulting from using the robust sheet feedback controller designed in Section 4.3.3 (black) and the fully linearizing sheet feedback controller designed in Section 3.2.2.1 (gray).

Given the high level sheet controllers designed in Section 4.3.3, the influence of changes in the low level bandwidths can again be studied. Also in this case, the results obtained using a 25 Hz low level bandwidth are taken as an example. From Fig. 6.16(a), which shows the experimentally obtained sheet tracking error, it can be seen that the second overall closed-loop subsystem appears to be close to instability. This can also be seen from Fig. 6.16(b), which shows that the Nyquist plot of the loop gain of the second overall subsystem closely approaches the point $(-1, 0)$. The fact that in this case this sec-

ond subsystem is close to instability, whereas this was not the case in the experiments of which the results are shown in Fig. 6.10, can be explained by the extra phase delay introduced by the low pass filter in the high level sheet controller, resulting in a smaller phase margin in the second subsystem. The first and third subsystem are not close to instability, since the low level bandwidths in these subsystems are slightly larger than the one in subsystem 2, resulting in a larger phase margin in subsystems 1 and 3. Because of the large steady state sheet tracking errors obtained in the first and second region, the performance properties defined in Section 1.4 are not satisfied in this case.

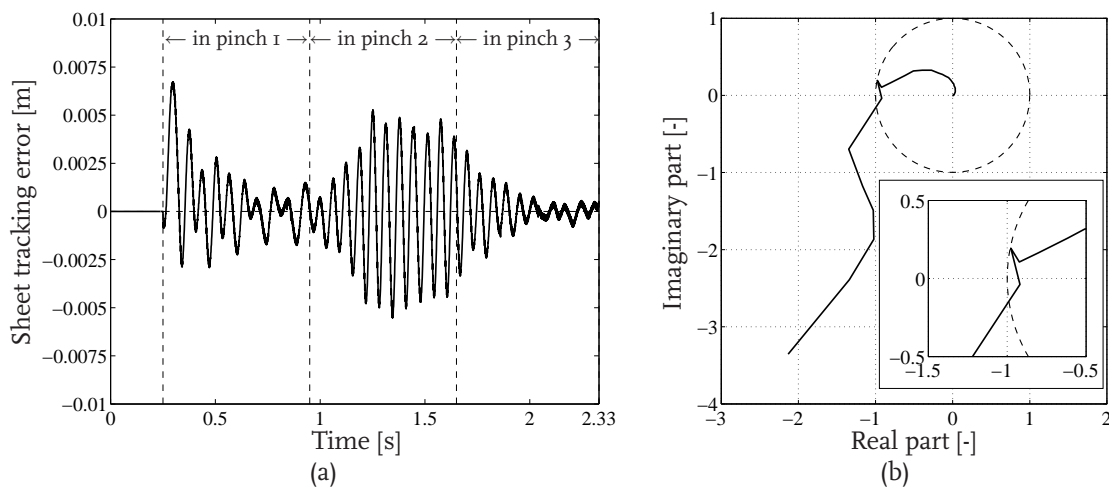


Figure 6.16 / Experimentally obtained sheet tracking error, using a low level bandwidth of 25 Hz (a), and the Nyquist plot of the loop gain of the second overall subsystem (b).

For a frequency domain analysis of the sheet tracking error, Fig. 6.17(a) shows the CPS of the measured sheet tracking error. From this figure, it can be seen that the majority of the frequency content of the error is located in the range around 15 Hz. This coincides with Fig. 6.17(b), which shows the FRF of the second overall closed-loop subsystem. In this figure, a large increase in magnitude in the frequency range around 15 Hz can be observed, resulting in the oscillatory behavior of the sheet tracking error.

As mentioned in Section 4.5, the computational effort on a CPU needed for the implementation of the controllers designed in Sections 3.2.2 and 4.3.3 can be analyzed to investigate to what extent the increase of the controller order results in an increase in computational effort. In the experiments discussed in Section 6.2, the average CPU time used for the calculation of the control scheme was $21.9 \cdot 10^{-6}$ s, whereas in Section 6.3.2 an average calculation time of $24.6 \cdot 10^{-6}$ s was needed. From this it can be concluded

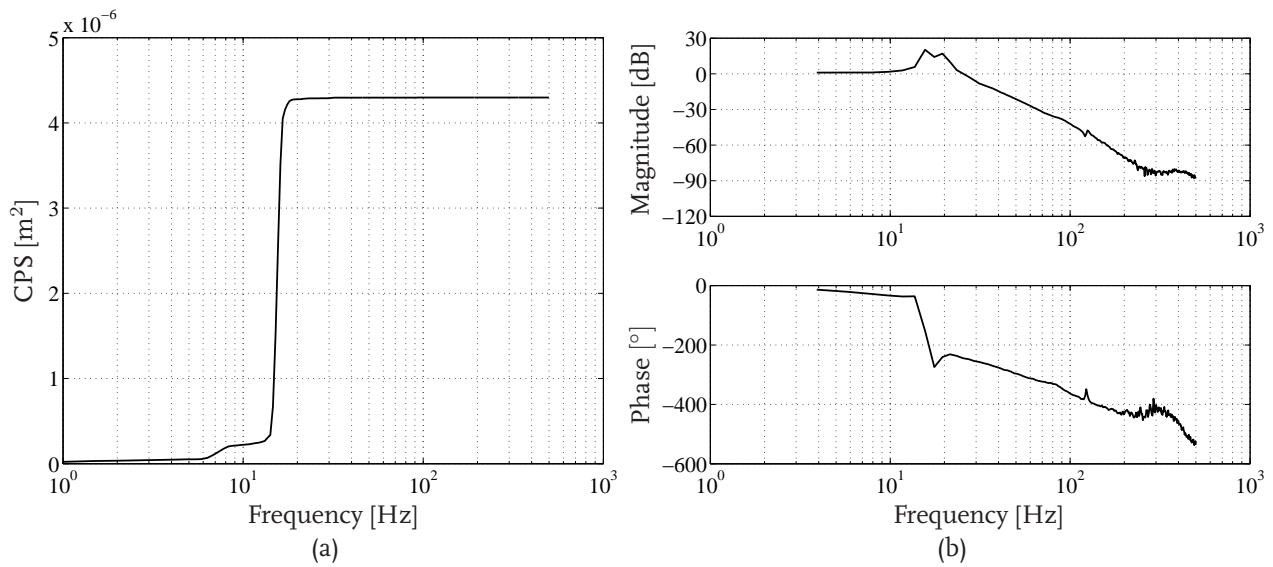


Figure 6.17 / Cumulative power spectrum of the sheet tracking error (a) and the FRF of the second closed-loop subsystem (b).

that using the PC-based control system in our experimental setup, the higher order controllers require approximately 12% more average CPU time. In this case, this was not a problem. However, the effect of such an increase in an embedded environment should be analyzed to guarantee the system will work properly.

Extensions of Sheet Feedback Control to Real Printer Paper Paths

7.1	Challenges in Industrial Paper Paths	107
7.2	Duplex Loop Modeling and Control	108
7.3	Sheet Transport via Multiple Pinches	113
7.4	Coupling Pinches into Sections	128
7.5	Evaluation	130

7.1 Challenges in Industrial Paper Paths

In Chapter 2, a basic paper path was chosen as a case-study for sheet feedback control design. So far, some of the challenging aspects of real printer paper paths have deliberately been left out of consideration to reveal the essence of the control problem. The three main differences between the basic paper path and real paper path layouts, as the one shown in Fig.1.3, are

1. the absence of a duplex loop for backside printing,
2. the distances between the pinches being equal to the sheet length,
3. and the actuation of each pinch by a separate motor.

To bridge the gap between the design of sheet feedback controllers for the basic paper path and a real paper path, this chapter will describe sheet feedback control design for

the case of a duplex loop and for the case a single sheet is driven by multiple pinches. Furthermore, initial ideas of applying sheet feedback control in case pinches are coupled into sections and driven by a single motor will be given, together with the consequences of integrating the approach in an embedded environment.

The choice for the control design approach to be used for the extensions of the basic paper path case study is based on the evaluation of both approaches given in Sections 3.4 and 4.5. The main concerns regarding the first approach, i.e. the fact that carrying out sheet feedback control design for robustness is not possible, the dependency of the control design and the controller structure on the order of the sheet reference profile, and the inability to apply frequency dependent weighting to the transfer functions of interest, were tackled by the second approach. On the other hand, one could argue that the dependency of the controller on the sheet position, needed for accurate switching, is a drawback since robustness against variations of the pinch positions cannot be obtained. However, this lack of robustness is also present when the controllers designed in Chapter 3 are used in case multiple sheets are present in the paper path, as will be the case in real printers. Based on the above mentioned considerations, it is decided to choose the control design approach described in Chapter 4 when extending the basic paper path case study.

7.2 Duplex Loop Modeling and Control

7.2.1 The Tracking Control Problem

For industrial high volume cut sheet document handling systems, the capability of back-side printing is indispensable. Therefore the paper paths in these systems have to be equipped with a mechanism that is capable of turning the sheet such that after printing the front side, also the back side can be printed. A common solution is to use a connection between the part of the paper path before and after the ITS, as can be seen in Fig. 1.3. This connection is here denoted as the duplex loop. After printing the front side, the sheet re-enters the first part of the paper path via the duplex loop. After leaving this loop, the direction of motion of the sheet is changed such that it is transported to the ITS again for back side printing.

To investigate the possibilities of modeling and controlling the sheet flow in a paper path equipped with a duplex loop, the basic paper path shown in Fig. 2.1 is adapted such that it contains a duplex loop, yielding the paper path shown in Fig. 7.1. The orientation of the pinches and the duplex loop are chosen in analogy with Fig. 1.3. As can be seen, the paper path consists of three pinches, each driven by a separate motor. The pinch locations

in the paper path are again represented by x_{P1} , x_{P2} , and x_{P3} , respectively, whereas their locations are again chosen such that both the distance between pinches P1 and P2 and the distance between pinches P2 and P3 is equal to the length of an A4 sheet, i.e. $L_s = 0.21$ m. As a reference, the location of pinch P1 is chosen to be $x_{P1} = 0$, as indicated in Fig. 7.1.

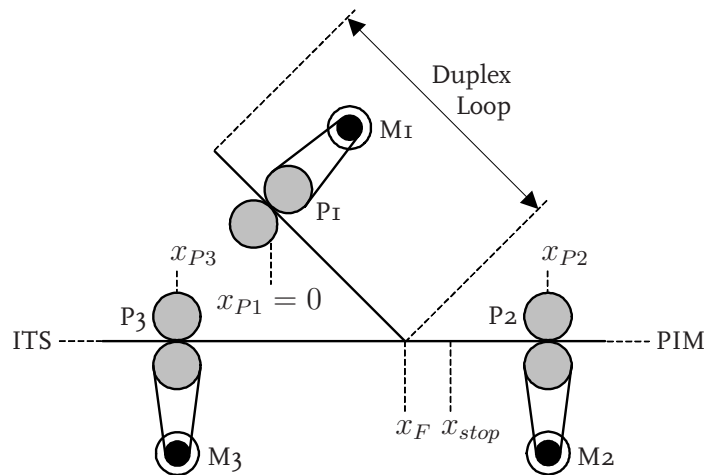


Figure 7.1 / Schematic representation of the basic duplex loop and its connection to the original basic paper path.

In Fig. 7.2, the sheet flow in the basic paper path with duplex loop is schematically depicted. From the first situation shown in this figure it can be seen that the sheet passes the points x_F and x_{stop} when it is transported from pinch P1 to pinch P2. After the trailing edge of a sheet has passed the point x_F , it is assumed that the sheet cannot re-enter the duplex loop due to the proper construction of the paper path. The point x_{stop} is the location in the paper path at which, when reached by the trailing edge of the sheet, the direction of motion of this sheet is supposed to change, as can be seen by situation 2 in Fig. 7.2. The trailing edge of the sheet now becomes the leading edge. After this change of direction the sheet is transported towards pinch P3, as indicated by situation 3.

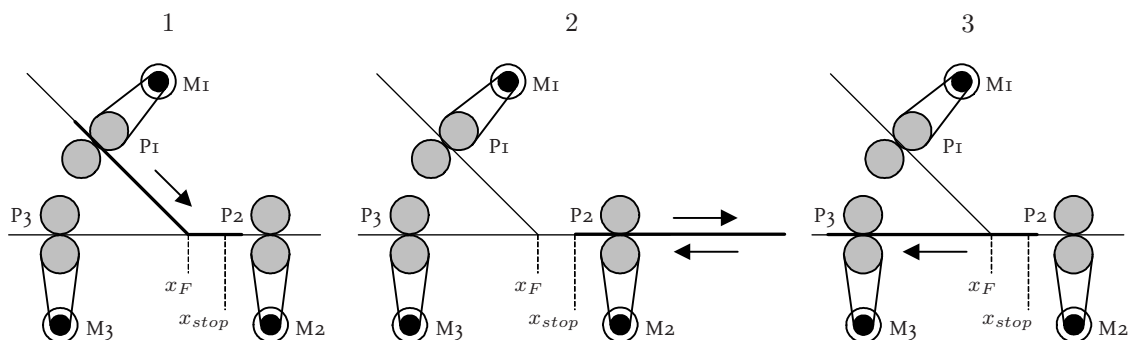


Figure 7.2 / Schematic representation of the sheet flow in the basic duplex loop.

The position of the sheet in the paper path is denoted by x_s . As long as the sheet is in the duplex loop, x_s is defined as the distance between the leading edge of the sheet and x_{P1} . As soon as x_s becomes equal to $x_F + L_s$, i.e. when the sheet has completely left the duplex loop, x_s is defined to increase when the sheet is transported towards the PIM, whereas x_s will decrease when the sheet is transported towards the ITS. This definition, in combination with the choice on the distances between pinches P1 and P2 and between pinches P2 and P3, leads to the fact that $x_s = 0$ when the sheet leaves the paper path. This implies that there is no unique correspondence between the sheet position and the location of a sheet in the paper path when $x_s < x_F + L_s$, since x_s is also equal to zero when the sheet enters the paper path. To solve this problem, the sheet flow model is extended with an additional state x_e that can be used to derive the actual location of a sheet. This state, with initial value $x_e(0) = 0$ will start to increase, e.g. with $\dot{x}_e = 1$, as soon as the trailing edge of the sheet becomes equal to x_F , i.e. when $x_s = x_F + L_s$. This can be seen in Fig. 7.3, which shows an example of the trajectory of both states. In the realization of both state trajectories, x_F and x_{stop} are chosen to be $x_F = 0.1$ m and $x_{stop} = 0.14$ m, respectively. Furthermore, the pinch positions are chosen to be $x_{P1} = 0$ m, $x_{P2} = L_s$ m, and $x_{P3} = 0$ m. From Fig. 7.3 it can be observed that the sheet position, indicated by the thick line, increases until the trailing edge reaches the point x_{stop} . At that point, the sheet is stopped for 0.25 s, i.e. the time assumed to be needed in real paper paths to align the sheets in lateral and skewness direction. After this time interval, the sheet position decreases until the new trailing edge leaves pinch P3. The additional state, indicated by the thin line in Fig. 7.3, remains zero when the sheet is in the duplex loop, i.e. until the moment the sheet position becomes equal to $x_F + L_s$. After that moment, x_e increases with $\dot{x}_e = 1$.

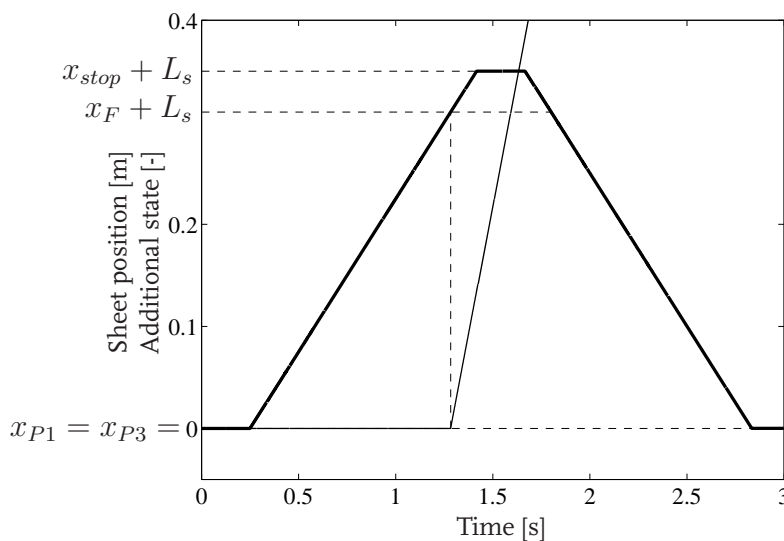


Figure 7.3 / Sheet position x_s (thick) and additional state x_e (thin) in case of sheet transport in a paper path with duplex loop.

The model describing the sheet flow through the simplified paper path with duplex loop is based on the sheet flow model described in Section 3.3. To incorporate the additional state x_e , however, an affine term \underline{a}_i is incorporated [52]:

$$\dot{\underline{x}} = (B_i + \Delta B_i) \underline{u} + \underline{a}_i \quad \text{for } x_s \in \mathcal{X}_i, i \in \mathcal{I}, \quad (7.1)$$

In this piecewise affine (PWA) sheet flow model, $\underline{x} = [x_s \ x_e]^T$ represents the state vector and $\underline{u} = [\omega_{M1} \ \omega_{M2} \ \omega_{M3}]^T$ is the column with high level control inputs. The input matrices B_i , the uncertainties in these matrices ΔB_i , and the affine terms \underline{a}_i are region dependent. In (7.1), \mathcal{I} represents the index set of the sheet regions. In this case, five different regions are defined. In the first region, denoted by ①, the sheet is driven by pinch P_I, and therefore $B_1 = \begin{bmatrix} n_1 r_{P1} & 0 & 0 \\ 0 & 0 & 0 \end{bmatrix}$. Since in this region the trailing edge of the sheet does not pass x_F , x_e remains equal to zero. Hence, $\underline{a}_1 = [0 \ 0]^T$. The first region in the state space is therefore represented by $\mathcal{X}_1 = \{x_s | x_s \in [x_{P1}, x_{P2}), x_e | x_e = 0\}$. In the second, third, and fourth region, denoted by ②, ③, and ④, respectively, the sheet is driven by pinch P₂, and therefore $B_2 = B_3 = B_4 = \begin{bmatrix} 0 & n_2 r_{P2} & 0 \\ 0 & 0 & 0 \end{bmatrix}$. The difference between these regions is determined by the location of the sheet in the paper path. When the trailing edge of the sheet has not yet passed the point x_F , $\underline{a}_2 = [0 \ 0]^T$ and therefore x_e remains zero. Consequently, the second region in the state space is represented by $\mathcal{X}_2 = \{x_s | x_s \in [x_{P2}, x_F + L_s), x_e | x_e = 0\}$. After the sheet has left the duplex loop, i.e. when the trailing edge of the sheet has passed x_F but has not yet passed the second pinch, the dynamics in the third regime become active. To prevent the sheet from going back into the duplex loop, and therefore to prevent the sheet flow model from re-entering the second regime, $\underline{a}_3 = [0 \ 1]^T$. Consequently, $\mathcal{X}_3 = \{x_s | x_s \in [x_F + L_s, x_{P2} + L_s), x_e | x_e \in [0, \infty)\}$. The fourth regime becomes active when the sheet has passed x_F on its way to pinch P₃, but is not yet driven by this pinch. In this regime, \underline{a}_4 is chosen to be $\underline{a}_4 = [0 \ 1]^T$ and the region in the state space is represented by $\mathcal{X}_4 = \{x_s | x_s \in [x_{P3} + L_s, x_F + L_s), x_e | x_e \in (0, \infty)\}$. In the final regime, denoted by ⑤, the sheet position has become smaller than $x_{P3} + L_s$ and pinch P₃ drives the sheet, and therefore $B_5 = \begin{bmatrix} 0 & 0 & n_3 r_{P3} \\ 0 & 0 & 0 \end{bmatrix}$. Furthermore, \underline{a}_5 is chosen to be $\underline{a}_5 = [0 \ 1]^T$. The conditions to be met for this regime to be active are given by $\mathcal{X}_5 = \{x_s | x_s \in [x_{P3}, x_{P3} + L_s), x_e | x_e \in (0, \infty)\}$. In all regions, the uncertainty terms of the i -th subsystem, ΔB_i , are defined in analogy with the input matrices B_i .

7.2.2 Sheet Feedback Control Design

Regarding the sheet flow control design in a duplex loop, the PWA sheet flow dynamics (7.1) are considered to be a switched linear system. This implies that the switching

conditions in (7.1) are neglected and, hence, the system is supposed to be able to switch arbitrarily. Consequently, the additional state x_e , which is only needed to properly specify the switching conditions, and the affine term \underline{a}_i are not needed for control design purposes. Hence, the control design can be carried out in analogy with the design presented in Section 4.3, based on the sheet flow dynamics in (3.42). Since the sheet is driven by one motor-pinch combination in the regions ②-④, the sheet flow dynamics in these regions are identical. Hence, the control design for these regions can be captured in a single LMI, yielding a total amount of four LMIs to be solved, as was the case in Section 4.3. Since the parameters used in the design have been chosen identical to the ones listed in Table 3.2, also the resulting sheet feedback controllers are identical to the ones presented in Section 4.3.3.

7.2.3 Simulation Results

For the validation of the control design approach, simulations of the basic printer paper path with duplex loop have been carried out using the PWA sheet flow model (7.1) and the sheet feedback controllers designed in Section 7.2.2. In these simulations, the sheet had to track the profile depicted in Fig. 7.3. The transmission ratios and pinch radii used in the simulation are equal to the actual values listed in Table 3.2. This implies that also in this case the actual transmission ratios used in the simulations have been perturbed with respect to the nominal ones to study the robustness properties of the closed-loop system. The results of the simulation are shown in Fig. 7.4. It can be seen that the additional state x_e , represented by the thin line and scaled by a factor 0.01 for visibility purposes, starts to increase as soon as the third regime of the model (7.1) becomes active, i.e. when the trailing edge of the sheet reaches the point x_F . The sheet tracking error obtained in the first two regimes is identical to the one shown in Fig. 4.15, resulting from the exact match between the control designs and simulation parameters. In the third region, two significant increases in sheet tracking error can be observed. These correspond to the jumps in sheet reference velocity when stopping the sheet and accelerating it in opposite direction. When entering region ⑤, the sheet tracking error deviates from zero, caused by the perturbation of the transmission ratio in this region. Comparing this deviation to the one shown in Fig. 4.15, it can be observed that in this case the sheet tracking error becomes negative, whereas Fig. 4.15 shows a positive deviation. This corresponds to the fact that the sign of the sheet reference velocities is different in both cases.

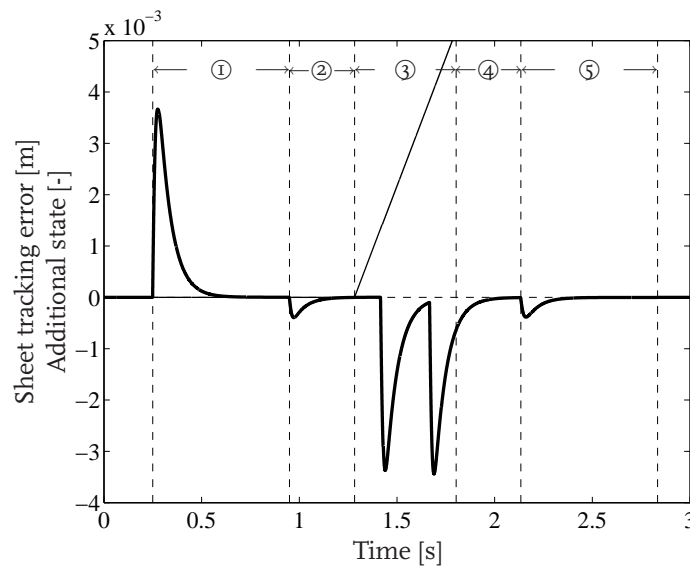


Figure 7.4 / Sheet tracking error (thick) and additional state (thin) obtained in simulation in case of sheet transport in a duplex loop.

7.3 Sheet Transport via Multiple Pinches

7.3.1 The Tracking Control Problem

Besides two-sided printing, another important requirement for document handling systems is the capability of transporting sheets with different dimensions. This implies that one of the assumptions made in Section 2.1, i.e. the distances between the pinches being equal to the sheet length, does not hold anymore. More specifically, these distances must always be smaller than or equal to the length of the smallest sheet to be transported. Hence, the situation in which multiple pinches are driving a single sheet will occur in real printers for the larger sheet sizes, resulting in a coupling of the dynamics of different motor-pinch combinations via the sheet.

Before going into further detail on the control problem at hand, we will first present the case-study adopted in this section, in order to facilitate the reasoning about the control problem. In this case study, the paper path depicted in Fig. 7.5 is considered. In this paper path an A3-format sheet, the length of which is 0.42 m, is transported by two pinches, each connected to a separate motor. The distance between these pinches is chosen to be 0.21 m, which corresponds to the size of an A4-format sheet. The sheet position x_s is again defined as the position of the leading edge of the sheet in the paper path.

From Fig. 7.5, it can be derived that when the sheet is in both pinches, two additional phenomena can occur in contrast with the case-study presented in Section 2.1. First of

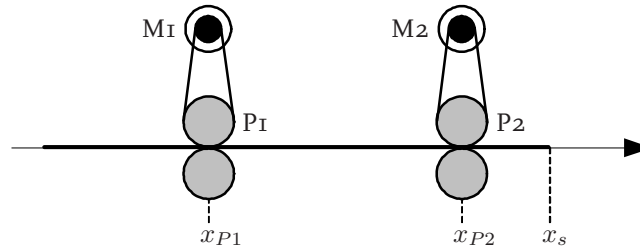


Figure 7.5 / Schematic representation of the printer paper path in which the sheet length exceeds the distance between the pinches.

all, when the circumferential velocity of pinch P_1 , v_{P_1} , is larger than the circumferential velocity of pinch P_2 , v_{P_2} , buckling of the sheet can occur. However, because of the limited available space in real printer paper paths, buckling is often not possible without obtaining a damaged or folded sheet. Therefore, in the case-study at hand a constraint has to be incorporated that enforces the sheet not to buckle when it is driven by both motor-pinch combinations. On the other hand, when $v_{P_1} < v_{P_2}$, a pulling force, imposed by the difference in pinch velocities, is transmitted via the sheet. When this force causes the contact force between the sheet and one of the driven rollers to become larger than the friction force present in the corresponding contact, slip will occur. Since this is not allowed, as it can damage the sheet or smudge the printed image, also this phenomenon imposes an additional constraint to be taken into account in the design of the sheet handling system.

In the case-study at hand, we choose the most downstream motor-pinch combination, i.e. motor M_2 and pinch P_2 in Fig. 7.5, to be the only one to influence the sheet motion when a sheet is in two pinches, as it is closest to the leading edge of the sheet, i.e. the edge that defines the sheet position. This implies that the first motor-pinch combination should behave such that it does not have a negative influence on the second motor-pinch combination. This can be realized both mechanically and via control. Examples of mechanical solutions are lifting the first pinch such that only the second pinch is in contact with the sheet, or equipping the first pinch with a unidirectional bearing. With such a bearing, the first motor-pinch combination does not drive the sheet as long as the circumferential velocity of pinch P_2 is larger than the circumferential velocity of pinch P_1 . As a result, the sheet reference velocity should slightly increase as soon as the sheet enters pinch P_2 . A benefit of both mechanical solutions is that they support the subdivision of the control problem into high level sheet control and low level motor control, as proposed in Chapter 2. A drawback of both mechanical solutions, however, is the increase in costs, since additional parts are necessary.

Therefore, in this section we propose to limit the influence of the first motor-pinch combination on the second one via a control approach. Given the no-slip and no-buckling constraints, the circumferential velocities of the two pinches driving the sheet should be

equal. To realize this goal, funnel-shaped velocity bounds, as proposed in [12, 13, 46], could be used in combination with the sheet feedback controllers designed in Section 4.3.3. However, in case parametric uncertainties are present in the paper path, perfect synchronization of the circumferential pinch velocities cannot be guaranteed. Hence, in this section the goal is to apply the systematic, model-based methodology for sheet feedback control design presented in Chapters 2 and 4, taking into account the two additional constraints. To realize this goal, two questions have to be answered first:

1. Can the control problem still be decoupled into low level motor control and high level sheet control?
2. Can we still ensure the difference in high level and low level bandwidth and a good low level tracking behavior, such that the controlled motor dynamics can be assumed to be ideal when designing the sheet control loop?

Regarding the first question, we know that if the pulling force in the sheet is limited, the contact forces present between the driven rollers and the sheet will be limited as well, and no slip will occur between the sheet and the pinches. Hence, similar to Section 2.3, a decoupling into low level motor control and high level sheet control is possible. Limitation of the pulling force in the sheet can be realized by adapting the low level control strategy of motor M_1 at the moment the sheet is driven by both pinches. In this adaptation, however, care has to be taken to ensure that buckling of the sheet does not occur either. The adaptation of the control strategy is necessary, since applying the original high gain PID feedback controller to both motors in case the sheet is in two pinches and in case the paper path parameters are perturbed will result in slip between the sheet and one of the pinches. This can be explained by the fact that in this case both controlled motors will try to closely track their reference velocities. However, due to the uncertainties in the paper path parameters, the values of the motor reference velocities can be such that the corresponding circumferential pinch velocities are not equal. Therefore, it is not possible for both motors to accurately track their reference velocities without slip between the sheet and both pinches. Hence, the control action for one or both motors, and therefore the contact force between the sheet and the driven roller and the pulling force transmitted via the sheet, will increase until slip between the sheet and one of the pinches will occur.

The answer to the second question follows from the choice that when the sheet is in two pinches, the downstream motor-pinch combination determines the sheet motion and the upstream motor-pinch combination follows this motion without strongly influencing the behavior of the downstream motor and pinch. Hence, if the downstream motor control loop, i.e. the control loop for motor M_2 , has a good tracking behavior and is designed to have a higher bandwidth than the sheet control loop, satisfying the rules of thumb used in hierarchical control design [75], the controlled motors can be assumed to be ideal.

Given the positive answers to the two questions posed, the sheet feedback control design can be carried out and the adaptations to the control strategy of motor M₁ can be made. Hence, in the next section we will present the modeling and control design of the sheet flow, after which the motor control design will be discussed.

7.3.2 High Level Sheet Flow Modeling and Control Design

From the previous section we know that the desired decoupling of the overall sheet handling control problem into low level motor control and high level sheet control can be maintained if the low level control strategies of motor M₁ and motor M₂ are adapted at the moment the sheet is driven by two pinches. This implies that the sheet flow modeling and control design can be done in analogy with the modeling and control design presented in Chapters 2 and 4.

The high level sheet flow model can be derived based on Fig. 7.5. As in Chapter 2, the inputs of the model that are acting on the sheet flow will change when the sheet is transported through the paper path. Hence, also in this case the sheet flow dynamics can be captured in the PWL modeling formalism. Furthermore, flexibilities in the gear belts connecting motors and pinches are again neglected, and slip between the pinches and the sheet is not taken into account as it will be prevented from occurring by the adaptation of the motor M₁ control strategy. In the derivation of the high level sheet flow model, the assumption that when a sheet is in two pinches, only the most downstream motor-pinch combination influences the sheet motion is incorporated. Given these modeling choices and assumptions, the resulting sheet flow model can be represented in analogy with (3.42):

$$\dot{x}_s = (B_i + \Delta B_i) \underline{u} \quad \text{for } x_s \in \mathcal{X}_i, i \in \mathcal{I}, \quad (7.2)$$

with the input matrices B_i defined as $B_1 = \begin{bmatrix} n_1 r_{P1} & 0 \end{bmatrix}$ and $B_2 = B_3 = \begin{bmatrix} 0 & n_2 r_{P2} \end{bmatrix}$, and with the uncertainty terms of the i -th subsystem, ΔB_i , defined in analogy with the input matrices B_i . Furthermore, \underline{u} represents the column with inputs of the high level sheet dynamics: $\underline{u} = \begin{bmatrix} \omega_{M1} & \omega_{M2} \end{bmatrix}^T$. The partitioning of the state space into the three regions is in this case represented by $\{\mathcal{X}_i\}_{i \in \mathcal{I}} \subseteq \mathbb{R}$, with $\mathcal{X}_1 = \{x_s | x_s \in [x_{P1}, x_{P2})\}$, $\mathcal{X}_2 = \{x_s | x_s \in [x_{P2}, x_{P1} + L_s)\}$, and $\mathcal{X}_3 = \{x_s | x_s \in [x_{P1} + L_s, x_{P2} + L_s)\}$.

Since the high level sheet flow model has exactly the same structure as the model used in Section 4.3, and since the parameters for the case-study at hand have been chosen identical to the ones used in Section 4.3, both the controller synthesis and the control design can be carried out in complete analogy with the synthesis and design presented in Sections 4.3.2 and 4.3.3, respectively.

7.3.3 Low Level Motor Control Design

From Section 7.3.1 we know that the control strategy of motor M_1 should be adapted such that the pulling force transmitted via the sheet is limited and such that buckling of the sheet, i.e. the occurrence of negative pulling forces, is avoided. To realize this goal, several control options are possible. The first option encompasses the implementation of a force controller for motor M_1 . Using this controller, the force transmitted via the sheet can be controlled by adaptation of the motion of the first motor-pinch combination. However, obtaining the transmitted force, needed in the control design, is far from trivial. Adding extra sensors is a possibility, but this is undesired as it adds extra costs and complexity to the system. Model-based estimation of the force is another possibility. However, as this force depends on the varying friction characteristics, detailed friction modeling is necessary to obtain a good estimate. Hence, this option also adds much complexity to the design. A second option is to compensate for the dynamics of the first motor-pinch combination via a motion control strategy such that the pulling force transmitted via the sheet will be limited and such that buckling of the sheet will not occur. In this section we propose the application of a feedforward controller for motor M_1 . In addition to this, we propose the use of an updated feedback controller for motor M_2 to realize accurate transportation of the sheet when driven by two pinches. By applying the feedforward controller, part of the dynamics of the first motor-pinch combination can be compensated for. Furthermore, buckling can be prevented and slip is likely to be avoided. On the other hand, the updated feedback controller for the second motor-pinch combination takes care of the compensation of the remaining dynamics of the first motor and the first pinch. The resulting control architecture of the printer paper path for the case the sheet is in both pinches is shown in Fig. 7.6.

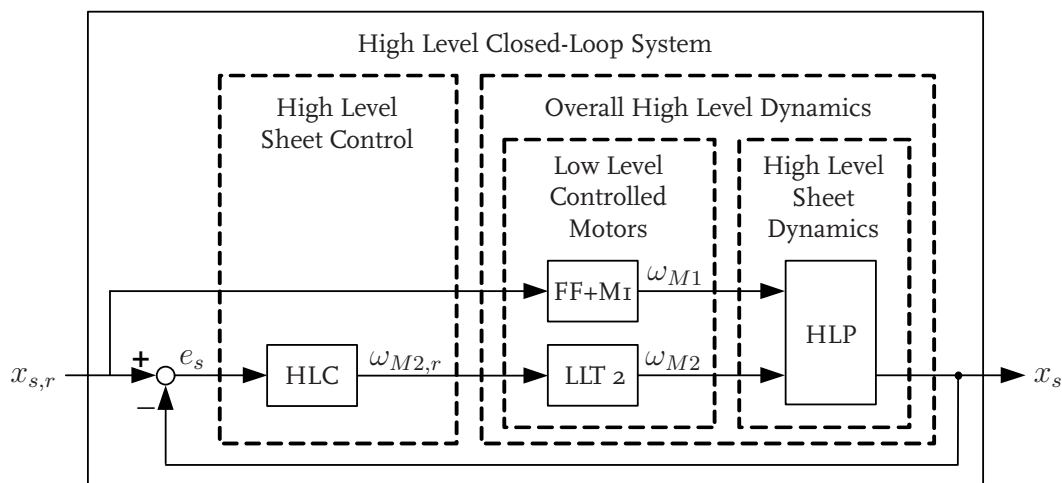


Figure 7.6 / Block diagram of the control scheme for the case the sheet is in two pinches.

From this block diagram it can be observed that the second motor is still controlled by a feedback controller, although this controller will be different from the one used in this thesis so far, yielding closed-loop motor dynamics LLT 2. On the other hand, the first motor is controlled by the feedforward controller, indicated by FF. When the sheet is only driven by one pinch, a block diagram similar to the one shown in Fig. 2.4 is obtained. Hence, switching of the low level controllers will be needed as the sheet is transported through the paper path. The design of both motion controllers will be discussed in the following two subsections.

7.3.3.1 Feedforward Control Structure

In the design of a motion feedforward controller for motor M_I, the sheet reference profile is chosen to be the input of the controller. In this section, this profile is assumed to be equal to the one used in the preceding chapters of this thesis, i.e. with $\ddot{x}_{s,r} = 0$. Hence, only the friction and damping of the first motor-pinch combination will be compensated for by the feedforward controller. When the sheet reference profile would also include nonzero acceleration parts, the inertia of the first motor-pinch combination should be compensated for as well. The feedforward control law to be implemented can be formulated as follows:

$$u_{FF,1} = \frac{1}{K_{A1}K_{M1}} (K_{S1}k_{d1}\dot{x}_{s,r} + k_{f1} \text{sign}(\dot{x}_{s,r})), \quad (7.3)$$

with k_{d1} the feedforward control parameter for the compensation of damping, in Nms/rad, and with k_{f1} the feedforward control parameter for dynamic friction compensation in Nm. Furthermore, K_{S1} represents a scaling factor needed to avoid buckling. The value of this scaling factor is determined such that in worst-case situations with respect to buckling, v_{P1} will be equal to $\dot{x}_{s,r}$ when the sheet is driven by both pinches. This worst-case situation will occur when the first and the second motor-pinch combination have maximum and minimum gain, respectively, as schematically depicted in Fig. 7.7. We know that in this case the following expression holds for v_{P1} :

$$v_{P1} = (B_1(1) + \Delta B_{1,max}(1)) \omega_{M1}, \quad (7.4)$$

with $\Delta B_{1,max}(1)$ the maximum possible perturbation of the gain of the first high level subsystem, i.e. the one equal to the uncertainty bound in Table 3.2. When we assume perfect compensation of the motor dynamics when using the feedforward control law (7.3), the following expression for ω_{M1} can be derived:

$$\omega_{M1} = K_{S1}\dot{x}_{s,r}. \quad (7.5)$$

Since we know that $v_{P1} = \dot{x}_{s,r}$ has to hold for the worst-case situation under consideration, the value of K_{S1} can be determined after substitution of (7.5) into (7.4):

$$K_{S1} = \frac{1}{(B_1(1) + \Delta B_{1,max}(1))}. \quad (7.6)$$

Given the values of the paper path parameters, shown in Table 3.2, the value of K_{S1} becomes $K_{S1} = 121.3$.

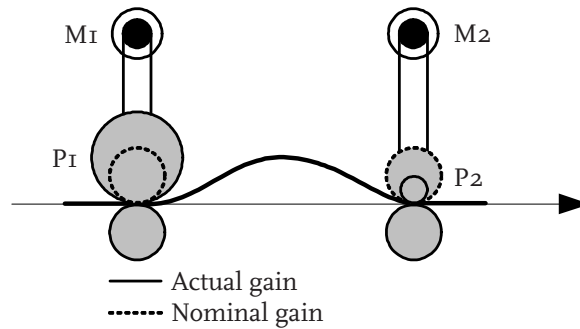


Figure 7.7 / Schematic representation of the worst-case situation with respect to buckling when $K_{S1} = 1$: the actual gains of the first and second motor pinch combination are maximal and minimal, respectively.

To analyze the effect of applying the feedforward control law (7.3) on the difference between v_{P1} and v_{P2} in the worst-case situation for buckling, simulations have been carried out. In these simulations, the sheet flow in the paper path depicted in Fig. 7.5 has been simulated. The A3-format sheet enters the paper path at $t = 0.25$ s and has to be transported at a velocity of 0.3 m/s. It leaves the paper path when its trailing edge has left pinch P2. The paper path parameters have been chosen such that the actual gain of the first motor-pinch combination is equal to $B_1(1) + \Delta B_{1,max}(1)$, whereas the actual gain of the second motor-pinch combination is equal to $B_2(2) - \Delta B_{2,max}(2)$. The choice of these gains leads to the largest buckle to be created if the scaling factor K_{S1} would be equal to 1. In the simulations, the sheet feedback controllers designed in Section 7.3.2 have been used. Furthermore, both the original model and the original feedback controller of motor M2, presented in Section 6.1, have been used. Regarding motor M1, damping and friction have been added to the model derived in Section 6.1, to be able to compensate for these effects using the feedforward controller. In case the sheet is only driven by pinch P1, the PID feedback controller derived in Section 6.1 has been used, whereas at the moment the sheet enters pinch P2 the switch in motor M1 control strategy is made from feedback control to feedforward control. To validate the choice of the scaling factor K_{S1} , perfect compensation via the feedforward controller has been applied.

The results of the simulation are shown in Fig. 7.8. In Fig. 7.8(a), the sheet tracking error obtained in the simulation is depicted. It can be seen that after the sheet enters pinch P2, the error starts increasing in the positive direction, which corresponds with the fact that the actual transmission ratio of the second motor-pinch combination in the simulation is smaller than the nominal value taken into account in the control design.

This also causes the circumferential velocity of pinch P2 to be smaller than 0.3 m/s when the sheet is only driven by pinch P1, as can be seen in Fig. 7.8(b). From this figure, it can also be seen that when the sheet enters pinch P2, the circumferential velocity of pinch P1 remains equal to 0.3 m/s. Hence, since perfect compensation of the dynamics of the first motor-pinch combination has been applied, it can be concluded that the scaling factor K_{S1} was chosen correctly. Since both circumferential velocities quickly become equal to each other when the sheet is in both pinches, no buckling and no slip are expected to occur.

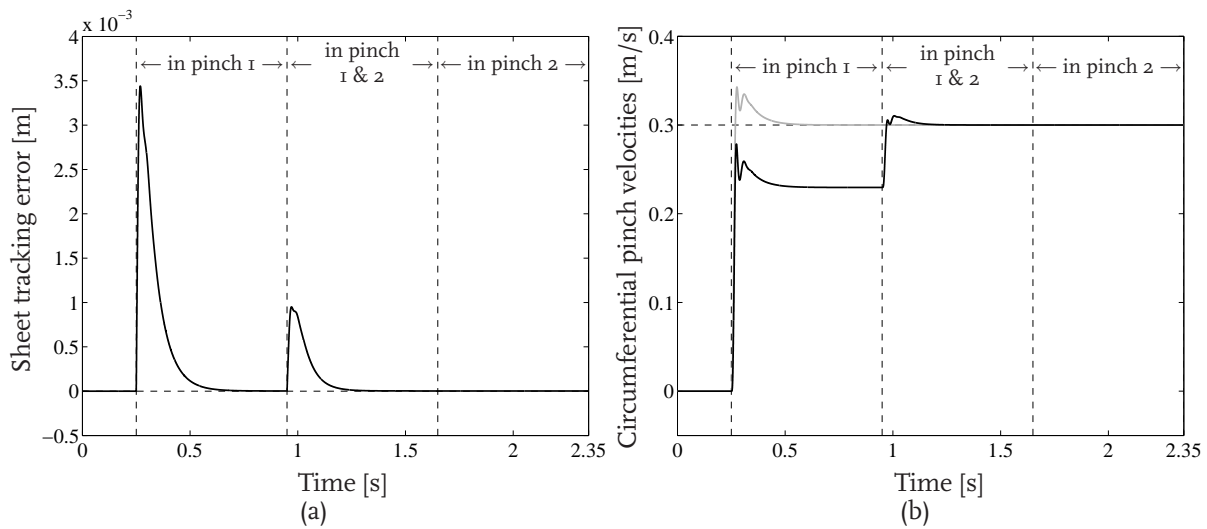


Figure 7.8 / Sheet tracking error obtained in simulation (a), together with the circumferential velocities of pinch P1 (gray) and pinch P2 (black) (b) in case the actual paper path parameters are chosen such that the chance of buckling to occur is largest.

7.3.3.2 Feedforward Control Design Results

To determine the values of the feedforward control parameters k_{d1} and k_{f1} in (7.3), an identification experiment has been carried out. In this experiment, the motor has been stabilized by a feedback controller and a number of constant velocity profiles had to be tracked. For each velocity, the average control input has been calculated, resulting in Fig. 7.9. In this figure, the average control inputs, indicated by the circles, are plotted as function of the velocity. Based on these values, a first order polynomial has been calculated that fits the measured data best in a least-squares sense, resulting in the feedforward control parameters $\frac{k_{d1}}{K_{A1}K_{M1}} = 4.6 \cdot 10^{-4}$ Vs/rad and $\frac{k_{f1}}{K_{A1}K_{M1}} = 0.22$ V. The fitted polynomial is shown in Fig. 7.9 as well, indicated by the solid line.

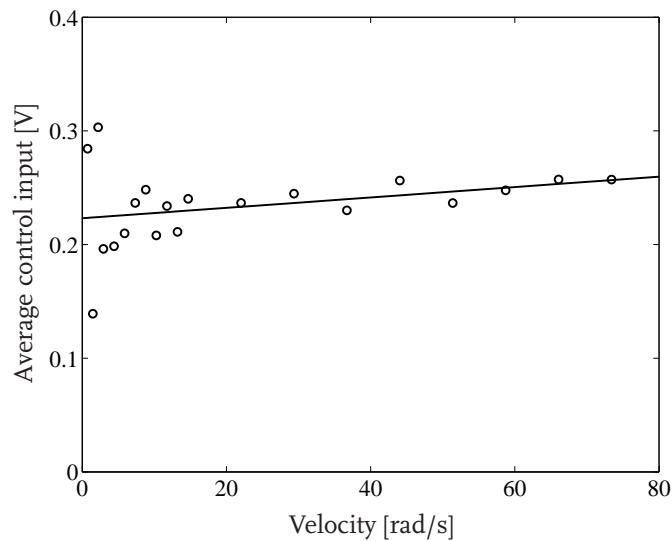


Figure 7.9 / Average control input of motor M_1 as a function of the angular motor velocity (circles), and the corresponding fitted first order polynomial (solid).

7.3.3.3 Feedback Control Design Results

The design of the feedback controller for motor M_2 , which is active when the sheet is driven by both pinches, is based on the dynamics of the two motor-pinch combinations that are connected via the sheet. To identify these coupled dynamics, FRF measurements have been carried out using the procedure presented in Section 6.1. During these measurements, motor M_2 , controlled by a low gain feedback controller, had to track a constant velocity. Since no control input was applied to motor M_1 , a pulling force was always present in the sheet, despite the addition of broadband noise to the output of the second motor controller, and the coupled dynamics could be identified. The results of the identification procedure are reliable in the frequency range above the bandwidth of the controlled system, which was 10 Hz in this case, since in this range the coherence of the measurement is good. This can be observed from Fig. 6.1, which shows the coherence of the sensitivity function, together with the FRF of the first motor-pinch combination. In analogy with Fig. 6.1, the decoupling of both the driven and the non-driven roller of pinch P_2 manifest themselves as antiresonance-resonance pairs around 120 Hz and 200 Hz, respectively. The main difference between the FRF shown in Fig. 7.10 with respect to the ones shown in Fig. 6.1 is the antiresonance-resonance pair in the frequency range between 60 – 100 Hz, resulting from the decoupling of the first motor-pinch combination.

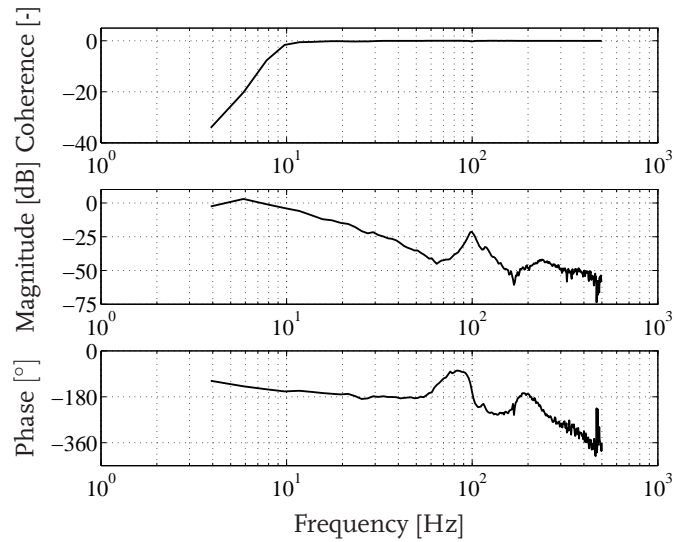


Figure 7.10 / Experimentally obtained FRF of motor M2, when the first motor-pinch combination is connected to the second one via the sheet.

Given the motor dynamics shown in Fig. 7.10, a collocated feedback controller has been designed using loopshaping techniques [25]. This controller consists of a lead filter in combination with an integral action and a notch to suppress the resonance peak at 100 Hz. Given this controller, which can be seen in Fig. 7.11(a), a bandwidth of 44 Hz has been realized, as shown in Fig. 7.11(b). Hence, also in this case the desired difference in bandwidth between the inner loop and the outer loop, discussed in Section 2.3, has been realized.

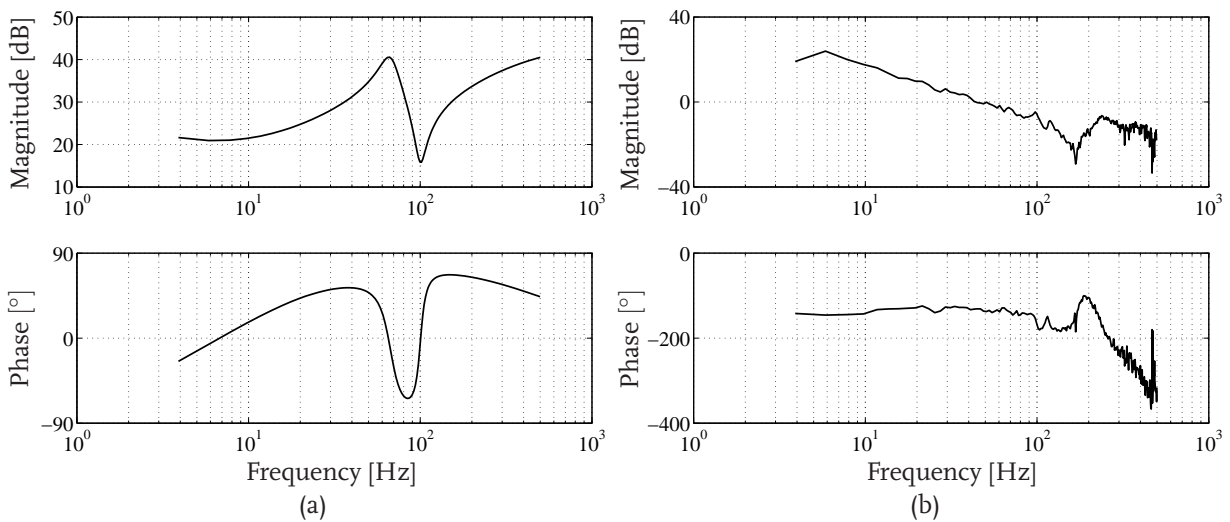


Figure 7.11 / Bode plot of the feedback controller (a), and the FRF of the loop gain (b) of the second controlled motor.

7.3.4 Validation Results

To validate the control design approach for the case a sheet is driven by two pinches, both simulations, in which the controlled motors were not taken into account, and experiments have been carried out. An A3-format sheet, the length of which is $L_s = 0.42$ m, enters the paper path at $t = 0.25$ s. It has to be transported with a velocity of 0.3 m/s and leaves the paper path when its trailing edge has left pinch P2. The distance between the pinches is chosen to be equal to the distances used in the description of the case-study in Section 7.3.1. With respect to its nominal value, the transmission ratio of the second motor-pinch combination has been perturbed by 14% to study the robustness properties. Also in this case, no disturbances and no feedforward sheet control input have been added to the sheet dynamics. Since the physical paper path parameters match the ones used in the simulation, the resemblance between simulations and experiments can be investigated.

The sheet tracking error obtained in the experiments is depicted in Fig. 7.12(a). It shows the stable behavior of the closed-loop system and it shows that for the parametric uncertainties under consideration the performance properties presented in Section 1.4 are still satisfied. The transient response, resulting from entering the second pinch, is controlled towards zero quickly. Furthermore, the harmonic component with a frequency in the range of 7 – 8 Hz in the sheet tracking error, caused by the rotation asymmetry of the first driven roller, can be observed during the time the sheet is in contact with the first pinch, which implies that the first motor-pinch combination still has some influence on the sheet motion. Fig. 7.12(a) also shows the sheet tracking error obtained in simulation, which was conducted without incorporating the low level controlled motor dynamics. Also in this case, the experimentally obtained tracking error shows much resemblance with the error obtained in simulation. For a frequency domain analysis of the sheet tracking error, Fig. 7.12(b) shows the CPS of the measured sheet tracking error, together with the CPS of the error obtained in simulation. The power of the error obtained in simulation and the experimentally obtained error is in the same order of magnitude as the power of the tracking errors obtained in Section 6.3.2, see Fig. 6.12(b), indicating that in case two motor-pinch combinations are coupled, a similar performance can be obtained compared to the case in which only one pinch is driving the sheet. From Fig. 7.12 it can be concluded that the resemblance between the experimentally obtained sheet tracking error and the error obtained in simulation, observed both visually in Fig. 7.12(a) and via the power spectrum of both errors in Fig. 7.12(b), is good. Hence, also in this case it can be concluded that the low-detailed simulation models have very good predicting capabilities.

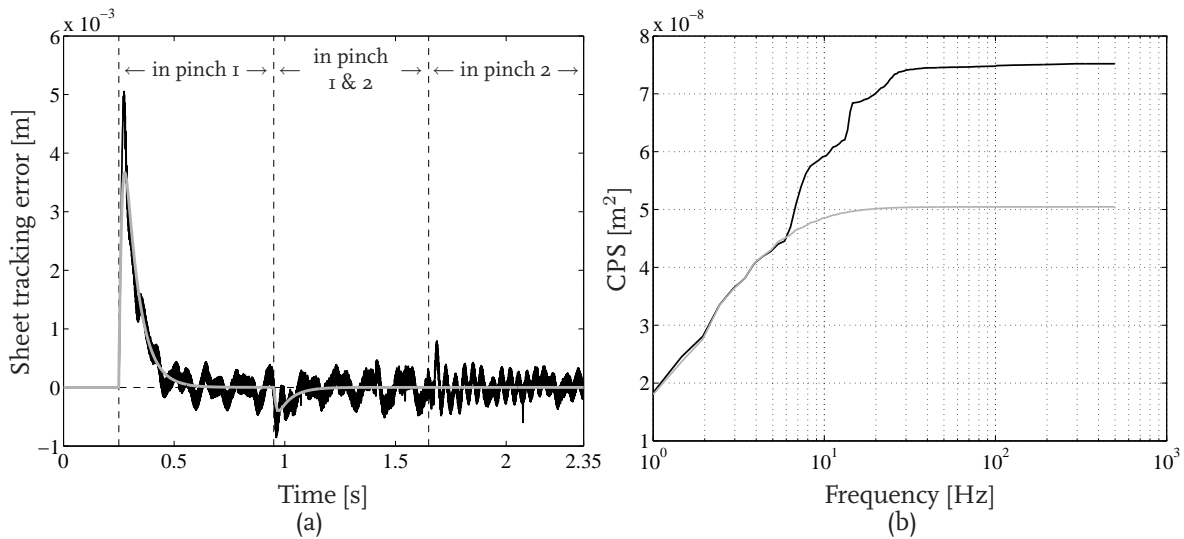


Figure 7.12 / Sheet tracking error obtained in experiments (black) and simulation (gray) (a), and their corresponding cumulative power spectra (b).

To investigate if buckling of the sheet or slip between the pinches and the sheet has occurred during the time the sheet was in contact with both pinches, the circumferential pinch velocities, calculated from the actual motor velocities via kinematic constraint relations, are depicted in Fig. 7.13(a). From this figure, it can be seen that the pinch velocities resemble each other, but are not exactly equal. For further analysis, the difference between both pinch velocities, i.e. $v_{P1} - v_{P2}$, is depicted in Fig. 7.13(b). Based on this figure, it can be concluded that both momentary buckling ($v_{P1} - v_{P2} > 0$) and momentary slip ($v_{P1} - v_{P2} < 0$) may have occurred. Since the integral of the velocity difference is smaller than zero, a net amount of slip has occurred, which is calculated to be $1.6 \cdot 10^{-3}$ m. To analyze in which pinch this slip has occurred, the difference between the sheet velocity and both circumferential pinch velocities has been depicted in Figs. 7.13(c) and 7.13(d), respectively. From these figures, it can be seen that the integral of both differences is larger than zero. This is confirmed by the calculation of these integrals, which equal $3.3 \cdot 10^{-3}$ m and $1.7 \cdot 10^{-3}$ m, respectively, indicating that a net amount of slip has occurred in both pinches. As expected, the difference between both net amounts equals the net amount of slip calculated from Fig. 7.13(b). From Fig. 7.13(d), it can also be observed that at many time instants the actual sheet velocity is larger than the circumferential velocity of pinch P2. Under the assumption of perfectly round driven rollers, this is unexpected, since it implies that the first pinch pushes the sheet through the second one without buckling to occur. This phenomenon is not likely to really have happened in the experiment, since the force needed to create a buckle is much smaller than the maximum friction force that should be exceeded for slip to occur. This unexpected result is probably caused by the way the sheet position is measured. More specifically, the sheet position is obtained via

sensors that are located between the pinches in the experimental setup. Hence, the actual velocities of the sheet in the pinches are not known if blousing occurs or if the sheet is stretched during pulling. From this we can conclude that the experimental results shown in Fig. 7.13 should be interpreted with some caution.

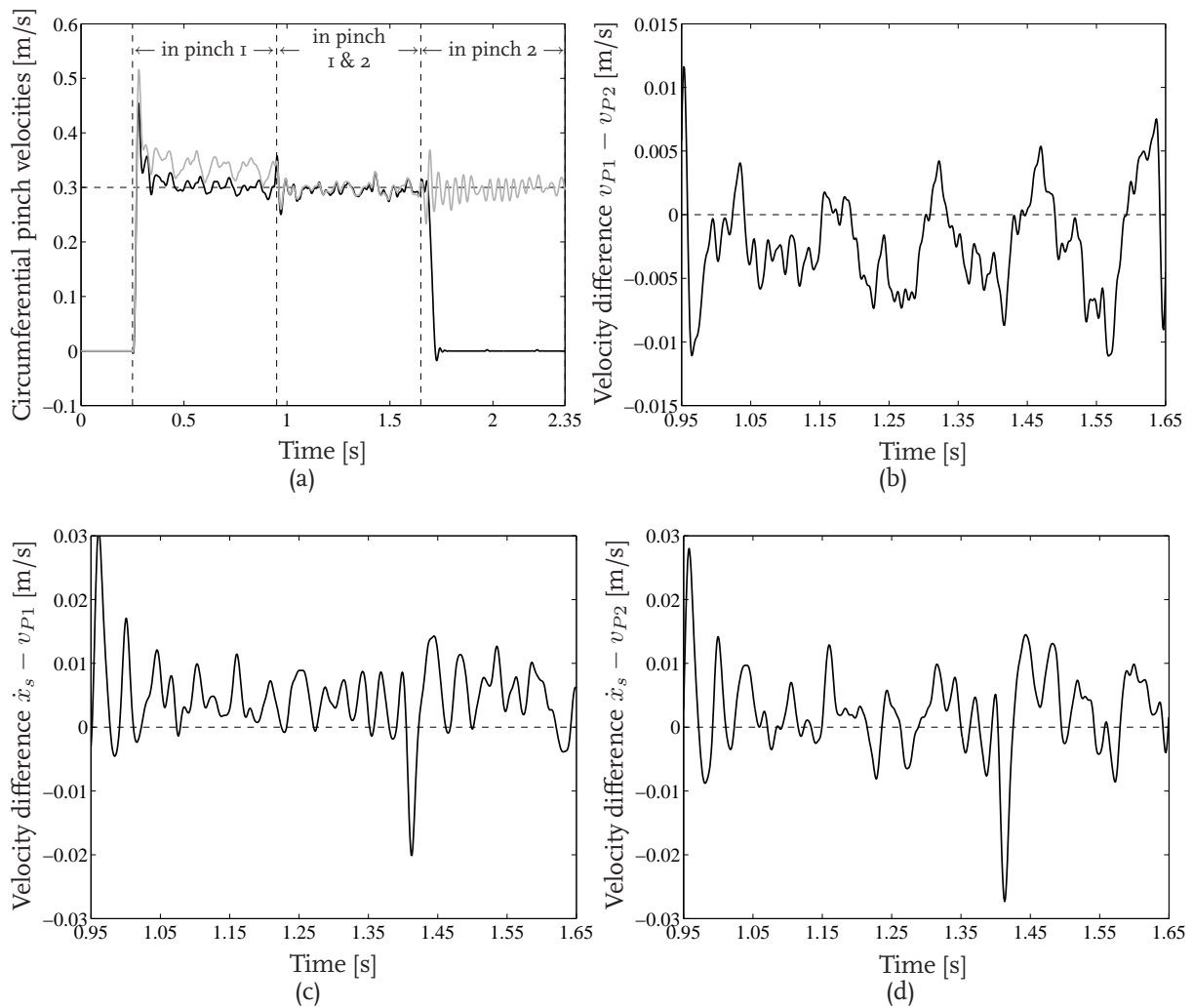


Figure 7.13 / The experimentally obtained circumferential velocity of pinch P₁ (black) and pinch P₂ (gray) (a), the velocity difference when the sheet is driven by both pinches (b), the difference between the sheet velocity and the circumferential velocity of pinch P₁ when the sheet is driven by both pinches (c), and the difference between the sheet velocity and the circumferential velocity of pinch P₂, also during the time the sheet is driven by both pinches (d).

From Fig. 7.13(a), it can also be seen that the first motor-pinch combination comes to a standstill once the sheet has left pinch P₁. This occurs since no switching back to the original feedback controller has been applied and since the feedforward control action is smaller than the control action needed to overcome the rotation asymmetry of pinch P₁.

For a frequency domain analysis of the difference between both pinch velocities, the CPS of this difference has been calculated and is depicted in Fig. 7.14(a). As can be seen from this figure, the contribution of the rotation asymmetry of the first driven roller can be observed, as it manifests itself as an increase of the frequency content in the range around 7 – 8 Hz. This implies that the first motor-pinch combination has to accelerate and decelerate, which is not compensated for. The contribution of the rotation asymmetry to the acceleration of motor M1 can be observed from Fig. 7.14(b), which shows the CPS of this motor acceleration, as it manifests itself as an increase of the frequency content around $7/n_1 \approx 14$ Hz. Based on the results presented so far, it is recommended to incorporate a compensation for the inertia of the first motor-pinch combination, for example via feedback linearization [45]. More specifically, the term $\frac{J_1}{K_{A1}K_{M1}}\ddot{\phi}_{M1}$ can be added to the feedforward control law (7.3). A practical implementation of the updated control law could be supported by making use of encoder time stamping techniques for obtaining accurate motor acceleration estimates [53].

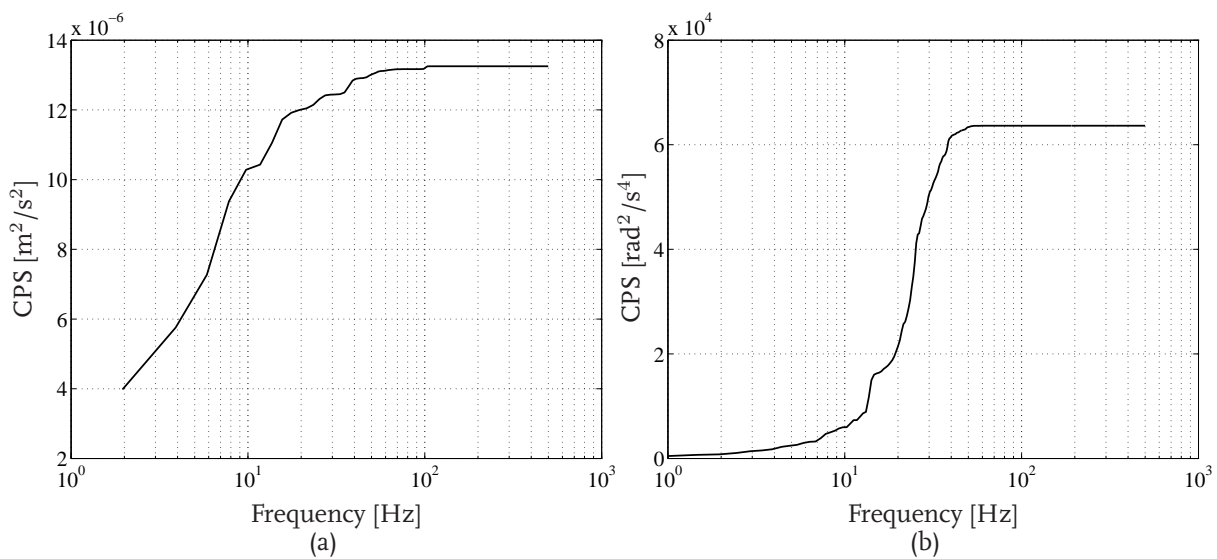


Figure 7.14 / Cumulative power spectra of the difference in circumferential pinch velocities (a), and of the actual acceleration of motor M1 (b).

Besides experiments with switching controllers for motor M1 and motor M2, also experiments have been conducted using a PID feedback controller for both motors. These experiments have been conducted using the same paper path settings as used in the first experiment discussed in this subsection. The sheet tracking error obtained in this experiment is shown in Fig. 7.15(a), together with the simulation results, again obtained without taking into account the controlled motors. It can be observed that when the trailing edge of the sheet leaves the first pinch, a large deviation from the zero tracking error

level takes place. This results from the the reaction of motor M2 to the sudden release of the sheet by pinch P1. The second striking characteristic of the tracking error is the fact that the influence of the perturbation of the transmission ratio of the second motor-pinch combination cannot be observed. This indicates that this motor-pinch combination has a limited influence on the sheet motion. This indication is confirmed by Fig. 7.15(b), which shows that the circumferential velocity of pinch P1 remains equal to 0.3 m/s as long as the sheet is in contact with this pinch. On the other hand, the circumferential velocity of pinch P2 equals approximately 0.34 m/s in this stage. Since the sheet velocity was equal to 0.3 m/s, it can be concluded that slip between the sheet and the second pinch has occurred and, hence, that the no-slip constraint of Section 7.3.1 has been violated. A possible reason for slip to occur between the sheet and the second pinch instead of the first pinch is a lower normal force applied by the non-driven roller of the second pinch.

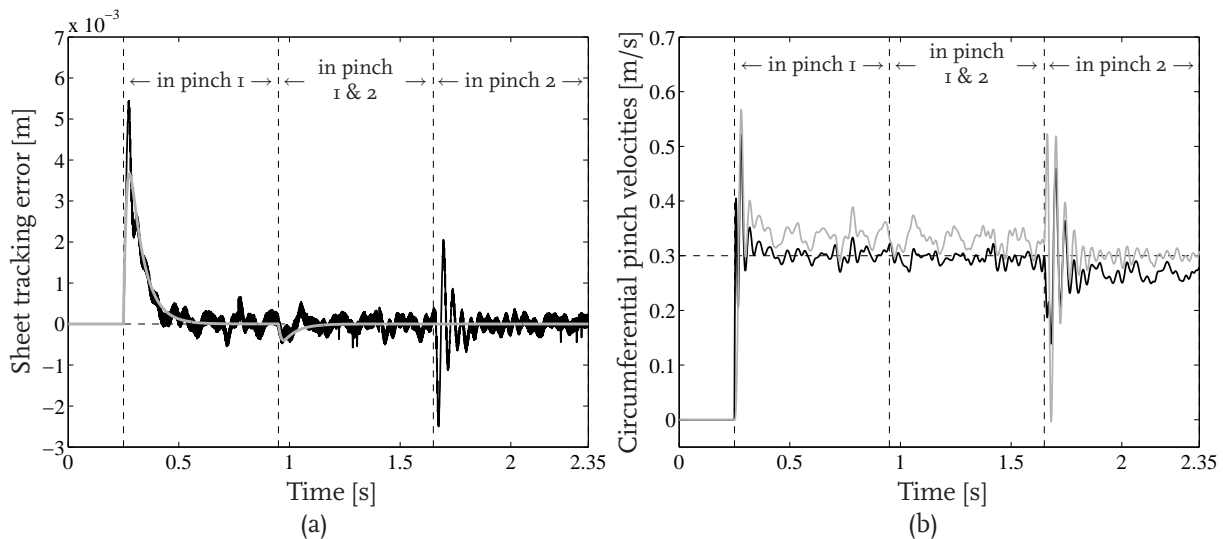


Figure 7.15 / Sheet tracking error obtained in simulations (gray) and experiments (black) (a), and the experimentally obtained circumferential velocity of pinch P1 (black) and pinch P2 (gray) (b), indicating the occurrence of slip between the sheet and pinch P2.

To investigate the influence of the normal force applied by the non-driven roller of the second pinch on the slip properties, an experiment has been conducted in which this normal force has been increased. As in the previous experiments, also here the actual paper path parameters listed in Table 3.2 have been used. The result of this increase in normal force on the sheet tracking error can be seen in Fig. 7.16(a). As in Fig. 7.15(a), it can be observed that when the trailing edge of the sheet leaves the first pinch, a deviation from the zero tracking error level takes place. This results again from the reaction of motor M2 to the sudden release of the sheet by pinch P1. The difference of the sheet

tracking error shown in Fig. 7.16(a) with respect to the one shown in Fig. 7.15(a) is that in the former case the deviation from the zero tracking error level, resulting from the perturbation of the transmission ratio of the second motor-pinch combination, can be observed. This coincides with Fig. 7.16(b), which shows the circumferential velocities of both pinches. From this figure it can be observed that the circumferential velocity of pinch P2 is approximately equal to \dot{x}_s , whereas the circumferential velocity of pinch P1 is not. Hence, it can be concluded that pinch P2 determines the sheet motion, whereas slip is present between the sheet and pinch P1. This slip occurs since the effect of using a PID feedback controller in both motor control loops results in a good tracking behavior in both loops.

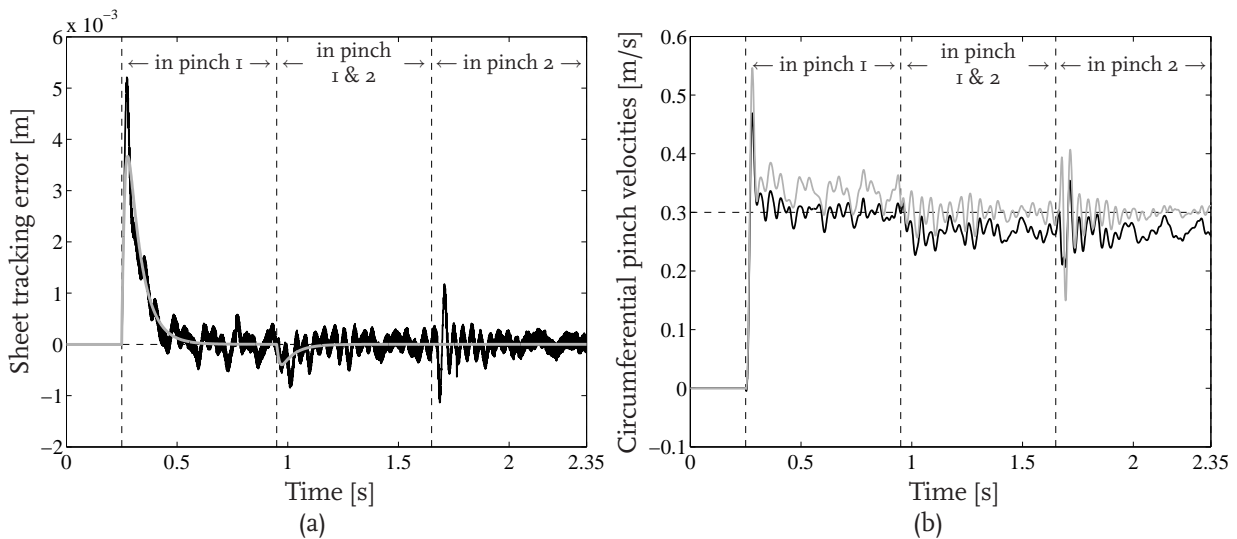


Figure 7.16 / Sheet tracking error obtained in simulations (gray) and experiments (black) (a), and the experimentally obtained circumferential velocity of pinch P1 (black) and pinch P2 (gray) (b), indicating the occurrence of slip between the sheet and pinch P1 due to the increased normal force in pinch P2.

7.4 Coupling Pinches into Sections

In Sections 7.2 and 7.3, two major items regarding the extension of the sheet feedback control design approach, presented in Chapter 4, towards real printer paper paths have been discussed. Consequently, as mentioned in Section 7.1, one important topic regarding the control design remains open, i.e. sheet feedback control design for cases in which pinches are coupled into sections, driven by a single motor. In real printer paper paths, sections are often created to realize a reduction of the cost price, since the number of motors and encoders can be decreased when pinches are coupled to one motor. To study the

application of sheet feedback control in paper paths with sections, the case in which two pinches are coupled to one motor is considered. Regarding the sheet flow in this section, three situations can be distinguished, as indicated in Fig. 7.17:

1. one single sheet S_1 , driven by one of the two pinches, is in the section (situation 1),
2. one single sheet S_1 , driven by both pinches, is in the section (situation 2),
3. and two sheets S_1 and S_2 , each driven by one of the two pinches, are in the section (situation 3).

In the remainder of this section, the sheet feedback control problem for the three individual situations is discussed.

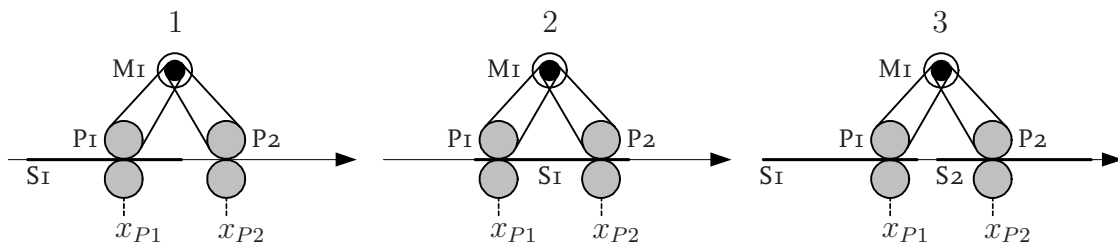


Figure 7.17 / Schematic representation of the sheet flow in the section.

In situation 1, only one motor-pinch combination drives the sheet. Hence, the control design for this situation can be carried out in analogy with the design presented in Section 4.3. It can be chosen to design one single sheet feedback controller that is robust for parameter perturbations of both the first and the second pinch. Alternatively, two feedback controllers can be designed: one controller for motor M_I in combination with pinch P_1 and one controller for motor M_I in combination with pinch P_2 . In analogy with Chapter 4, in this case switching between both controllers has to be enforced at the moment the sheet enters pinch P_2 . From a mechanical design point of view, the transmission ratios and pinch radii present in the section will be chosen to be approximately equal to each other to avoid slip and buckling in situation 2. Hence, it is expected that one single sheet feedback controller can be used to obtain a robustly stable system that satisfies the performance specifications.

When considering situation 2, it can be seen that the pinches cannot be individually controlled due to the coupling to the same motor. Hence, the paper path will have to be designed such that the circumferential pinch velocities will be equal to each other to prevent buckling and slip between the sheet and the pinches. However, when the paper

path parameters deviate from their nominal values, slip or buckling can in this case not be prevented, unless mechanical solutions are applied. As mentioned in Section 7.3.1, examples of mechanical solutions are lifting of pinch P_1 as soon as the sheet enters pinch P_2 or equipping pinch P_1 with a unidirectional bearing and designing the sheet reference velocity such that it increases when the sheet enters pinch P_2 . Since these mechanical solutions support the decomposition of the control problem into two levels, the control design approach proposed in this thesis can still be applied. However, as already recognized in Section 7.3.1, additional costs in the design are needed. If high level sheet feedback control is applied without the mechanical adaptations, the paper path should be designed such that blousing can occur without damaging the sheet. On the other hand, slip between the sheet and one of the pinches cannot be prevented in case of parameter perturbations. However, if it is ensured that this slip occurs between the sheet and the upstream pinch by enforcing the largest normal force applied by the downstream pinch, the high level sheet feedback control design approach proposed in this thesis can be applied. More specifically, if the downstream pinch determines the sheet motion and no slip occurs between this pinch and the sheet, the control problem can be decomposed into two levels and a sheet feedback controller can be designed. An a posteriori performance analysis can be carried out to study the effect of slip in the upstream pinch on the tracking behavior.

In the third situation, multiple sheets present in the section cannot be controlled independently, since changing the motor reference velocity based on one of the sheet tracking errors affects the motion of both sheets. In that case, the tracking requirements for individual sheets must be adjusted since they cannot independently be realized in case multiple sheets are in a single section. Hence, it should be decided based on which sheet tracking error the motor reference velocity of the section should be calculated. One possibility is to add additional logic to the sheet feedback control level, which itself is designed using the control design approach presented in Section 4.3, possibly using the extensions presented in Sections 7.2 and 7.3. This design approach, which is based on one single sheet, can be used since the sheet flow dynamics are identical for each sheet. However, a new model of the sheet flow dynamics will have to be designed, based on the paper path configuration.

7.5 Evaluation

In this chapter, it has been shown that the systematic methodology for applying sheet feedback control in a basic paper path, presented in Chapters 2 and 4, can also be applied in paper paths equipped with a duplex loop and in cases in which sheets are driven by multiple motor-pinch combinations. Furthermore, directions for solutions for cases in

which pinches are coupled into sections are presented. Hence, the technical feasibility of the sheet feedback control design approach has been proven, which opens the way towards the integration and implementation in a real printer paper path. Regarding this implementation and integration step, a number of important subjects plays a role. First of all, it should be investigated if additional elements present in the paper path, e.g. a registration unit for sheet corrections in lateral and skewness direction, impose complications to the sheet feedback control design process. Furthermore, the reproducibility of the mouse sensors should be improved in order to obtain accurate absolute sheet position information, needed to realize the desired printing quality. An alternative for improving the reproducibility is making use of other contactless sheet position sensors. From a broader perspective, another important subject is the integration of the high level control software into the existing embedded control software. It is interesting to analyze the effect of the synchronous sheet position updates on the predictability of the real-time software [42], in comparison with the asynchronous updates obtained by the I/O sheet sensors used in current printer paper paths. Moreover, it is interesting to investigate to what extent the presented approach results in an increase in computational effort, compared with the current event-driven sheet feedback control approach.

Besides the integration and implementation of the sheet feedback control design approach in a real printer paper path, the economical feasibility of the approach should be investigated. More specifically, it should be studied whether economic benefits of the approach, e.g. the possible reduction of the paper path design time and the possible reduction of the costs of the mechanical parts resulting from the decreased demands on their tolerances, are profitable with respect to the economic drawbacks, e.g. the increased costs resulting from the use of additional sheet sensors. A positive outcome of this study will open the way to application of the sheet feedback control design approach in industrial printer development.

Conclusions and Recommendations

8.1	Conclusions	133
8.2	Recommendations	135

8.1 Conclusions

In this thesis a systematic, model-based design methodology for controlling the longitudinal sheet flow in a printer paper path has been developed. In describing the sheet flow in the basic paper path case-study that was initially adopted, low-detailed, kinematic models were used. In the derivation of these models, flexibilities between motors and pinches and slip between sheets and pinches were assumed not to be present, as a result of which a decoupling of the overall control problem into low level motor control and high level sheet control became possible. The benefit of the resulting hierarchical control setup is the independent design of motor control and sheet control, resulting in a significant simplification of the overall design problem.

For the design of the sheet feedback control loop, two approaches have been presented. In the first approach, the control design has been carried out based on the piecewise linear nominal sheet flow model which was written in terms of its error dynamics. A distinguishing feature with respect to the derivation of the error dynamics of linear systems was the introduction of jump conditions describing the system behavior at the switching boundary. Hence, unlike the linear case, a discontinuous, piecewise linear model has been obtained. Given this model, it was shown that to be able to define zero to be a globally asymptotically stable equilibrium point of the system in the sense of Lyapunov, dependencies between a part of the controller parameters had to be introduced. Based on

this observation, two types of controllers have been designed, yielding either a linear or a PWL, discontinuous closed-loop system. Stability analysis of both systems has yielded much insight in the relation between the type of controller used and the type of Lyapunov function needed to prove the stability of this type of systems. In case parametric uncertainties are considered, it can be concluded that the control design approach presented is not suitable, since in case of uncertainties it is not possible to define the origin to be a globally asymptotically stable equilibrium point of the error dynamics. Hence, control design for robustness is not possible. However, a posteriori analysis has been used to investigate the influence of parametric uncertainties on the tracking performance of the system. From this analysis it can be concluded that in case the sheet tracking error and the sheet velocity error are zero before the sheet enters the next pinch, the controller parameters do not influence the jump in the sheet velocity error resulting from the perturbation of the system parameters. More specifically, in this case the performance guarantees should be obtained from the mechanical design of the system, as the jumps are only influenced by the paper path parameters.

The second control design approach is based on the high level sheet flow model itself. Using this approach, dynamic output feedback controllers for the switching dynamics at hand are designed, taking into account parametric uncertainties into the control design. By combining linear H_∞ control design techniques for the individual regimes of the sheet flow dynamics with stability and performance requirements for the overall switched system, robustness against parameter perturbations within prespecified bounds can be obtained. By using this approach, the closed-loop dynamics in each regime can be shaped according to the designer's demands, and therefore this approach can be very well used to solve the sheet feedback control problem.

The experiments performed on an experimental paper path setup, used for the practical validation of both control design approaches, have shown that the desired tracking performance can be realized, even when the system is subject to parameter perturbations within a prespecified bound. The experimental results for the basic paper path case-study have also shown that slip between the sheet and the pinches does not occur. Hence, the no-slip assumption made in the modeling process has been justified. The most appealing outcome of the validation experiments is the close resemblance between the experimentally obtained responses and the ones obtained in simulation. From this resemblance, it can be concluded that in case of the basic paper path case-study the combination of sheet feedback controllers together with simple sheet flow models, that do not contain the closed-loop motor dynamics, are very well capable of predicting the sheet flow in reality. Hence, using these models in early stages of the design process has been justified.

With the experimental validation of the sheet feedback control design approaches, the design cycle is complete. The PWL modeling *formalism* and the controller synthesis *tech-*

niques, together with the supportive *tools* for the calculation of the controller gains and the systematic *method* of applying these in combination with simulations and experiments have resulted in the desired methodology for applying sheet feedback control in a basic printer paper path. Because of the model-based character of this methodology, fast design cycles can be realized, as the sheet flow model allows for an easy adaptation of model parameters, pinch locations, etc. The modeling and control design can be carried out as soon as the first paper path design ideas are ready and the first sheet schedules have been designed. Hence, an early stage integration of the methodology in the paper path design process is possible. Based on these observations, the proposed approach is expected to contribute to both a decrease of the development time and an increase of the predictability of the design process of the printer paper path, possibly resulting in a decrease of the development costs. With respect to the application of the systematic design methodology to the printer case, it can be observed that performance does not depend that heavily on accurate mechanics anymore. Hence, the robustness against disturbances and uncertainties might be increased and it may be possible to build less expensive printers with equal performance. The application of sheet feedback control might also provide an increase of the sheet handling capabilities. Consequently, the sheet flow might become more predictable, especially in case disturbances and uncertainties are present in the paper path, which might result in an increase of the throughput.

Starting from the control design for the basic printer paper path, two extensions have been made towards real printer paper paths, i.e. modeling and control design in case the paper path is equipped with a duplex loop for back-side printing, and sheet handling in which multiple motor-pinch combinations are driving a sheet. Regarding the latter extension, the low level motor control loops have been adjusted to prevent buckling and slip from occurring. An alternative would have been to lift the upstream pinch or to use unidirectional bearings. However, by using the control approach as presented, no additional expenses are needed in the design of the sheet handling system. With the extensions presented, the basis of a reusable, systematic design approach for sheet handling in printer paper paths has been created, opening the way towards the integration and implementation in a real paper path.

8.2 Recommendations

For future research, a few suggestions are considered to extend the work presented in this thesis. These recommendations are divided into recommendations concerning the control design approaches on the one hand, and recommendations regarding the integration and implementation of sheet feedback control in a real paper path on the other hand.

8.2.1 Recommendations for the Control Design Approaches

First of all, it is recommended to carry out additional research on the calculation of the controller parameters and the Lyapunov functions in Section 3.2.1.2. Currently, a rather ad-hoc approach is used, whereas more structured approaches are desirable. Reformulation of the control problem in terms of LMIs or BMIs might be a proper starting point for future research.

Secondly, it is recommended to perform additional research on the possible benefits of sheet feedback controllers that result in partial linearization of the sheet dynamics. Compared with feedback controllers that yield a linear closed-loop system, the design of this type of controllers allows more freedom in the choice of the controller parameters. This could result in an improved behavior of the system, such as an improvement of the performance index containing the control input, or in the introduction of additional characteristics, such as the possibility to design for different control bandwidths in the various subsystems.

A third recommendation regarding the control design presented in Chapter 3 is to investigate the possibility of incorporating additional dynamics in the sheet feedback controllers. This way, a high frequency roll-off can be included in the controllers, as done in Sections 4.2 and 4.3. Furthermore, available a priori knowledge on frequency ranges in which disturbances are likely to be present can be taken into account in the design.

Since so far only first order reference profiles have been considered in the control design approach presented in Chapter 3, a final recommendation concerning this chapter is to carry out sheet feedback control design based on sheet flow models in error space that are derived from more realistic sheet reference profiles.

Considering the practical implementation of the control design approaches, in Chapter 5 it was observed that an exact continuous absolute position measurement of the sheets in the paper path cannot be obtained using the current implementation of the mouse sensors in the experimental setup. Therefore, more research on determining the absolute sheet position, needed to realize the desired printing quality, will have to be carried out before implementing continuous sheet feedback control in a real paper path. One could think of, for example, improving the reproducibility of the mouse sensors or the exploration of other possibilities for contactless sheet position measurement.

As far as extensions of sheet feedback control design for real printer paper paths are concerned, two main recommendations can be given. First of all, in case a single sheet is driven by two pinches, more analysis on the occurrence of slip between the sheet and one of the pinches should be carried out. Moreover, the effect of these slip properties on the low level control design for the upstream motor should be explored.

The second recommendation concerning the extensions to real printer paper paths encompasses sheet flow modeling and control design for cases in which pinches are coupled into sections, driven by a single motor. Starting from the initial ideas on this topic presented in Section 7.4, the modeling, control design, and validation should be considered in more detail.

8.2.2 Recommendations for Integration and Implementation

Also with respect to the integration and implementation of sheet feedback control in a real paper path and in the paper path design process a few recommendations can be given. First of all, the integration of the high level control software into the existing embedded control software should be investigated. More specifically, since the current implementation of discrete-event sheet controllers results in asynchronous updates of the sheet position information, whereas using the approach presented in this thesis synchronous updates are obtained, it is interesting to analyze if the predictability of the real-time software has increased. Moreover, it is interesting to investigate to what extent the presented approach results in an increase in computational effort.

Secondly, the economical feasibility of the approach should be investigated. More specifically, it should be studied whether the economic benefits of the approach, e.g. the possible reduction of the paper path development time and the possible reduction of the costs of the mechanical parts resulting from the decreased demands on their tolerances, are profitable with respect to the economic drawbacks, e.g. the increased costs resulting from the use of optical mouse sensors, the additional wiring needed, and possible increased maintenance sensibility.

With respect to the economical feasibility, a few additional recommendations can be given. First of all, the possibilities of using a sheet position estimation algorithm based on the information obtained from the optical I/O sheet sensors already present in most printer paper paths is an interesting option to be investigated. Hence, the additional costs on extra sheet sensors can be saved. As an alternative, the use of high level sheet sensors for motor control purposes can be investigated. This way, position encoders at the motor shafts are not needed anymore and a non-collocated control setup is obtained that can be used for controlling the sheets. The benefit of using only one type of sensors for control is again a decrease of the printer's cost price.

A final recommendation results from the fact that the use of stepper motors is becoming a serious option in printer paper path design [76]. Hence, it would be interesting to examine the possibilities of applying sheet feedback control as proposed in this thesis in

paper paths equipped with stepper motors. As the no-slip assumptions in the modeling process can still be made and since these stepper motors are controlled in an open-loop fashion, it is expected that this type of motors also supports the decoupling of the sheet handling control problem into high level sheet control and low level motor control.

Linearizing Change of Variables

The first step in the linearizing change of variables is the partitioning of \mathcal{P} and \mathcal{P}^{-1} as

$$\mathcal{P} = \begin{bmatrix} Y & N \\ N^T & * \end{bmatrix}, \mathcal{P}^{-1} = \begin{bmatrix} X & M \\ M^T & \bullet \end{bmatrix}, \quad (\text{A.1})$$

where X and Y are $n \times n$ symmetric matrices, with n the number of states of the augmented plant. In (A.1), $*$ and \bullet represent matrices satisfying

$$\mathcal{P}\mathcal{P}^{-1} = \begin{bmatrix} YX + NM^T & YM + N\bullet \\ N^T X + *M^T & N^T M + *\bullet \end{bmatrix} = I. \quad (\text{A.2})$$

From (A.2) we know that $\mathcal{P} \begin{pmatrix} X \\ M^T \end{pmatrix} = \begin{pmatrix} I \\ 0 \end{pmatrix}$, which leads to

$$\mathcal{P}\Pi_1 = \Pi_2, \quad (\text{A.3})$$

with $\Pi_1 = \begin{bmatrix} X & I \\ M^T & 0 \end{bmatrix}$ and $\Pi_2 = \begin{bmatrix} I & Y \\ 0 & N^T \end{bmatrix}$. Next, the following change of controller variables is defined:

$$\begin{aligned} \widehat{A}_i &= NA_{K,i}M^T + NB_{K,i}C_{v,i}X + YB_{u,i}C_{K,i}M^T + Y(A_i + B_{u,i}D_{K,i}C_{v,i})X \\ \widehat{B}_i &= NB_{K,i} + YB_{u,i}D_{K,i} \\ \widehat{C}_i &= C_{K,i}M^T + D_{K,i}C_{v,i}X \\ \widehat{D}_i &= D_{K,i} \end{aligned} \quad , i \in \mathcal{I}. \quad (\text{A.4})$$

The motivation for this transformation lies in the following identities, that are derived

from (A.3), (A.4), and (4.11):

$$\begin{aligned}
\Pi_1^T \mathcal{P} \mathcal{A}_i \Pi_1 &= \Pi_2^T \mathcal{A}_i \Pi_1 \\
&= \begin{bmatrix} (A_i + B_{u,i} D_{K,i} C_{v,i}) X + & & A_i + B_{u,i} D_{K,i} C_{v,i} \\ & + B_{u,i} C_{K,i} M^T & \\ Y (A_i + B_{u,i} D_{K,i} C_{v,i}) X + Y B_{u,i} C_{K,i} M^T + & & Y (A_i + B_{u,i} D_{K,i} C_{v,i}) + \\ & + N B_{K,i} C_{v,i} X + N A_{K,i} M^T & + N B_{K,i} C_{v,i} \end{bmatrix} \\
&= \begin{bmatrix} A_i X + B_{u,i} \widehat{C}_i & A_i + B_{u,i} \widehat{D}_i C_{v,i} \\ \widehat{A}_i & Y A_i + \widehat{B}_i C_{v,i} \end{bmatrix}, i \in \mathcal{I} \tag{A.5}
\end{aligned}$$

$$\begin{aligned}
\Pi_1^T \mathcal{P} \mathcal{B}_i &= \Pi_2^T \mathcal{B}_i \\
&= \begin{bmatrix} B_{w,i} + B_{u,i} D_{K,i} D_{vw,i} \\ Y (B_{w,i} + B_{u,i} D_{K,i} D_{vw,i}) + N B_{K,i} D_{vw,i} \end{bmatrix} \\
&= \begin{bmatrix} B_{w,i} + B_{u,i} \widehat{D}_i D_{vw,i} \\ Y B_{w,i} + \widehat{B}_i D_{vw,i} \end{bmatrix}, i \in \mathcal{I} \tag{A.6}
\end{aligned}$$

$$\begin{aligned}
C_i \Pi_1 &= \begin{bmatrix} C_{z,i} X + D_{zu,i} D_{K,i} C_{v,i} X + D_{zu,i} C_{K,i} M^T & C_{z,i} + D_{zu,i} D_{K,i} C_{v,i} \end{bmatrix} \\
&= \begin{bmatrix} C_{z,i} X + D_{zu,i} \widehat{C}_i & C_{z,i} + D_{zu,i} \widehat{D}_i C_{v,i} \end{bmatrix}, i \in \mathcal{I}. \tag{A.7}
\end{aligned}$$

Pre- and postmultiplication of (4.19) with Π_1^T and Π_1 , respectively, results in (4.21):

$$0 \prec \Pi_1^T \mathcal{P} \Pi_1 = \Pi_1^T \Pi_2 = \begin{bmatrix} X & I \\ I & Y \end{bmatrix}. \tag{A.8}$$

Furthermore, pre- and postmultiplication of the analysis LMI (4.20) with $\text{diag}(\Pi_1^T, I, I)$ and $\text{diag}(\Pi_1, I, I)$, respectively, yields

$$0 \succ \begin{bmatrix} \Pi_1^T \mathcal{A}_i^T \mathcal{P} \Pi_1 + \Pi_1^T \mathcal{P} \mathcal{A}_i \Pi_1 & \Pi_1^T \mathcal{P} \mathcal{B}_i & \Pi_1^T C_i^T \\ \mathcal{B}_i^T \mathcal{P} \Pi_1 & -\gamma I & \mathcal{D}_i^T \\ C_i \Pi_1 & \mathcal{D}_i & -\gamma I \end{bmatrix}. \tag{A.9}$$

Substitution of (A.4)-(A.7) into (A.9) yields the synthesis LMI (4.22).

Bibliography

- [1] AVAGO TECHNOLOGIES. *ADNB-6011-EV and ADNB-6012-EV High Performance Laser Mouse Bundles (Data Sheet)*. <http://www.avagotech.com/assets/downloadDocument.do?id=13561>.
- [2] BANNER ENGINEERING. <http://www.bannerengineering.com>.
- [3] BECKERS, J.M.J., HEEMELS, W.P.M.H., BUKKEMS, B.H.M., and MULLER, G.J. Effective Industrial Modeling for High-Tech Systems: The Example of Happy Flow. In *Proc. of the 17th Symposium International Council on Systems Engineering (INCOSE)*. Orlando, Florida, USA, 2007 (accepted).
- [4] BELL, D., BOBROW, D., FALKENHAINER, B., FROMHERZ, M., SARASWAT, V., and SHIRLEY, M. RAPPER: The Copier Modeling Project. In *Int. Workshop on Qualitative Reasoning about Physical Systems*. Nara, Japan, 1994, pp. 1–12.
- [5] BOSGRA, O.H., KWAKERNAAK, H., and MEINSMA, G. *Design Methods for Control Systems*. Lecture notes for the DISC course, Dutch Institute of Systems and Control, 2003.
- [6] BOYD, S., EL GHAOU, L., FERON, E., and BALAKRISHNAN, V. *Linear Matrix Inequalities in System and Control Theory*. Volume 15 of SIAM Studies in Applied Mathematics, Philadelphia, PA, USA, June 1994.
- [7] BUEDE, D.M. *Engineering Design of Systems - Models and Methods*. John Wiley & Sons, Inc., New York, NY, USA, 2000.
- [8] BUKKEMS, B.H.M., DE BEST, J.J.T.H., VAN DE MOLENGRAFT, M.J.G., and STEINBUCH, M. Robust Piecewise Linear Sheet Control in a Printer Paper Path. In *Proc. of the 2nd IFAC Conference on Analysis and Design of Hybrid Systems (ADHS'06)*. 2006, pp. 142–147.

- [9] BUKKEMS, B.H.M., SANDEE, J.H., BECKERS, J.M.J., YUAN, Z., VAN DER WIJST, B., and VAN DE MOLENGRAFT, M.J.G. A Case-Study in Multidisciplinary Modeling of Dynamic Embedded Systems. In *Proc. of Mechatronics and Robotics 2004 (MechRob 2004)*. Aken, Germany, 2004, pp. 26–31.
- [10] BUKKEMS, B.H.M., VAN DE MOLENGRAFT, M.J.G., HEEMELS, W.P.M.H., VAN DE WOUW, N., and STEINBUCH, M. A Piecewise Linear Approach Towards Sheet Control in a Printer Paper Path. In *Proc. of the American Control Conference 2006*. 2006, pp. 1315–1320.
- [11] CHEN, M., ZHU, C.R., and FENG, G. Linear-matrix-inequality-based approach to H_∞ controller synthesis of uncertain continuous-time piecewise linear systems. *IEEE Proc.-Control Theory Appl.*, vol. 151(3): (2004), pp. 295–300.
- [12] CLOET, C. *A Mechatronics Approach to Copier Paperpath Design*. Ph.D. thesis, University of California Berkeley, CA, USA, 2001.
- [13] CLOET, C., KRUCIŃSKI, M., HOROWITZ, R., and TOMIZUKA, M. A Hybrid Control Scheme for a Copier Paper Path. In *Proc. of the American Control Conference*. San Diego, CA, USA, 1999, pp. 2114–2118.
- [14] CLOET, C., KRUCIŃSKI, M., TOMIZUKA, M., HOROWITZ, R., and LI, P. Intersheet Spacing Control and Controllability of a Copier Paper Path. In *Proc. of the 1998 IEEE International Conference on Control Applications*. Trieste, Italy, 1998, pp. 726–730.
- [15] CLOET, C., TOMIZUKA, M., and HOROWITZ, R. Design Requirements and Reference Trajectory Generation for a Copier Paperpath. In *Proc. of the 2001 IEEE/ASME International Conference on Advanced Intelligent Mechatronics*. 2001, pp. 911–916.
- [16] CLOOSTERMAN, M.B.G., VAN DE WOUW, N., HEEMELS, W.P.M.H., and NIJMEIJER, H. Robust Stability of Networked Control Systems with Time-Varying Network-Induced Delays. In *Proc. of the 45th IEEE Conference on Decision and Control*. San Diego, California, USA, 2006, pp. 4980–4985.
- [17] DAMEN, A. and WEILAND, S. *Robust Control*. Lecture notes for the course Robust Control (5P430), Technische Universiteit Eindhoven, 2001.
- [18] DE BEST, J.J.T.H., BUKKEMS, B.H.M., VAN DE MOLENGRAFT, M.J.G., and STEINBUCH, M. Piecewise Linear Sheet Control in an H_∞ Framework. In *IEEE Multi-conference on Systems and Control (MSC2007)*. Singapore, 2007 (accepted).
- [19] DECARLO, R.A., BRANICKY, M.S., PETTERSSON, S., and LENNARTSON, B. Perspectives and Results on the Stability and Stabilizability of Hybrid Systems. *Proc. IEEE*, vol. 88(7): (2000), pp. 1069–1082.

- [20] DOYLE, J.C., PACKARD, A., and ZHOU, K. Review of LFTs, LMIs, and μ . In *Proc. of the 30th IEEE Conference on Decision and Control*. Brighton, England, 1991, pp. 1227–1232.
- [21] EMBEDDED SYSTEMS INSTITUTE. *Summary of the Boderc Project Plan*. <http://www.esi.nl/>.
- [22] FENG, G. Controller Design and Analysis of Uncertain Piecewise-Linear Systems. *IEEE Trans. Circuits Syst. I*, vol. 49(2): (2002), pp. 224–232.
- [23] FENG, G., LU, G.P., and ZHOU, S.S. An Approach to H_∞ Controller Synthesis of Piecewise Linear Systems. *Communications in Information and Systems*, vol. 2(3): (2002), pp. 245–254.
- [24] FLORESCU, O., VOETEN, J.P.M., and CORPORAAL, H. A unified model for analysis of real-time properties. In *Proc. of the 1st International Symposium on Leveraging Applications of Formal Methods (ISoLa 2004)*. Paphos, Cyprus, 2004, pp. 220–227.
- [25] FRANKLIN, G.F., POWELL, J.D., and EMAMI-NAEINI, A. *Feedback control of dynamic systems*. Prentice Hall, Upper Saddle River, New Jersey, USA, 2002.
- [26] FRERIKS, H.J.M., HEEMELS, W.P.M.H., MULLER, G.J., and SANDEE, J.H. On the Systematic Use of Budget-Based Design. In *Proc. of the 16th symposium International Council on Systems Engineering (INCOSE)*. Orlando, Florida, USA, 2006.
- [27] FROMHERZ, M.P., CRAWFORD, L.S., and HINDI, H.A. Coordinated Control for Highly Reconfigurable Systems. In *Hybrid Systems: Computation and Control (HSCC) 2005*. Zurich, Switzerland, 2005, pp. 1–24.
- [28] GAHINET, P., NEMIROVSKI, A., LAUB, A.J., and CHILALI, M. *LMI Control Toolbox for Use with Matlab*. The Mathworks Inc., Natick, MA, USA, May 1995.
- [29] GAHINET, P. Explicit Controller Formulas for LMI-based H_∞ Synthesis. *Automatica*, vol. 32(7): (1996), pp. 1007–1014.
- [30] GAHINET, P. and APKARIAN, P. A Linear Matrix Inequality Approach to H_∞ Control. *Int. J. of Robust and Nonlinear Control*, vol. 4: (1994), pp. 421–448.
- [31] GUPTA, V., SARASWAT, V.A., and STRUSS, P. A model of a Photocopier Paper Path. In *Proc. of the 2nd IJCAI Workshop on Engineering Problems for Qualitative Reasoning*. 1995.
- [32] GUPTA, V. and STRUSS, P. Modeling a Copier Paper Path: A Case Study in Modeling Transportation Processes. In *Proc. of the 9th Workshop on Qualitative Reasoning*. Amsterdam, The Netherlands, 1995.

- [33] HAMBY, E.S. and GROSS, E.M. A Control-Oriented Survey of Xerographic Systems: Basic Concepts to New Frontiers. In *Proc. of the American Control Conference*. Boston, MA, USA, 2004, pp. 2615–2620.
- [34] HANG, C.C., LOH, A.P., and VASNANI, V.U. Relay Feedback Auto-Tuning of Cascade Controllers. *IEEE Trans. Contr. Syst. Technol.*, vol. 2(1): (1994), pp. 42–45.
- [35] HASSIBI, A. and BOYD, S. Quadratic Stabilization and Control of Piecewise-Linear Systems. In *Proc. of the American Control Conference*. Philadelphia, PA, USA, 1998, pp. 3659–3664.
- [36] HEEMELS, W.P.M.H., MULLER, G.J., and VAN DEN BOSCH, P.F.A. *Boderc: Model-Based Design of High-Tech Systems (Chapter 1)*. Embedded Systems Institute, Eindhoven, The Netherlands, 2006.
- [37] HEEMELS, W.P.M.H., SOMERS, L., VAN DEN BOSCH, P.F.A., MULLER, G.J., YUAN, Z., VAN DER WIJST, B., and VAN DEN BRAND, A. The Use of the Key Driver Technique in the Design of Copiers. In *Proc. of the International Conference on Software and Systems Engineering and their Applications (ICSSEA)*. Paris, France, 2006.
- [38] HEEMELS, W.P.M.H., VAN DE WAAL, E., and MULLER, G.J. A Multi-Disciplinary and Model-Based Design Methodology for High-Tech Systems. In *Proc. of the Conference on System Engineering (CSER)*. Los Angeles, CA, USA, 2006.
- [39] HENZINGER, T.A. The Theory of Hybrid Automata. In *Proc. of the 11th Symposium on Logic in Computer Science (LICS '96)*. New Brunswick, New Jersey, USA, 1996, pp. 278–292.
- [40] HINDI, H.A., CRAWFORD, L.S., and FROMHERZ, M.P.J. Synchronization of State Based Control Processes with Delayed and Asynchronous Measurements. In *Proc. of the 44th IEEE Conference on Decision and Control and the European Control Conference 2005*. Sevilla, Spain, 2005, pp. 6370–6375.
- [41] HOL, C.W.J. *Structured Controller Synthesis for Mechanical Servo-Systems; Algorithms, Relaxations and Optimality Certificates*. Ph.D. thesis, Delft University of Technology, Delft, The Netherlands, 2006.
- [42] HUANG, J. *Predictability in Real-Time Software Design*. Ph.D. thesis, Technische Universiteit Eindhoven, Eindhoven, The Netherlands, 2005.
- [43] INCOSE. *What is Systems Engineering?* <http://www.incose.org/practice/whatissystemseng.aspx>.
- [44] JOHANSSON, M. and RANTZER, A. Computation of Piecewise Quadratic Lyapunov Functions for Hybrid Systems. *IEEE Trans. Automat. Contr.*, vol. 43(4): (1998), pp. 555–559.

- [45] KHALIL, H.K. *Nonlinear Systems*. Prentice Hall, Upper Saddle River, New Jersey, USA, 2002.
- [46] KRUCIŃSKI, M. *Feedback Control of Photocopying Machinery*. Ph.D. thesis, University of California Berkeley, CA, USA, 2000.
- [47] KRUCIŃSKI, M., CLOET, C., HOROWITZ, R., TOMIZUKA, M., and LI, P. Asynchronous Observer for a Copier Paper Path. In *Proc. of the 37th IEEE Conference on Decision and Control*. Tampa, Florida, USA, 1998, pp. 2611–2612.
- [48] KRUCIŃSKI, M., CLOET, C., HOROWITZ, R., TOMIZUKA, M., and LI, P. Inter-object Spacing Control and Controllability of a Manufacturing Transportation System. In *Proc. of the American Control Conference*. Philadelphia, Pennsylvania, USA, 1998, pp. 1259–1265.
- [49] LAMBRECHTS, P.F. *The Application of Robust Control Theory Concepts to Mechanical Servo Systems*. Ph.D. dissertation, Delft University of Technology, 1990.
- [50] LEE, Y. and PARK, S. PID Controller Tuning To Obtain Desired closed-loop Responses for Cascade Control Systems. *Ind. Eng. Chem. Res.*, vol. 37(5): (1998), pp. 1859–1865.
- [51] LOGITECH. *Logitech G5 Laser Mouse*. <http://www.logitech.com/index.cfm/products/details/NL/EN,CRID=2464,CONTENTID=10715>.
- [52] MAAS, J.W.L.H. *Sheet Flow Modeling in a Printer Paper Path*. Department of Mechanical Engineering, Technische Universiteit Eindhoven, Eindhoven, The Netherlands, 2006.
- [53] MERRY, R.J.E., VAN DE MOLENGRAFT, M.J.G., and STEINBUCH, M. Error Modeling and Improved Position Estimation for Optical Incremental Encoders by means of Time Stamping. In *Proc. of the American Control Conference*. New York City, USA, 2007 (accepted).
- [54] POLITECNICO DI MILANO - DIPARTIMENTO DI INGEGNERIA AEROSPAZIALE. *RTAI - the RealTime Application Interface for Linux*. <https://www.rtai.org/>.
- [55] POTTS, C. Software-engineering Research Revisited. *IEEE Software*, vol. 10(5): (1993), pp. 19–28.
- [56] RAI, S. and JACKSON, W.B. A Hybrid Hierarchical Control Architecture for Paper Transport Systems. In *Proc. of the 37th IEEE Conference on Decision and Control*. Tampa, Florida, USA, 1998, pp. 4249–4250.
- [57] RANTZER, A. and JOHANSSON, M. Piecewise Linear Quadratic Optimal Control. *IEEE Trans. Automat. Contr.*, vol. 45(4): (2000), pp. 629–637.

- [58] REPENNING, N.P. Understanding Fire Fighting in New Product Development. *Journal of Product Innovation Management*, vol. 18(5): (2001), pp. 285–300.
- [59] RODRIGUES, L., HASSIBI, A., and HOW, J.P. Output Feedback Controller Synthesis for Piecewise-Affine System with Multiple Equilibria. In *Proc. of the American Control Conference*. Chicago, Illinois, USA, 2000, pp. 1784–1789.
- [60] SAKAMURA, K. and SUGIE, T. Trajectory tracking control of bimodal piecewise affine systems. *Int. J. of Control*, vol. 78(16): (2005), pp. 1314–1326.
- [61] SANCHEZ, R., ERGUETA, E., FINE, B., HOROWITZ, R., TOMIZUKA, M., and KRUCIŃSKI, M. A Mechatronic Approach to Full Sheet Control Using Steer-able Nips. In *Proc. of the 4th IFAC-Symposium on Mechatronic Systems*. Heidelberg, Germany, 2006, pp. 277–282.
- [62] SANCHEZ, R., HOROWITZ, R., and TOMIZUKA, M. Paper Sheet Control Using Steerable Nips. In *Proc. of the American Control Conference*. Boston, Massachusetts, USA, 2004, pp. 482–487.
- [63] SANCHEZ, R., HOROWITZ, R., TOMIZUKA, M., and SIMIĆ, S.N. Full Paper Sheet Control Using Hybrid Automata. In *Hybrid Systems: Computation and Control. Vol. 2993 of Lecture Notes in Computer Science*. Berlin, Germany, 2004, pp. 523–538.
- [64] SANDEE, J.H. *Event-Driven Control in Theory and Practice - Trade-offs in Software and Control Performance*. Ph.D. thesis, Eindhoven University of Technology, Eindhoven, The Netherlands, 2006.
- [65] SANDEE, J.H., HEEMELS, W.P.M.H., MULLER, G.J., VAN DEN BOSCH, P.F.A., and VERHOEF, M.H.G. Threads of Reasoning: A Case-Study in Printer Control. In *Proc. of the 16th symposium International Council on Systems Engineering (INCOSE)*. Orlando, Florida, USA, 2006.
- [66] SANDEE, J.H., HEEMELS, W.P.M.H., and VAN DEN BOSCH, P.P.J. Event-Driven Control as an Opportunity in the Multidisciplinary Development of Embedded Controllers. In *Proc. of the American Control Conference*. Portland, Oregon, USA, 2005, pp. 1776–1781.
- [67] SCHERER, C.W., GAHINET, P., and CHILALI, M. Multiobjective Output-Feedback Control via LMI Optimization. *IEEE Trans. Automat. Contr.*, vol. 42(7): (1997), pp. 896–911.
- [68] SHRAGER, J., JORDAN, D.S., MORAN, T.P., KICZALES, G., and RUSSELL, D.M. Issues in the Pragmatics of Qualitative Modeling: Lessons Learned from a Xerographics Project. *Communications of the AMC*, vol. 30(12): (1987), pp. 1036–1047.

- [69] SKOGESTAD, S. and POSTLETHWAITE, I. *Multivariable Feedback Control*. John Wiley & Sons Ltd., West Sussex, England, 2005.
- [70] SLOTINE, J.J.E. and LI, W. *Applied Nonlinear Control*. Prentice Hall, Englewood Cliffs, New Jersey, USA, 1991.
- [71] SOLYOM, S. and RANTZER, A. The servo problem for piecewise linear systems. In *Proc. of the Fifteenth International Symposium on Mathematical Theory of Networks and Systems*. Notre Dame, IN, 2002.
- [72] SONTAG, E.D. Nonlinear Regulation: The Piecewise Linear Approach. *IEEE Trans. Automat. Contr.*, vol. 26(2): (1981), pp. 346–381.
- [73] STEINBUCH, M. and NORG, M.L. Industrial Perspective on Robust Control: Application to Storage Systems. *Annual Reviews in Control*, vol. 22: (1998), pp. 47–58.
- [74] STEINBUCH, M., VAN GROOS, P.J., SCHOOTSTRA, G., WORTELBOER, P.M., and BOSGRA, O.H. μ -Synthesis for a Compact Disc Player. *Int. J. Robust Nonlinear Control*, vol. 8: (1998), pp. 169–189.
- [75] STEPHANOPOULOS, G. *Chemical Process Control*. Prentice Hall, Englewood Cliffs, New Jersey, USA, 1984.
- [76] STOLTE, J., VAN DEN BOSCH, A.V.P.P.J., and VAN DE WAAL, E. *Boderc: Model-Based Design of High-Tech Systems (Chapter 10)*. Embedded Systems Institute, Eindhoven, The Netherlands, 2006.
- [77] TERLOUW, J., LAMBRECHTS, P.F., BENNANI, S., and STEINBUCH, M. Parametric uncertainty modelling using LFTs. In *1992 AIAA Guidance, Navigation and Control Conference*. South Carolina, United States of America, 1992.
- [78] THE MATHWORKS. Matlab & Simulink. Natick, Massachusetts, USA.
- [79] TUNESTÅL, P. and KRUCINSKI, M. Hybrid Control of a Manufacturing Transport System. In *Proc. of the 36th IEEE Conference on Decision and Control*. San Diego, California, USA, 1997, pp. 84–89.
- [80] VAN DE MOLENGRAFT, M.J.G., DE KRAKER, A., and STEINBUCH, M. Integrating Experimentation into Control Courses. *IEEE Control Syst. Mag.*, vol. 25(1): (2005), pp. 40–44.
- [81] VAN DEN BOSCH, P.F.A., FLORESCU, O., VERHOEF, M.H.G., and MULLER, G.J. *Boderc: Model-Based Design of High-Tech Systems (Chapter 8)*. Embedded Systems Institute, Eindhoven, The Netherlands, 2006.

- [82] WITVOET, G. *The Design of an Experimental Paper Path Setup*. Department of Mechanical Engineering, Technische Universiteit Eindhoven, Eindhoven, The Netherlands, DCT Report No. 2005.141, 2005.
- [83] YOUNG, P.M., NEWLIN, M.P., and DOYLE, J.C. μ Analysis with Real Parametric Uncertainty. In *Proc. of the 37th IEEE Conference on Decision and Control*. Brighton, England, 1991, pp. 1251–1256.
- [84] ZHOU, K., DOYLE, J.C., and GLOVER, K. *Robust and Optimal Control*. Prentice Hall, Upper Saddle River, New Jersey, USA, 1996.

Summary

Sheet Feedback Control Design in a Printer Paper Path

The design of a sheet handling system is an important part of the design of document handling systems, such as high volume cut sheet printers, as this system is crucial for realizing important requirements such as reliability, high printing quality and large throughput. Standard approaches of designing sheet handling systems often rely on the high-precision mechanics of the system, i.e. all mechanical parts are manufactured with very low tolerances. As a result, a predictable sheet flow can be realized and error correction during the sheet transport can be done at a few fixed locations in the paper path only. At present, there is no systematic approach to design these discrete-event sheet controllers; for each new printer to be designed, it takes much effort to determine where and how feedback needs to be applied. Hence, fast design cycles in an early stage of the design are difficult to realize.

To improve the design trajectory of a sheet handling system, this thesis proposes a systematic, model-based methodology for applying closed-loop sheet control based on continuous feedback of the sheet position information. Because of the model-based character of the methodology, fast design cycles can be realized that can be applied in early stages of the paper path design process. Hence, the proposed approach is expected to contribute to both a decrease of the development time and an increase of the predictability of this design process, possibly resulting in a decrease of the development costs. The application of sheet feedback control might also result in an increase of robustness against disturbances and uncertainties present in the paper path. Examples of such disturbances are the asymmetry of the rollers driving the sheet through the paper path and slip between the rollers and the sheet, whereas tolerances on the radii of the rollers or on transmission ratios between motors and rollers are examples of paper path uncertainties. Hence, the main focus of the control design presented in this thesis is on the systematic synthesis for robust stability and robust performance of the closed-loop system.

The overall sheet handling control problem is decomposed into the design of low level motor control loops and a high level sheet control loop, as a result of which a hierarchical control structure is obtained. For a further simplification of the design problem, the controlled motor dynamics are assumed to be ideal. This leads to a simple, yet adequate model of the sheet flow, which serves as the basis for sheet feedback control design. The dynamics of this sheet flow are captured in the piecewise linear modeling (PWL) formalism, resulting in a model that encompasses both the consecutive switching of the driving input acting on the sheet as well as the uncertainties present in the paper path.

Based on the sheet flow model, two control design approaches are proposed. In the first approach, the sheet flow model is written in terms of its error dynamics. By working in the error domain, stability of these error dynamics is directly linked to the tracking performance of the sheet flow dynamics. Based on the nominal, discontinuous model in error space, a stabilizing state feedback control law is proposed. Two types of controllers are synthesized based on the formulation of a set of linear matrix inequalities (LMIs), yielding either a linear or a PWL, discontinuous closed-loop system. Furthermore, relations between the controllers and the Lyapunov function for proving the closed-loop stability are analyzed, together with the influence of parameter perturbations on the sheet tracking and velocity errors. The second control design approach is directly based on the sheet flow dynamics. In this approach, dynamic output feedback controllers are synthesized that result in robust stability and robust performance of the closed-loop system. The latter synthesis is also formulated in terms of a set of LMIs and combines linear H_∞ control design techniques for the individual regimes of the sheet dynamics with stability and performance requirements for the overall switched system.

Both control design approaches are validated in practice. For this purpose, an experimental paper path setup is realized, in which the sheet position information is made available by using optical mouse sensors. The results of the experiments show the stable behavior of the closed-loop system and they show that in the presence of parametric uncertainties the prespecified performance properties are satisfied. Moreover, the experimentally obtained responses can be very well predicted by the basic sheet flow models used in the controller synthesis.

After showing the proof of concept for sheet control in a basic paper path, and given the requirements in a real paper path, the second control design approach is selected to be extended for application in such a paper path. This approach has been chosen because of its design freedom and because of the possibility to carry out robust control design. Given this approach, extensions to sheet transport for backside printing and transport of different sheet sizes are carried out. With these extensions, the basis of a reusable, systematic design approach for sheet handling in printer paper paths has been created, opening the way towards integration and implementation in a real paper path.

Samenvatting

Het ontwerp van een papiertransport systeem is een belangrijk onderdeel in het ontwerp van reproductiesystemen, zoals hoog volume cutsheet printers, aangezien dit systeem cruciaal is voor het realiseren van belangrijke systeemeisen, zoals betrouwbaarheid, een hoge printkwaliteit en een hoge doorvoersnelheid. Standaard ontwerpbenaderingen van papiertransport systemen maken vaak gebruik van de hoge nauwkeurigheid van de mechanische constructie van het systeem. Als gevolg hiervan kan een voorspelbare velloop worden gerealiseerd en kan foutcorrectie tijdens het veltransport worden toegepast op een beperkt aantal vaste locaties in het papierpad. Tot dusver bestaat er geen systematische aanpak om dergelijke event-gedreven regelaars te ontwerpen; voor elke nieuw te ontwerpen printer is veel tijd nodig om te bepalen waar en hoe terugkoppeling toegepast moet worden. Als gevolg hiervan zijn snelle ontwerpcycli in een vroeg stadium van het ontwerptraject moeilijk te realiseren.

Om het ontwerptraject van een papiertransport systeem te verbeteren, wordt in dit proefschrift een systematische, modelgebaseerde methodologie voorgesteld voor het toepassen van een gesloten-lus regeling van de velloop, gebaseerd op continue terugkoppeling van de positie-informatie van het vel. Vanwege het modelgebaseerde karakter van de methodologie kunnen snelle ontwerpcycli in een vroeg stadium van het ontwerpproces gerealiseerd worden. Hierdoor is de verwachting dat de voorgestelde aanpak bij kan dragen aan zowel een afname van de ontwerptijd als een toename van de voorspelbaarheid van het ontwerpproces van papiertransport systemen, wat mogelijk leidt tot een afname van de ontwerpkosten. Het toepassen van een gesloten-lus regeling van de velloop leidt mogelijk ook tot een toename van de robuustheid voor verstoringen en onzekerheden in het papierpad. Voorbeelden van zulke verstoringen zijn de asymmetrie van de knepen die het vel door het pad transporteren en slip tussen het vel en de knepen, terwijl toleranties op de stralen van de knepen of op overbrengingen tussen de motoren en de knepen voorbeelden zijn van onzekerheden. Als gevolg van de mogelijke toename van de robuustheid ligt de nadruk van het regelaarontwerp dat wordt gepresenteerd in dit proef-

schrift op het systematisch ontwerpen voor robuuste stabiliteit en robuuste performance van het geregelde systeem.

Het totale papiertransport probleem wordt opgedeeld in het ontwerp van laag-niveau motorregelingen en een hoog niveau papierregeling, waardoor een hiërarchische regelaarstructuur wordt verkregen. Voor een verdere vereenvoudiging van het ontwerpprobleem wordt aangenomen dat de geregelde motoren zich ideaal gedragen. Dit leidt tot een eenvoudig, maar adequaat model van de velloop dat dient als basis voor het ontwerp van de terugkoppelingsgebaseerde regeling van de velloop. De dynamica van deze velloop wordt beschreven met behulp van het stuksgewijs lineair (PWL) modelvormingsformalisme, wat resulteert in een model dat zowel het achtereenvolgend schakelen van de aandrijvende kneep en de in het papierpad aanwezige onzekerheden bevat.

Gebaseerd op dit model van de velloop worden twee methoden voor regelaarontwerp gepresenteerd. In de eerste methode wordt het model van de velloop geschreven in termen van zijn foutdynamica. Door in het foutdomein te werken, is de stabiliteit van deze foutdynamica direct gekoppeld aan de prestaties van het volgedrag van de velloop dynamica. Om het nominale model in het foutdomein, dat discontinuïteiten bevat, te stabiliseren, wordt een regelwet voorgesteld die gebaseerd is op toestandsterugkoppeling. Er worden twee typen regelaars ontworpen op basis van de formulering van een set lineaire matrix ongelijkheden (LMIs). Toepassing van het eerste type regelaar resulteert in een lineair gesloten-lus systeem, terwijl met het tweede type een stuksgewijs lineair, discontinu, gesloten-lus systeem wordt verkregen. De relaties tussen beide regelaars en de Lyapunov functie, gebruikt voor het stabiliteitsbewijs van het gesloten-lus systeem, worden geanalyseerd, evenals de invloed van parameter perturbaties op de positie- en snelheidsfout van het vel. De tweede methode voor regelaarontwerp is direct gebaseerd op het model van de velloop. Met behulp van deze methode worden dynamische regelaars ontworpen die gebaseerd zijn op de terugkoppeling van de uitgang van het systeem. Deze regelaars garanderen stabiliteit en prestaties van het gesloten-lus systeem, dat onderhevig is aan onzekerheden in de parameters. Dit tweede ontwerp wordt ook geformuleerd in termen van een set LMIs en combineert technieken voor lineair H_∞ regelaarontwerp voor de individuele regio's van de velloop dynamica met stabiliteits- en prestatie-eisen voor het totale schakelende systeem.

Beide methoden voor het regelaarontwerp zijn in de praktijk gevalideerd. Hiertoe is een experimentele papierpad-opstelling gerealiseerd, waarin de verplaatsing van de vellen gemeten wordt met behulp van optische muissensoren. De experimenten laten een stabiel gesloten-lus gedrag zien en ze laten zien dat voldaan wordt aan de performance eisen in het geval dat parametrische onzekerheden aanwezig zijn in het papierpad. Bovendien kunnen de experimenteel verkregen responsies erg goed voorspeld worden met behulp van de eenvoudige modellen van de velloop die gebruikt zijn in het regelaarontwerp.

Na het aantonen dat terugkoppelingsgebaseerd regelen van de velloop in een eenvoudig papierpad mogelijk is, en gegeven de vereisten in een echt papierpad van een printer, is de tweede methode voor het regelaarontwerp gekozen om uitgebreid te worden voor toepassing in zo'n papierpad. Deze methode is gekozen vanwege mogelijkheid tot robuust regelaarontwerp en vanwege het feit dat deze methode de meeste ontwerpvrijheid biedt. Gegeven deze methode worden uitbreidingen naar veltransport voor tweezijdig printen en naar transport van verschillende velformaten uitgevoerd. Met deze uitbreidingen wordt de basis voor een herbruikbare, systematische ontwerpaanpak voor papierdoorvoer in papierpaden gecreëerd, wat de weg opent naar integratie en implementatie in een echt papierpad.

Dankwoord

Het aanbreken van de eerste zonnige lentedagen van het jaar vormt voor mij een mooi moment om stil te staan bij de afgelopen vier jaar. Een periode die met het schrijven van het dankwoord van dit proefschrift wordt afgesloten en die getypeerd kan worden als uitdagend en intensief, maar bovenal als erg leerzaam. Een periode ook die vorm heeft gekregen met hulp van een groot aantal mensen, waarvan ik er enkele hier persoonlijk wil bedanken.

Als eerste wil ik Maarten Steinbuch en René van de Molengraft bedanken voor de mogelijkheid die ze me gegeven hebben om het promotietraject te doorlopen en voor hun coaching gedurende de afgelopen vier jaren. Maarten en René, jullie enthousiasme, positieve instelling en vertrouwen zijn voor mij een grote steun geweest, vooral in de perioden dat het onderzoek wat minder vlot verliep dan ik graag zou willen. Ik heb onze samenwerking als bijzonder prettig ervaren en ik denk ook met veel plezier terug aan de onderwijstaken die we samen vervuld hebben en die ik ervaren heb als een mooie aanvulling op en afwisseling van het dagelijkse onderzoek.

Ook wil ik Maurice Heemels bedanken voor zijn bijdrage aan het werk beschreven in de Hoofdstukken 3 en 4. Maurice, jouw scherpe en kritische blik hebben me veel inzicht gegeven en ik heb veel geleerd van onze discussies. Bedankt dat ik gedurende de laatste maanden regelmatig bij je aan kon kloppen. Ook wil ik jou, evenals Carsten Scherer, Job van Amerongen en Paul van den Bosch bedanken voor het lezen van mijn proefschrift en het geven van feedback, zodat ik de puntjes op de “i” heb kunnen plaatsen.

Een woord van dank gaat ook uit naar het Embedded Systems Institute voor het leiding geven aan het Boderc project. Verder wil ik alle Boderc collega’s bedanken voor de fijne samenwerking en voor alle kennis buiten het domein van de regeltechniek om die ik dankzij hen heb vergaard. Mijn mede-AiO’s Peter, Marcel, Oana en Marieke wil ik veel succes toewensen met het afronden van hun promotie-onderzoek en mijn (oud)

mede-AiO Heico wil ik bedanken voor de lol tijdens diverse conferenties [64]. Vooral het kamperen in St. Malo, samen met Maurice, en de zoektocht naar een blauwe Ford Escort in Aken zullen me nog lang bijblijven.

Mijn collega's van de DCT groep wil ik graag bedanken voor het creëren van een fantastische werksfeer. Ik ben altijd met veel plezier naar mijn werk gekomen en dat komt mede door de lol die ik heb gehad tijdens en buiten werktijd. Van deze DCT-ers wil ik Nathan van de Wouw bedanken voor de bijeenkomsten die we, vooral in een vroeg stadium van het project, gehad hebben en die mede richting gegeven hebben aan mijn werk. Harrie van de Loo en Peter Hamels wil ik graag bedanken voor de ondersteuning van de experimenten die ik heb uitgevoerd. Ook de studenten die hebben bijgedragen aan het werk beschreven in dit proefschrift wil ik bedanken: Jeroen de Best, Koen Evers, Gert Witvoet, Nico Weel, Sebastiaan Elling, Wiebo Kamphuis en Jeroen Maas. Uiteraard mogen ook de collega's van het Tech United Robocup Team niet vergeten worden. De wekelijkse klusavonden vormden een mooie afleiding van het dagelijkse werk en ons allereerste toernooi zal ik zeker niet snel vergeten.

Natuurlijk zijn er ook buiten het werk om veel mensen die belangrijk voor mij zijn geweest gedurende de afgelopen tijd. Mijn familie en vrienden wil ik bedanken voor de getoonde interesse in mijn werk en voor de broodnodige, niet-werkgerelateerde afleiding in de vorm van (verjaardags)feestjes, uitjes en vakanties. Een speciaal woord van dank wil ik richten aan mijn ouders. Jullie hebben me altijd de vrijheid en de mogelijkheden gegeven om mezelf te ontplooiën en de liefde, de steun en het vertrouwen die ik van jullie heb gekregen is fantastisch, bedankt hiervoor! Last, but most certainly not least, wil ik Daphne bedanken voor haar liefde, haar vertrouwen en haar grenzeloze geduld, dat vooral in de laatste fase van het promotietraject flink op de proef is gesteld. Je bent gedurende de hele periode een grote steun voor me geweest en daarvoor ben ik je bijzonder dankbaar!

Björn Bukkems
Maart 2007

Curriculum Vitae

Björn Bukkems was born on June 25, 1978 in Geldrop, The Netherlands. After finishing Atheneum at the “College Asten Someren” in Asten in 1996, he started his study Mechanical Engineering at the Technische Universiteit Eindhoven. In 2003, he received his Master’s degree (cum laude), after successfully finishing his graduation project, entitled “Advanced Control of an RRR-robot Tip”, which was carried out within the Control Systems Technology group. For the thesis resulting from this project, he was awarded with the “KIVI Regeltechniekprijs 2003”. In February 2003, he started as a Ph.D. student in the Boderc (**B**eyond the **O**rdinary: **D**esign of **E**mbodied **R**eal-time **C**ontrol) research project on the topic of “Sheet Feedback Control Design in a Printer Paper Path”, resulting in this thesis.

